




ADVERTIMENT. L'accés als continguts d'aquesta tesi queda condicionat a l'acceptació de les condicions d'ús establertes per la següent llicència Creative Commons:  <https://creativecommons.org/licenses/?lang=ca>

ADVERTENCIA. El acceso a los contenidos de esta tesis queda condicionado a la aceptación de las condiciones de uso establecidas por la siguiente licencia Creative Commons:  <https://creativecommons.org/licenses/?lang=es>

WARNING. The access to the contents of this doctoral thesis it is limited to the acceptance of the use conditions set by the following Creative Commons license:  <https://creativecommons.org/licenses/?lang=en>

Identification of novel genes expressed during mammalian spermatogenesis. Analysis of their functions and implication for fertility

Thesis submitted by
Yan Huang

To opt for the title of
Doctor in Cell Biology

Doctoral thesis directed by
Dr. Ignasi Roig Navarro

Departament de Biologia Cel·lular, Fisiologia i Immunologia
Institut de Biomedicina i Biotecnologia (IBB)
Universitat Autònoma de Barcelona

Director
Dr. Ignasi Roig Navarro

PhD candidate
Yan Huang

Bellaterra (Cerdanyola del Vallès), 2022

This work was supported by:

- Ministerio de Economía y Competitividad:
 - Research project (BFU2016-80370-P)
 - Research project (PID2019-107082RB-I00)
 - Excellence network MeioNet (BFU2015-71786-REDT).

- China Scholarship Council Fellowship:
 - Pre-doctoral fellowship (201607040048)

Do What You Love

— My mom

Cuando bebas agua, recuerda la fuente.

昔者庄周梦为胡蝶，
栩栩然胡蝶也，
自喻适志与，不知周也。
俄然觉，则蘧蘧然周也。
不知周之梦为胡蝶与，胡蝶之梦为周与？

——《齐物论》

INDEX

ABSTRACT	11
ACRONYMS AND ABBREVIATIONS.....	13
CHAPTER 1 INTRODUCTION.....	16
1.1. GAMETOGENESIS	18
1.1.1. Meiotic entry	20
1.1.2. Spermatogenesis	21
1.1.3. Oogenesis	24
1.1.4. Genetic cause of infertility.....	27
1.2. MEIOSIS.....	30
1.2.1. Meiosis overview	30
1.2.2. Meiotic chromosomes and the synaptonemal complex (SC)	32
1.2.3. Recombination.....	45
1.2.4. Meiotic checkpoint	57
CHAPTER 2 OBJECTIVES.....	65
CHAPTER 3 MATERIALS AND METHODS.....	69
3.1. GENE SCREEN	71
3.1.1. RNA purification	71
3.1.2. Reverse transcription polymerase chain reaction (RT-PCR)	72
3.2. GENE CLONING.....	75
3.2.1. High-fidelity PCR	75
3.2.2. DNA purification	76
3.2.3. DNA digestion	79
3.2.4. DNA ligation.....	81
3.2.5. Transformation	82
3.2.6. Colony screening	82
3.2.7. Plasmid isolation	83
3.3. GENE EXPRESSION ANALYSIS	85

3.3.1.	Transfection in HEK 293T cell line.....	85
3.3.2.	Electroporation in live mouse testis.....	86
3.3.3.	Spermatocyte spreading from frozen testis	87
3.3.4.	Seminiferous tubule Squash.....	88
3.3.5.	Immunofluorescence staining	89
3.3.6.	Western blot	90
3.3.7.	5' Rapid Amplification of cDNA Ends (RACE)	94
3.4.	POLYCLONAL ANTIBODY GENERATION.....	99
3.4.1.	Purification of recombinant protein	99
3.4.2.	Sample preparation for animal injection	108
3.4.3.	Immunization of animals	111
3.5.	MOUSE MUTATION AND PHENOTYPING	111
3.5.1.	CRISPR/Cas9 knockout.....	111
3.5.2.	Mouse Genotyping.....	112
3.5.3.	Tissue fixation, embedding, and sectioning	114
3.5.4.	Immunohistochemistry staining.....	115
3.5.5.	PAS-Hematoxylin staining.....	116
3.5.6.	TUNEL assay- <i>In situ</i> cell death detection	117
3.5.7.	Oocyte nuclei spreading.....	118
3.5.8.	Follicle count and classification	119
3.6.	MICROSCOPY, IMAGING PROCESS, AND DATA ANALYSIS	120
3.6.1.	Microscopy and image capture.....	120
3.6.2.	Image process and analysis.....	120
3.6.3.	Statistical analysis.....	120
CHAPTER 4	RESULTS.....	122
4.1.	EXPRESSION PROFILE OF CANDIDATE GENES IN MOUSE TISSUES	124
4.2.	EXPRESSION PATTERN OF CANDIDATE GENES IN HEK 293T CELLS.....	128
4.3.	EXPRESSION PATTERN OF CANDIDATE GENES IN MOUSE SPERMATOCYTES.....	131
4.3.1.	Gene 20P1.....	132
4.3.2.	Gene 25 P1	133
4.3.3.	Gene 62P1 and 62P2	134
4.3.4.	Gene 136P1.....	136

4.3.5.	Gene 151P1.....	137
4.3.6.	Gene 255P1.....	137
4.3.7.	Gene 273P2.....	138
4.3.8.	Gene 310P1.....	139
4.3.9.	Gene 333P1.....	140
4.3.10.	Gene 355P1.....	141
4.4.	FUNCTIONAL ANALYSIS OF 255P1/BEND2 IN MEIOSIS	143
4.4.1.	Localization of BEND2 in meiocytes	143
4.4.2.	Detection of BEND2 during spermatogenesis	147
4.4.3.	Phenotyping of <i>Bend2</i> mutant mice.....	150
4.5.	FUNCTIONAL ANALYSIS OF 355P1/USP44 IN MEIOSIS.....	169
4.5.1.	The distinction between 355P1 and USP44 in testis	170
4.5.2.	Localization of USP44 in meiocytes	171
4.5.3.	Phenotyping of <i>Usp44</i> mutant mice	175
CHAPTER 5	DISCUSSION	186
5.1.	IDENTIFICATION OF MEIOTIC GENES ESSENTIAL FOR FERTILITY	188
5.1.1.	The efficiency of electroporation in live mouse testis.....	189
5.2.	ROLES OF BEND2 IN MEIOTIC PROPHASE	190
5.2.1.	The source of persistent DSBs in <i>Bend2</i> mutants	191
5.2.2.	Increased DSBs levels might be formed in <i>Bend2</i> mutants	193
5.2.3.	DSB repair might be impaired in <i>Bend2</i> mutants	195
5.3.	USP44 AS A NOVEL MEIOTIC GENE	197
5.3.1.	Ubiquitination and deubiquitination protein regulation.....	197
5.3.2.	Roles of USP44 in mammals	198
5.3.3.	Roles of USP44 in meiosis	201
CHAPTER 6	CONCLUSIONS	207
REFERENCES	212
SUPPLEMENTARY TABLES.....	250

Abstract

Meiosis is a specialized cell division, generating haploid gametes during gametogenesis for successful reproduction. Meiotic failure leads to infertility in mammals. In humans, infertility has become a major social health issue with many unknown genetic causes. Thus, in this work, we aimed to identify novel meiotic genes required for mammalian gametogenesis for better clinically relevant diagnosis and therapeutics. This work builds on the finding of several unannotated transcripts detected in 14 dpp mouse testis that we predicted to be novel genes. To test this hypothesis, we performed a sequential screen and eventually identified two novel meiotic prophase-specific genes *Bend2* and *Usp44*. Then, we went through characterizing their localization in meiocytes using our *in-house* polyclonal antibodies and analyzing mutant mice focusing on fertility and meiotic major events (synapsis and recombination). On one hand, BEND2 is a BEN domain-containing protein likely involved in chromatin and transcriptional regulation. BEND2 is highly expressed in nuclei from spermatogonia until early pachytene during spermatogenesis, independently of either DSB formation or completion of recombination. The deletion of BEND2 leads to a significant loss of primordial follicles in adult females with reduced fertility but has minor effects on spermatogenesis, despite increased apoptosis. BEND2 deficient meiocytes exhibited normal synapsis and considerably increased γ H2AX during late prophase. A subtle change of RPA and RAD51 foci numbers and altered meiotic progression in *Bend2* mutant spermatocytes and a reduced CO number in *Bend2* mutant oocytes were also found. These results indicate BEND2 is required for female fertility but not male's and the BEND2 mutation leads to insufficient DSB repair during prophase. On the other hand, USP44 is a deubiquitinating enzyme that localizes at synapsed chromosome axes during meiotic prophase, in a SPO11- and DMC1-dependent manner. In the absence of USP44, meiosis was arrested in most seminiferous tubules. Spermatocytes exhibited extensive defects in homolog pairing and synapsis, substantial γ H2AX signals persisted in zygotene-like cells with accumulations of RPA and RAD51 foci, and only a minority of spermatocytes progressed to the diplotene stage. These results suggest that USP44 is essential for homolog pairing, synapsis, and DSB repair as well as male fertility. In conclusion, our results confirm our approach is valid for identifying novel genes involved in mammalian gametogenesis. Using this strategy, we successfully identified two novel meiotic genes essential for mammalian fertility, thus providing new insights into understanding, diagnosing, and treating human infertility.

Acronyms and abbreviations

#	- Number	dpc	- Day postcoitum
%	- Percentage	dpp	- Day postpartum
µg	- Microgram	DSB	- DNA double-strand break
µl	- Microliter	DUB	- Deubiquitinating enzyme
µm	- Micrometer	EP	- Electroporated/electroporation
AE	- Axial element	FMR1	- Fragile X mental retardation 1
AMH	- Anti-Mullerian hormone	FSH	- Follicle-stimulating hormone
ANK	- Ankyrin repeats	g	- G-force
ATM	- Ataxia telangiectasia mutated	GnRH	- Gonadotropin-releasing hormone
ATR	- Assisted reproductive technology	GO	- Gene Ontology
ATR	- ATM/ ATM and Rad3-related	GSP	- Gene-specific primer
AZF	- Azoospermia factor	GTP	- Genotyping
BRCA1	- Breast cancer 1 protein	h	- Hour/hours
BRCA2	- Breast cancer 2 protein	H1t	- Histone 1t
BTB	- Blood-testis barrier	HJ	- Holliday junction
cAMP	- Cyclic adenosine monophosphate	HORMAD1	- HORMA domain containing 1
CDS	- Coding sequence	HORMAD2	- HORMA domain containing 2
CE	- Central element	HR	- Homologous recombination
CFTR	- Cystic fibrosis transmembrane conductance regulator	lbs	- Inclusion bodies
cGMP	- Cyclic guanosine monophosphate	IF	- Immunofluorescence
CMV	- Cytomegalovirus	IH	- Inter-homolog
CO	- Crossover	IMAC	- Immobilized metal affinity chromatography
CR	- Central region	IS	- Inter-sister
CS	- Cleavage site	IS-HR	- Inter-sister homologous recombination
CYP26B1	- Gene cytochrome P450, family 26, subfamily b, polypeptide 1	KRAB	- Krueppel-associated box
DAZL	- RNA-binding protein deleted in azoospermia-like	L	- Liter
DdM	- DNA demethylation	L1	- LINE1
DDR	- DNA damage response	LE	- Lateral element
dHJ	- Double Holliday junction	LH	- Luteinizing hormone
DM	- DNA methylation	MCS	- Multiple cloning site

min	- Minute/minutes	POI	- Primary ovarian insufficiency
ml	- Milliliter	RA	- Retinoic acid
mM	- Millimolar	RACE	- Rapid amplification of cDNA ends
mPGCLCs	- Mouse primordial germ cell-like cells	RPA	- Replication protein A
MR	- Meiotic recombination	RT	- Reverse Transcription
MRN	- MRE11-RAD50-NBS1	RT-PCR	- Reverse transcription polymerase chain
MRX	- Mre11-Rad50-Xrs2	s	- Second
MSCI	- Meiotic Sex Chromosome Inactivation	SAC	- Spindle assembly checkpoint
MSUC	- Meiotic silencing of unsynapsed chromatin	SAP130	- Sin3-associated protein 130
MutLy	- MLH1/MLH3	SC	- Synaptonemal complex
MutSy	- MSH4/MSH5	SDSA	- Synthesis-dependent strand annealing
MW	- Molecular weight	SEIs	- Single-end invasions
NCO	- Non-crossover	SMC	- Structural maintenance of chromosome
N-CoR	- Nuclear receptor co-repressor	SN	- Supernatant
NGN3	- Neurogenin 3	spc	- Spermatocyte
NHEJ	- Non-homologous end joining	SSCs	- Spermatogonial stem cells
nm	- Nanometer	Stra8	- Retinoic Acid gene 8 genes
NPC	- Nuclear pore complex	TdT	- Terminal deoxynucleotidyl transferase
NUP96	- Nuclear protein 96	TEVp	- Tobacco Etch Virus protease
NUP98	- Nuclear protein 98	TF	- Transverse filaments
°C	- Celsius degree	TOPOVIBL	- TopoVIB-like subunit
ON	- Overnight	TS	- Turner syndrome
P	- Pellet	TSO	- Template-switch oligonucleotide
PAR	- Pseudoautosomal region	UBE2C	- Ubiquitin-conjugating enzyme-E2C
PB	- Polar body	UPM	- Universal primer mix
PCOS	- Polycystic ovary syndrome	UPS	- Ubiquitin-proteasome system
PCR	- Polymerase chain reaction	USP	- Ubiquitin-specific protease
PGCs	- Primordial germ cells	ZZS	- Zip2-Zip4-Spo16
Plk1/Plx1	- Polo-like kinase 1	γH2AX	- Phosphorylates H2AX
PMF	- Peptide Mass Fingerprinting		-

Chapter 1

INTRODUCTION

1.1. Gametogenesis

The perpetuation of most living beings and their genetic information across generations relies on a critical biological process-gametogenesis. In mammals, this process includes oogenesis and spermatogenesis, through both of which unipotent diploid precursor cells develop into mature haploid gametes, egg in females, or sperm in males. After fertilization, the united egg and sperm form the embryo that develops into a new diploid organism carrying maternal and paternal genomic material.

Primordial germ cells (PGCs) are singled out as a cluster of germ cells at the epiblast in early mouse embryonic development at ~E7.25 (Chiquoine 1954; Ginsburg, Snow, and McLaren 1990). They are recruited from pluripotent embryonic cells and specified by inductive signals arising from the surrounding tissue (Extavour and Akam 2003). From the epiblast, PGCs undergo migration along the elongating hindgut endoderm and eventually colonize the developing gonads, the genital ridge, at E10.5, forming syncytia in which multiple cells share one cytoplasm. These arise due to PGCs dividing by mitosis with incomplete cytokinesis (Molyneaux et al. 2001; R. Anderson et al. 2000; Tam and Snow 1981; Western 2009).

During the migration period, PGCs proliferate rapidly and are transcriptionally quiescent. Soon after the colonization of the developing gonads, PGCs enter a transitional period. They switch from multipotential to bipotential and obtain the competence to initiate sexual differentiation and meiosis (Lesch and Page 2012). At around E12.5, the genital ridge develops into testes in males determined by the Y-chromosome-encoded gene, *Sry*, while ovaries are formed in females due to the absence of *Sry* (Y.-T. Lin and Capel 2015). Consequently, PGCs commit to divergent development based on the cues from the somatic environment that female and male PGCs differentiate to their specialized gamete precursors: oogonia and spermatogonia, to form eggs through oogenesis or sperm through spermatogenesis (Edson, Nagaraja, and Matzuk 2009; Griswold 2016) (Figure 1-1).

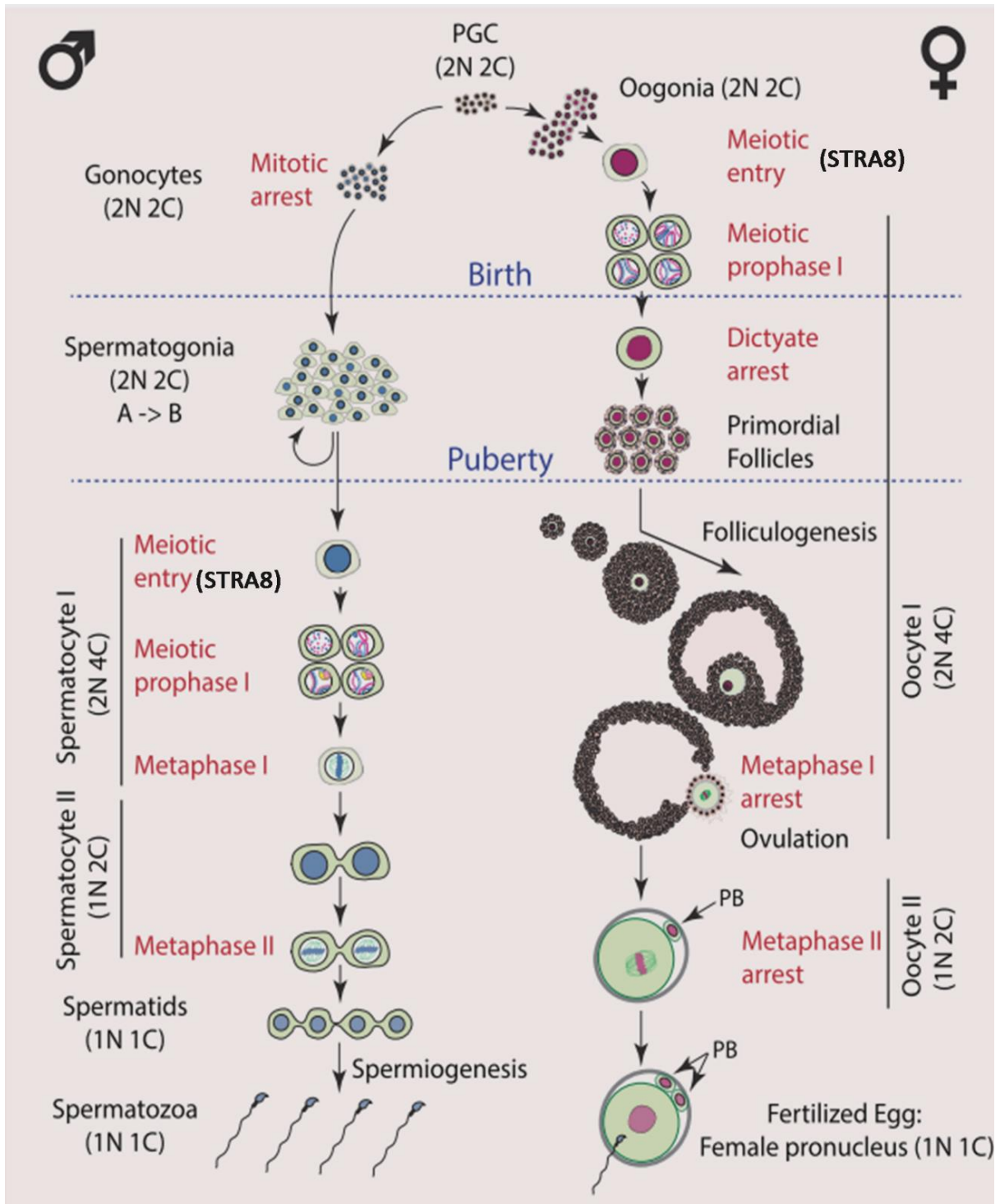


Figure 1-1. Gametogenesis overview.

The schematic illustrates sexually dimorphic progressive events of gametogenesis in mammalian males (left) and females (right). Red fonts indicate meiosis events. DNA content: C value and number of sets of chromosomes: N value, ploidy. Sexually undifferentiated primordial germ cells (PGCs) migrate and colonize at the fetal gonads. Soon, PGCs switch from multipotential to bipotential, subsequently, sex-specific differentiation programs initiate. In males (left panel), PGCs undergo a short mitotic proliferation after sex determination and then arrest at the G₀/G₁ phase, forming quiescent gonocytes. After birth, gonocytes differentiate into spermatogonial stem cells (SSCs)-As spermatogonia. SSCs either self-renew to maintain the stem cell pool or differentiate into B spermatogonia, through Apr (progenitor spermatogonia), Aal, A₁, A₂, A₃, A₄, and In spermatogonia. B spermatogonia form

preleptotene spermatocytes, thus initiating meiosis (depending on *STRA8* expression). Diploid spermatocytes proceed through prophase I and complete two rounds of cell division without interruption, eventually generating haploid spermatids. Spermatids undergo spermiogenic differentiation (spermiogenesis) to form spermatozoa. In females (right panel), oogonia undergo mitotic proliferation, forming germ cell cysts. Oogonia in the cysts enter meiotic prophase I during fetal development (depending on *STRA8* expression). The diploid oocytes complete meiotic recombination, forming primary oocyte arrested at the dictyate stage around birth. Shortly after birth, as cysts breakdown, somatic pre-granulosa cells enclose primary oocytes to form primordial follicles. Around puberty, primordial follicles are recruited and activated to initiate follicular development with the growth of oocytes and the proliferation of granulosa cells. which remains arrested at dictyate. Prior to ovulation, the arrested oocytes resume meiosis and then arrest at metaphase I. Upon ovulation, the first meiotic division is completed and the first polar body (PB) is extruded into the space under the zona pellucida. The ovulated oocytes arrest again, at metaphase II. Until fertilization, meiosis resumes second meiotic division and extrusion of the second PB (the first PB rarely undergoes its second division). Image adapted from Bolcun-Filas et al. 2018.

1.1.1. Meiotic entry

In mammals, meiotic initiation is sexually dimorphic and requires a switch-off from the mitotic program (Handel and Schimenti 2010). In mice, meiosis initiates during embryonic development in females (E12.5) but during the postnatal period in males. Despite the difference in the entry timing, retinoic acid (RA) signaling is considered the extrinsic key driver for initiating meiosis (Y. Lin et al. 2008; Raverdeau et al. 2012). Intrinsic factors, such as the Stimulated by Retinoic Acid gene 8 genes (*Stra8*), are also needed. *Stra8* is a mammalian germ cell-specific gene required to induce the meiotic program. It is expressed in embryonic ovaries (Menke, Koubova, and Page 2003) and the postnatal testis before meiotic entry (Oulad-Abdelghani et al. 1996). *Stra8* plays a crucial role in regulating the meiotic initiation by responding to RA (E. L. Anderson et al. 2008; Dokshin et al. 2013; Mark et al. 2008; Baltus et al. 2006).

During mouse embryonic development, germ cells obtain the competence to respond to RA, which depends on the RNA-binding protein deleted in azoospermia-like (DAZL) (Lesch and Page 2012; Soh et al. 2015). RA synthesizes in the mesonephric ducts (Bowles et al. 2006), responsible for initiating female meiosis by inducing *Stra8* expression (Baltus et al. 2006; Koubova et al. 2006a). In males, RA is degraded by CYP26B1 (gene cytochrome P450, family 26, subfamily b, polypeptide 1) from male Sertoli cells. Consequently, CYP26B1 prevents the induction of *Stra8* and blocks the meiotic entry (Bowles et al. 2006). Postnatally, the expression of CYP26B1 is repressed in male gonads, which enables male spermatogenic precursors to respond to RA, expressing

Stra8, and ultimately enter meiosis (Lesch and Page 2012; Koubova et al. 2006b; Bowles et al. 2006; E. L. Anderson et al. 2008).

The exact RA-*Stra8* meiotic initiation pathway remains elusive. A recent study suggests that STRA8 may initiate meiosis in mice as a common factor in a broad transcriptional network by binding and upregulating meiotic prophase I genes, G₁-S cell-cycle genes, and factors that specifically inhibit the mitotic program and germline-specific genes (Kojima, De Rooij, and Page 2019). MEIOSIN, a recent-discovered factor, seems to trigger meiosis initiation in mice. MEIOSIN works together with STRA8 in the same transcriptional complex. Both activate genes responsible for suppressing the mitotic program and establishing a meiosis-specific chromosome structure under the presence of RA (Oatley and Griswold 2020). Interestingly, it is also suggested that RA and STRA8 are not sufficient to induce meiosis *in vitro* in mouse primordial germ cell-like cells (mPGCLCs) (Miyachi et al. 2017). The BMP-ZGLP₁ pathway, which activates critical oogenic programs, is required to initiate meiosis synergistically with RA, contributing to oogenic maturation and PGC program repression by employing the common downstream effector STRA8 on mPGCLCs (Nagaoka et al. 2020). Besides, a STRA8 independent pathway is suggested for RA-mediated meiosis initiation, in which RA directly promotes *Rec8* expression (a component of cohesin complex) (Soh et al. 2015; Koubova et al. 2014a). Apart from RA, some other regulators such as epigenetic restriction (Yamaguchi et al. 2012; Yokobayashi et al. 2013; Endoh et al. 2017), DMRT₁ (Matson et al. 2010), and MAX (Suzuki et al. 2016) are also thought to contribute to the meiotic entry through negative controls.

1.1.2. Spermatogenesis

Mammalian male fertility requires millions of sperm produced daily by continuous spermatogenesis throughout reproductive life. The continual spermatogenesis is founded on a stem cell pool supplied by spermatogonial stem cells (SSCs) (de Rooij and Russell 2000; Oatley and Brinster 2008). Spermatogenesis continues with the mitotic expansion of spermatogonia, the meiotic divisions of spermatocytes, and the morphological transformations of spermatids (Griswold 2016) (Figure 1-1).

SSCs are testis-specific stem cells derived from PGCs. In mice, male PGCs undergo a short proliferation after sex determination and arrest at the G₀/G₁ phase at

around E13.5, referred to as gonocytes (prospermatogonia). Around 3 dpp, gonocytes migrate from the center of the seminiferous cords to the basement membrane, where they differentiate into SSCs (McLean et al. 2003; Bellve et al. 1977). One subpopulation of cells develops into morphologically distinct SSCs, which express Neurogenin 3 (NGN3) and supply SSC for spermatogenesis during adulthood. The other subpopulation does not pass through the NGN3-expressing stage and directly forms differentiating spermatogonia, which initiates the first round of spermatogenesis (S. Yoshida et al. 2006).

SSCs are defined by their self-renewal capability to maintain the stem cell pool and differentiation to support spermatogenesis. In mice, SSCs (As (A-single) spermatogonia) undergo symmetric division to produce SSCs for self-renewal or progenitor spermatogonia (Apr (A-paired) spermatogonia) for differentiation, which marks the beginning of spermatogenesis. SSCs self-renewal predominate during the neonatal period to establish a stem cell pool (Shinohara et al. 2001), but only occurs periodically under steady-state conditions during adulthood to maintain the SSC pool (Oatley and Brinster 2012). Progenitor spermatogonia divide into Aal spermatogonia, together with the As and Apr spermatogonia forming the undifferentiated heterogeneous spermatogonia population. Aal spermatogonia give rise to differentiating A1 spermatogonia, which subsequently undergoes five rounds of mitotic cell divisions to form differentiating A2, A3, A4, In (Intermediate), and B spermatogonia. B spermatogonia result in preleptotene spermatocytes via a final round of mitosis and initiate meiosis (Rato et al. 2012; Russell et al. 1993; de Rooij and Russell 2000).

Diploid spermatocytes proceed through meiosis, which starts with DNA replication, followed by two rounds of cell division, resulting in haploid round spermatids. Subsequently, these round spermatids undergo structural and functional changes, including nuclear remodeling by chromatin condensation, removing the excess cytoplasm, and forming an acrosome and a sperm tail (spermiogenesis) (Herms et al. 2010; Lehti and Sironen 2016). As a result, spermatids become motile spermatozoa and are released to the central seminiferous lumen (spermiation). Spermatozoa will complete the final maturation to become fertilizable sperm in the epididymis.

Spermatogenesis is strictly controlled by hormone regulators such as RA, follicle-stimulating hormone (FSH), luteinizing hormone (LH), and testosterone globally (O'Donnell, Stanton, and de Kretser 2000; Kretser et al. 1998). Locally, biochemical interactions between germ cells and somatic cells (de Rooij and Russell 2000)

and sequential and coordinated gene expression programs also contribute to the regulation of spermatogenesis (Bettegowda and Wilkinson 2010).

Spermatogenesis occurs within the seminiferous tubules of the testis, in which germ cells in different stages of development are organized into a series of cell associations, known as stages. For each stage, a particular spermatogonial cell type is always associated with a specific stage of meiosis and spermatid development (O'Donnell, Stanton, and de Kretser 2000). In mouse testis, 12 stages have been identified and are successively arranged along the length of the tubules showing a spatial continuity based on the differentiation steps (Hasegawa and Saga 2012). A complete series of these stages is termed the epithelial cycle, resulting in the release of mature spermatozoa. RA pulses progressively stagger along the tubule and stimulate the spermatogonia to enter the rigidly timed pathway committed to meiosis. This defines the seminiferous epithelial cycle initiation and eventually enables the continuous release of spermatozoa (de Rooij and Russell 2000).

The developing germ cells and Sertoli cells comprise the seminiferous epithelium within the seminiferous tubules (Figure 1-2). Sertoli cells form tight junctions at their base to separate the seminiferous epithelium into basal (where the spermatogonial population resides) and the adluminal compartments (where the meiotic and haploid germ cells reside). These tight junctions constitute the so-called "blood-testis barrier" (BTB). The BTB restricts the entry of elements from the interstitial space, such as immune cells and specific molecules, into the adluminal compartment. Thus, the BTB is required to maintain homeostasis to develop meiotic and haploid germ cells in the adluminal compartment (Oatley and Brinster 2008; O'Donnell, Stanton, and de Kretser 2000). The BTB remodels periodically to ensure preleptone spermatocytes enter the adluminal compartment to initiate meiosis. The effects of RA on Sertoli cells are suggested to contribute to this remodeling through dynamic gene expressions (Hasegawa and Saga 2012).

The interstitial tissue between the seminiferous tubules contains Leydig cells, vascular network, and immune cells (Figure 1-2). The steroidogenic interstitial Leydig cells secrete testosterone under the influence of LH. Testosterone acts on various testicular cells, including Sertoli cells, to stimulate and maintain germ cell development throughout life and is required for spermatogenesis. Under the influence of FSH and testosterone, Sertoli cells secrete paracrine factors (e.g. GDNF) and express cell-surface

receptors needed to offer direct nourishment and support for spermatogenesis. (Griswold 1998; Oatley and Brinster 2012; Hasegawa and Saga 2012). Besides, dynamic gene expression through each stage strictly controls the extraordinarily complex spermatogenesis process (Bettegowda and Wilkinson 2010). For instance, many germ cell-specific transcripts resulting from the highly prevalent alternative splicing of mRNA in the testis are required for the ordered germ cell development. Non-coding RNAs play multiple roles in meiosis and spermiogenesis transcriptional regulation (O'Donnell, Stanton, and de Kretser 2000).

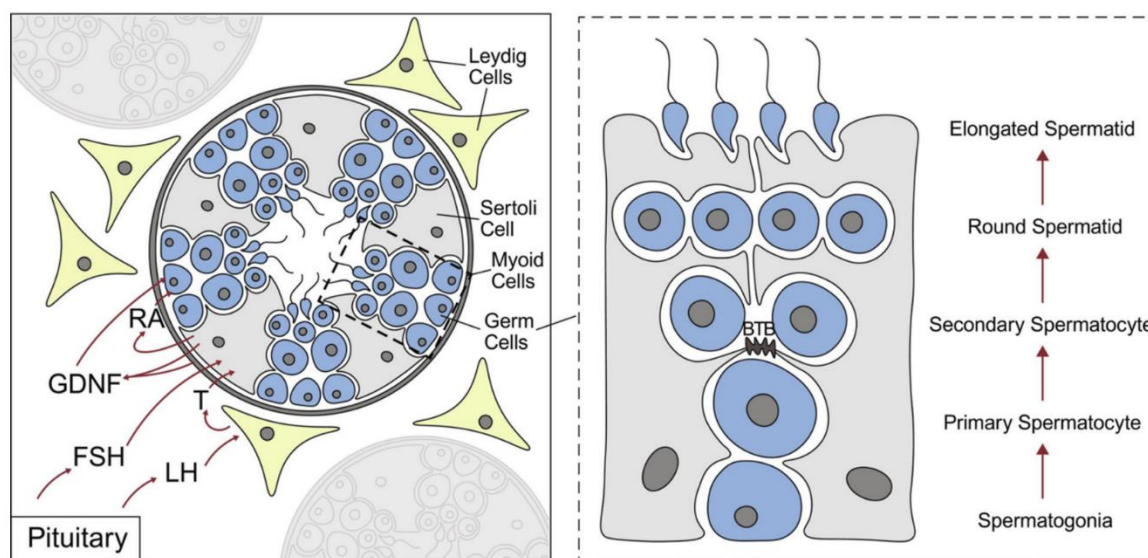


Figure 1-2. Schematic of testis cross section.

Major testis somatic and germ cell types are shown (left), along with select paracrine and endocrine signaling molecules. FSH, follicle-stimulating hormone; LH, luteinizing hormone; RA, Retinoic acid; T, testosterone; GDNF, Glial derived neutrophic factor. Zoom-in of progression of spermatogenesis (right). BTB, blood-testis barrier. Image adapted from Larose et al. 2019.

1.1.3. Oogenesis

Mammalian oogenesis begins during embryonic development and generates primary oocytes assembled in primordial follicles perinatally. The establishment of the pool of primordial follicles determines mammalian female fertility. Post-pubertally, primordial follicles are recruited irreversibly and develop into mature follicles during the estrous/menstrual cycle, eventually releasing mature and fertilizable oocytes. As a result, the ovarian reserve is gradually reduced, defining a finite female reproductive life span

(Kerr, Myers, and Anderson 2013; Hunter 2017; Wear, McPike, and Watanabe 2016; R. Li and Albertini 2013; Ruth et al. 2021) (Figure 1-1).

In mice, after differentiation of PGCs, oogonia undergo mitotic divisions with incomplete cytokinesis, forming germ cell cysts in which daughter cells are connected by intercellular bridges (McLaren and Monk 1981; M E Pepling and Spradling 1998). On E13.5, oogonia in the cysts initiate meiosis and eventually differentiate into primary oocytes, arrested at dictyotene of meiotic prophase I perinatally (Borum 1961). After cyst breakdown, primary oocytes are further enclosed in a layer of pre-granulosa cells, forming primordial follicles by 4 dpp (Melissa E. Pepling and Spradling 2001).

The formation of primordial follicles is a complex process. It requires the presence of germ cells (McLaren 1984) and involves communication between oocytes and pre-granulosa cells (Melissa E. Pepling 2012). Multiple aspects have been suggested to regulate the process, including transcription factors (*Figa* and *Foxl2*), signaling pathways (*Notch*, *TGF β* , and *Kit*), steroid hormones estrogen, bisphenol-A (BPA), testosterone, and progesterone (reviewed in Pepling, 2012).

In mammals, massive oocyte culling accompanies the oogenesis process for primordial follicle pool setup. In humans, around six to seven million primary oocytes enter meiosis during fetal development, with only one million oocytes remaining by birth and approximately 250,000 at the onset of puberty (T. G. Baker 1963; Hunter 2017). In mice, oocyte numbers begin to decline since E14.5, remain about half at birth, and continue reducing postnatally. At 4 dpp, eventually, only 20% of fetal oocytes remain in the ovaries (Martínez-Marchal et al. 2020; Malki et al. 2014; Hunter 2017).

The occurrence of this massive oocyte death has been indicated to be a consequence of oocyte quality control (Hunter 2017). Oocytes with potential defects due to the activation of LINE1 transposon are eliminated during embryonic development (E15.5-18.5), leaving only oocytes with limited LINE1 activity (Malki et al. 2014). Postnatally, oocyte culling occurs in response to errors in meiotic prophase I to remove oocytes that might have chromosomal defects (Di Giacomo et al. 2005). Additionally, the loss of oocytes is also suggested to be the self-sacrifice of nursing cells, which donate their cytoplasm through intercellular transfer within the cysts before undergoing apoptosis. Consequently, the surviving oocytes obtain most of the dying oocytes' cytoplasmic content and organelles and become primary oocytes (Lei and Spradling 2016). Through all these possible oocyte quality control processes, the most suitable oocytes are selected

for the next generation.

Newly formed primordial follicles remain quiescent until puberty, except for that a cohort of primordial follicles located at the anterior-dorsal region of mouse ovary are activated to grow during the first week of postnatal development (so-called the first wave of folliculogenesis) (Cordeiro et al. 2015). After puberty, quiescent primordial follicles are recruited continually through primordial follicle activation to initiate follicular development, forming primary follicles featured with a single-layer of cuboidal granulosa cells (Lintern-Moore and Moore 1979).

The exact mechanisms regulating the recruitment of primordial follicles are not well understood. Experimental evidence shows that the activation of primordial follicles is likely under both stimulatory and inhibitory regulations, involving both intrinsic and extrinsic factors (Larose et al. 2019; Durlinger et al. 2002). Potential inhibitory factors have been suggested, including oocyte-extrinsic anti-Mullerian hormone (AMH) (Durlinger et al. 2002), FOXL2 (Schmidt et al. 2004) and oocyte-intrinsic PTEN (Reddy et al. 2008), and various transcription factors SOHLH1, SOHLH2, LHX8, etc. (Pangas et al. 2006; Y. Choi, Yuan, and Rajkovic 2008; Y. Choi et al. 2008). At the same time, stem cell factor SCF, and growth factors GDF9, bFGF, and NGF are indicated to induce the development of primordial follicles (Vitt et al. 2000; Nilsson, Parrott, and Skinner 2001; Dissen et al. 2001; Durlinger et al. 2002).

Primary follicles continue developing through two phases: pre-antral and antral phases. Primary follicles become secondary/pre-antral follicles with two or more layers of granulosa cells through the pre-antral phase. The pre-antral phase development is independent of gonadotropins and mainly regulated by autocrine and paracrine signaling. Specifically, TGF- β family members play a crucial role in facilitating follicle development at this phase, such as oocyte-secreted GDF-9 and BMP-15, activins, and inhibins (Günesdogan and Surani 2016; Namwanje and Brown 2016; C. Yan et al. 2001).

Through the antral phase, antral follicles are formed. These are characterized by containing a granulosa cell-secreted fluid-filled cavity, called the antrum. Also, at this stage, the granulosa cells consist of two populations – the cumulus cells and the mural cells. The follicle development during this phase depends on gonadotropins FSH and LH (Williams and Erickson 2000). FSH stimulates granulosa cells to proliferate and to secrete estrogen. LH stimulates the theca cells to produce progesterone and testosterone. More importantly, the rise of the FSH level during the menstrual cycle allows the selection of

dominant follicles, enabling only a few antral follicles to develop into ovulatory follicles (Zelevnik 2004).

Since the initiation of follicular development, oocytes start to grow in size and are transcriptionally and translationally active (Lintern-Moore and Moore 1979). However, they remain arrested at the end of the meiotic prophase, marked by a large nucleus-the germinal vesicle with a prominent nucleolus. When the follicles reach the preovulatory stage, oocytes will resume meiosis and complete maturation in response to LH surge, as seen by the germinal vesicle breakdown (R. Li and Albertini 2013). Subsequently, oocytes arrest at metaphase II upon ovulation and resume meiosis again after fertilization, eventually generating a mature oocyte and two or three polar bodies that will undergo apoptosis.

In developing follicles, the oocyte arrest is maintained by the combined effects of the cyclic adenosine monophosphate (cAMP) and cyclic guanosine monophosphate (cGMP). LH acts on mural granulosa cells, triggering a series of signaling cascades. This results in a decrease of cGMP and cAMP in oocytes and thus reduced effects on oocyte arrest, eventually initiating meiosis resumption (Jaffe and Egbert 2017; R. Li and Albertini 2013). Besides the nuclear maturation, which involves the haploidization of the genome, the oocyte cytoplasm must also mature through major translational, post-translational, and organellar modifications, which are essential for the completion of meiosis, fertilization, and early embryonic development (reviewed in Li and Albertini, 2013).

1.1.4. Genetic cause of infertility

Successful reproduction requires precise regulations of complex processes essential for the development of reproductive organs, gametogenesis, neuroendocrine competency, and the ability to carry a pregnancy (S. A. Yatsenko and Rajkovic 2019). Infertility, a common, multifactorial pathological condition defined as the inability to establish a clinical pregnancy after at least one year of regular unprotected sexual intercourse, affects approximately 50 million couples worldwide (Mascarenhas et al. 2012). Among the infertility cases with identified causes, one third is due to a female factor, another third is due to a male factor, and the remaining third is due to combined female and male factors (Mallepaly et al. 2017). Furthermore, genetic defects are estimated to contribute to nearly 50% of these infertility cases. More unknown genetic

causes are suggested in infertility and need to be uncovered (Zorrilla and Yatsenko 2013).

Male infertility derives etiologically from quantitative spermatogenic defects, ductal obstruction or dysfunction, hypothalamic-pituitary axis dysfunction, and qualitative spermatogenic defects (from most to least common) (Tournaye, Krausz, and Oates 2017). Known genetic factors account for at least 15% of male infertility and involve in all these etiological categories (Csilla Krausz and Riera-Escamilla 2018). Diagnosing male infertility mainly relies on semen (and hormone) analysis, which results in two major phenotypes of oligozoospermia (reduced sperm count) and azoospermia (no spermatozoa in the ejaculate) (Tüttelmann, Ruckert, and Röpke 2018). Qualitative spermatogenic defects or ductal obstruction usually manifest as azoospermia, and multiple genetic factors are validated as the causes. They include numerical and structural chromosomal anomalies (e.g., Klinefelter's syndrome, 46, XX male syndrome), Y-chromosome micro-deletions (e.g., azoospermia factor (AZF) deletions), gene mutations (e.g., *TEX11* deletions), and cystic fibrosis transmembrane conductance regulator (*CFTR*) mutations (Csilla Krausz and Riera-Escamilla 2018). AZF deletions are the most frequent genetic cause of azoospermia (C. Krausz et al. 2014). Most numerical and structural chromosomal anomalies and *TEX11* deletions are thought to cause spermatogenic defects due to errors during meiosis (Sun et al. 2007; A. N. Yatsenko et al. 2015; Yang et al. 2015). Currently, some of these genetic infertility causes can be clinically diagnosed by widely applied analyses, such as karyotyping, AZF deletion screening, and *CFTR* mutation analysis (Tournaye, Krausz, and Oates 2017).

Female infertility can result from a wide range of factors affecting ovarian development, oocyte maturation, fertilization competence, and the potential of a fertilized egg for implantation and development (S. A. Yatsenko and Rajkovic 2019). Ovulation disorders are the leading cause of female infertility, which often occur as a result of conditions classified into three categories: hypothalamic failure, dysfunction of hypothalamic-pituitary-ovarian axis—mostly polycystic ovary syndrome (PCOS), and primary ovarian insufficiency (POI) (National Institute for Health and Care Excellence [NICE] 2013). Genetic factors are suggested to play a role in all these disorders. For example, mutations of the *GNRHR* gene encoding the gonadotropin-releasing hormone (GnRH) receptor and genes causing Kallmann syndrome have been identified in women affected by hypothalamic amenorrhea. Alternations in multiple genes such as *CYP17*, *CYP19*, *LHCGR*, *DENND1A* are linked to PCOS, suggesting its polygenicity (reviewed in

Beke, 2019).

POI has become a significant cause of female infertility, which occurs due to premature exhaustion of the primordial follicular pool in most cases (Rossetti et al. 2017). The most common contributors to POI are the X chromosome-linked defects, in which Turner syndrome (TS) is the primary cause for syndromic POI. In contrast, premutation of the *FMR1* (fragile X mental retardation 1) gene is the most common gene mutation associated with non-syndromic POI. The absence of one X chromosome in TS causes oocyte loss during early meiotic prophase and ovarian development, leading to ovarian dysgenesis and primary amenorrhea since infancy (Fechner et al. 2006). How *FMR1* premutation leads to POI is not clear yet. It's possibly due to the insufficiency of necessary proteins for oocyte development or follicle development and survival resulting from *FMR1* premutation (Rossetti et al. 2017). Identification of the causative genetic alterations in POI patients is beneficial for her female relatives, who can undertake precautionary measures (e.g., egg freezing, embryo cryopreservation, anticipated pregnancy planning, etc.) in case of being positive in the genetic screening (Rossetti et al. 2017). This perspective is becoming increasingly important due to the modern tendency to delay childbirth in societies.

Despite the revealed genetic factors contributing to female and male infertility, the genetic causes remain unexplained for the majority of infertility cases, including idiopathic infertility cases, which are identified in 25-30% infertility couples and likely have a genetic etiology (Mallepaly et al. 2017; S. Smith, Pfeifer, and Collins 2003). Furthermore, with the increasing use of assisted reproductive technology (ART), which removes the natural barrier to egg fertilization, the concerns about its safety and possible adverse outcomes are rising (M. J. Davies et al. 2012). Diagnosing the genetic causes of infertility becomes more clinically significant for infertility treatment and the health of patients and their children. Thus, identifying unknown genes involved in mammalian gametogenesis, which could contribute to human infertility, is demanding and essential for clinical infertility diagnosis in the near future.

1.2. Meiosis

1.2.1. Meiosis overview

Meiosis is a specialized cell division critical for gametogenesis in all sexually reproducing organisms. Through meiosis, a diploid parental cell gives rise to haploid daughter cells, and this is achieved by a single round of DNA replication followed by two rounds of cell divisions (Kleckner 1996). In mammals, homologous chromosomes separate during the first division (meiosis I), and sister chromatids separate during the second division (meiosis II) analogously to mitosis, resulting in the generation of haploid cells.

Consistent with the sexually dimorphic features of gametogenesis, meiosis exhibits substantial sexual dimorphism in mammals, including the different timing of meiosis (Handel and Eppig 1997; Morelli and Cohen 2005). In females, meiosis is initiated roughly at the same time in all germ cells during fetal development. Subsequently, arrest at the end of meiotic prophase I (diplotene stage) around the time of birth and resume to produce eggs periodically after puberty over a defined reproductive lifetime. In contrast, male meiosis is initiated in separate cohorts of germ cells after the onset of puberty and provides continuous sperm production throughout most of adult life (Feng, Bowles and Koopman, 2014). The two meiotic cell divisions in males are consecutive and result in four identical haploid sperm from each spermatogonium that initiates meiosis. On the contrary, female meiosis I do not complete until ovulation, and meiosis II only occurs under the trigger of fertilization, eventually generating one haploid oocyte from one oogonium (Bolcun-Filas and Handel 2018).

Meiosis is characterized by extended prophase I. The meiotic recombination (MR), comprised of the formation and repair of programmed DNA double-strand breaks (DSBs), occurs during this stage. MR results in crossovers (COs) forming with reciprocal exchange of chromosome arms flanking the DSB site. COs establish the connections between homologous chromosomes to ensure their accurate segregation at meiosis I and reshuffle parental alleles to increase genetic diversity in offspring. (Hunter 2015; Lam and Keeney 2015).

MR initiates in early prophase I with the formation of numerous DNA DSBs

catalyzed by the conserved SPO11 protein (Scott Keeney 2001). DSB ends undergo resection and generate 3' ssDNA ends, subsequently bound by the RecA family of strand exchange proteins (DMC1, RAD51) (San Filippo, Sung, and Klein 2008). This protein nucleofilament searches and invades homologous repair templates, initiating the repair pathways to form COs or non-crossovers (NCOs, with no exchange of flanking parental sequences) (S. Keeney and Neale 2006; Hunter 2015). Most COs arise from the resolution of double Holliday junction (dHJ) intermediates and are evenly distributed subject to a known process called CO interference (Berchowitz and Copenhaver 2010). In contrast, most NCOs are formed by synthesis-dependent strand annealing (SDSA) (Hunter 2015). NCOs promote homolog pairing while COs provide physical linkages between homologs. COs coupled with cohesion between sister chromatids ensure the correct homolog orientation on the meiotic spindle and proper segregation in meiosis I (Bolcun-Filas and Handel 2018; Van Heemst and Heyting 2000).

Meiotic recombination is tightly integrated with a highly-organized and dynamic chromosome structure during meiotic prophase I (D Zickler and Kleckner 1999). According to the chromosome morphology, the meiotic prophase is divided into five substages (leptonema, zygonema, pachynema, diplonema, and diakinesis) (Figure 1-3). During leptonema, the chromatin condenses at the developing chromosomal axes, and recombination initiates. The axes provide a rod-like center for the loops of every pair of chromatids to anchor. This well-defined loop-axis structure is essential for DSB formation and repair template choice (Subramanian and Hochwagen 2014). During zygonema, homologs begin to pair, and synapsis initiates, forming a tripartite proteinaceous scaffold, the synaptonemal complex (SC), between the paired homologous chromosomes to create their intimate association. Pachynema starts when an SC is formed along the entire length of all homologous chromosomes. During pachynema, recombination completes the final steps in the context of SC. At diplonema, the SCs disassemble between homologs. At diakinesis, bivalents are highly condensed and only remain connected by chiasmata, the cytological manifestation of COs. Subsequently, homologous chromosomes segregate, and the first meiotic division completes with maternal and paternal chromosomes separated into daughter cells. The second meiotic division is similar to mitosis, during which sister chromatids separate and haploid gametes generate.

Meiosis must be carefully monitored to preserve the order of meiotic events and

avoid producing aberrant chromosomes and defective gametes (Subramanian and Hochwagen 2014). In mice, surveillance mechanisms monitor recombination and synapsis at the pachytene stage (meiotic checkpoint) (Roeder 2000) and control bipolar attachment to the spindle at metaphase I (the spindle assembly checkpoint, SAC) (Touati and Wassmann 2016).

1.2.2. Meiotic chromosomes and the synaptonemal complex (SC)

1.2.2.1. Meiotic chromosome axis

After DNA replication in the pre-meiotic S-phase, each pair of sister chromatids are tightly held together by cohesin complexes, comprising meiotic homologous chromosomes, which are also known as homologs. The chromatin of sister chromatids is organized in a linear array of loops emanating from a chromosome axis, forming the meiotic axis-loop organization, which allows the possible close juxtaposition of homolog axes during meiotic prophase (Zickler and Kleckner, 2015). In mammals, there are several components of the chromosome axis, including meiosis-specific cohesin complexes (J. Lee et al. 2003; J. Lee and Hirano 2011; Ekaterina Revenkova et al. 2004; Prieto et al. 2001), the axial element proteins (AEs)(Lammers et al. 1994; Offenbergl et al. 1998), and the HORMA domain containing proteins (HORMADs) (Wojtasz et al., 2009) (Figure 1-3).

Axial proteins-The cohesin complex

The cohesin complex is an evolutionary conserved multi-protein complex that binds to DNA and mediates the cohesion between sister chromatids (Nasmyth and Haering 2009). Although the cohesin complex is essential for faithful chromosome segregation in mitosis and meiosis, it differs in meiosis from mitosis in respect of their components and functions (K. ichiro Ishiguro 2019) (Figure 1-4).

In mammalian somatic cells, the cohesin complex comprises four conserved core subunits: the structural maintenance of chromosomes (SMC) protein, SMC1 α and SMC3, the kleisin family protein RAD21, and either one of the two accessory protein SA1 or SA2 (reviewed in (Nasmyth and Haering 2009) (Figure 1-4). . Cohesins are loaded onto the chromatin before DNA replication and establish cohesion during DNA replication with the help of several cohesion-associated proteins (reviewed in

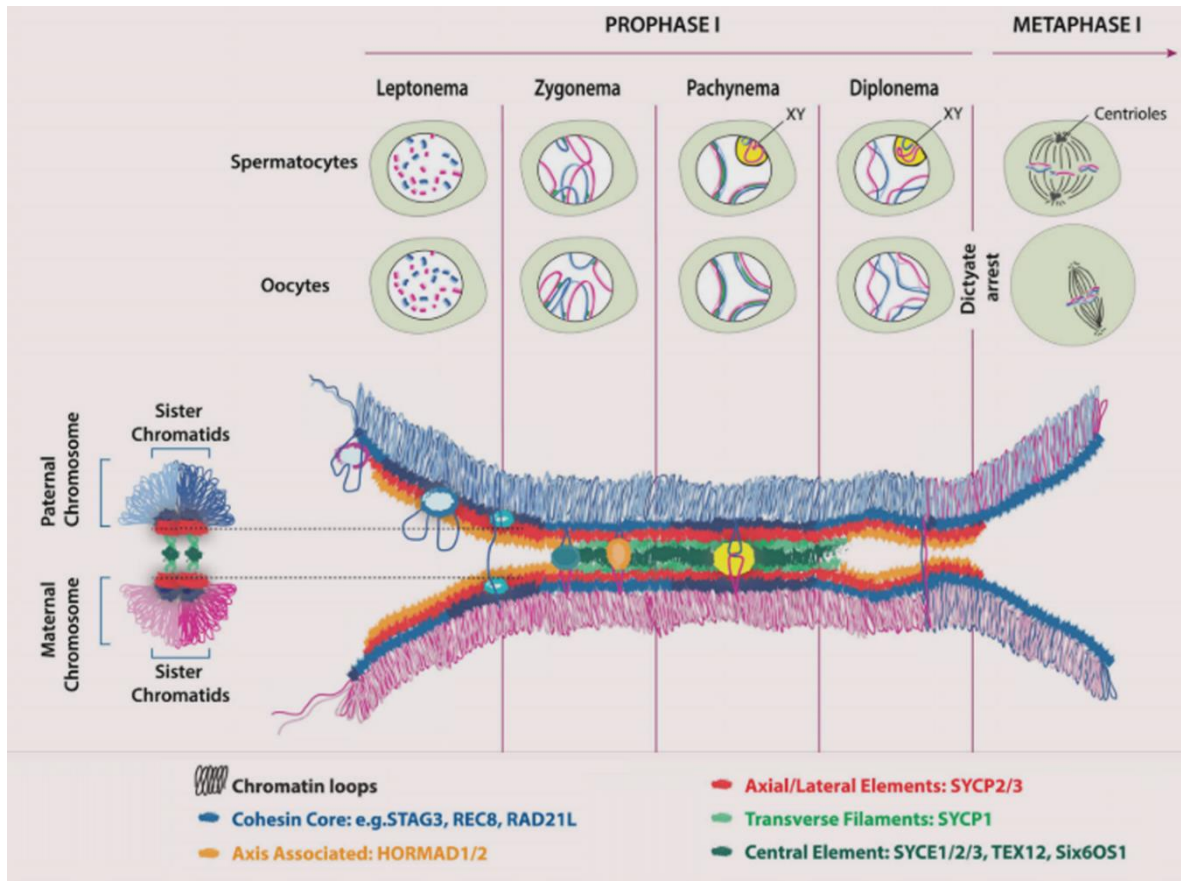


Figure 1-3. Meiotic chromosomal axis.

This schematic representation illustrates chromosome dynamics during meiotic prophase I (upper) and the organization of the chromosomal axis and synaptonemal complex (SC) (lower). Each meiotic homolog chromosome consists of two sister chromatids (darker and lighter blue or red) connected by cohesins. Cohesins load onto chromatin, forming cohesin core axis, where chromatin of sister chromatids are progressively organized as loops. During leptotema, axial elements (AEs) develop along this cohesion core axis. During zygotema, synapsis is initiated between subteleric regions; this synapsis gradually extends along with the entire AE as two layers of transverse filaments (TFs) and the central element (CE) of the SC are installed between the AEs. AEs are then designated as lateral elements (LEs) of SC. Throughout zygotema, HORMAD proteins disappear from axial regions where the deposition of the CE occurs. By pachynema, homologous chromosomes are fully synapsed, except for the heteromorphic X and Y chromosomes in the male. Sex chromosomes synapse only in a short pseudoautosomal region and form a transcriptionally silent chromatin compartment known as the sex body (yellow in upper panel). By the end of pachynema, all DSBs are repaired. Finally, during diplonema, the CE is disassembled and homologous chromosomes are held together by chiasmata. At this time, HORMAD proteins reload onto the desynapsed axes. From diplonema, spermatocytes progress to metaphase I, completing meiotic divisions without interruption, while in contrast, oocytes arrest at the dictyate stage until meiotic resumption around puberty. Image adapted from Bolcun-Filas et al. 2018.

Ishiguro, 2019). Subsequently, as cohesins are removed from chromosomes through mitosis, cohesion between sister chromatids is lost. The removal of cohesins occurs first during prophase, leading the bulk of cohesins disassociated from chromosome arms through the so-called prophase pathway mediated by Polo-like kinase 1 (Plk1/Plx1) and

Wapl (Gandhi, Gillespie, and Hirano 2006; Kueng et al. 2006). The small amounts of cohesin at centromeres are protected and will not be cleaved until anaphase I by separase (Sakuno and Watanabe 2009). In mitosis, apart from facilitating chromosome segregation through significant effects on chromosome alignment and bipolar attachment, the cohesin complex also contributes to transcriptional regulation by collaborating with insulator-binding factor, CTCF, and transcriptional coactivator, Mediator (Wendt et al. 2008; Kagey et al. 2010).

In mammalian germ cells, in addition to the four somatic core subunits (SMC1 α , SMC3, RAD21, and SA1/ SA2), the cohesin complex contains other five meiosis-specific subunits: REC8 (J. Lee et al. 2003) and RAD21L (J. Lee and Hirano 2011), SMC1 β (E. Revenkova et al. 2001) and SA3/STAG3 (Prieto et al. 2001). SMC1 β and SA3 replace most SMC1 α and SA1/SA2 in cohesin complexes during meiosis (E. Revenkova et al. 2001; Prieto et al. 2001). SMC1 α and/or SA2 are only found in a small portion of the cohesin complex in spermatocytes with unclear functions (Ekaterina Revenkova et al. 2004). These meiosis-specific and canonical somatic subunits combine into three types of cohesin complexes in germ cells: REC8-, RAD21L- and RAD21-type. Each class contains a different kleisin subunit (REC8, RAD21L, or RAD21) and three common subunits SA3, SMC1 β , and SMC3 (K. I. Ishiguro et al. 2011; J. Lee and Hirano 2011) (Figure 1-4). The REC8-type cohesin complex is loaded along chromosomes before or during DNA replication (preleptotene) and persists throughout prophase I. Later, REC8-containing cohesin complexes are removed from chromosome arms by separase at anaphase I. But they persist at centromeres until metaphase II (Kudo et al. 2009). Differently, the RAD21L-type cohesin complex mostly appears on chromosomes after DNA replication, reaches a peak around leptotene/zygotene, and dissociates from chromosomes after late pachytene. The removal of RAD21L-type cohesin is mediated by WAPL (Briño-Enríquez et al. 2016), a process that is conserved in multiple organisms (K. ichiro Ishiguro 2019) and has similar mechanisms to the prophase pathway in mitosis (Gandhi, Gillespie, and Hirano 2006; Kueng et al. 2006). In sharp contrast to REC8 and RAD21L, RAD21 does not appear on chromosomes until late pachytene, concomitantly with the dissociation of RAD21L. RAD21 dissociates from chromosomes at the diplotene stage in spermatocytes, remaining only at the centromeres until metaphase I (K. I. Ishiguro et al. 2011; J. Lee and Hirano 2011; Parra et al. 2004). Like mitotic cohesins, meiotic cohesins facilitate chromosome segregation through effects on chromosome alignment and bipolar

attachment. Moreover, the role of meiotic cohesion in regulating gene transcription has also been inferred recently. Meiotic cohesins are suggested to collaborate with CTCF to establish transcriptional hubs for early embryonic development in meiotic prophase I and fine-tuning subsequent spermatogenesis progression (Vara et al. 2019).

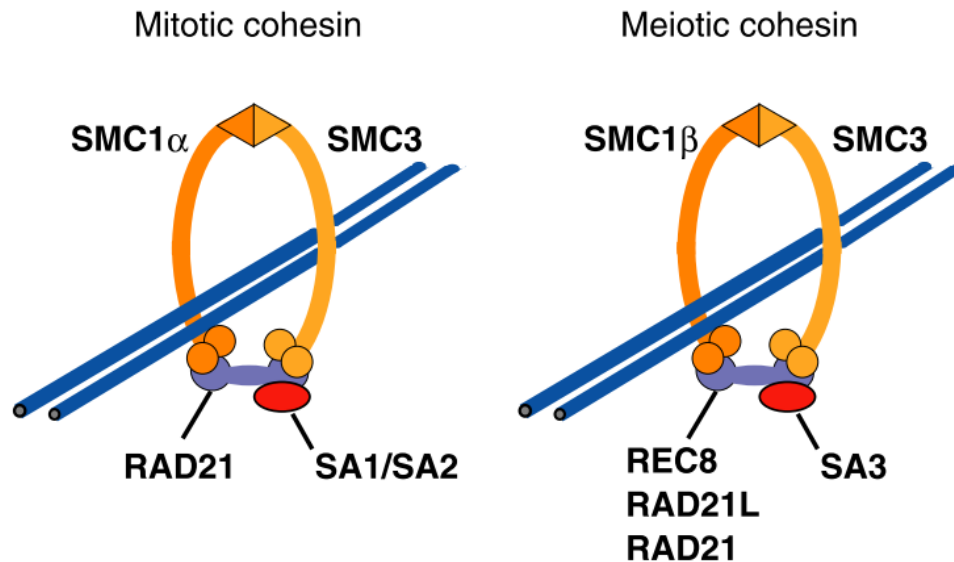


Figure 1-4. The cohesin complex in mitosis and meiosis

Mitotic cohesin contains four core subunits, SMC1 α , SMC3, the kleisin family protein RAD21, and SA1 or SA2. Differently, the meiotic cohesin complex has two meiosis-specific kleisin subunits, REC8 and RAD21L, and two meiosis-specific cohesin subunits, SMC1 β and SA3, which substitute SMC1 α and SA1/SA2 respectively.

Axial proteins – The HORMADs

HORMAD₁ and HORMAD₂ are mammalian members of the meiotic HORMAD family (Wojtasz et al. 2009), characterized by the conserved N-terminal HORMA (Hop1, Rev7, Mad2) domain that interacts with short sequence motifs termed ‘closure motifs’ (Rosenberg and Corbett 2015). They play crucial roles in DSB and CO formation and meiotic chromosomal behaviors in various organisms (West et al. 2019).

In mice, HORMADs load onto the chromosome axes during leptotene (Figure 1-3). As cells progress to pachytene, HORMADs disappear from synapsed regions and precisely localize on unsynapsed regions of homologous axes. In males, HORMADs accumulate on unsynapsed regions of XY chromosomes in pachytene and diplotene cells. Interestingly, HORMAD₁ reloads onto desynapsed autosomal axes in diplotene spermatocytes. In females, because the two X chromosomes fully synapse during pachytene, HORMADs are barely detected on chromosomes. However, during diplotene,

not only HORMAD₁, but also HORMAD₂ substantially appear on desynapsed axes in oocytes (Wojtasz et al. 2009; Fukuda et al. 2010; Kogo, Tsutsumi, Inagaki, et al. 2012).

The assembly of HORMADs on the meiotic chromosome axis is mediated through binding their N-terminal HORMA domains to closure motifs from both their C-termini and other meiotic chromosome axis proteins (Kim et al. 2014). The depletion of HORMADs from synapsed chromosome axes depends on the meiosis-specific AAA+ ATPase-TRIP13. This is revealed by the fact that HORMAD₁ and -2 substantially remain on nearly entirely synapsed chromosome axes in TRIP13 defective cells (Wojtasz et al. 2009; Roig et al. 2010; Kogo, Tsutsumi, Inagaki, et al. 2012). The unfolding of the N-termini of HORMADs might contribute to this removal of HORMADs by TRIP13 (Ye et al. 2017).

AE is a proteinaceous structure whose main components, SYCP₂ and SYCP₃, load along the sister chromatid axis, forming a continuous linear structure at leptotene (Figure 1-3). As homologous chromosomes physically pair and recombine, other proteins associate with AEs creating the tripartite SC, and AEs are integrated as SC's lateral elements (LEs). During meiotic prophase I, the cohesin complexes play specialized roles in forming AEs and the SC assembly in addition to its role in chromosome segregation as in mitosis (Cahoon and Hawley 2016). The HORMADs are also responsible for SC development, and required for DSB formation and homolog-directed DSB repair (Shin et al. 2010; Daniel et al. 2011; Kogo, Tsutsumi, Ohye, et al. 2012; Kogo, Tsutsumi, Inagaki, et al. 2012; Roig et al. 2010; Wojtasz et al. 2012). Additionally, HORMADs are part of the surveillance mechanisms that control homologous chromosome synapsis (Paigen and Petkov 2018a; Ichijima et al. 2011; Wojtasz et al. 2012; Kogo, Tsutsumi, Inagaki, et al. 2012). The details of these roles will be explained in the following sections.

1.2.2.2. Homologous chromosomes dynamics

During meiotic prophase I, paternal and maternal homologs progressively coalign with each other (pairing), concomitantly with the condensation of individual chromosomes. Subsequently, homologs form an intimate association (synapsis) as the SC installs between closely-aligned homologous axes along their lengths. After homologous recombination is completed in the SC context, SC disassembly is followed by the segregation of bivalent homologs ensured by their inter-homologous connections

(Denise Zickler and Kleckner 2015) (Figure 1-3).

In some organisms (e.g., *Neurospora*, *Coprinus*, and higher plants), all homolog pairs complete close alignments before SC formation. Differently, in budding yeast and mammals, synapsis initiates concomitantly with the pairing of homologs in zygotene. Namely, the central region (CR) proteins assemble along segmentally aligned homolog axes (Zickler 2006). Synapsis often initiates at the telomeres and several interstitial sites of DSB-mediated inter-homolog associations along chromosomes (Fung et al. 2004). Once initiated, synapsis quickly spreads into both directions in a zipper-like manner and is completed at pachytene as the SC is fully assembled between paired homologs (Fraune et al. 2012). In mice and several organisms with metacentric chromosomes, including humans, centromeres are the last regions to synapse (Roig et al. 2010; Qiao et al. 2012; Bisig et al. 2012).

The last recombination steps occur in the SC context, which further helps keep the homologs in association, generating COs at the end of pachytene. Subsequently, the SC disassembles throughout late prophase (diplotene and diakinesis) accompanied by changes in chromosome compaction and the configuration of additional proteins regulating the release of cohesin between sister chromatids at meiosis I (Gao and Colaiácovo 2018), resulting in the characteristic cruciform bivalents by late diakinesis. The separated homologs remain connected by chiasmata. Chiasmata persist until the chromosome arm cohesion is cleaved at the anaphase I. Chiasmata ensure correct segregation under tension at meiosis I by allowing homolog pairs to stably bi-orient at the metaphase I spindle (Handel and Schimenti 2010). Differently, the segregation of meiosis II is ensured by the centromeric cohesion of the sister chromatids (K. ichiro Ishiguro 2019).

Homolog pairing

The loop-axis chromosome organization, with the chromatin emanating from the same side of the axis, makes possible close alignment of homolog axes (Denise Zickler and Kleckner 2015). But how these DNA molecules can achieve base-pair resolution of pairing in the complex architecture is still limitedly understood. Several regulation layers have been suggested to promote homolog pairing, including meiotic recombination and dynamic chromosome movement (Bolcun-Filas and Handel 2018).

In most organisms, including mammals, recombination initiated by SPO11-

induced DSBs plays a central role in the meiotic program, according to which DSBs are essential for efficient homolog pairing and synapsis (Baudat, Imai, and De Massy 2013; Gerton and Hawley 2005; Denise Zickler and Kleckner 2015). In yeast and mice, DSB numbers are correlated with the extent of homolog pairing and SC formation (Kauppi et al. 2013; Henderson and Keeney 2004). DSB repair mediates homology search within the nucleus to recognize the homolog in early prophase I and initiates interhomolog interactions, promoting close juxtaposition of homolog axes. The close juxtaposition of homolog axes can be cytologically seen as bridges between the homolog axes (Denise Zickler and Kleckner 1999). Recombinational interactions occur at these bridging sites and further facilitate the overall chromosome pairing by associating the recombination machinery with the chromosome axis. (Denise Zickler and Kleckner 2015). Reduction in DSB numbers impairs homology search and homolog alignment, eventually leading to delayed and even nonhomologous synapsis (Kauppi et al. 2013). Thus, although DSBs are not essentially required for SC assembly, they are needed for proper SC formation between paired homologous chromosomes (Baudat et al. 2000; Romanienko and Camerini-Otero 2000).

Other DSB-independent mechanisms support homolog pairing by bringing chromosomes together and enhancing local homolog interactions (Bolcun-Filas and Handel 2018). During the pre-meiotic interphase, a global DSB-independent homolog pairing is established before DSB formation, and the pairing at telomere persists in the early meiotic prophase. This global pre-DSB pairing depends on meiotic cohesin REC8 (K. I. Ishiguro et al. 2014) and SPO11 protein but is independent of its role in DSB formation (Boateng et al. 2013). The global pre-DSB pairing reduces the complexity of homology scanning and the likelihood of entanglement, promoting DSB-mediated homolog pairing (Denise Zickler and Kleckner 2015).

Later during the leptotene/zygotene stage, telomeric regions cluster at a particular zone of the nuclear envelope, forming the “bouquet” (Scherthan 2001), and undergo rapid movements, facilitating alignment and pairing of homologous chromosomes. These quick telomere-led movements are mediated by SUN and KASH domain proteins, which transmit forces generated by the cytoskeleton across NE to telomeres (Burke 2018; C. Y. Lee et al. 2015). Meiotic cohesin proteins SA3 and RAD21L have also been suggested to be involved in ‘bouquet’ organization and its movement. SA3 transmits the driving force for the chromosome movement by connecting the

chromosome axis with the telomere-binding protein TERB1 (Shibuya et al., 2014). On the other hand, RAD21L plays a dominant role in bouquet exit. *Rad21*^{-/-} spermatocytes exhibit prolonged telomere clustering along their nuclear membrane and defects in homologous pairing (K. I. Ishiguro et al. 2014). The telomere-led fast movements likely facilitate homolog pairing by bringing homologous DNA sequences to close proximity as pre-DSB pairing and promoting the resolution of entanglements (Denise Zickler and Kleckner 2015).

1.2.2.3. The synaptonemal complex and its role

Synaptonemal complex components

In eukaryotes, the SC is a highly conserved meiosis-specific feature in function and structure. The SC serves as the scaffold for the close juxtaposition of homologous chromosomes and is intimately associated with chromosome pairing, synapsis, and recombination (Gao and Colaiácovo 2018; Cahoon and Hawley 2016; Fraune et al. 2012; Geisinger and Benavente 2017).

Fully formed SC is revealed as a tripartite structure by electron microscopy, consisting of two LEs that run along the electron-dense chromatin and flank a CR (Moses 1969), composed of a central element (CE) and numerous transverse filaments (TFs). LEs assemble onto meiotic chromosome axes (referred to as AEs before SC assembly). TFs span the central region and bridge the parallel homologous axes. CEs line along the center of the SC and are thought to help stabilize the structure. (Figure 1-3) In mammals, eight meiotic-specific SC proteins have been identified and characterized so far (Schücker, Sauer, and Benavente 2018): SYCP2 and SYCP3 as the LE proteins (Lammers et al. 1994; Offenbergl et al. 1998); SYCP1 as the TF protein (Meuwissen et al. 1992), and SYCE1, SYCE2, SYCE3, TEX12, and SIX6OS1 as the CE proteins (Costa et al. 2005; Hamer et al. 2006; Schramm et al. 2011; Gómez-H et al. 2016).

Although the general structure is highly conserved across yeasts and mammals, SC proteins share little similarity at the amino acid sequence level (Grishaeva and Bogdanov 2014; Fraune et al. 2016). The structural and functional conservation observed for the SC might be attributed to some conserved protein features and similarities in the SC organization, e.g., the coiled-coil domains (Gao and Colaiácovo 2018). The coiled-coil domains possess the capability of homotypic and heterotypic protein interactions

(Newman, Wolf, and Kim 2000). They are found in CR and LE components across many species (Cahoon and Hawley 2016; Baier, Alsheimer, and Benavente 2007). Moreover, some of these coiled-coil domain-containing proteins, such as mammalian SYCP₁ and SYCP₃, can self-organize to higher-order structures in the absence of other SC components, thereby probably providing a platform for SC assembly (Fraune et al. 2016; Gao and Colaiácovo 2018).

SYCP₂ binds to SYCP₃ through its C-terminal coiled-coil domain (Yang et al. 2006) and oligomerizes into filaments *in vitro* (West et al. 2019). SYCP₂ is speculated to associate with cohesin complex to mediate the anchoring of chromatin loops to the axis through the N-terminal domain (Feng et al. 2017; Xu et al. 2019). It possesses 'closure motifs' responsible for HORMADs recruitment (West et al. 2019).

SYCP₁ and SYCP₃ can self-assemble, forming higher-order structures in the absence of the other SC components, thereby considered the two bona fide structural proteins (Öllinger, Alsheimer, and Benavente 2005; Fraune et al. 2012; Yuan et al. 1998). SYCP₃ is the main component of the LEs, which can form thin fibrils *in vitro* (Yuan et al. 1998). Its coiled-coil domain and the short flanking sequences at the C-terminal region are essential for polymerization (Baier, Alsheimer, and Benavente 2007). Interestingly, SYCP₃ codes for two isoforms rather than one in mice and rats, as in most other species. The shorter isoform is conserved among metazoans. The longer isoform, containing an extra N-terminal domain, appeared after the mouse and rat separated from the hamster lineage 15 million years ago with unclear properties (Alsheimer et al. 2010).

SYCP₁ contains a large coiled-coil domain and constitutes the major part of TFs in dimers or tetramers (Meuwissen et al. 1992). Its C-termini is positioned in the LEs (Schücker et al. 2015) and interacts with SYCP₂ (Winkel et al. 2009). In contrast, the N-termini is located in the CEs (J. G. Liu et al. 1996), thereby mediating homologs synapsis. SYCP₁ is proposed to act as a structural framework for the CR assembly of the SC (Öllinger, Alsheimer, and Benavente 2005). It spans the distance between the homologs, probably with the help of other CR proteins (J. G. Liu et al. 1996). The width of the SC is approximately 90–150 nm in all species, and SYCP₁ appears to be its primary determinant (Öllinger, Alsheimer, and Benavente 2005).

Among the five CE proteins, SYCE₁ and SYCE₃ are essential for synapsis initiation, likely through contacting the TFs of homologs (Schramm et al. 2011; Costa et al. 2005; Bolcun-Filas et al. 2009). SYCE₂ and TEX₁₂ are required to propagate synapsis

by spreading along the entire length of the axes from the initiation sites (Bolcun-Filas et al. 2007; Hamer et al. 2008; O. R. Davies, Maman, and Pellegrini 2012). These CE proteins contain a predicted coiled-coil domain, and they interact interdependently to promote the assembly and stabilization of the SC (Geisinger and Benavente 2017; Cahoon and Hawley 2016). All these CR proteins are required for fertility in female and male mice, unlike LE proteins. Knockout SYCP2 or SYCP3 leads to sterile males but subfertility in females, whereas mutant mice lack any CR proteins (SYCP1, SYCE1, SYCE2, SYCE3, and SIX6OS1) are infertile (Yang et al. 2006; Bolcun-Filas et al. 2007; Gómez-H et al. 2016).

Synaptonemal complex assembly and disassembly

The SC undergoes a dynamic cycle through its assembly, a highly dynamic steady-state, and disassembly (Gao and Colaiácovo 2018). The SC is assembled by integrating its CR proteins to connect two LEs, a poorly understood process that might occur in different ways in different organisms because of the divergent component protein sequences in various organisms (Cahoon and Hawley 2016). At pachytene, the SC is fully assembled between all the paired homologs. Interestingly, studies in yeast and worms indicated that the SC is not static but highly dynamic during early pachytene (Voelkel-Meiman et al. 2012; Pattabiraman et al. 2017). The SC shifts to a more stable state in late pachytene as recombination progresses. After CO formation, the SC starts to disassemble asymmetrically throughout the late prophase. Certain SC proteins are retained at specific chromosome subdomains until late prophase I, facilitating proper homolog segregation at meiosis (Obeso, Pezza, and Dawson 2014).

A picture of how SC proteins are assembled in order has been inferred from studies in knockout mice, although SC assembly mechanisms' details are not well elucidated (Geisinger and Benavente 2017; Fraune et al. 2012). During meiotic prophase I, each pair of sister chromatids are held together by the inter cohesin complex and organized into a chromosome axis (D Zickler and Kleckner 1999). The cohesin proteins appear during the pre-meiotic S phase or early leptotema and act as a framework for the AE assembly (Peltari et al. 2001; K. ichiro Ishiguro 2019). The AE/LE proteins: SYCP2 and SYCP3 first appear to load along with the cohesion complex during leptotene together with chromosomal proteins HORMADs (Wojtasz et al. 2009)a and create the chromosome axis by establishing the loop-axis meiotic chromatin structure (Yang et al. 2006; Yuan et al. 2000; D Zickler and Kleckner 1999). Then, the CR proteins: SYCP1,

SYCE₃, SYCE₁, which are essential for synapsis initiation, are assembled between the AEs in sequence: the TF protein SYCP₁ first associates with the AEs, likely through interacting with SYCP₂ (Schücker et al. 2015; Winkel et al. 2009); and then SYCE₃ is required downstream through direct interaction with SYCP₁ (Schramm et al. 2011; Hernández-Hernández et al. 2016). Subsequently, SYCE₁ is loaded likely through interacting with SYCE₃ (J. Lu et al. 2014). Additionally, SYCE₁ interacts and stabilizes SYCP₁ (Costa et al. 2005). Recently, a novel CE protein SIX6OS₁ has been shown to bind SYCE₁ through its N-terminal half and suggested to be required downstream of SYCP₁, at a similar hierarchy level to SYCE₃ (Gómez -H et al., 2016b). Finally, synapsis spread along the entire length of homolog axes with the required loading of SYCE₂ and TEX₁₂ (Hamer et al. 2006), which are thought to be recruited as hetero-octameric complexes (O. R. Davies, Maman, and Pellegrini 2012) and interact with the SC through SYCE₂ binding to SYCP₁, SYCE₃ and SYCE₁ (Costa et al. 2005; Bolcun-Filas et al. 2007; Schramm et al. 2011).

The SC is completely assembled at the interface of nearly all lengthwise-aligned homologous chromosome pairs in pachytene cells. And this SC structure is thought to be dynamic in yeast and *C.elegans* (Voelkel-Meiman et al. 2012; Pattabiraman et al. 2017). After CO formation, SCs start to disassemble as SYCP₁ is lost from chromosome arms in diplotene. But SC fragments remain at CO sites, presumably to coordinate local chromosome organization and separate the homologous axes, and centromeres, until diakinesis (Qiao et al. 2012; Bisig et al. 2012). After removing SYCP₁ from the centromeres, SYCP₃ accumulates and persists in these regions until late diplotene, before the nuclear-envelope breakdown. It has been speculated that SYCP₃ may promote proper centromere bi-orientation leading to appropriate homolog segregation (Bisig et al. 2012; Qiao et al. 2012).

Synaptonemal complex regulation

Multiple layers of regulation are imposed on the SC formation and disassembly dynamics to coordinate these mechanisms with the homologous recombination in various organisms (Gao and Colaiácovo 2018; Denise Zickler and Kleckner 2015). These include the regulation from structural axial protein (cohesin and HORMAD), the transcriptional regulation of the SC genes, translational control of SC mRNAs, the association of nonstructural regulators with SC components, protein modifications, etc. (Gao and Colaiácovo 2018; Denise Zickler and Kleckner 2015).

As mentioned above, the axial proteins (cohesin complexes and HORMAD proteins) are required for SC and LE/AE formation. Cohesin loads before AE formation and forms a core axis to organize AE's loading. They are essential for AE formation as the deletion of the common subunit of the meiotic cohesin complex, SA₃, leads to the failure of AE assembly with only short stretches of axes (Fukuda et al. 2014). Although AE formation depends on meiotic cohesin, the cohesin subunits contribute differently to AE formation. The deletion of REC8 or RAD21L causes partial impairment of AE formation, a shorter AE in REC8 KOs (Bannister et al. 2004), but a discontinuous and fragmented AE in RAD21L KOs (K. I. Ishiguro et al. 2014). Significantly, in the absence of both REC8 and RAD21L, AE formation is completely disrupted, suggesting REC8-type and RAD21L-type cohesin complexes are required for normal chromosome axis formation (K. I. Ishiguro et al. 2014). In addition to the essential roles of cohesins in forming AE, cohesins are also inferred to regulate the loop-axis organization by interacting with AE components. In SYCP3-deficient meocytes, chromosomes display shortened chromatin loops. Also, their axes marked by cohesins are twice as long as the wild-type chromosome axes, suggesting AE components contribute to the cohesin core axis compaction (Yuan et al. 2000). The loss of SMC1 β gives rise to a heterogeneous size of loops at shortened cohesin axes, indicating the cohesin bound to the chromosome axis acts as chromatin loop attachment sites (Novak et al. 2008). Furthermore, both the chromatin loop size and the cohesin core axis length are restored to wild-type levels in meocytes lacking both SMC1 β and SYCP3 (Novak et al. 2008), indicating the AE components contribute to the longitudinal axial compaction of the cohesin core axis.

HORMAD₁ is essential for homolog pairing and synapsis (Shin et al. 2010; Paigen and Petkov 2018a; Kogo, Tsutsumi, Ohye, et al. 2012). HORMAD₁ promotes efficient DSB formation. The depletion of HORMAD₁ leads to an extensive defect in homologous pairing and synapsis in mice due to failed homology search (Shin et al. 2010; Paigen and Petkov 2018a; Kogo, Tsutsumi, Ohye, et al. 2012). Moreover, HORMAD₁ can also promote SC formation independently from its role in homolog-directed DSB repair (Paigen and Petkov 2018a). In DSB-deficient *Spo11*^{-/-} mice where SC forms between non-homologous partners, the removal of HORMAD₁ exacerbates the SC defect, indicating HORMAD₁ has a direct role in SC formation (Paigen and Petkov 2018a). Additionally, both HORMAD₁ and HORMAD₂ are required to surveillance homolog synapsis. (Paigen and Petkov 2018a; Kogo, Tsutsumi, Inagaki, et al. 2012; Wojtasz et al. 2009). Their absence

rescues the loss of asynaptic oocytes in the SPO11-deficient background (details in section 1.2.4.2).

Synapsis initiates at CO-designated inter-homologous engagement sites in yeast, controlled by a protein complex named synapsis initiation complex, composed of at least eight members from a group of proteins, 'ZMM' (an acronym for Zip1-4, MSH4-5, Mer3, Spo16) (Gao and Colaiácovo 2018). Studies have revealed that several SC component proteins, including the AE protein Red1, can be SUMOylated, and this SUMOylation is required for SC assembly in yeast (Humphryes et al. 2013; Leung et al. 2015). In mice, SC initiation depends on the total number of interhomolog engagements. Reduced DSBs lead to fewer interhomolog engagements, causing delayed synapsis (Kauppi et al. 2013). Although more DSBs can be generated through a DSB feedback loop in unsynapsed axes, homologs may fail to pair, and eventually, SC assembly occurs between nonhomologous chromosomes (Kauppi et al. 2013). Whether SUMOylation is involved in SC assembly in mice is unclear, although similar to yeast Red1, mouse SYCP3 can also be SUMOylated (Xiao et al. 2016).

A positive feedback system in yeast controls SC polymerization. The initial assembly of the transverse filament recruits central-element proteins, which in turn recruit more transverse filaments. The mechanism controlling SC polymerization in mice remains unknown (Cahoon and Hawley 2016).

The control of the timing between the formation of a CO and SC disassembly is vital for proper chromosome segregation. In mice, this relies on cell-cycle kinases (PLK1, Aurora B, CDK1-Cyclin B1), which in turn are regulated through transcriptional and translational mechanisms (Gao and Colaiácovo 2018). PLK1 is directly involved in the disassembly of the central element SYCP1 and TEX12, likely through phosphorylation (Jordan, Karppinen, and Handel 2012). Aurora B mediates the disassembly of lateral elements SYCP2 and SYCP3 from chromosome arms (Parra et al. 2003). CDK1-Cyclin B1 is also required for SC disassembly. CDK1 has to interact with HSPA2 for its activation in late prophase and provably to be recruited to the SC. Then, CDK1 mediates the SC disassembly by phosphorylating SYCP1 (Allen et al. 1996; Cahoon and Hawley 2016).

Synaptonemal complex roles

The SC plays a universal role in all species, which is to provide order within the nucleus during late prophase, as well as it may have diverse roles in many organisms

(Denise Zickler and Kleckner 2015). The SC is required for stabilizing chromosome structure during late prophase I and segregation at meiosis I (Denise Zickler and Kleckner 2015). After NCO-fated DSBs are repaired, the SC is responsible for holding homologs and thus ensuring the interhomolog interactions before COs are formed (Denise Zickler and Kleckner 1999; Qiao et al. 2012). The retention of SC proteins at centromeres until metaphase I is proposed to promote biorientation of the homologs, ensuring proper segregation (Qiao et al. 2012).

The SC is required to repair SPO11-induced DSBs and CO formation (Denise Zickler and Kleckner 2015). In mice, recombination can not be completed without the CR proteins (Fraune et al. 2012; Bolcun-Filas et al. 2007; Gómez-H et al. 2016; Schramm et al. 2011). The AE proteins are closely associated with the development of recombination protein complexes. At the same time, the CR plays a more significant structural role for the assembly, maintenance, and turnover of the complexes and thus enables the maturation of the DSBs into COs subject to interference (Handel and Schimenti 2010; Fraune et al. 2012). SC formation also shuts off the SPO11 activity (Kauppi et al. 2013). Moreover, analysis of mutant mice indicates that the HORMAD_{1/2} regulates recombination-dependent DSB formation (Wojtasz et al. 2009; Paigen and Petkov 2018a). Furthermore, the SC might be centrally important in the surveillance of meiotic recombination and HORMAD-regulated monitoring of synapsis.

1.2.3. Recombination

Meiotic recombination consists of the formation and repair of DSBs and is essential for fertility and allelic shuffling. In many organisms, recombination promotes the close juxtaposition of each pair of homologous chromosomes and thus facilitates chromosome synapsis. Interhomolog interactions generate CO products in the context of synapsed chromosomes, resulting in the exchange of alleles between homologs. In addition to creating genetic diversity, COs facilitate the proper orientation of homologous pairs at metaphase and thus ensure they segregate accurately at the first meiotic division, eventually supporting functional gametes formation (Hunter 2015; Lam and Keeney 2015; Marsolier-Kergoat et al. 2018) (Figure 1-5).

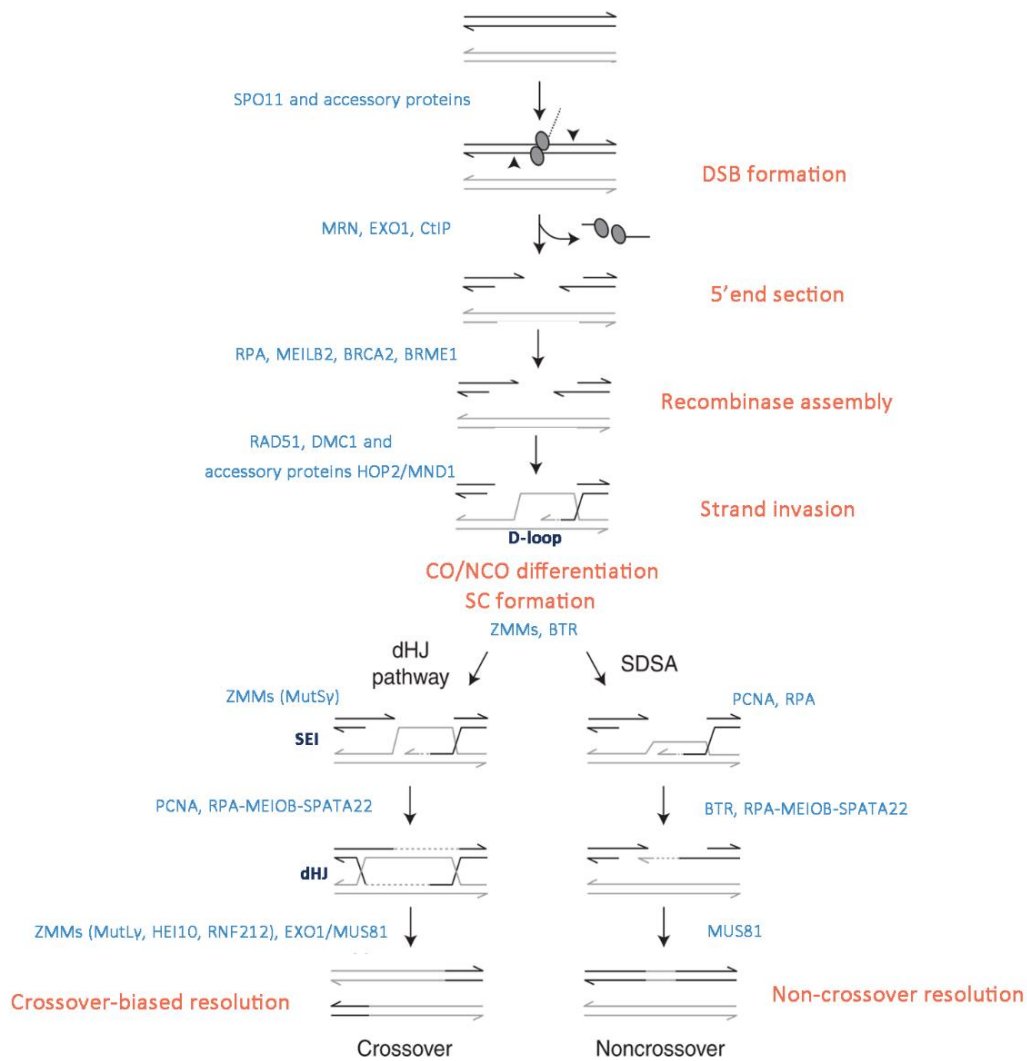


Figure 1-5. The meiotic recombination pathway.

The schematic diagram shows the major events and key transitions (fonts in orange), selected factors involved in each event (fonts in blue), and major DNA intermediates (fonts in dark blue) during meiotic recombination. A segment of one sister chromatid from each homolog (black, gray) is shown. SPO₁₁ (ovals) catalyzes DSB formation, in association with its accessory proteins. Endonucleolytic cleavage on either side of the DSB (black arrowheads) by MRN complex (MRE₁₁-RAD50-NBS1) and CtIP releases SPO₁₁ covalently attached to a short oligonucleotide (SPO₁₁ oligo) and generates a nick. Then, the DNA ends undergo 5'→3' resection by exonuclease activity from MRE₁₁, EXO₁, and DNA₂. Recombinases DMC₁ and RAD₅₁ subsequently assemble at resected 3' ssDNA tails, promoted by recombination proteins such as RPA, MEILB₂, BRCA₂, and BRME₁. RAD₅₁ and DMC₁ coated ssDNA are stabilized by HOP₂-MND₁ and engage in homology search and strand exchange, resulting in D-loop formation. The repair can proceed by either a double Holliday junction (dHJ) pathway or synthesis-dependent strand annealing (SDSA). This is controlled by ZMM proteins and other factors through processing and stabilizing the recombination intermediates. In the dHJ pathway, D-loops are further stabilized by MutS γ (MSH₄ and MSH₅) and the second end of the DSB is captured to form a dHJ, requiring PCNA and RPA-MEIOB-SPATA₂₂ complex. ZMM proteins such as HEI₁₀ and RNF₂₁₂ facilitate the recruitment of mismatch repair factors MutL β (MLH₁, MLH₃). MutL β and together with EXO₁ mediate the resolution of dHJ, primarily giving rise to crossover (CO) products. In SDSA, the invading strand is displaced after DNA synthesis and reanneals to the other end of the DSB, followed by further DNA synthesis

(PCNA) and nick ligation, ultimately giving rise to noncrossover (non-CO) products. Image adapted from Lam and Keeney 2015.

1.2.3.1. Recombination initiation

Recombination begins with programmed DSBs catalyzed by the conserved SPO11 protein and accessory DSB proteins in meiosis. Most DSBs are repaired by MR, a particular kind of homologous recombination (HR) where the homologous chromosomes are used as the template, generating NCO and CO products. (Lam and Keeney 2015; Scott Keeney 2008).

DSBs formation

SPO11 is the orthologue of the catalytic subunit (TopoVIA) of the archaeal Topo VI subfamily, a type II DNA topoisomerase family (Scott Keeney, Giroux, and Kleckner 1997; Bergerat et al. 1997). It catalyzes meiotic DSBs formation by a transesterification reaction. As a result, SPO11 covalently binds to the 5' end of the DSB through an essential and conserved tyrosine residue likely acting as the catalytic center of topoisomerase function (J. Liu, Wu, and Lichten 1995) (Figure 1-5).

In addition to SPO11, accessory DSB proteins are required for SPO11 mediated DSB formation in many organisms (Lam and Keeney 2015). Notably, a TopoVIB-like subunit (TOPOVIBL), structurally similar to the TopoVIB subunit of Topo VI topoisomerase, has been demonstrated to be essential for meiotic DSB formation. TOPOVIBL directly interacts and forms a complex with SPO11 in plants and mice. Most likely, this requirement is conserved among most eukaryotic species (Vrielynck et al. 2016; Thomas Robert et al. 2016; T. Robert et al. 2016). This is inferred by identifying meiotic recombination proteins Rec102 and Rec6, in budding and fission yeast, and MEI-P22, in flies, as homologs to the transducer domain TopoVIB.

In budding yeast, eight other accessory proteins are required for DSB formation. These form different subcomplexes: Ski8 directly interacts with Spo11 (Arora et al. 2004), Rec102-Rec104 form another complex, Rec114 interacts with Mei4 and Mer2. Finally, the MRX complex, formed by Mre11-Rad50-Xrs2, is also required for DSB formation (Lam and Keeney 2015). Rec114-Mei4-Mer2, which is regulated through phosphorylation, is likely to be bridged with Spo11-Ski8 by Rec102-Rec104. On the other hand, the MRX complex plays a role in DNA resection and repair (Lam and Keeney 2015).

In mice, three evolutionarily conserved proteins are also identified to be required for SPO11-mediated DSB formation, including IHO1, MEI4, and REC114, the mouse orthologs of yeast Mer2, Mei4, and Rec114. These three proteins co-localize on the axes of the meiotic chromosome independently of SPO11 activity. (Kumar et al. 2018; Stanzione et al. 2016; Kumar, Bourbon, and De Massy 2010). IHO1 probably acts as a platform to recruit REC114 and MEI4 to the axes (Kumar et al. 2018).

IHO1 is a direct interactor of the axial component protein HORMAD1 in mice (Stanzione et al. 2016). It is required for the axis-localization of REC114 and MEI4 *in vivo* and interacts directly with REC114 *in vitro* (Kumar et al. 2018; Stanzione et al. 2016). However, IHO1 axial localization is independent of MEI4 or REC114, suggesting that IHO1 recruits REC114 and MEI to the axis. IHO1 might recruit REC114 and MEI4 as a complex as these two mutually interacting proteins are reciprocally required for their localization *in vivo* and form a stable complex *in vitro* (Kumar et al. 2018).

In mice, REC114 may control the SPO11/TOPOVIBL catalytic activity via ataxia telangiectasia mutated (ATM)-dependent inhibition of DSBs (Subramanian and Hochwagen 2014; Boekhout et al. 2019). The loss of ATM/ATR and Rad3-related (ATR) leads to an increased level of DSBs in many organisms, suggesting the activation of ATM/ATR kinases downregulate DSBs formation (Joyce et al. 2011; Kurzbauer et al. 2012; Lange et al. 2011). REC114 is inferred to be the target of ATM in this context in mice as studies in *S. cerevisiae* show that Tel1/Mec1 (ATM/ATR)-dependent phosphorylation of REC114 is related to the downregulation of DSBs (Carballo et al. 2013). Alternatively, REC114 could be involved in this inhibition through its novel interactor-ANKRD31, which is proposed to be a direct ATM target as it has an ATM phosphorylation motif (clustered SQ/TQ sites) (Boekhout et al. 2019).

DSB distribution

DSBs are nonrandomly distributed along the chromosomes. DSBs tend to accumulate preferentially at regions called recombination hot spots (Székvölgyi, Ohta, and Nicolas 2015). This exceptional spatial distribution is under multiple layers of control in various organisms. In most mammals, PRDM9 determines the locations of recombination hot spots (Paigen and Petkov 2018b). PRDM9 binds to specific DNA sequences in the genome complementary to its Zinc finger array. Once bound to a specific DNA sequence, PRDM9 methylates histone H3 lysines 4 and 36 (H3K4me3 and

H3K36me₃) of nearby nucleosomes using its PR/SET domain. As a result, PRDM9 targets SPO11 to specific genome regions (Grey, Baudat, and de Massy 2018).

PRDM9 activating hot spots occurs in the DNA loops while SPO11 catalyzing DNA cleavage with accessory proteins occurs along the chromosomal axis (Scott Keeney 2008; Kumar et al. 2015; Stanzione et al. 2016; T. Robert et al. 2016). Thus, it is necessary to associate the activated hot spots with the chromosomal axis where DSBs are formed. Indeed, several proteins (EWSR1, CDYL, EHMT2, and CXXC1) have been implicated in mediating the linking by binding the KRAB domain of PRDM9 and interacting with the proteins located at axes (Parvanov et al. 2017; Imai et al. 2017). Nevertheless, some DSBs sites are targeted independently of PRDM9 in meiosis, e.g., the pseudoautosomal region (PAR) in male meiosis (Brick et al. 2012).

DSB regulation

DSB formation is tightly controlled to occur in a narrow time window within prophase I. ATM plays an essential role in regulating further DSB formation via negative feedback loop both in *trans* and *cis* (L. Zhang et al. 2011; Lange et al. 2011; Garcia et al. 2015; Pacheco et al. 2015; Barchi et al. 2008). The depletion of ATM leads to significantly increased DSBs in multiple organisms (Joyce et al. 2011; Kurzbauer et al. 2012). In mice, ATM-deficient spermatocytes cannot cope with the amount of DSBs, resulting in the activation of surveillance mechanisms that arrest the cells at the pachytene stage (Lange et al. 2011; Pacheco et al. 2015). In this context, a particular function of ATM is preventing repeated DSB formation at the same chromosomal locus. This is inferred by detecting a strong increase of SPO11 oligos but a mild increase in RAD51 foci in *Atm*^{-/-} mice (Barchi et al. 2008; Lange et al. 2011). The finding that Tel1 prevents clusters of DSBs and suppresses DSBs within the surrounding chromosomal region in yeast further supports this function of ATM (Garcia et al. 2015). ATM might also be involved in other feedback circuits to ensure enough DSBs are formed to support homolog interactions and recombination (Cooper et al. 2014).

1.2.3.2. DSB resection

After DSB formation, DSB ends are processed through a series of nuclease activities, called DSB resection, to generate ssDNA tails. ssDNA subsequently will be

coated with strand-exchange proteins (DMC1 and RAD51), catalyzing the invasion into the homologous repair template (Lam and Keeney 2015; Baudat, Imai, and De Massy 2013) (Figure 1-5).

DSB resection process involves several steps. In budding yeast, MRX complex recognizes Spo11 and generates nicks nearby with Sae2 via endonuclease activity, leading to the release of Spo11 bound to short oligonucleotides (Spo11 oligos) (Cannavo and Cejka 2014; Neale, Pan, and Keeney 2005). The nicks serve as entry points for short- and long-range nuclease activity. Short-range 3'→5' Mre11 exonuclease activity degrades dsDNA back to the DSB end. Long-range 5'→3' Exo1 exonuclease activity to exclusively resect the same strand away from the DSB end in cooperation with Dnaz nuclease (Zakharyevich et al. 2010; Garcia et al. 2011; Manfrini et al. 2010). The consequence is the generation of 3' ssDNA tails on both sides of the DSB. The full-length resection requires the DSB-responsive kinase Tel1, which promotes resection initiation, likely through Sae2 phosphorylation (Cartagena-Lirola et al. 2008), and regulates resection length (Mimitou, Yamada, and Keeney 2017).

Although the homolog of Mre11 (MRE11) is predicted to catalyze the endonucleolytic cleavage in *mus musculus* (Neale, Pan, and Keeney 2005), the role of the mammalian MRX complex and Sae2 homologs, the MRN complex (MRE11- RAD50-NBS1) and CtIP, respectively, in meiotic DSB repair is poorly understood. The embryonic lethality of knocked-out mice of any MRN component hinders the study of MRN function in meiotic DSB repair, and several viable mutant mice of MRN do not show a severe defect in meiotic DSB repair (B. Zhang et al. 2020; Pacheco et al. 2015).

NBS1 is a critical component of the MRN complex given that it is not only required for the nuclear localization of the MRN complex (Desai-Mehta, Cerosaletti, and Concannon 2001; Carney et al. 1998) but it is also responsible for sensing CtIP phosphorylation and activating MRE11's endonuclease activity (Anand et al. 2019). Mice harboring hypomorphic *Nbs1* mutations are subfertile. Their spermatocytes display slight asynaptic aberrations and decreased CO markers (Cherry et al. 2007). Moreover, a recent study demonstrates that conditional disruption of NBS1 in male mice causes a dramatic reduction of DNA end resection and severe defect in chromosome synapsis, eventually leading to meiotic arrest and infertility (B. Zhang et al. 2020). Thus, the MRN complex, like MRX in yeast, seems essential for SPO11-catalyzed DSB repair in mammals and required for DSB resection. Notably, the nucleotide-excision repair factor, DNA

polymerase- β , is also implicated in SPO11 removal during DSB processing in addition to its requirement for normal synapsis and DSB repair (Kidane et al. 2010). Finally, *Exo1*^{-/-} mice are not defective in homologous interactions, suggesting EXO1 is dispensable for DSB resection in mammals (Wei et al. 2003).

Homology search and interhomolog bias

Resected 3' ssDNA tails resulting from nuclease activities are immediately bound by replication protein A (RPA) as well as RPA1-related MEIOB protein, and its associated factor, SPATA22, at the DSB sites. These are further replaced by the recombinases DMC1 and RAD51. Then, one of the RAD51/DMC1-coated ssDNA commences engaging in homology search and interhomolog interactions. Consequently, unstable nascent D-loop intermediates are likely generated *in vivo*. These are either destabilized in the NCO pathway or stabilized to form SEI intermediate targeting the CO pathway (Hunter 2015; Brown and Bishop 2015) (Figure 1-5).

DMC1 and RAD51 are structural and functional homologs of the bacterial strand-exchange protein RecA. RAD51 functions in somatic and meiotic cell cycles, whereas DMC1 is meiosis-specific (Brown and Bishop 2015). Both are detected as discrete foci on chromosome axes in leptotene soon after DSB formation, marking sites of ongoing recombination (Moens et al. 2002; Barlow et al. 1997; Brown and Bishop 2015). In yeast, DMC1 is the essential DNA strand-exchange factor, while RAD51 is dispensable but performs a critical regulatory role (Cloud et al. 2012). This might also be the case in mammals since a recent study has shown that DMC1 binds preferentially at the 3' end of the ssDNA filament, responsible for strand exchange, while RAD51 binds away from the 3' end (Hinch et al. 2020).

The assembly of both proteins is ATP-dependent and promoted by several recombination factors in mammals such as ATR, breast cancer 2 protein (BRCA2), TRIP13, the Shu complex SWS1-SWSAP1, and PALB2, etc. (Zelensky, Kanaar, and Wyman 2014; Abreu et al. 2018; Roig et al. 2010; Pacheco et al. 2018; Felipe-Medina et al. 2020; J. Zhang et al. 2020; 2019; Widger et al. 2018). ATR promotes the loading of both proteins, likely through its effector CHK1, in response to RPA-coated ssDNA (Pacheco et al. 2019; Widger et al. 2018). TRIP13 might be specifically required for the assembly of RAD51 (Koubova et al. 2014b). BRCA2 replaces RPA with RAD51 by direct binding to RAD51 and ssDNA (Zhao et al. 2015; Jensen, Carreira, and Kowalczykowski 2010). Several recent studies identified

BRCA2 localizer (MEILB2) and MEILB2's stabilizer (BRME1). These two meiosis-specific proteins have been proposed to form a complex with BRCA2 and function as the recruiter of RAD51 and DMC1 onto ssDNA (Felipe-Medina et al. 2020; J. Zhang et al. 2019; 2020).

The activity of the DMC1-RAD51 complex to promote homology search and strand exchange is driven by the stability of the formed nucleoprotein filament (Brown and Bishop 2015). The HOP2-MND1 complex enhances the DMC1-RAD51 nucleoprotein (Petukhova, Romanienko, and Camerini-Otero 2003). The *Hop2*^{-/-} mice analysis has shown HOP2 stabilizes the RAD51/DMC1 complex on ssDNA, reduces the affinity of RAD51 to dsDNA, and modulates the conformation of the nucleoprotein filament *in vitro* (Chi et al. 2007; Petukhova et al. 2005; Pezza et al. 2007).

In stark contrast to the exclusive inter-sister (IS) recombination interactions occurring in the somatic cell cycle, MR interactions are biased between homologous chromosomes. Thus, promoting pairing, synapsis, and formation of chiasmata between homologous chromosomes. The precise mechanism of this meiotic inter-homolog (IH) bias is unclear but is likely achieved both by inhibiting IS bias and promoting IH bias. The so-far best-understood mechanism was uncovered in yeast. Involves Tel1/Mec1, Hop1 (homolog of HORMAD1/2), effector kinase Mek1 (homolog of CHK2), and RAD54, an SWI/SNF-family ATPase (Subramanian and Hochwagen 2014). Tel1/Mec1 phosphorylates the axial protein Hop1, leading to the recruitment and activation of the effector kinase Mek1. The binding of Mek1, in turn, stabilizes the phosphorylation mark on Hop1 and the activated Mek1 inhibits RAD54, which stimulates RAD51-recombinase activity for inter-sister repair. As a result, IH bias is promoted (Niu et al. 2005; 2007; 2009; Carballo et al. 2008; Chuang, Cheng, and Wang 2012; H. Y. Wu, Ho, and Burgess 2010).

1.2.3.3. DSB repair pathway

In the contemporary meiotic recombination models, single strand invasions result in less stable nascent joint molecules, presumably D-loops. The differentiation of D-loops leads to either NCOs via SDSA or COs subject to interfering (class I) via forming CO-specific intermediates single-end invasions (SEIs) and dHJs (Figure 1-5). D-loops are stabilized along the CO pathway to form SEIs, which are the earliest detectable CO-specific joint molecules. Subsequently, SEIs become more stable dHJs joint molecules through a process including a second-end capture and DNA synthesis. Eventually, dHJs

are resolved exclusively into class I COs. By contrast, unstable D-loops are not stabilized in the NCO pathway after the invading strand extends. The nascent DNA is annealed to the other end of the broken DNA molecule by DNA synthesis, resulting in NCOs. Additionally, a minority of D-loops escape from these two pathways and generate NCOs and class II COs (Ranjha, Howard, and Cejka 2018; Hunter 2015; Baudat, Imai, and De Massy 2013).

Crossover/Noncrossover Differentiation

The differentiation of the CO and NCO pathways is controlled by a panel of factors through processing and stabilizing the recombination intermediates. That D-loops are fated to give rise to COs or NCOs is determined by the opposite activities of ZMM proteins and a helicase complex, STR/BTR (yeast Sgs1–Top3–Rmi1, metazoan BLM–TOPIII α –RMI1–RMI2) (Hunter 2015).

ZMMs stabilize recombinational joint molecules and promote the formation of SC, ultimately required for the formation of class I COs. In budding yeast, ZMMs are CO-specific, given that most ZMM-stabilized D-loops are processed as COs. However, ZMM-staining foci vastly outnumber the final COs in mouse, and several other species, suggesting that ZMMs' stabilization of recombinational interactions may be a prerequisite for CO designation in these organisms. Indeed, D-loops bound by ZMMs could also form NCOs products (S. S. De Vries et al. 1999; Edelman et al. 1999; Kneitz et al. 2000; Higgins et al. 2008; Yokoo et al. 2012; De Muyt et al. 2014; L. Zhang, Liang, et al. 2014).

ZMM is a group of functionally diverse proteins, and several mammalian ZMM proteins have been studied to have a role in the CONCO decision: MSH4, MSH5, TEX11, RNF212, HEI10, HFM1, and SPO16. All of these proteins partially colocalize with recombination foci (defined by RAD51 and DMC1) on synapsed axes (S. S. De Vries et al. 1999; Edelman et al. 1999; Kneitz et al. 2000; Guiraldelli et al. 2013; 2018; Q. Zhang et al. 2019; Adelman and Petrini 2008; Qiao et al. 2014; Prasada Rao et al. 2017).

MSH4 and MSH5 are related to MutS, the bacterial mismatch repair (MMR) proteins, and form the MutS γ heterodimer (Pochart, Woltering, and Hollingsworth 1997), which specifically binds to D-loops and Holliday junctions (HJs) *in vitro* (Snowden et al. 2004). MutS γ is essential for chromosome synapsis, CO formation, and thus fertility in mice (S. S. De Vries et al. 1999; Edelman et al. 1999; Kneitz et al. 2000). MSH4 has also

been indicated to protect dHJs from being dissociated by anti-recombinases Sgs1/BLM *in vivo* (Jessop et al. 2006; Oh et al. 2007).

HFM1 is the mammalian ortholog of yeast DNA helicase Mer3. Mer3 can unwind D-loops, Holliday junctions, and substrates with a 3' overhang and stimulate D-loop extension *in vitro* (Nakagawa and Kolodner 2002; Mazina et al. 2004; Hunter 2015). Mer3 is also likely to stabilize the nascent recombinational intermediates into SEIs *in vivo* (Börner, Kleckner, and Hunter 2004). Mutated HFM1 was found in human patients with azoospermia or POI syndromes, indicating the importance of HFM1 for fertility (Baudat, Imai, and De Massy 2013; Jian Wang et al. 2014; W. Zhang et al. 2017). Removing HFM1 causes a drastic reduction of COs and partially affects synapsis in mice (Guiraldelli et al. 2013). Mer3 is also found to limit the extension of D-loops during DNA synthesis by recruiting MutL β , a mismatch repair related heterodimer, to recombination hotspots, consequently limiting the length of gene conversion tracts. Interestingly, HFM1 is also revealed to interact with MutL β *in vitro* (Duroc et al. 2017).

Yeast Zip2, Zip4, and Spo16 (mammalian SHOC1, TEX11, and SPO16) are shown to form a functional complex (ZZS) which is required for CO formation likely through physical interaction with chromosomal axes and CO machinery (De Muyt et al. 2018). In mice, the deficiency of SHOC1, TEX11, and SPO16 causes reduced COs with a relatively minor synapsis defect, suggesting a conserved role of the ZZS complex in recombination repair (Q. Zhang et al. 2019; Guiraldelli et al. 2018; Adelman and Petrini 2008).

Mouse RNF212, the ortholog of yeast E3 ligase-Zip3, and HEI10, a ubiquitin-ligase, regulate CO by modifying recombination factors (MutS γ) at CO-designated sites in an antagonistic manner. Subsequently, stabilized recombination factors enable the recruitment of CO-specific factors (MLH1-MLH3, MutL γ) for CO maturation (Gray and Cohen 2016; Qiao et al. 2014; Prasada Rao et al. 2017; Reynolds et al. 2013; Hunter 2015).

Apart from the regulation of ZMMs, Mcm8, MEIOB, and its associated factor, SPATA22, are also involved in regulating DNA synthesis, the annealing of DSB ends during NCO formation, and the establishment of dHJs during CO formation. MEIOB and SPATA22 are associated with RPA, and this complex is required for intermediate steps of recombination and normal synapsis (La Salle et al. 2012; Ishishita, Matsuda, and Kitada 2014; Luo et al. 2013; Souquet et al. 2013). MEIOB-SPATA22 is inferred to promote strand annealing in both SDSA and dHJ pathways, acting analogously to the budding yeast Rad52 protein (Lao et al. 2008; Luo et al. 2013). Also, MEIOB-SPATA22-RPA is

proposed to mediate digestion of 3'-flaps to remove the excess DNA synthesis relative to DSB resection (Luo et al. 2013).

Recombination intermediates resolution

The STR (BTR) is the yeast (metazoan) "dissolvase" complex, comprising RecQ helicase, Sgs1 (BLM), type-I topoisomerases, Top3 (TOPIII α), and accessory factors Rmi1 (RMI1-RMI2), respectively. During early recombination steps, STR is required for channeling early joint molecules into CO and non-CO pathways. Later, STR/BTR promotes the resolution of the final recombination intermediates into NCOs by its dissolution activity via SDSA (Hunter 2015). STR/BTR unwinds D-loops and dHJs *in vitro* and has anti-CO activity *in vivo*. In mice, in the absence of BLM, chiasma numbers are increased, and aberrant chiasma-like structures are detected (Raynard et al. 2008; L. Wu et al. 2006; Holloway et al. 2010).

Distinguishingly, in the CO pathway, the resolution of joint molecules is mediated by the endonuclease activity of mismatch repair factors MLH1, MLH3, and EXO1 to generate class I COs. For Non-interfering class II COs, resolution of joint molecules is mediated by structure-specific endonucleases, MUS81, GEN1, and SLX1/4 (Holloway et al. 2008; De Muyt et al. 2012; Zakharyevich et al. 2012; Hunter 2015). Interfering COs are estimated to account for most COs (~90%) in mice (Serrentino and Borde 2012; Holloway et al. 2008).

It is indicated that the MSH4-MSH5 complex interacts with the MLH1-MLH3 complex and activates its activity to process dHJs into COs (Gray and Cohen 2016; Santucci-Darmanin et al. 2002). Consistently, the deletion of MLH1, MLH3, or EXO1 in mice causes significant loss of chiasmata and, consequently, mice sterility (Wei et al. 2003; S. M. Baker et al. 1996; Edelman et al. 1996; Lipkin et al. 2002). Both MLH1 and MLH3 localize precisely to future CO sites in many organisms, including mice. Thus, they are invaluable markers of crossovers in the cytological analysis (Kolas and Cohen 2004).

Crossover control

Finally, another layer of control tightly regulates the outcome of DSB repair. CO numbers per meiosis show a low variation despite a much more considerable variation in the numbers of recombinational interactions. This phenomenon is called CO homeostasis, which is underpinned by the lower and upper limits for the CO numbers

regulated by CO assurance and interference. (Martini et al. 2006; Rosu, Libuda, and Villeneuve 2011; Cole et al. 2012; Yokoo et al. 2012; Hunter 2015). CO assurance guarantees that each homolog pair obtains at least one CO to segregate properly at meiosis I. Meanwhile, interference is defined by an inhibitory zone around CO-designated sites where DSBs are prevented from becoming COs. Interference results in COs being widely and evenly spaced along the genome (Hillers 2004; Berchowitz and Copenhaver 2010; L. Zhang, Liang, et al. 2014).

The molecular mechanisms responsible for CO assurance and interference have been long elusive. Until recently, studies in the fission yeast *S. pombe* elucidate the molecular basis of CO interference and repression of CO near centromeres more clearly (G. R. Smith and Nambiar 2020; Nambiar and Smith 2018; Fowler et al. 2018). A clustering model was suggested for CO interference, based on the finding of three DSB hotspot determinant proteins cluster at particular nucleus regions (Rec25, Rec27, and Mug20). In this model, in each cluster containing several DSB hotspots, only one single DSB is formed. Consequently, at most, a single CO is made in the chromosomal interval corresponding to the DSB hotspot-clustered interval (G. R. Smith and Nambiar 2020; Fowler et al. 2018). In *S. cerevisiae* and *S. pombe*, as DSB interference (in which the occurrence of a DSB suppresses adjacent DSB formation) depends on DNA damage response protein Tel1, CO interference also depends on Tel1. In the absence of Tel1, both DSB and CO interference become negative or reduced (Fowler et al. 2018; Garcia et al. 2015; C. M. Anderson et al. 2015). Moreover, studies in male mice show that ATM is required for forming the obligate CO in the small pseudoautosomal region of homology between sex chromosomes and controlling the numbers and distributions of COs on autosomes (Barchi et al. 2008).

In fission yeast, RNAi and heterochromatin are responsible for pericentric DSB and CO repression (Ellermeier et al. 2010). The heterochromatin protein Swi6 binds to methylated H3K9 in heterochromatin and plays negative and positive roles in pericentric DSB and CO formation by regulating cohesins (Nambiar and Smith 2018). Furthermore, this molecular mechanism elucidated in *S. pombe* is likely conserved in diverse organisms, including flies and mice, based on the features of meiotic recombination and pericentric regions in these species (Hartmann, Umbanhowar, and Sekelsky 2019; Prieto et al. 2001; Fukuda et al. 2012; Manheim and McKim 2003; Bhattacharyya et al. 2019; G. R. Smith and Nambiar 2020).

The SC is required for efficient interhomolog crossing-over in most organisms. Deleting CR proteins of the SC prevents completion of homologous recombination (Denise Zickler and Kleckner 2015; Börner, Kleckner, and Hunter 2004; F. A. T. De Vries et al. 2005; Reynolds et al. 2013; Qiao et al. 2014). Locally, the SC plays a pro-CO role via stabilizing pro-CO factors and facilitating the exchange of homolog axes (Börner, Kleckner, and Hunter 2004; Qiao et al. 2012; Voelkel-Meiman et al. 2015).

1.2.4. Meiotic checkpoint

DSBs formation and repair are carefully monitored to choreograph nuclear dynamics and cell division programs. An intricate meiotic checkpoint network has emerged to create dependencies between independent processes when homologous chromosomes pair, synapse, and recombine.

Given the central role of DSB formation and repair during meiotic prophase, not surprisingly, many of the canonical DNA damage response (DDR) signaling proteins appear to be the players of the meiotic checkpoint machinery. Like the DDR signaling pathway, the meiotic checkpoint mechanism is centered on the role of the two evolutionarily conserved checkpoint sensor kinases, ATM and ATR (MacQueen and Hochwagen 2011). They detect and respond to DSBs with the help of checkpoint cofactors in many organisms. Once activated, ATM and ATR phosphorylate a large set of substrates, preferentially containing serine/threonine-glutamine (S/TQ) cluster domains (Traven and Heierhorst 2005). Many of these target proteins act directly to implement the checkpoint response, while others work as transmitters to relay the checkpoint signals to downstream effectors, such as CHK1 and CHK2 kinases (Subramanian and Hochwagen 2014).

The roles of meiotic checkpoint machinery in preserving the order of chromosomal events during meiotic prophase have been discussed in previous sections. This section will discuss how the surveillance mechanisms monitor these meiotic events (Subramanian and Hochwagen 2014; MacQueen and Hochwagen 2011; Hochwagen and Amon 2006).

In response to DSB repair or synapsis defects, the meiotic checkpoints trigger a cell cycle arrest at the pachytene stage to provide sufficient time to fix the errors. This mechanism can eventually lead to activation of apoptosis to cull meiocytes, if defects

persist, in various organisms (Roeder 2000; Di Giacomo et al. 2005; W. J. Lu et al. 2010; Bhalla and Dernburg 2005). In mammals, observations in mutant mice deficient in meiotic recombination suggest that two genetically distinct surveillance mechanisms may contribute to the checkpoint arrest at the pachytene stage: the recombination checkpoint monitoring DSB repair process and the synapsis checkpoint monitoring axis formation and synapsis (Joshi et al. 2015; Roeder 2000; MacQueen and Hochwagen 2011; Subramanian and Hochwagen 2014).

In males defective in DSB repair like *Trip3^{mod/mod}* and *Dmc1^{-/-}* mice, most spermatocytes arrest before incorporating testis-specific histone H1t at pachynema (Barchi et al. 2005; Widger et al. 2018). In contrast, *Spo11^{-/-}* spermatocytes, which do not have programmed DNA damage, progress further and incorporate H1t, suggesting that they reach mid/late pachytene. Nonetheless, these cells arrest before completing meiotic prophase and ultimately apoptose (Barchi et al. 2005; Pacheco et al. 2015). Additionally, the removal of DSBs confers a *Spo11^{-/-}*-like phenotype to these DSB repair-deficient mutants (*Dmc1^{-/-}* and *Trip13^{mod/mod}*) (Barchi et al. 2005; X. Li and Schimenti 2007).

In females, elimination of oocytes defective for DSB repair (*Trip13^{mod/mod}*) or both DSB repair and synapsis (*Dmc1^{-/-}*, *Msh5^{-/-}*) occurs earlier (around birth) than those defective for synapsis alone (*Spo11^{-/-}*, up to 2 months postpartum) (Di Giacomo et al. 2005; X. Li and Schimenti 2007). Mutations disrupting DSB formation (*Spo11* and *Mei1*) are epistatic to those affecting DSB repair, further supporting the existence of DNA damage and synapsis checkpoints (Di Giacomo et al. 2005; Reinholdt and Schimenti 2005; X. Li and Schimenti 2007; Finsterbusch et al. 2016). These results suggest that spermatocytes could respond differently to meiotic defects, irrespective of the common apoptosis consequence. This difference indicates the existence of two distinct checkpoint mechanisms, sensing recombination and synapsis, which mediate pachytene arrest.

1.2.4.1. Recombination checkpoint

The recombination checkpoint is likely to be activated when recombination intermediates persist at pachynema in mammals (Di Giacomo et al. 2005; MacQueen and Hochwagen 2011; Burgoyne, Mahadevaiah, and Turner 2009). So far, the study of the recombination checkpoint in mammals has been challenged by the fact that most mutations that compromise recombination also affect synapsis. However, a gene trap-

disrupted allele of *TRIP13*, *Trip13^{mod/mod}* (X. Li and Schimenti 2007; Roig et al. 2010), which cannot complete DSB repair but complete synapsis, has proven to be helpful to study the recombination-dependent arrest and meiotic cells elimination. Analyses of mice doubly or triply deficient for *TRIP13* and other DDR genes uncover several signaling pathways involved in the recombination checkpoint-mediated arrest and/or apoptosis in both males and females (Pacheco et al. 2015; Marcet-Ortega et al. 2017; Bolcun-Filas et al. 2014; Rinaldi et al. 2017; Rinaldi, Bloom, and Schimenti 2020).

In males, MRN, ATM, CHK2, and p53 family members, p53 and TAp63, are required for the recombination-dependent arrest at early pachynema before incorporating Hit into chromatin (Pacheco et al. 2015; Marcet-Ortega et al. 2017)(Figure 1-6).

Compared to the single mutant *Trip13^{mod/mod}* spermatocytes, there is a significant increase of Hit positive cells with a high level of unrepaired DSBs in *Trip13^{mod/mod} Spo11^{+/-}Atm^{-/-}* mutants, suggesting that the elimination of ATM activity allows spermatocytes to progress further from an Hit-negative stage to an Hit-positive state despite a high level of unrepaired DSBs. The MRN complex is responsible for DSBs sensing and ATM activating in somatic cells (Stracker and Petrini 2011). The MRN complex is also required for meiotic recombination in many organisms, including mammals (S. Keeney and Neale 2006; Cherry et al. 2007). CHK2 is an effector kinase of ATM signaling in response to ionizing radiation (Matsuoka, Huang, and Elledge 1998). Interestingly, disruption of the MRN complex and CHK2 kinase in *Trip13^{mod/mod}* mutants confer a similar meiotic progression phenotype as in *Trip13^{mod/mod} Spo11^{+/-}Atm^{-/-}* mutants (Pacheco et al. 2015). Thus, ATM may be required for the recombination-dependent arrest at early pachynema. (Barchi et al. 2005; Pacheco et al. 2015; Burgoyne, Mahadevaiah, and Turner 2009; Hélne Royo et al. 2010). Additionally, the MRN-ATM-CHK2 signaling cascade is likely to respond to persistent unrepaired DSBs and mediates the recombination-dependent arrest at pachynema in male mice (Pacheco et al. 2015). Similarly, p53 and TAp63 have been inferred to act downstream of the MRN-ATM-CHK2 signaling in the recombination-dependent arrest mechanism as *Trip13^{mod/mod} p53^{-/-}* and *Trip13^{mod/mod} TAp63^{-/-}* spermatocytes phenotypically resemble *Trip13^{mod/mod} Chk2^{-/-}* concerning the further meiotic progression, high levels of DSBs and the pachytene arrest and apoptosis (Marcet-Ortega et al. 2017).

In *Trip13^{mod/mod}* mutants with deficiency of ATM or MRN, spermatocytes can

not correctly repair abundant DSBs caused by the disability of ATM's negative regulation in DSBs generation (Lange et al. 2011), thus failing to complete synapsis and indirectly causing sex body failure (Barchi et al., 2008; Burgoyne et al., 2009; Pacheco et al., 2015; Roig et al., 2010). In *Trip13^{mod/mod} Chk2^{-/-}*, *Trip13^{mod/mod} p53^{-/-}* and *Trip13^{mod/mod} TAp63^{-/-}* spermatocytes, the existence of subtle defects in the sex body in these mutants explains why spermatocytes eventually undergo arrest and apoptosis at late pachynema (Pacheco et al. 2015; Marcet-Ortega et al. 2017), further supporting that an alternative checkpoint mechanism mediates sex body deficient arrest in male mice (Barchi et al. 2005).

In females, CHK2 is essential for eliminating oocytes bearing unrepaired DSBs, and an ATR-CHK1/CHK2-*p53/TAp63* signaling pathway is proposed to mediate the DNA damage checkpoint response in meiosis (Bolcun-Filas et al. 2014; Rinaldi, Bloom, and Schimenti 2020; Rinaldi et al. 2017; Martínez-Marchal et al. 2020) (Figure 1-6).

Deletion of CHK2 rescues developing oocytes in 3-week-postnatal *Dmci^{-/-}* mice. Although the absence of primordial follicles eventually results in a nearly complete oocyte depletion by two months postpartum. This pattern of oocyte loss has high similarity to that in *Spoi1^{-/-}* or *Spoi1^{-/-} Dmci^{-/-}* mice, suggesting that the loss of CHK2 allows the deficient oocytes to surpass the DSB repair but not the synapsis checkpoint. Moreover, the deletion of CHK2 can reach a more successful rescue in *Trip13^{mod/mod}* mice. *Trip13^{mod/mod} Chk2^{-/-}* mice have a significant pool of oocytes at three weeks postpartum, a high number of all types of follicles after two months postpartum, and sustained fertility for many months. Abundant γ H2AX staining was detected in all dictyate *Trip13^{mod/mod} Chk2^{-/-}* oocytes indicating the persistence of unrepaired DSBs like in *Trip13^{mod/mod}*. Thus, CHK2 is required for the DNA-damage checkpoint mediated elimination of oocytes. (Bolcun-Filas et al. 2014).

Remarkably, the lack of both *p53* and *TAp63* enables nearly a complete rescue of *Trip13^{mod/mod}* oocytes. The triple mutants *Trip13^{mod/mod} p53^{-/-} TAp63^{-/-}* mice have indistinguishable numbers of primordial and growing follicles from wild-type mice (Rinaldi, Bloom, and Schimenti 2020). As CHK2 deficiency only rescues *Trip13^{mod/mod}* oocytes to around one-third of wild-type levels (Bolcun-Filas et al. 2014), another pathway is implied to signal these two effectors *p53* and *TAp63* in parallel with CHK2. Indeed, CHK1 has been suggested to perform this function (Rinaldi, Bloom, and Schimenti 2020; Martínez-Marchal et al. 2020). CHK1 is activated to an increased degree by persistent DSBs when CHK2 is absent in ovaries, and it can eliminate *Chk2^{-/-}* oocytes

after birth (Rinaldi, Bloom, and Schimenti 2020) (Figure 1-6).

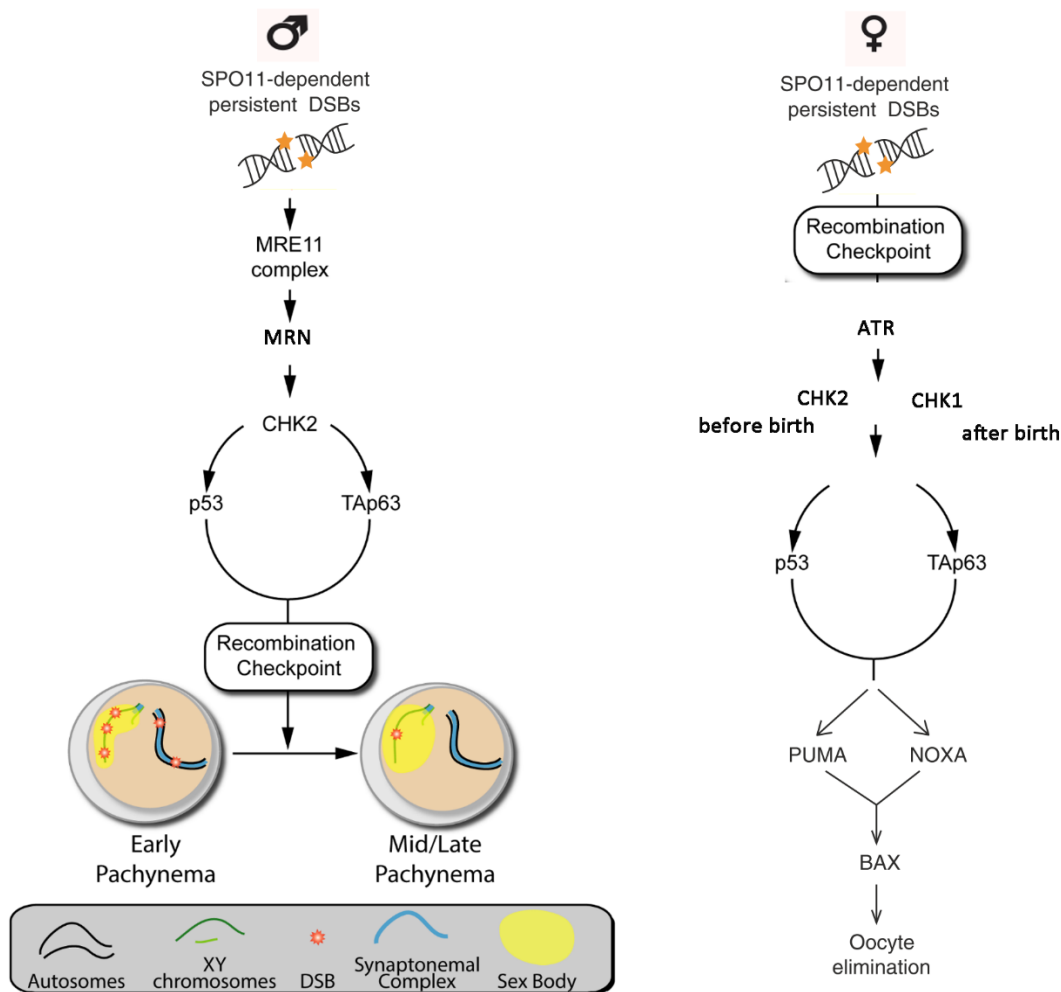


Figure 1-6. Recombination checkpoint pathway in males and females.

Model showing the proposed signaling pathway in response to unrepaired SPO11-dependent DSBs in male (left) and female (right) mice. In males, DSBs are sensed by the MRN complex, leading to activation of ATM, which in turn activates effector CHK2. CHK2 acts on target proteins p53 and TAp63, which implement the recombination-dependent arrest that blocks progression to mid/late pachynema. In females, ATR is activated responding to unrepaired DSBs, leading to oocyte elimination before birth via CHK2-dependent pathway and after birth via CHK1-dependent pathway. CHK1 and CHK2 also signal to p53 and TAp3 and pro-apoptotic BCL-2 pathway components PUMA, NOXA, and BAX act downstream to trigger oocyte apoptosis. Image adapted from Marcet-Ortega, Maria et al. 2017 and Ellnati et al. 2020.

The loss of ATM triggers oocyte elimination by the DNA damage checkpoint in female mice, which could be rescued by the deficiency of CHK2 to a degree similar to the rescue by CHK2 in *Dmc^{-/-}* ovaries. Thus, unlike males, ATR rather than ATM is proposed to activate CHK2 in the recombination checkpoint in females. (Bolcun-Filas et al. 2014; Rinaldi, Bloom, and Schimenti 2020). Recently, it has been demonstrated that the pro-apoptotic BCL-2-dependent pathway is responsible for eliminating recombination-

defective oocytes and suggested acting downstream of CHK2/p53/TAp63 to trigger oocyte apoptosis (ElInati et al. 2020). The BCL-2-dependent pathway consists of PUMA, NOXA, and BAX, which are known targets of p53 and TAp63 transcription factors in somatic cells (Su, Chakravarti, and Flores 2013). PUMA/NOXA or BAX deletion rescue oocyte numbers in DSB-repair mutants (*Dmcr1^{-/-}* and *Msh5^{-/-}*) and like CHK2 deletion, the rescue did not reach wild-type levels, suggesting the existence of other components in DNA damage checkpoint (Bolcun-Filas et al. 2014; Rinaldi et al. 2017; ElInati et al. 2020) (Figure 1-6).

1.2.4.2. Synapsis Checkpoint

Defects in chromosome axis formation or SC assembly can activate a cell response to asynapsis independently of DSBs formation in many organisms, leading to cell cycle arrest and even apoptosis (MacQueen and Hochwagen 2011).

In mammals, the synapsis checkpoint response is closely associated with the meiotic silencing of unsynapsed chromatin (MSUC). The MSUC is a chromatin remodeling process by which unsynapsed regions are transcriptionally inactivated during meiotic prophase I (Turner 2015). The MSUC is achieved through the crosstalk between the axially located sensors signaling asynapsis, such as the axial component proteins HORMAD_{1/2} proteins, etc. (Fukuda et al. 2010; Wojtasz et al. 2009), and the loop-located effectors mediating gene silencing such as the variant histone H2AX (Fernandez-Capetillo et al. 2003). HORMAD_{1/2} load onto chromosome axes at leptotema and are depleted from the axes by TRIP13 once homologs have synapsed (Fukuda et al. 2010; Wojtasz et al. 2009; Koubova et al. 2014b). By the late zygotene stage, HORMAD_{1/2} recruit the breast cancer 1 protein (BRCA1) to the unsynapsed axes (Turner et al. 2004; Hélène Royo et al. 2013). Then, in HORMAD_{1/2}- and BRCA1-dependent manner, ATR is recruited to unsynapsed axes (Turner et al. 2004; Paigen and Petkov 2018a; Wojtasz et al. 2012), which further promotes the enrichment of BRCA1 and ATR-activating cofactors: TOPBP1, ATRIP (Hélène Royo et al. 2013; Perera et al. 2004; Refolio et al. 2011) as well as regulate phosphorylation of HORMAD_{1/2} (Fukuda et al. 2012). If asynapsis persists until pachytene, ATR translocates into the chromatin loops and phosphorylates H2AX (γ H2AX) with the help of the γ -H2AX-binding factor MDC1, resulting in the irreversible silencing of this region (Ichijima et al. 2011).

In males, spermatocytes loss mediated by DSB-independent response to asynapsis involves the failure of Meiotic Sex Chromosome Inactivation (MSCI) (Burgoyne, Mahadevaiah, and Turner 2009). MSCI is a physiological MSUC process that responds to the unavoidable partial asynapsis of the sex chromosomes without leading to cell death (Turner et al. 2006). MSCI is reflected by the formation of the sex body, a specialized subnuclear domain encompassing most portions of the X and Y chromosomes in pachytene spermatocytes. The sex body is characterized by the lack of RNA synthesis and sequestration of an array of proteins not found elsewhere in the spermatocyte's nucleus (Handel 2004).

In mutant mice with extensive asynapsis (e.g., *Spo11*^{-/-}, *Dmci*^{-/-}), MSCI can not occur. Most probably, due to the limited association of silencing factors with XY axes (e.g., ATR, BRCA1 are sequestered at unrepaired DSBs sites in *Dmci*^{-/-} mice) (Mahadevaiah et al. 2008; Kouznetsova et al. 2009). MSCI failure leads to the expression of lethal sex-linked genes, thus resulting in spermatocyte progression arrest and apoptosis (Hélne Royo et al. 2010).

In females, ablation of HORMAD1, HORMAD2, or H2AX prevents prophase I oocyte loss in *Spo11*^{-/-} mice (Jeffrey M. Cloutier et al. 2015; Paigen and Petkov 2018a; Wojtasz et al. 2012), suggesting a potential role of HORMADs in the checkpoint response to asynapsis in females (Turner 2015). In fact, oocyte elimination due to asynapsis is proposed to be caused by the transcriptional inactivation of oogenesis essential genes via MSUC (Jeffrey M. Cloutier et al. 2015; J. M. Cloutier et al. 2016).

Chapter 2

OBJECTIVES

Meiosis is a critical process of gametogenesis in all sexually reproducing organisms, in which haploid gametes are generated through reductional cell division, eventually allowing the formation of a diploid embryo after fertilization. The success of ploidy reduction requires accurate homologous chromosome segregation during the first meiotic division, which is assured mainly by the two coordinated major events, homologous synapsis and meiotic recombination occurring during meiotic prophase I. Errors in these processes can dramatically impact fertility in mammals (Baudat, Imai, and De Massy 2013). Human infertility is an emerging major health issue, and genetic factors significantly contribute to its origin (Zorrilla and Yatsenko 2013). More unknown genes, genetic variants, or mutations affecting mammalian gametogenesis need to be discovered for better clinically relevant diagnosis and therapeutics. Thus, identifying new players involved in meiosis is essential for a better understanding of the genetic regulation of mammalian meiosis but also has profound implications for understanding, diagnosing, and treating human infertility.

Our previously unpublished RNA sequencing analysis detected many unannotated transcripts in 14 dpp mouse testis. Using this data, in this work, we aimed to identify novel genes involved in meiotic prophase and study their functions in gametogenesis.

To achieve this aim, we set the following objectives:

1. Describe the expression profile of the candidate genes in different mouse tissues.
2. Study the ability to express proteins of the selected candidate genes in vitro and in vivo.
3. Characterize the protein localization of putative meiotic prophase genes in mouse meiocytes using immunostaining.
4. Study the meiotic function of identified genes using knock-out mouse models:
 - a. Generate mutant mice using the CRISPR-Cas9 technique.
 - b. Analyze the gametogenesis phenotype of mutant mice.
 - c. Analyze the synapsis and recombination processes in mutant mice.

Chapter 3

Materials and Methods

3.1. Gene screen

3.1.1. RNA purification

Mouse organs (testis, ovary, fetal ovary, prepubertal testis, brain, fat, kidney, liver, spleen, and stomach) were harvested right after euthanasia and preserved by flash freezing with liquid nitrogen. Each organ was collected from 3 different 3-5 months old wild-type individuals for adult tissues, 16-18 days *postcoitum* (dpc) for fetal ovary, and 2-16 days *postpartum* (dpp) for prepubertal testis. RNA of each tissue was purified using the RNeasy Plus Mini Kit (Qiagen) and applied for the downstream RT-PCR.

Protocol, following the manufacturer's instructions:

- Remove a piece of frozen tissue ($3 \times 3 \times 3 \text{ mm}^3$) and place it inside a clean Eppendorf.
- Disrupt the tissue by grinding it thoroughly with a clean pestle.
- Add 350 μl Buffer RLT Plus and homogenize the lysate by pipetting.
- Centrifuge the lysate for 3 min at 13,200 rpm.
- Transfer the supernatant carefully to a gDNA Eliminator spin column placed in a 2 ml collection tube. Centrifuge for 1 min at 13,200 rpm. Discard the column and save the flow-through.
- Add 350 μl of 70% ethanol to the flow-through and mix well by pipetting.
- Transfer all the mix to an RNeasy spin column placed in a 2 ml collection tube. Close the lid gently, and centrifuge for 1 min at 13,200 rpm. Discard the flow-through.
- Add 700 μl Buffer RW₁ to the RNeasy spin column. Close the lid and turn the tube upside down gently and centrifuge for 1 min at 13,200 rpm. Discard the flow-through.
- Add 500 μl Buffer RPE to the RNeasy spin column. Close the lid, and centrifuge for 1 min at 13,200 rpm. Discard the flow-through.
- Add 500 μl Buffer RPE to the RNeasy spin column. Close the lid gently, and centrifuge for 2 min at 13,200 rpm, Discard the flow-through.
- Place the RNeasy spin column in a new 2 ml collection tube, centrifuge

at 13,200 rpm for 1 min, discard the flow-through.

- Place the RNeasy spin column in a new 1.5 ml collection tube. Add 30–50 µl RNase-free water directly to the spin column membrane. Close the lid gently, and centrifuge for 1 min 13,200 rpm.
- Measure the concentration using Nanodrop™ Spectrophotometers. Store RNA sample at -80°C for up to 1 year.

3.1.2. Reverse transcription polymerase chain reaction (RT-PCR)

Total RNA or RNA treated with DNase as described below was transcribed into cDNA using the iScript™ cDNA Synthesis Kit (Bio-Rad). Then, cDNA was amplified with gene-specific primers designed using Primer-BLAST (NCBI) as well as β -actin primers, as control. A minus Reverse Transcription control (RT-) containing all the reaction components except the reverse transcriptase was included for testing for contaminating DNA.

Primer design

All primers were designed using the tool Primer-BLAST and the following criteria (Table 3-1):

- 1) The primer pair should be specific to each gene.
- 2) The melting temperature should be $60 \pm 1^\circ\text{C}$.
- 3) The length should be 16-30 bp.
- 4) The GC content should be 40-70%.

Table 3- 1. RT-PCR primers

Gene name	Forward primer	Reverse primer
12P1	AGGGGGATGGTTCGTGTAAG	TCAGAGGGAAGTGCCTGTAG
14P1	AGAACCTCACTGCCATAGGGT	ACTGTTTCTTGCAAAGGCTCC
17P1*	agggATGTTCCCTGACAATTTTCG	CTATGGGTCAGGCTTTGGAGC
20P1	TTCAGAGTTCAGCAACGCCT	AAGCCTTCAAGTGCCCTTACTT
22P1*	tagtATGACAACACCAGCTGTGC	TTATGACAGACTATGACCGCTCAG
25P1	GCCAAATCCACAGGATCCGA	ATCCTATAGCAATGAAGTTCCTGT
36P1	GATAGGTTCTTGACAACAGGGCAT	TTCTGGAAAAGAGGGACAGGC
60P2	GACTCCATCCCTTCTGTAGCC	AGATGCTCGGGACAAGTTCGT
62P1	ATGCGTGAGAAGGCTGTTTCG	TAACCTGATTGAGCCAGGCG
62P2	TGGGCTCGTTTACCTGGATT	AGCACTACCCGCAGTAAGTT
80P1	AGCTGTAGGATACAATTGGGAAGA	TCAATCCGACTTACAAAGGCT
83P1	TACTTGTCACGGTCACCGAA	TTGGCCTCGTGTCTTCATCT
86P1	CTGCATCCCTCTTCCATGG	GGTCTACCCACATTGAACC
89P1*	gaagATGGGTCAAAGTCAGAGTG	TCATCCATTAGCACCCCTATCAC
94P1	TCAGGAACACGTCCTGTGTG	TCGTTTTTACCCTATGAAACTGCAC
96P2	TGCACTTCTGTTCTACGGCAA	TGGATGGGAAATCCTGTGACC
119P4	GATCAGCTATGGCTGTGGGG	TCCTTTAGGCTGCACCTTGG
136P1	GACGGATGGCCATGGAAGG	TGTCAGCAGAGACGGGTAGT
151P1	AAGGACGCACAGTAGAGAGA	CTCACTCGAGCATGAAGAGAGT
160P2	CCTCACTGCTATAGGCATGAAAGA	GCACTCGAAGATTGCAATGATGT
172P1	TGGAGGCATCTCTGTAGGGG	TGTCTTGGCCTTGCAGGTTTA
199P1	GCCTTTCCAATACCCAGTCA	GACATTGGAGATGACCACGA
251C	AGAAAGGCTAGCTGTGTCTGT	CACCGACATTTGGGGCTCAT
255P1	TAGGGACCAAGAACCTGCTG	TCCTGAAGCCACTGAGAAGG
273P2	ACACTGCTCTGCATTACGCT	TCCAGTTGGGAAACCAAGAGAA
303C	ATCTGATCAAGATGCAGAGAAAAG	GCCCTGGTAACGGCTTTTAG
305P1	GCTTCGACAGTGGCTTGTTG	ACTCTCCACAATCCCTGTTTCT
310P1	CACTGAAGGAAGTGACCCAGAG	TCATTGTGCTTCCTTTGATGCT
319P1	AAGCCTGTTCAACAAGGGAGA	AAACGCCTTAAAATTAAGCAAACA
325P1	AGAGTCCCATCCAGCAATGG	TCCTGGATGTTGAGTCCTGG
333P1	CCAGAACATCACTGCTATAGGCT	TGGATATGGAGACTACACTGCCAA
346P1	TCTTTCTGAGTACCACATCTTCCAG	CTACTGAAGAAGAGCCTGGTTTTG
355P1	CTCAGGTTCTCAGACTGCAC	CTTACTGGGGTGCTGGCTAT
361P1	AGACCTATAGGAACCTCACTGCT	AGACCACTGGTTGGTGCAAA
368P1	TTCCAGAAGACATGGAAGGCATA	GTTCCGAGTTCAGTGTTCGG
β-Actin	AGGTCTTTACGGATGTCAACG	ATCTACGAGGGCTATGCTCTC

* Primers are used for both RT-PCR and cloning PCR.

DNase treatment of RNA

To avoid the unintended genomic DNA amplification during PCR for single-exon putative genes, the RNA sample was pretreated with DNase I (Qiagen) to remove contaminating DNA before cDNA synthesis.

Protocol:

- Mix 2 µg of RNA with 2 µl of 10X DNase I.
- Incubate at RT for 15 min.
- Add 2 µl of 25 mM EDTA to the mix.
- Inactivate the DNase I at 65°C for 10 min.
- Continue the reverse transcription protocol.

Reverse transcription (RT)

Protocol, according to the manufacturer's instructions:

- Mix 2 µg RNA with the reaction components in a 0.2 ml PCR tube as follows (Table 3-2):

Table 3-2. RT-PCR Reaction mix

Component	20 µl Reaction
5× Reaction Mix*	4 µl
Reverse Transcriptase	1 µl
Total RNA	2µg
Nuclease-free water	Up to 20 µl

* The reaction mix contains a blend of oligo (DT) and random hexamer primers.

- Incubate the reaction mix at 42°C for 30 min and then inactivate the enzyme at 85°C for 5 min in a thermal cycler. Store cDNA at -20°C until use.

Polymerase chain reaction (PCR)

Protocol:

- Prepare a master mix for the appropriate number of samples to be amplified in a 1.5 ml tube as Table 3-3 and distribute the proper amount

to each PCR tube. The used primers are displayed in Table 3-1.

Table 3-3. PCR master mix

Component	20 μ l Reaction
10 \times PCR Buffer	2 μ l
dNTPs 8 mM	2 μ l
MgCl ₂ 25 mM	1.36 μ l
Forward Primer 10 μ M	1 μ l
Reverse Primer 10 μ M	1 μ l
cDNA	1 μ l
Horse-Power Taq DNA Polymerase 5U/ μ l	0.4 μ l
Milli-Q Water	11.24 μ l

- Add Horse-Power Taq DNA polymerase to each reaction and immediately start the incubation in a thermal cycler using the following program (Table 3-4):

Table 3-4. PCR cycling program

Cycle Step	Temp. \times Time	Cycles
Initial Denaturation	95°C \times 2'	1
Denaturation	95°C \times 15"	
Annealing	59°C \times 50"	40
Extension	68°C \times 30"	
Final Extension	68°C \times 5'	1

- Load 10 μ l of the reaction mix with 5 μ l molecular weight marker in agarose gel (0.7-1.5%) stained with 0.0085% SYBR safe (Thermo Fisher Scientific). Determine the size of the amplification product.

3.2. Gene cloning

3.2.1. High-fidelity PCR

In order to obtain the correct full-length coding sequence (CDS) of the gene of interest for inserting into the pEGFP-C₁ and pEGFP-N₁ vector (Figure 3-1), adult mouse testis cDNA was amplified using Phusion High-Fidelity DNA Polymerase (Thermo Fisher Scientific).

Primer design

All primers were designed manually according to the following criteria (Table 3-5):

- 1) Each gene-primer pair should target at both ends of the putative gene CDS to amplify the full length.
- 2) Each primer pair should have a sufficiently large target sequence at its 3'-end (usually >15 bases).
- 3) The melting temperature (only target sequence) should be $70 \pm 4^{\circ}\text{C}$ based on the formula, $Tm = 4 \times G/C + 2 \times A/T$.
- 4) To allow the insert DNA in frame with tagged EGFP in vectors, each gene-specific forward primer (for both pEGFP-C₁ and pEGFP-N₁ cloning) should be added at its 5' end by 4 bases upstream to its CDS in the mouse genome; each gene-specific reverse primer (only for pEGFP-N₁ cloning) should exclude the stop codon sequence and replace it by a G/C base.

Protocol:

- Prepare a master mix for the appropriate number of samples to be amplified as follows and distribute the proper amount to each PCR tube (Table 3-6).
- Add the polymerase right before starting the cycling (Table 3-7).
- Determine the size of the amplification product by gel electrophoresis.

3.2.2. DNA purification

Amplified DNAs were purified by cleaning up at least from two independent reactions using the NucleoSpin Gel and PCR Clean-up (Macherey-Nagel). Depending on the specificity, DNAs were extracted directly from PCR reactions or excised agarose gels containing desired DNA fragment.

Protocol, following the manufacturer's instruction:

Mix 1 volume of PCR reaction with 2 volumes of Buffer NTI or add 200

- μ l Buffer NT1 for each 100 mg of agarose gel (< 2%) and incubate for 10 min at 50°C with vortexing until the gel slice is completely dissolved.
- Place a Column into a Collection Tube (2 ml) and load up to 700 μ l sample.
 - Centrifuge for 30 s at 11,000 x g. Discard flow-through and place the column back into the collection tube. Load the remaining sample if necessary and repeat the centrifugation step.
 - Add 700 μ l Buffer NT3 to the Column. Centrifuge for 30 s at 11,000 x g.
 - Discard flow-through and place the column back into the collection tube.
 - Centrifuge for 1 min at 11,000 x g to remove Buffer NT3 completely.
 - Incubate the column for 5 min at 70°C to evaporate the residual ethanol from NT3 Buffer.
 - Place Column into a new 1.5 ml microcentrifuge tube.
 - Add 20 μ l Buffer NE and incubate at RT for 1 min.
 - Centrifuge for 1 min at 11,000 x g. Confirm the DNA sequence by sanger-sequencing.

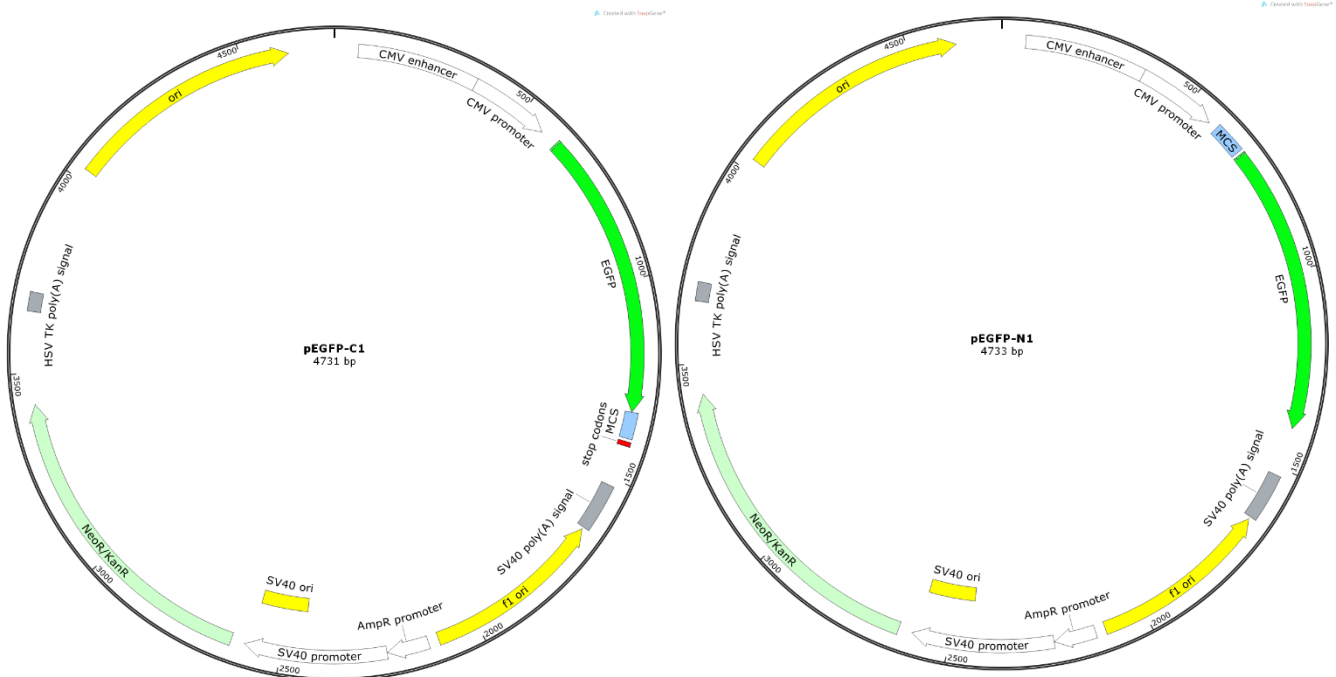


Figure 3-1. pEGFP-C1 and pEGFP-N1 plasmid map

Table 3-5. pEGFP-C₁/N₁ Cloning Primer

Gene name	Forward primer (5' → 3') ^a	Reverse primer C1 (5' → 3')
		Reverse primer N1 (5' → 3') ^b
20P1	gccgATGACTGCTACTGAAGCTGC	TTACTGTGAAGCAAATAAGCCTTCAAG gCTGTGAAGCAAATAAGCCTTCAAG
25P1	tgctATGCCAAATCCACAGGATC	TTAAAGAACTGGATAGGGTTCCTC cAAGAACTGGATAGGGTTCCTCTC
62P1	cagcATGCGTGAGAAGGCTG	CTAACCTGATTGAGCCAGGC gACCTGATTGAGCCAGGCG
62P2	gggcATGCGTGAGAAGGCTG	TCACTGGCTCCCAACAGTCAG gCTGGCTCCCAACAGTCAGTT
96P2	taagATGATGGAATGGCGGCCT	TCACTGGTGTCTGGGCTAGGG gCTGGTGTCTGGGCTAGGGAA
136P1	caagATGAAATCTGTGCCACTTGATG	CTCACCTTTGAAGCTCTTCACAC cTACTCACCTTTGAAGCTCTTCAC
151P1	tgccATGAAAGGATTCACAGTGAAG	TTACTTACATACACAAGGTTTCTCTCC gCTTACATACACAAGGTTTCTCTCCA
255P1	agaaATGCCAGGAAAACTGAAG	TTAAGCTATTGCATTCTTGGG gAGCTATTGCATTCTTGGGC
273P2	cattATGGACTGTAGCGAGAAC	TCAAACCTTCTCCCTCTTTTTTC gAACTTCTCCCTCTTTTTTCC
310P1	gaggATGCAGAGAAAGACAGGAAAG	TCACACCTGGCTGGTAAACAGTAAG gCACCTGGCTGGTAAACAGTAAGG
333P1	ggtgATGCTAGAGACATAACC	CTAAGGGTTTTTCTAAAATGTG gAGGGTTTTTCTAAAATGTGTTCC
355P1	tgacATGTTGGACAAATTTACAGAAACAG	TCAGCTAAGGACTTCATTAGAAGAGGC gGCTAAGGACTTCATTAGAAGAGGC

^a Lowercase sequence indicates genomic sequences upstream of each gene. ^b Lowercase sequence indicates the sequence replacing stop codon for pEGFP-N₁ cloning

Table 3-6. High-Fidelity PCR master mix

Component	50 μ l Reaction
5 \times HF Buffer	10 μ l
dNTPs 8 mM	1.25 μ l
DMSO	1.5 μ l
Forward Primer 10 μ M	2 μ l
Reverse Primer 10 μ M	2 μ l
cDNA	2 μ l
Phusion DNA Polymerase 2U/ μ l	0.4 μ l
Milli-Q Water	30.85 μ l

Table 3-7. High-Fidelity PCR cycling program

Cycle Step	Temp. \times Time	Cycles
Initial Denaturation	98°C \times 1'	1
Denaturation	98°C \times 15"	
Annealing	X°C \times 20"	35
Extension	72°C \times 1'	
Final Extension	72°C \times 5'	1

3.2.3. DNA digestion

Vector DNA Digestion and Dephosphorylation

The recipient vectors, pEGFP-C₁, and pEGFP-N₁ vector were digested by FastDigest SmaI (Thermo Fisher Scientific) to create blunt ends and dephosphorylated by FastAP Thermosensitive Alkaline Phosphatase (Thermo Fisher Scientific) simultaneously to prevent re-circularization.

Protocol, following the manufacturer's instruction:

- Prepare the scaled-up reaction mixture as Table 3-8.
- Mix thoroughly, spin briefly and incubate at 37°C for 10 min.
- Leave on ice while checking the result by electrophoresis loaded with 1 μ l reaction diluted in 9 μ l Milli-Q water.

Table 3-8. SmaI digestion and dephosphorylation master mix reaction

Component	50 μ l Reaction
Plasmid DNA	5 μ g
10 \times Fast Digest buffer	5 μ l
Fast Digest SmaI enzyme	5 μ l
Fast AP, alkaline phosphatase	5 μ l
Nuclease-free Water	up to 50 μ l

- If the band is linear and clear, stop the reaction by heating at 65°C for 15 min. If not, return the Eppendorf to incubate at 37°C for another 5 min.

Insert DNA Phosphorylation

The purified PCR product was phosphorylated by T₄ Polynucleotide Kinase (Thermo Fisher Scientific) before being inserted into the dephosphorylated vectors.

Protocol, following the manufacturer's instruction:

- Prepare the following reaction mixture (Table 3-9):

Table 3-9. Phosphorylation of insert DNA

Component	Final Conc.
Amplified DNA	Variable
10 \times Reaction Buffer A	1 \times
ATP 10 mM	1 mM
T ₄ Polynucleotide Kinase	1 μ l

- To maximize the final concentration of insert DNA, the reaction was prepared by adding all the pre-purified amplification DNA mostly around 15-18 μ l and without adding any water. In this case, the volumes of reaction buffer and ATP were adjusted according to the final concentration and the DNA volume.
- Mix thoroughly, spin briefly and incubate at 37°C for 20 min.
- Heat at 75°C for 10 min.

3.2.4. DNA ligation

The insert DNA was ligated with both pEGFP-C1 and EGFP-N1 vectors that were SmaI-digested and dephosphorylated using the Rapid DNA Ligation Kit (Thermo Fisher Scientific). The molar ratio of insert: vector was set to 3: 1 and the DNA concentrations of vector and insert were estimated by electrophoresis described as below.

Protocol:

- Load 1 µl of each linearized vector DNA and phosphorylated insert DNA in a 1% agarose gel side by side along with 5 µl DNA marker. Run the gel.
- Compare the intensity of the bands and determine, the ratio of DNA concentrations ($\frac{C_i}{C_v}$).
- Determine the $\frac{S_v}{S_i}$ by comparing the size of the vector and inserting DNA.
- Calculate the V_i by the following formula to decide the required volume of insert DNA to reach a 3:1 insert: vector molar ratio.

$$\frac{C_i \times V_i}{C_v \times 1\mu L} \times \frac{S_v}{S_i} = 3 : 1$$

- Add the following to a 1.5 ml tube (Table 3-10):

Table 3-10. Ligation of insert DNA to plasmid vector DNA

Component	20 µl Reaction
Vector DNA	1 µl
Insert DNA	Variable
5× Rapid Ligation Buffer	4 µl
T4 DNA Ligase 5 U/µl	1 µl
Nuclease-free water	Up to 20 µl

- Vortex and spin briefly to collect drops.
- Incubate the mixture at 22°C for 15-20 min.
- Store the ligation mixture at 4°C until transformation.

3.2.5. Transformation

5-alpha Competent *E. coli* cells from New England Biolabs (NEB) or Dr. Joaquín Ariño Carmona's lab (IBB, UAB; JAC) were transformed with a ligation mixture.

Protocol:

- Thaw 100 µl from NEB cells or 200 µl of the JAC cells on ice.
- Mix gently and carefully pipette the cells into a new 1.5 ml tube on ice.
- Add 4 µl of the ligation reaction mixture in every 100 µl of the *E. coli* cells.
- Carefully flick the tube 4-5 times to mix cells and DNA. Do not vortex.
- Place the mixture on ice for 30 min. Do not mix.
- Heat shock at 42°C for 30-45 s. Do not mix.
- Place on ice for 5 min. Do not mix.
- Pipette 1 ml of RT LB medium into the mixture.
- Place at 37°C and shake at 220 rpm for at least 3 h.
- Centrifuge the LB mixture at 13200 rpm for 30 s.
- Remove most of the supernatant but keep ~50 µl.
- Mix the cells thoroughly by pipetting gently.
- Spread all the mixture onto pre-warmed kanamycin (50 µg/ml) selection plate using an aseptic technique to avoid contamination.
- Incubate overnight at 37°C.

3.2.6. Colony screening

To identify the transformed colonies containing a DNA insert with correct size and orientation, a direct PCR from colonies was performed as described below.

Protocol:

- Pick up 16-20 colonies from each plate and incubate in 1 ml LB medium with kanamycin (50 µg/ml) at 37°C for 4-16 h.
- Seed 1 µl of each cultured colony into the PCR reaction as the DNA template sample.
- Use a combined primer set, including an insert-specific primer and a

vector-specific primer, to detect the presence of the insert and its orientation (Figure 3-2).

The PCR reaction mix preparation and cycling program were performed following previously described methods (Table 3-3 and 3-4). The annealing temperature for each PCR was estimated by NEB Tm Calculator. All the PCR products were run by gel electrophoresis and the results were evaluated. The whole process starting from colonies pick-up was repeated at most 3 times more if there was not any expected amplification.

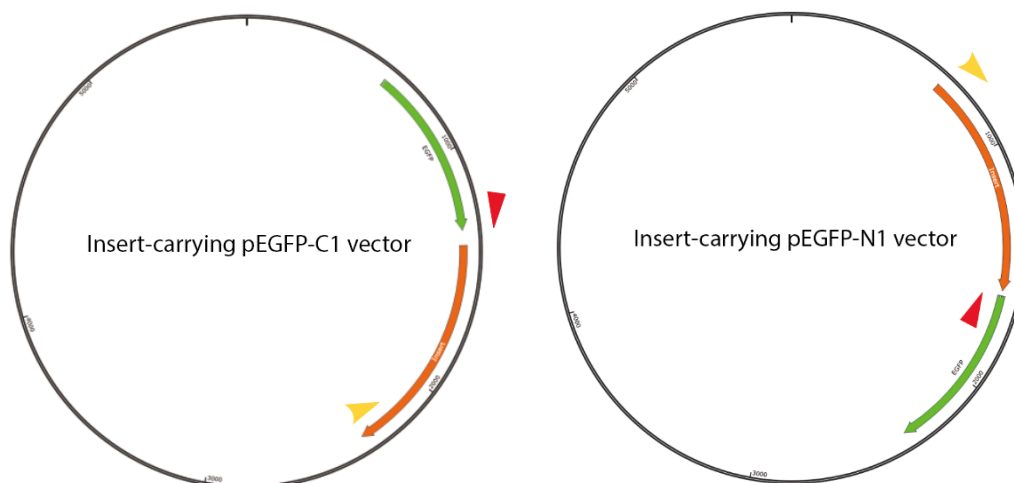


Figure 3-2. Primer design for colony PCR

PCR for pEGFP-C1 cloning: forward primer (red arrowhead) is located at the EGFP region – CATGGTCCTGCTGGAGTTCGTG and reverse primer (yellow arrowhead) is the gene-specific reverse primer C1. For pEGFP-N1 cloning: forward primer (red arrowhead) is the gene-specific forward primer and reverse primer (yellow arrowhead) is located at the EGFP region – CGTCGCCGTCCAGCTCGACCAG.

3.2.7. Plasmid isolation

The plasmid was then isolated using NucleoSpin Plasmid (Macherey-Nagel) from the corresponding LB samples showing the expected amplicon size and finally, the sequence was confirmed by sanger sequencing.

Miniprep isolation protocol, following the manufacturer's instructions:

- Use 0.5-1 ml of the E.coli LB culture, centrifuge cells in an Eppendorf for 30 s at 11,000 x g. Discard the supernatant and remove as much of the liquid as possible.
- Add 250 µl Buffer A1. Resuspend the cell pellet completely by vortexing. Make sure no cell clumps remain.

- Add 250 µl Buffer A2. Mix gently by inverting the tube 6–8 times. Do not vortex to avoid shearing of genomic DNA.
- Incubate at RT for up to 5 min until lysate appears clear.
- Add 300 µl Buffer A3. Mix thoroughly by inverting the tube 6–8 times until blue samples turn completely colorless. Do not vortex to avoid shearing of genomic DNA.
- Centrifuge for 5 min at 11,000 x g at RT.
- Place a NucleoSpin® Plasmid Column in a Collection Tube (2 ml) and pipette a maximum of 700 µl of the supernatant onto the column.
- Centrifuge for 1 min at 11,000 x g. Discard flow-through and place the NucleoSpin® Plasmid Column back into the collection tube. Repeat this step to load the remaining lysate.
- Preheat Buffer to 50°C and add 500 µl to the column. Centrifuge for 1 min at 11,000 x g.
- Add 600 µl Buffer A4. Centrifuge for 1 min at 11,000 x g. Discard flowthrough and place the NucleoSpin® Plasmid Column back into the empty collection tube.
- Centrifuge for 2 min at 11,000 x g and discard the collection tube.
- Incubate the column for 10 min at 37°C to evaporate the residual ethanol from Buffer A4.
- Place the NucleoSpin® Plasmid Column in an Eppendorf and add 30-50 µl Buffer AE. Incubate for at least 1 min at RT. Centrifuge for 1 min at 11,000 x g.
- Store the isolated plasmid DNA at -20°C until use.

1 µl of the correct gene-containing plasmid was transformed into *E.coli* cells following the previously described protocol and incubated in 200 ml LB medium overnight for a large amount of plasmid preparation. The plasmid was then isolated by NZYMaxiprep (NYZTECH).

Maxiprep isolation protocol, following the manufacturer's instructions:

- Pellet 100-150 ml of an *E. coli* LB culture by centrifugation for 10 min at 6,000 x g at 4°C. Discard supernatant.
- Re-suspend cell pellet in 12 ml of Buffer M1, containing RNase A, by

vigorous vortexing.

- Add 12 ml of Buffer M₂ and mix gently by inverting the tube 5 times. Do not vortex. Incubate at RT for 5 min.
- Add 12 ml of pre-cooled Buffer M₃ to the suspension. Mix gently by inverting the tube 10-15 times. Do not vortex. Immediately proceed to the next step.
- Centrifuge for 30 min at 20,000 x g at 4°C. During this time, equilibrate an NZYTech Plasmid Maxi Column with 6 ml Buffer MEQ. Allow the column to empty by gravity flow.
- Apply the lysate to the equilibrated NZYTech Plasmid Maxi Column. Allow the column to empty by gravity flow.
- Wash the NZYTech Plasmid Maxi Column with 32 ml of Buffer MW. Allow the column to empty by gravity flow.
- Heat buffer ME to 50°C in the water bath and elute the plasmid DNA with 15 ml. Allow the column to empty by gravity flow.
- Collect the eluate in a clean tube.
- Add 10.5 ml of isopropanol to precipitate the eluted plasmid DNA.
- Mix well and let the mixture sit for 2 min. Centrifuge at 20,000 x g for 30 min at 4°C. Carefully discard the supernatant.
- Add 5 ml of 70% ethanol to the pellet and centrifuge at 20,000 x g for 15 min at RT. Carefully remove ethanol completely from the tube with a pipette tip. Allow the pellet to dry at RT.
- Dissolve the DNA pellet in 200 µl Buffer TE.
- Determine plasmid concentration by Nanodrop.

3.3. Gene expression analysis

3.3.1. Transfection in HEK 293T cell line

All the successful cloned plasmids containing 12 genes of interest (9 carried in both pEGFP-C₁ and pEGFP-N₁ vectors, 2 carried only in pEGFP-C₁ vector and 1 carried only in pEGFP-N₁ vector, Table 4-1) were first introduced into the human embryonic

kidney cell line (HEK 293T) by transfection to assess their expression ability *in vitro*. The transfection procedure was performed by using jetPEI® DNA transfection reagent (Polyplus Transfection).

Protocol, following the manufacturer's instruction :

- Seed 200,000 – 400,000 cells/per well 24 h before transfection in 6-well plate.
- On the day of the transfection, change the medium of the 6-well plate.
- For the transfection, per well, dilute 3 µg of DNA in 150 mM NaCl to a final volume of 100 µl. Vortex gently and spin down briefly.
- Vortex jetPEI® reagent and spin down before use. Per well, dilute 6 µl of jetPEI® reagent in 150 mM NaCl to a final volume of 100 µl. Vortex gently and spin down briefly.
- Add the 100 µl jetPEI® solution to the 100 µl DNA solution all at once. Vortex the solution immediately and spin down briefly.
- Incubate for 30 min at RT.
- Per well, add the 200 µl jetPEI®/DNA mix drop-wise to the cells in 2 ml of serum-containing medium and homogenize by gently swirling the plate.
- Return the plates to the cell culture incubator and incubate for 24-48 h.
- Check eGFP expression with an inverted fluorescence microscope (Nikon Eclipse TE2000-E or TS2R-FL).

3.3.2. Electroporation in live mouse testis

The *in vivo* electroporation (EP) experiment was performed in collaboration with the group of Dr. A. Pendás (CIC-CSIC, Salamanca, Spain). This particular transfection technique allows a transient expression of the delivered plasmid in live mouse testis cells, facilitating *in vivo* gene function analysis.

Protocol, adapted from (Shibuya, Morimoto, and Watanabe 2014):

- Anesthetize a 16-18 dpp wild-type mouse with isoflurane by inhalation and then pull out the testis from the abdominal cavity.
- Prepare DNA solution in 5 µg/µl by diluting plasmid in 1x HBS (HEPES

buffered saline: 20 mM HEPES, 140 mM NaCl, 5 mM KCl, 0.1% glucose, 0.7 mM Na₂HPO₄·12H₂O) and stained with 1 µl of 0.1% FastGreen (Sigma-Aldrich).

- Inject 10 µl of DNA solution to the rete testis, the region surrounded by the white dotted line, using a glass capillary.
- Leave the testes to rest for 1 h to allow the DNA to penetrate the seminiferous tubules.
- Wet the testes with PBS. Hold it between a pair of electrodes and apply 4 electric pulses of 35 V for 50 ms in each direction using a CUY21 BEX electroporator (BEX Ltd).
- Place the testes back into the abdominal cavity and sew up the incision.
- Sacrifice the mouse after 24–72 h and dissect the testis for downstream spermatocyte spread and squash.

3.3.3. Spermatocyte spreading from frozen testis

A small portion of frozen testes was used for spreading spermatocyte nuclei on a glass slide in a 2D preparation of nuclear chromatin. Even though this technique caused the loss of soluble cellular components, chromatin-bound molecules were retained to study protein localization coupling with immunofluorescence microscopy.

Protocol, adapted from (Liebe et al. 2004):

- Cut a small portion with a pre-cooled sterile blade in a Petri dish on dry ice.
- Transfer the Petri dish with the sample to ice.
- Immediately add 10–25 µl of cold 1 × PBS (pH 7.4) containing 1 × protease inhibitor, PI (Roche Diagnostics).
- Mince the sample with the blade thoroughly for 2–3 min.
- Gradually add more 1 × PBS up to 100 µl while mincing.
- Transfer the cell mixture to a sterile Eppendorf and let it sit on ice for 15 min so large tissue pieces sediment
- Distribute 25 µl of the upper cell suspension on a slide and place it in a humid chamber. Repeat up to three times this process.

- Add 80 µl of 1% Lipsol containing 1 × PI in Milli-Q water onto the cell suspension, mix gently and leave for 15-20 min.
- Add 150 µl of the PFA fixative solution (1% Paraformaldehyde in Milli-Q water pH 9.2-9.4, 15% Triton X-100, 1x PI). Mix gently and spread over the slide.
- Let the slides sit in a closed humid chamber at RT for 2 h.
- Open de humid chamber in a fume hood and let slides dry for 30-45 min.
- Wash the slides four times in 0.4% Photoflo (Kodak) solution for 2 min. Samples of different genotypes were washed separately.
- Let the slides air dry and store at -80°C until use.

3.3.4. Seminiferous tubule Squash

Compared to the surface-spreading technique, which is useful for studying the meiotic chromosome as it presents a flattened-out nuclear chromosome structure, the seminiferous tubule squash technique preserves the integrity of spermatocytes as well as other cells involved in spermatogenesis. Therefore, many cellular structures, e.g., centromeres, telomere attachment, and the nuclear envelope, etc. were maintained and could be assessed via immunofluorescence microscopy. Two different protocols were applied for frozen or fresh testicular seminiferous tubules squash respectively.

Cells preparation for frozen testis, adapted from (Liebe et al. 2004)

- Cut a small piece of frozen testes with sterile blade scalpel in a petri dish on dry ice.
- Add 10 µl PFA fixative solution (2% Paraformaldehyde in PBS pH 9.4-9.5) by 2 times up to 20 µl while mincing the seminiferous tubules completely.
- Transfer the cell solution to a sterile Eppendorf and let it sit at RT for 10 min to deposit.
- Transfer 6 µl of the cell suspension to a marked slide, 3 slides in total.
- Continue with the squashing of the seminiferous tubules as described below.

Cells preparation for fresh testis, adapted from (Page et al. 1998)

- Cut a small portion of fresh testes with sterile blade and forceps in 1x PBS, pH 7.4 in a Petri dish.
- Remove the testicular tunica albuginea by puncturing the tissue with sharp-tipped forceps and collecting the loose seminiferous tubules.
- Outline the edges of 3 poly-L-lysine coated glass slides with a liquid blocker pen.
- Transfer a few long tubules to each slide and add 60 μ l fixative solution (1.875% PFA in PBS pH 9.0).
- Incubate the tubules in the PFA solution for 5 min at RT.
- Mince seminiferous tubules into 2 mm segments using the blade.
- Arrange 10-20 tubule segments to be distributed evenly in the center part of the slide by forceps. Avoid tissue overlaps.
- Remove excess liquid using a paper towel.

Squashing of the seminiferous tubules

- Put a 24*24mm coverslip on top of the tubules.
- Fix the coverslip with a finger on one corner upon a sheet of paper towel. Roll a pencil all over the coverslip with even force.
- Place the paper towel on top of the coverslip. Press the coverslip with the thumb for seconds to squash the tubules.
- Immediately flash freeze the slide in liquid nitrogen until the noise subsides.
- If immunostaining is performed immediately after, remove the coverslip with a blade and place the slide into PBS, wash 5 min for 3 times. Then, the preparation is ready for blocking.
- If the slides are not going to be used right away, wrap the slides with the coverslip in tinfoil and store them at -80°C for long-term storage. When immunostaining a stored slide, dip it into liquid nitrogen again until the noise disappears. Remove the coverslip and wash in PBS as described above.

3.3.5. Immunofluorescence staining

Indirect immunofluorescence staining was applied for chromatin preparation to study the presence and subcellular localization of the protein of interest in cell nuclei.

Protocol:

- Block the slides with freshly made blocking solution (0.2% BSA, 0.2% gelatin, 0.05% Tween-20 in PBS) for 15 min at RT under agitation.
- Dilute the primary antibody in 80 µl blocking solution per slide. Primary antibodies used for detection in transfected samples are listed in Table 3-12.
- Add the primary antibody solution on each slide and cover it with parafilm.
- Incubate the slides in a humid chamber overnight at 4°C.
- Wash the slides 4 times in blocking solution for 3 min under agitation.
- Dilute the secondary antibody in 80 µl blocking solution per slide.
- Add the secondary antibody solution on each slide and cover it with parafilm.
- Incubate the slides in a humid chamber for 1 h at 37°C.
- Wash the slides 4 times in blocking solution for 3 min under agitation.
- Drain the slides at RT.
- Mount each slide with 15 µl DAPI (0.1 µg/ml in Vectashield antifade mounting medium) and cover with a coverslip.
- Analyze the results with an epifluorescence microscope (Zeiss Axioskop). Stained slides were stored at 4°C for the short term and -20°C for the long term.

Antibodies used for IF in transfected samples are listed in Table 3-12.

3.3.6. Western blot

Western blot analysis was performed to detect the protein expression level of genes of interest in the transfected cells and the electroporated testis with their corresponding plasmids.

Protein sample preparation from adherent cells

- Place the cell culture plate on ice and gently wash the cells with ice-cold

PBS.

- Discard the PBS and add ice-cold 1× RIPA lysis buffer (50 mM Tris pH 8, 1% Triton X-100, 0.1% SD, 150 mM NaCl, 1 mM EDTA, 0.5% Sodium Deoxycholate, 10 mM NaF, 1× PI), 100-150 µl per well of 6-wells plate.
- Scrape the cells off the plate using a cold plastic cell scraper and gently collect the cell suspension into a pre-cooled 1.5 ml tube.
- Let the tube stand on ice for 30 min, vortex every 10 min vigorously.
- Centrifuge for 10-20 min at 12,000 rpm at 4°C.
- Place the tubes onto the ice and gently transfer the supernatant into a fresh tube kept on ice.

Protein sample preparation from mouse testis

- Add ice-cold 1× RIPA lysis buffer to the tissue in a 1.5 ml tube. 100-150 µl for half of a 16 dpp mouse testes.
- Disrupt and homogenize the tissue using a plastic pestle for 3-5 min.
- Incubate the tube in the thermomixer for 10 min at 95°C.
- Disrupt and homogenize again with the pestle for min.
- Centrifuge at 13200 rpm for 10 min at 4°C.
- Transfer the supernatant into a new 1.5 ml tube.

Determine the concentration of each lysate sample by using Pierce™ BCA Protein Assay Kit (Thermo Scientific).

Protocol, following the manufacturer's instruction:

- Prepare WR by mixing 50 parts of BCA Reagent A with 1 part of BCA Reagent B (50:1, Reagent A:B). The total volume of WR required is determined by the following formula:

$$(9 \text{ standards} + \# \text{ unknowns}) \times (2 \text{ replicates}) \times (200 \mu\text{l of WR per sample}) = \text{total volume WR required}$$
- Dilute each unknown sample in 1:10.
- Pipette 10 µl of each standard or diluted unknown sample replicate into a 96-Well Plate.
- Add 200 µl of the WR to each well and mix the plate thoroughly on a plate shaker for 30 s.

- Cover plate and incubate at 37°C for 30 min.
- Cool plate to RT. Measure the absorbance near 540 nm on a plate reader.
- Subtract the average 540 nm absorbance measurement of the Blank standard replicates from measurements of all other individual standard and unknown sample replicates.
- Prepare a standard curve by plotting the average Blank-corrected measurement for each BSA standard vs. its concentration in µg/ml.
- Use the standard curve to determine the protein concentration of each diluted unknown sample.
- Multiply by 10 each diluted sample concentration to determine the final protein concentration.

Protein separation by SDS-PAGE

Casting the gel

- Prepare a 10% SDS-PAGE resolving gel solution and a 4% SDS-PAGE stacking gel solution separately according to the following recipes (Table 3-11).

Note: add and mix TEMED in the end just right before casting.

Table 3-11. Recipe for preparing resolving and stacking gels

Component	10 % Resolving Gel	4 % Stacking Gel
Milli-Q Water	3.8 ml	3 ml
Acrylamide/bis (30% 37.5:1; Bio-Rad?)	3.4 ml	670 µl
Tris-HCl (1.5 M, pH 8.8)	2.6 ml	/
Tris-HCl (0.5 M, pH 6.8)	/	1.25 ml
SDS (20%, w/v)	50 µl	25 µl
APS	100 µl	50 µl
TEMED (Bio-Rad)	13 µl	6.5 µl

- Pour half of the resolving gel solution into the pre-stalled glass cassette.
- Add 50 µl isopropanol to remove the bubbles.
- Leave the gel for 15 min to solidify. Meanwhile, check if the leftover gel solution solidifies to confirm that the gel solution behaves as expected.

- Remove the isopropanol with a clean filter paper.
- Load half of the stacking gel solution over the resolving gel.
- Immediately insert the comb into the upper gel.
- Leave the gel for 5 min to solidify. Meanwhile, check if the leftover gel solution solidifies.

Reduce and denature the protein sample

- Add 15 μ l 2x Laemmli sample buffer containing β ME to each 30 μ g protein sample as well as an appropriate volume of water up to 30 μ l per well.
- Boil the mixed sample at 95°C for 10 min and leave the sample cool down.

Gel loading and running

- Mount the cassette into the electrophoresis apparatus and pour enough amount of 1 \times Running buffer (25 mM Tris, 190 mM glycine, 0.1% SDS in Milli-Q Water) into the cassette and the tank.
- Remove the comb from the cassette carefully and load the prepared protein extracts to the wells along with protein ladders.
- Run the gel at 80 volts at the beginning, speed up to 120 volts after the samples pass the stacking gel, and stop when the samples reach the bottom of the resolving gel.

Protein transference

- Gently disassemble the cassette.
- Take out the gel and remove the stacking part.
- Prepare the stack with the preassembled nitrocellulose membrane pack (Bio-Rad).
- Transfer the protein using Trans-Blot® Turbo™ Transfer System (Bio-Rad) for 10 min at 25V/1.3A.
- Rinse the membrane with water and air dry.

Antibody labeling

- Block the membrane for 1 h at RT in blocking solution (0.5% fat-free milk in 0.1% TTBS).

- Incubate with the primary Ab diluted in blocking solution ON at 4°C under agitation.
- Wash the membrane for 5 min in TBST 3 times.
- Incubate the membrane with the secondary Ab diluted in TBST for 1 h at RT under agitation.
- Wash the membrane for 5 min in TBST 3 times.
- Prepare the substrate detection buffer (Clarity Western ECL Substrate, Bio-Rad) and add 2 ml to the membrane.
- Incubate for 5 min and remove the excess substrate.
- Expose the membrane and acquire images using Versadoc (Bio-Rad).

Antibodies used for WB in transfected samples are listed in Table 3-12.

Table 3-12. Antibodies used for the analysis of the transfected sample

Antibody	Host	Dilution	Source
Anti-SCP3	Mouse	1:200 for IF	Abcam
Anti-GFP	Rabbit	1:200 for IF, 1:2000 for WB	Thermo Fisher Scientific
Cy3 anti-mouse	Goat	1:200 for IF	Jackson Immunoresearch
FITC anti-Rabbit	Goat	1:200 for IF	Jackson Immunoresearch
anti-Rabbit-HRP	Goat	1:10000 for WB	Bio-Rad

3.3.7. 5' Rapid Amplification of cDNA Ends (RACE)

An adapted in-house designed 5' rapid amplification of cDNA ends (RACE) analysis (Pinto and Lindblad 2010) is used to determine the transcription start points. The technique takes advantage of the propensity of the murine leukemia reverse transcriptase (M-MuLV) to add an extra 2–4 cytosines to the 3' end of newly synthesized cDNA on reaching the cap structure at the 5' end of the template mRNA.

Thus, in the synthesis of cDNA primed by a gene-specific primer (GSP₁), a template-switch oligonucleotide (TSO) containing 3' poly-G terminus pairs with the cDNA 5' poly-C tail, becoming a template for RT to add its complementary sequences at the cDNA terminus as a linker sequence. As the template-independent addition of cytosines is cap-dependent, the TSO is appended only to full-length cDNA ends, assuring the mRNA 5' region is included in these template-switch cDNA containing linker

sequences.

Then a universal primer mix (UPM) and a gene-specific antisense primer (GSP₂) were used for a step-out PCR. The UPM is composed of a long primer and a short primer. The long primer is present in low concentration and contains part of the TSO at its proximal end and the short primer at its distal end. Therefore, it specifically but inefficiently primes the template-switched cDNA in the PCR. Subsequently, the short primer specific for the distal part of the long primer and in high concentration drives the PCR product amplification together with gene-specific antisense primer. The PCR products, including the mRNA 5' region, are then cloned and sequenced.

The presence of the poly G 3' end of TSO can cause unspecific cDNA synthesis if it binds to C-rich sequences in the mRNA of interest. To avoid this unspecific cDNA synthesis during RT and product synthesis by the unspecific cDNA during PCR, TSO was blocked by adding C₃-spacer at its 3' end and the unspecific TSO-primed cDNA was flanked by in- inverted terminal sequences that act as PCR suppressors due to the use of the UPM (Siebert et al. 1995).

Primer design

A collection of primers was designed manually according to the following criteria (Table 3-13):

TSO criteria:

- 1) the sequence is absent from the mouse genome.
- 2) the 3' poly-G should be 5 bases long.
- 3) the 5' section should have a melting temperature of $68 \pm 1^\circ\text{C}$ (USENSE).
- 4) any putative secondary structures should have free energy values above -4 kcal/mol.

UPM-SHORT criteria:

- 1) The melting temperature should be $68 \pm 1^\circ\text{C}$.
- 2) The sequence similarity to U_SENSE should be low.
- 3) It should result in a UPM-LONG having free energy values for secondary structures above -8 kcal/mol.

GSP₁

- 1) The length should be 16-20bp with 40-70% GC.
- 2) It should specifically prime to the 3' end of 355P₁ and USP44 without 3' mis-priming.

- 3) The sequence should be stable at the central part and 5' end and unstable at 3' end.

GSP₂

- 1) The melting temperature should be $68 \pm 1^\circ\text{C}$.
- 2) Any putative secondary structures should have free energy values above -4 kcal/mol.
- 3) It should specifically prime to the 3' end of 355P1 and USP44 upstream of GSP1 without 3' mis-priming.
- 4) The sequence should be stable at the central part and 5' end and unstable at 3' end.

Table 3-13. Primers for 5' RACE

Primer	Sequence (5' → 3')
TSO	GTCGCACGGTCCATCGCAGCAGTCACAGGGGG ^a or CGCCGATTACGCTCGTCGTTACGCTTggggg ^b
USENSE	GTCGCACGGTCCATCGCAGCAGTC ^a or CGCCGATTACGCTCGTCGTTACGCTT
UPM long	ACGCTGACGCTGAGCCTACCTGACGTCGCACGGTCCATCGCAGCAGTC ^a
UPM short	ACGCTGACGCTGAGCCTACCTGAC ^a
GSP1	TCCATTCTCAGTAACTCGC or CTTACTGGGGTGCTGGCTAT
GSP2	ACCCAGAACCTCCTTCGGAATTGTAGC

^aPrimers are adopted from Pinto and Lindblad, 2010; ^b absent sequence in the mouse genome is from Herold, Kurtz and Giegerich, 2008.

The second structure was predicted by Oligo 7 and the specificity in the mouse genome was checked by Primer-BLAST.

cDNA synthesis for 5' RACE

2-steps cDNA synthesis from total mouse testis RNA and mouse liver or spleen RNA as control was carried out using SuperScript™ II or SuperScript™ III Reverse Transcriptase (Invitrogen):

Protocol:

- Combine the following in a 0.2ml tube to denature the samples (Table 3-14):

Table 3-14. RT Denaturation Mix for 5' RACE

Component	3.5 μ l Reaction
Total RNA	1 μ g
GSP1 10 μ M	0.2 μ l
dNTPs 10 mM	1 μ l
Nuclease-free water	Up to 3.5 μ l

- Incubate the tube at 65°C for 5 min, then place on ice for at least 1 min.
- Prepare the following cDNA elongation Mix, adding each component in the indicated order (Table 3-15):

Table 3-15. RT Elongation Mix for 5' RACE

Component	6.5 μ l Reaction
10 \times RT Buffer	1 μ l
MgCl ₂ 25 mM	2 μ l
DTT 0.1 M	2 μ l
RnaseOut 40 U/ μ l	1 μ l
RT 200 U/ μ l	0.5 μ l

- Add 6.5 μ l of cDNA elongation Mix to each denatured RNA/primer mixture, mix gently, and collect by brief centrifugation. Incubate for 60 min at 50°C.
- Prepare the cDNA template-switching Mix, adding each component in the indicated order in Table 3-16.
- Add 10 μ l of cDNA template-switching Mix to each mixture, mix gently, and collect by brief centrifugation. Incubate at 42°C for 90 min.
- Terminate the reactions at 85°C for 5 min.
- Chill on ice.
- Collect the reactions by brief centrifugation.
- Add 1 μ l of RNase H to each tube and incubate the tubes for 20 min at 37°C. cDNA synthesis reaction can be stored at –30°C to –10°C or used

for PCR immediately.

Table 3-16. RT Template-Switch Mix for 5' RACE

Component	10 μ l Reaction
10 \times RT Buffer	1 μ l
MgCl ₂ 25 mM	2 μ l
TSO 10 μ M	2 μ l
Nuclease-free water	4.5 μ l
RT 200 U/ μ l	0.5 μ l

H-F PCR for 5' RACE

Protocol:

- Add 1 μ l of each cDNA as a template.
- Prepare a master mix for the appropriate number of samples to be amplified as follows and distribute the proper amount to each PCR tube (Table 3-17). Add the polymerase right before starting the cycling (Table 3-18).
- Check the amplified products by electrophoresis.
- Purify the PCR products and clone them into pEGFP vectors as described in section 3.2. Confirm the sequence by sanger-sequencing.

Table 3-17. PCR Reaction Mix for 5' RACE

Component	20 μ l Reaction		
5 \times HF Buffer	4 μ l		
dNTPs 8 mM	0.5 μ l		
GSP2 10 μ M	1 μ l	0.4 μ l	0.4 μ l
UPM LONG 10 μ M	0.14 μ l	0.06 μ l	/
UPM SHORT 10 μ M	1 μ l	0.4 μ l	/
U SENSE 10 μ M	/	/	0.4 μ l
cDNA	1 μ l		
Phusion DNA Polymerase 2U/ μ l	0.2 μ l		
Milli-Q Water	Up to 20 μ l		

Table 3-18. PCR cycling program for 5' RACE

Cycle Step	Temp. × Time	Cycles
Initial Denaturation	98°C × 30"	1
Denaturation	98°C × 10"	40
Extension	72°C × 45"	
Final Extension	72°C × 10'	1

3.4. Polyclonal antibody generation

To generate custom antibodies to the studied proteins, recombinant full-length proteins were expressed in *E.coli* and then purified protein was injected into rabbits for immunization. As a result, polyclonal antibodies against multiple epitopes throughout the sequence were obtained and used for the downstream applications.

3.4.1. Purification of recombinant protein

The recombinant target protein was produced in collaboration with the lab of Dr. Neus Ferrer Miralles (NBT, IBB-UAB, Barcelona, Spain) using a bacterial expression system. The whole process involves cloning the genes of interest into modified bacterial expression vector pET-28a (+)-TEV, the transformation of cloned genes into *E. coli* BL21(DE3) competent cells, inducing the bacterial host to highly express target protein, and purifying the target protein by affinity chromatography from *E. coli* cell lysate.

Cloning

Full-length sequences of the genes of interest were introduced to modified (+)-TEV vectors (NBT) (Figure 3-3) which carry an N-terminal 6xHis tag/TEV protease (TEVp) cleavage site/T7 tag configuration for bacteria expression. This results in the expression of the target protein having an N-terminal 6xHis-tag, which is necessary for its purification with immobilized metal affinity chromatography (IMAC). The recombinant protein also contains a TEVp cleavage site between the His-tag and the protein sequence

which is required for the removal of the His-tag before the injection to animals.

The cloning procedure mostly follows the standard cloning method as previously described (Section 3.2). Any modifications and additions are indicated below. Briefly, High-Fidelity PCR was performed using pre-constructed plasmid DNA (pEGFP-N1-gene of interest, Section 3.2) as a template and specifically designed primers (Table 3-19). PCR products were then purified and digested with restriction enzymes FastDigest NdeI and XhoI (Thermo Scientific). Meanwhile, the pET-28a (+)-TEV vector plasmid (NBT, UAB, Barcelona) was cut by NdeI and XhoI. A 3:1 molar ratio of digested insert DNA and vector DNA were ligated as the suggested amount by NEBioCalculator. 4ul of ligation reactions were transformed into 5-alpha Competent *E. coli* cells (New England Biolabs). 20 colonies were screened by a direct PCR (colony PCR, Section 3.2.6). Briefly, the PCR was performed using colonies as a template and a pair of primers including a 3' end gene-specific primer and a primer complementary to T7 promoter region (TAATACGACTCACTATAGGG) from the vector (schematic of primer design seen in Figure 3-2). Then plasmids were isolated from the culture of these colonies containing the correct size and orientation of the insert DNA. Once the sequences of isolated plasmids were confirmed by Sanger sequencing, the plasmids were transformed into BL21(DE3) competent cells (NBT, IBB-UAB, Barcelona).

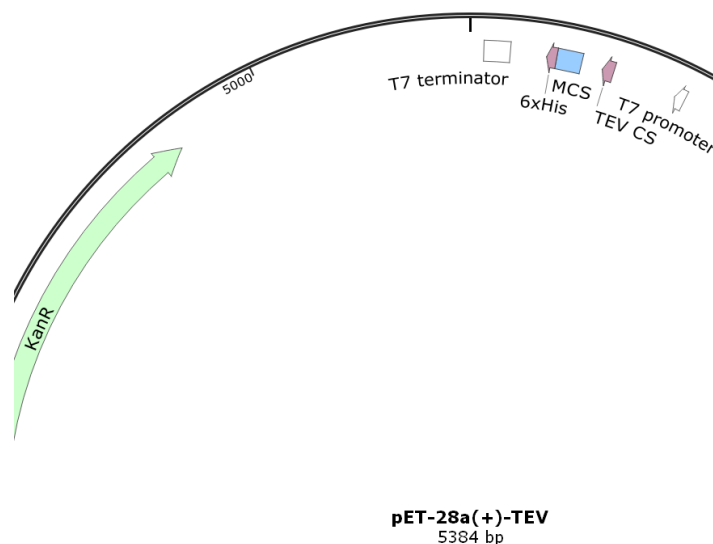


Figure 3-3. pET-28a(+)-TEV plasmid map

The sequence of gene of interest is inserted at multiple cloning sites (MCS) between TEVp cleavage site (CS) and 6xHis tag.

Table 3-19. pET-28a (+)-TEV cloning primer

Gene	Forward primer (5' → 3')	Reverse primer (5' → 3')
255P1	CAAc ^u catatgCCAGGAAAACTGAAGTTATCATG	CCGCctcgagtt ^a AGCTATTGCATTCCTTGGGC
355P1	CAAc ^u catatgTTGGACAAATTTACAGAAACAG	CGTActcgagtt ^a GCTAAGGACTTCATTAGAAGAGG

The uppercase sequences indicate the specific sequence to each gene; the italic uppercase sequences indicate the sitting sequence; the lowercase sequences indicate the NdeI (forward) and XhoI (reverse) cleavage sites; the underlined sequences indicate the stop codons.

The transformation was plated onto an LB agar plate with 30-50 µg/ml kanamycin and incubated overnight at 37°C. The next day, a single colony was streaked consecutively over four quadrants of the entire surface of a new kanamycin LB agar plate and incubated overnight at 37°C. Finally, well-isolated discrete colonies were obtained on the streaking plate. These single colonies were used directly for inoculating starter/overnight culture for protein expression and/or for preparing stock culture in 25% glycerol.

3.4.1.1. Protein expression – condition screen and scale-up

Transformed BL21(DE3) *E. coli* cells were grown in LB culture and induced with IPTG to express the target protein. For each target protein expression, a single colony was grown in LB with kanamycin first to obtain small freshly saturated cultures, called overnight or starter cultures. Then, starter cultures were used to inoculate small-scale cultures for screening the optimal protein expression condition, or large-scale cultures for purifying the target protein after the optimal expression condition was determined. The growth curves of *E. coli* cells from small or large-scale cultures were monitored by measuring cell density with a spectrophotometer. Once cell growth reached mid-way through the exponential phase, IPTG was added to induce protein expression at the designated conditions. Finally, post-induction cells were harvested and lysed for protein expression analysis by Western blot or protein purification.

Protocol:

Growing starter/overnight culture, day 1

- Work quickly and use an aseptic technique to avoid contamination under a class II laminar flow hood.
- Transfer 10 ml LB in 50ml conical tube for small-scale culture or 150 ml

LB in 1 L Erlenmeyer flask for large-scale culture with 30-50 µg/ml kanamycin.

- Inoculate each LB medium with a single colony from the streaking plate or glycerol stock of starter culture by touching the colony with a sterile tip or glycerol stock with a disposable inoculation loop, then dipping the tip or loop into the LB.
- Incubate at 37°C at 250 rpm ON.

Growing expression culture and monitoring growth curve, day 2

- Measure OD₅₅₀ of starter culture with a spectrophotometer (GENEQUANT 1300, Biochrom), referred to as OD_s.
- Prepare small-scale (150 ml) or large-scale (2-4 L) expression culture for monitoring growth curve:
 - Transfer LB medium (referred to as V_c) with 30-50 µg/ml kanamycin in Erlenmeyer flask: 150 ml in one 1 L flask for small scale, and 700 ml in 3-6 2 L flasks for large-scale.
 - Add the required volume of starter culture (referred to as V_s) based on the following formula:

$$OD_s \times V_s = OD_c \times V_c$$

$$OD_c = 0.05-0.1/\text{ml}$$

- Incubate at 37°C at 250 rpm.
- Measure OD_c after 1h incubation and then at every 10-15 min.
- Proceed to the next induction step when OD_c reaches 0.4-0.6/ml.

IPTG induction for expression, day 2

- For small-scale expression, before induction, remove 5 OD of culture (~ 4.0 x 10⁹ cells) as a negative control and harvest the cells as described below. For large-scale expression, a negative control is unnecessary.
- Calculate remained V_c after the removal for OD₅₅₀ measurements or/and negative control.
- Add the required volume of IPTG (1 M) to induce protein expression based on the following formula:

$$V_{IPTG} \times 1M = \text{Remained } V_c \times C_{IPTG}$$

$$C_{\text{IPTG}} = 0.5 \text{ mM}$$

- For small-scale expression, to screen the optimal condition, transfer 10 ml of culture to 9 new 50ml conical tubes and incubate every 3 tubes (as triplicates) at the following conditions:

37°C for 3 h (Harvest on the same day)

25°C ON

16 or 18°C ON

For large-scale expression, incubate all the cultures at the optimal condition.

Harvest the induced cells, day 3

For small-scale expression

- Measure OD_i of all the 9 cultures in tubes and transfer 5 OD of each culture to a new 50ml conical tube.
- Centrifuge for 5–10 min at 11000g at 4°C.
- Discard the supernatant.
- Resuspend each pellet with 1ml 1x PBS containing PI (EDTA-free protease inhibitor, Roche Diagnostics).
- Centrifuge for >1 min at 11000g at 4°C.
- Remove the supernatant carefully. The pellets can be stored at -80°C until cell lysis.

For large-scale expression

- Transfer each 700 ml culture to 1 L bottle (Beckman).
- Centrifuge at 5000 rpm at 4°C for 15 min.
- Discard the supernatant.
- Resuspend each pellet with 20 ml 1x PBS containing PI in 30 ml tubes.
- Centrifuge at 8000 rpm at 4°C for 15 min.
- Discard the supernatant. The pellets could be stored at -80°C until cell lysis.

3.4.1.2. Protein expression analysis for small-scale expression

The behaviors and favorable expression conditions of each target protein are unknown, hence the whole protein expression from small-scale cultures at different induction conditions was analyzed by SDS-PAGE electrophoresis and Western blot. According to the results, the best strategy for large-scale protein expression was made in terms of volumes for scale-up culture, induction time, temperature, and the requirement for protein solubilization.

Protocol:

- Resuspend each cell pellet with 1 ml 1x PBS with PI.
- Disrupt the cells by sonication (Sonifier, Marshall scientific) with 1 second on and 1 second off, at 10% amplitude for 2 min and then at 15% amplitude for 2 min.
- Centrifuge the disrupted cells at 13000 rpm at 4°C for 45 min.
- Transfer each supernatant (soluble protein) to a new tube without touching the pellet.
- Resuspend each pellet (insoluble protein) in 1ml 1xPBS with PI.
- Load both the soluble and insoluble protein samples for SDS-PAGE electrophoresis or store them at -80°C until use.
- Prepare the following samples with 4x Laemmli buffer and 1x PBS in 2ml screw-capped tubes,
 - Positive control–GFP protein
 - Negative control (without induction)-soluble, insoluble
 - Inducted at 37°C-soluble, insoluble x 3
 - Inducted at 25°C-soluble, insoluble x 3
 - Inducted at 16 or 18°C-soluble, insoluble x 3
- Denature at 95°C for 20 min for soluble samples and 40 min for insoluble samples.
- Load 10 ul of each denatured protein to TGX gel (Bio-Rad) along with 2 µl of protein standards-Precision Plus Protein™ All Blue Prestained Protein Standards and Unstained Protein Standards, Bio-Rad.
- Run the TGX gel at 300 volts for 27 min in Running buffer (25 mM Tris, 190 mM glycine, 0.1% SDS in distilled water).
- Expose the gel using a ChemiDoc Touch Imaging system.

- Prepare the transference sandwich:
 - Wet the bottom filter paper in the transfer buffer.
 - Activate the membrane in 100% ethanol for 30 s.
 - Rinse the membrane with transfer buffer.
 - Place it on top of the bottom filter.
 - Add the gel on top of the membrane.
 - Wet the top filter paper in transfer buffer and put it on the top.
- Perform protein transfer at 25 volts for 3 min with Trans-Blot® Turbo™ transfer system.
- Block the membrane in 5% non-fat milk in PBS at 4°C ON and incubate with 3 µl 6x His monoclonal antibody (1:5000, TAKARA 631212) in 15 ml milk at RT for 2 h. Alternatively, block at RT for 2 h followed by primary antibody incubation at 4°C ON.
- Wash the membrane with 1x PBST for 15 min twice and 1x PBS for 10 min.
 - Incubate with goat anti-mouse HRP conjugate antibody (Biorad 170-6516, 1:2000) in 10 ml PBS.
- Add ECL substrate (Bio-Rad) and expose the membrane with ChemiDoc Touch Imaging system .
- Analyze the images with the Imagelab software.

3.4.1.3. Protein extraction for large-scale expression

In the case that the expressed target protein was soluble, the cell pellets from large-scale *E.coli* culture were lysed with a high-pressure homogenizer (AVESTIN EMULSIFLEX C5, ATA scientific) and the cell lysate in the supernatant was directly used for protein purification.

Protocol:

- Resuspend all the cell pellets with binding buffer (20 mM Tris-HCl pH 8.0, 0.5 M NaCl, in Milli-Q water, 50 ml per 1 L culture) with PI by pipetting on ice.
- Transfer all the suspension to a new 250 ml beaker.
- Disrupt the cells with a high-pressure homogenizer (AVESTIN EMULSIFLEX C5, ATA Scientific) at 1000–1500 psi pressure for 2-3

rounds.

- Centrifuge the lysis at 12000 g at 4°C for 45 min.
- Pass the supernatant through 0.45 µm and 0.22 µm PVDF membrane filter (Merck) in turn before application for chromatography.

In the case that the expressed target protein was insoluble and accumulated in so-called inclusion bodies (IBs) in the pellets after cell lysis, the IBs were solubilized to release protein for purification.

Protocol adapted from (Peternel et al. 2008):

- Weigh the pellets from *E. coli* culture and resuspend in Tris-HCl buffer (10mM pH 8.0 in Milli-Q water, in 4 ml/g).
- Perform 3 rounds of disruption with a high-pressure homogenizer at 1000–1500 psi pressure.
- Collect all the lysate together and centrifuge at 10,000 g for 45 min. Save the supernatant (SN₁).
- Wash the pellet with Milli-Q water and centrifuge at 10,000 g for 30 min. Save the supernatant (SN₂).
- Repeat the previous step and save the supernatant (SN₃).
- Weigh the pellet and resuspend with the solubilization buffer (40 mM Tris-HCl, 0.2% N-lauroyl sarcosine, 40 ml/g).
- Incubate for 16-24 at RT with rotary shaker gently.
- Centrifuge at 15000 g for 30 min. Save both the pellet (P₁) and the supernatant (SN₄). SN₄ is supposed to contain the solubilized protein.
- Add the proper volume of 1 M NaCl to SN₄ to reach a final concentration of Tris-HCL at 20 mM and NaCl at 0.5 M.
- Pass the sample through a 0.22 µm PVDF membrane filter before application for chromatography. The samples of SN₁, SN₂, SN₃, SN₄, and P₁ could be loaded along with purified protein when performing SDS-PAGE electrophoresis analysis after protein purification.

3.4.1.4. His-tag protein purification with affinity chromatography

The cell lysate or solubilized protein samples were loaded onto HisTrap HP

column (Cytiva) operated with ÄKTA pure liquid chromatography system to purify His-tagged target protein using the IMAC method. IMAC is based on the interaction of a protein with certain amino acid residues (e.g., histidine, cysteine, and tryptophan) on the surface with metal ions (e.g., Ni²⁺, Cu²⁺, Zn²⁺, Co²⁺) immobilized via a chelating ligand. HisTrap HP column (Cytiva) is pre-charged with immobilized nickel (Ni²⁺) by a chelating resin. When the sample passes through the column, target proteins are retained as they strongly bind to the resin due to the 6 Histidine residues, while other proteins in the cell lysate or solubilized protein sample do not bind at all or just weakly. Then the captured His-tagged protein was recovered by eluting the column with a high concentration of imidazole.

Protocol:

- Install HisTrap HP column to ÄKTA pure chromatography system.
- Wash the ÄKTA pure system and pump with Milli-Q water.
- Wash the column with 5 column volumes of Milli-Q water at a flow rate of 1 column volume/min.
- Equilibrate ÄKTA pure system and pump by binding buffer (20 mM Tris-HCl pH 8.0, 0.5 M NaCl in Milli-Q water, 0.22 µm PVDF membrane filtered).
- Equilibrate the column with 5–10 column volumes of binding buffer at a flow rate of 1 column volume/min.
- Load the filtered cell lysate sample or solubilized protein sample with an external pump or 50 ml superloop onto the column at a flow rate of 1 column volume/min. Collect the flow-through sample.
- Wash the column with binding buffer until the absorbance reaches a steady baseline. Collect the washed sample.
- Elute the column with elution buffer (20 mM Tris-HCl pH 8.0, 0.5 M NaCl, 0.5 M Imidazole in Milli-Q water, 0.22 µm PVDF membrane filtered) using linear gradient over 20 column volumes a flow rate <1 column volume/min.
- Monitor the absorbance. Hold the elution buffer at a certain percentage when a peak of absorbance appears and continue the gradient when the peak ends. Collect the elution samples.
- Regenerate the column by washing it with 5–10 column volumes at a flow

rate of column volume/min.

- Wash the system and pump with Milli-Q water at a flow rate of column volume/min.
- Wash the system, pump, and column with 20% ethanol at a flow rate < column volume/min.
- Uninstall the column. Cover with parafilm and store at 4°C. The column could be repeatedly used up to 3 times.
- Load the sample before purification, the flow-through sample, the washed sample, and the three elution samples corresponding to the starting point, the highest point, and the ending point of each peak.
- Perform Western Blot analysis to identify the existence and purity of target protein in elution samples as seen in section 3.4.1.2.
- Group the elution samples from identified peaks and transfer them to a new tube as initial purified protein sample Go. Save 100 µl Go aliquot.
- Measure the protein concentration of Go by Nanodrop (Thermo Scientific) and calculate the total amount of protein in Go.

3.4.2. Sample preparation for animal injection

The His-tags of purified target protein might cause immune response during animal immunization and generate unspecific antibodies. Hence, removing His-tags from target protein is necessary before animal injection whenever possible. The removal was done by the cleavage of TEV protease at the TEV cleavage site of the purified protein. Then, any proteins with an affinity of binding to the column were separated from the target protein with removed His-tag using IMAC. Finally, the target protein was prepared in PBS and sterilized filter before injecting it to animals.

Protocol:

- Dialyze sample Go in 3 L TEVp reaction buffer at RT for 3 h:
 - Submerge the tubing (12-14 kDa, Spectrum) containing all the Go samples in 1 L TED buffer (50 mM Tris-HCl pH 8.0, 0.5 mM EDTA, 1 mM DTT in Milli-Q water).
 - Gently spin the tubing at RT for 1 h by stirring.

- Submerge the tubing in 1 L new TED buffer and spin at RT for 1 h.
 - Repeat the previous step.
 - Transfer the sample from tubing to a new tube.
 - Centrifuge at 14000 g at 4°C for 15 min.
 - Observe if there is any precipitation and transfer the supernatant to a new tube as TED-dialyzed sample G₁. Save 100 µl G₁ aliquot.
- Measure the G₁ protein concentration by Nanodrop and estimate the total amount of protein in G₁. Estimate the protein loss during dialysis by comparing the amount of protein in G₀ and G₁ if there is any precipitation observed.
 - Add 1 mg TEV protease (NBT or Thermo Fisher Scientific) to each 3 mg G₁ protein.
 - Gently shake the tube at RT ON.
 - Centrifuge at 14000 g at 4°C for 15 min.
 - Transfer the supernatant in a new tube as TEVp-digested sample G₂. Save 100 µl G₂ aliquot.
 - Dialyze sample G₂ in 3 L binding buffer at RT for 3 h:
 - Submerge the tubing containing all the G₂ samples in 1 L binding buffer (20 mM Tris-HCl pH 8.0, 0.5 M NaCl in Milli-Q water, 0.22 µm PVDF membrane filtered).
 - Gently spin the tubing at RT for 1 h by stirring.
 - Submerge the tubing in 1 L new binding buffer and spin at RT for 1 h.
 - Repeat the previous step.
 - Transfer the sample from tubing to a new tube.
 - Centrifuge at 14000g at 4°C for 15 min.
 - Observe if there is any precipitation and transfer the supernatant to a new tube as binding buffer-dialyzed sample G₃. Save 100 µl G₃ aliquot.
 - Pass sample G₃ through 0.22 µm PVDF membrane filter.

- Load the filtered sample G₃ to HisTrap HP column with ÄKTA pure chromatography system and wash the column with binding buffer.
- Monitor the absorbance to confirm the detection of protein without His-tag while loading and washing.
- Collect carefully the flow-through sample and the wash sample and load both of them along with sample G₀–G₃ to TGX gel.
- Perform Western blot analysis. The flow-through sample should contain most of His-tag removed target protein and the washed sample might also contain some.
- Based on the WB result, dialyze the flow-through or/and wash sample in 3 L PBS buffer at RT for 3 h:
 - Submerge the tubing containing protein sample in 1 L 1X PBS buffer (pH 7.2-7.6).
 - Gently spin the tubing at RT for 1 h by stirring.
 - Submerge the tubing in 1 L new PBS buffer and spin at RT for 1 h.
 - Repeat the previous step.
 - Transfer the sample from tubing to a new tube.
 - Centrifuge at 14000 g at 4°C for 15 min.
 - Observe if there is any precipitation and transfer the supernatant to a new tube.
- Measure protein concentration in the supernatant by Nanodrop and estimate the total amount of target protein without his tag.
- Load the sample to Amicon® Ultra centrifugal filter (Millipore).
- Spin the device at 4°C to concentrate the sample to at least 0.2 mg/ml. While spinning, the sample volume decreases. When the remained sample volume reaches the expected volume (calculated by the total amount of protein/0.2 mg/ml), stop the spinning and confirm the concentration by Nanodrop.
- Sterilize the concentrated sample using a 0.2 µm filter.
- The sterile His-tag removed target protein sample in PBS is ready for animal injection.

3.4.3. Immunization of animals

Two rabbits were immunized for each polyclonal antibody in collaboration with Dr. Antoni Iborra (SCAC, Barcelona, Spain). Briefly, pre-immune serum was collected from each animal on Day 0 as control; then animals were injected with 0.05-0.5 mg/dose of antigen on Day 1 as a primary injection, on Day 14 as of 1st booster, on Day 28 as 2nd booster and/or on Day 42 as 3rd booster. Post 2nd or 3rd booster, 1-2 ml sera were tested by ELISA titration to verify the immunization response. Once verified, immunization was stopped and two bleeds (~100 ml total per rabbit) were collected from the rabbits. Immunoglobulins (IgG) were isolated from 1-2 ml sera by affinity chromatography using Affi-Prep protein A resin cartridge (Bio-Rad) and used for the required applications.

3.5. Mouse mutation and phenotyping

3.5.1. CRISPR/Cas9 knockout

To analyze the functions of the genes of interest, CRISPR/Cas9 system was used to generate *Bend2* knockout mice in collaboration with Dr. Anna Pujol (CBATEG, UAB, Barcelona, Spain) and *Usp44* knockout mice in collaboration with Dr. A. Pendás (CIC-CSIC, Salamanca, Spain).

For *Bend2* knockouts, sgRNAs were designed using CRISPR DESIGN TOOLS (Millipore Sigma) (Table 3-20). A pair of gRNAs with minimum off-target and maximum on-target activity were selected to specifically target at sequences that encode essential protein domains of each gene. sgRNAs were synthesized by Sigma and microinjected together with Cas9 protein into the pronucleus of C57BL/6JOlaHsd zygotes. Edited founders were identified by PCR with primers flanking the targeted region and HincII digest. PCR products were further purified and determined by Sanger sequencing. 3-4 selected founders carrying desired deletions were crossed with wild-type C57BL/6JOlaHsd to eliminate possible off-target mutations to generate pure heterozygotes. Female heterozygotes (+/-) were crossed with wild-type male (+/y) for wild-type female (+/+), heterozygous female (+/-), wild-type male (+/y), and mutant

male (-/y) offsprings, and crossed with mutant male (-/y) for mutant female (-/-), heterozygous female (+/-), wild-type male (+/y) and mutant male (-/y) offsprings. Mice from at least F₂ generation were analyzed for their phenotyping. Male mutants were all analyzed together with their wild-type littermates. Female mutants were analyzed with wild-type mice from other litters at the same age.

For Usp44 knockouts, crRNAs were designed using Custom Alt-R® CRISPR-Cas9 guide RNA (https://eu.idtdna.com/site/order/designtool/index/CRISPR_CUSTOM) (Table 3-20). The crRNAs were produced by chemical synthesis at IDT and pre annealed to form the final gRNA. A mixture containing the sgRNAs, recombinant Cas9 protein (IDT) was microinjected to both pronucleus and cytoplasm of zygotes (F₂ hybrids between strains C57BL/6J and CBA/J). Edited founder mice were identified by PCR with primers flanking the targeted region. PCR products were subcloned into pBlueScript (Stratagene) followed by standard Sanger sequencing. 3-4 selected founders carrying desired deletions were crossed with wild-type C57BL/6J OlaHsd to eliminate possible off-target mutations to generate pure heterozygotes. Female and male heterozygotes were interbred. Mice from at least F₂ generation were analyzed. Mutants were all analyzed together with their wild-type littermates.

Table 3-20. gRNAs for CRISPR/Cas9 knockout

Name	Target Region	Sequence (5' → 3')	PAM	Strand
BEND2 gRNA1	EXON4 within	AGTAGCAGGCTGCATAAGT	GGG	Antisense
BEND2 gRNA2	EXON4 downstream	AGACCAGCCTTATTGACCA	TGG	Sense
USP44 gRNA1	EXON3 upstream	AGCAACCTAGACCTAATCTA	TGG	Sense
USP44 gRNA2	EXON3 downstream	AGTCTAACCCAAGATAAACT	TGG	Antisense

3.5.2. Mouse Genotyping

3.5.2.1. Genomic DNA extraction

Genomic DNA was extracted from mouse tails and applied for the downstream genotyping PCR.

Protocol:

- Place 0.5 cm of the tail into a 1.5ml tube.
- Add 490µl lysis buffer (0.1 M Tris-HCl pH 8.5-9, 0.2 M NaCl, 0.2% SDS and 5 mM EDTA in Milli-Q water) and 10µl proteinase K (20 mg/ml, Roche Diagnostics).
- Incubate at 56°C overnight.
- Centrifuge at 13200 rpm for 15 min.
- Transfer the supernatant to a new 1.5 ml tube with pre-added 500µl isopropanol. Shake vigorously to allow DNA precipitating.
- Centrifuge at 13200 rpm for 3 min.
- Discard the supernatant as much as possible.
- Add 500 µl cold 70% ethanol and mix by shaking.
- Centrifuge at 13200 rpm for 3 min.
- Remove the supernatant and dry the pellet at 60°C for 10-15 min.
- Resuspend the pellet with 100µl Milli-Q water and incubate at 60°C for 10 min.

3.5.2.2. Genotyping PCR

Genomic DNA was amplified by using NZYTaQ II 2x Green Master Mix with self-designed primers to identify wild-type or mutated alleles by the product size (Table 3-21 and 22). Primers were specific to each genomic sequence of each gene and designed using Primer-BLAST (NCBI). For each mouse line, two pairs of primers were employed. One primer pair (BEND2 GenoF and GenoR or USP44 GTP-F and GTP-R) was used in the first round of PCR; the identified possible homozygous BEND2 females and USP44 animals were subjected to the second round of PCR using the second pair primers, BEND2 GTP Forward and Reverse wt or USP44 GTP Forward and Reverse Wildtype, to confirm the homozygosity.

Protocol:

- Thaw the master mix and set up the PCR reaction on ice.
- Add 1 µl of template genomic DNA to the PCR tubes.
- Mix appropriate times of the remained components specified in Table 3-23 and quickly vortex.

- Pipette 19 μ l of the mix to each tube.
- Perform PCR using the cycling as Table 3-4.

Table 3-21. BEND2 genotyping primers

Primer	Allele specificity	Sequence (5' \rightarrow 3')	Product size (bp)
BEND2 GenoF	+/-	TTGCCAGTGGGGTATTACGA	
BEND2 GenoR	+/-	CTGGAAGGCAGGAAGTTTAACA	693 and 200-400
BEND2 GTP Forward	+/-	TTTGCTCCACTGTTTCACGC	
BEND2 GTP Reverse wt	+	TCCCTTAAACTGCCAACAACA	539

Table 3-22. USP44 genotyping primers

Primer	Allele specificity	Sequence (5' \rightarrow 3')	Product size (bp)
USP44 GTP-F	+/-	GCCAAAGAAACACACATCCCTCC	
USP44 GTP-R	+/-	TGTACCCTCAACCCACCAAAAAGT	551/263
USP44 GTP Forward	+/-	ACACGGCTGGCGTTCATTTC	
USP44 GTP Reverse Wildtype	+	CAGCTCTACCTCCTTCGGAAT	697

Table 3-23. Genotyping PCR reaction mix

Component	20 μ l Reaction
genomic DNA	1 μ l
Forward Primer 10 μ M	0.5 μ l
Reverse Primer 10 μ M	0.5 μ l
Milli-Q Water	8 μ l
NZYTag II 2x Green Master Mix	10 μ l

3.5.3. Tissue fixation, embedding, and sectioning

To perform microscopic analysis, fresh mouse tissues were fixed with PFA for immunofluorescence/TUNEL assay or with Bouin's for the use of PAS (Periodic Acid Schiff) staining. After fixation, tissues were embedded in wax and cut into very thin slices mounted on glass slides.

Protocol:

- Dissect the tissue from the animal and immediately immerse it into

- fixative solution, freshly made 4% PFA (0.4 g paraformaldehyde dissolved in 10 ml PBS, pH 7.4) or Bouin's fixative. Let it sit ON at 4°C.
- Wash in PBS for 30 min at 4°C twice.
 - Dehydrate the tissue in a series of ethanol with increasing concentration:
 - 50% Ethanol 30 min 4°C
 - 70% Ethanol 30 min 4°C (can be kept for months)
 - 85% Ethanol 30 min RT
 - 96% Ethanol 30 min RT (plus 0.1% eosin for fetal ovaries)
 - 100% Ethanol 30 min RT x2
 - Clear the ethanol with histoclear and infiltrate paraffin:
 - Histoclear 30 min RT x3
 - Histoclear: Paraffin (1:1) 45 min 56°C (held in cassettes)
 - Paraffin 2 h 56°C
 - Paraffin 16 h 56°C
 - Embed the tissue in paraffin to form a block:
 - Place the tissue infiltrated with paraffin in a mold filled with molten paraffin.
 - Carefully orientate the tissue to determine the plane of the section.
 - Place a cassette on top of the mold.
 - Leave it to solidify on a cold plate.
 - Remove the block and its attached cassette.
 - Store the block at 4°C.
 - Section the paraffin block:
 - Cut the block into 6-7 µm slices using a microtome.
 - Flatten the sections in the floatation bath.
 - Transfer the sections onto poly-L-lysine coated slides.
 - Leave the slides dry at 37°C ON.

3.5.4. Immunohistochemistry staining

To detect the location of the target protein in mouse tissues, immunohistochemistry staining was applied to the tissue sections. After deparaffinized

and rehydrating the slides, an antigen retrieval step was performed to expose the epitopes masked by PFA fixation to allow antibodies to bind.

Protocol:

Deparaffinization and rehydration

Immerse the slides in the following sequence:

Xylene	5 min	x3
100% Ethanol	3 min	x2
96% Ethanol	2 min	x2
70% Ethanol	2 min	
distilled water	2 min	(can be kept until next step)

Antigen retrieval

- Pre-heat sodium citrate buffer (10 mM Sodium citrate, 0.05% Tween 20, pH 6.0) or Tris-EDTA buffer (10 mM Tris, 1 mM EDTA, 0.05% Tween 20, pH 9.0) to 95-100° C in a Coplin jar placed in a water bath.
- Put the slides into the jar and heat the slides for 30 min.
- Remove from the water bath and cool down by rinsing with running distilled water for 2 min.

Immunostaining was performed as described in section 3.3.5 and antibodies were indicated in Table 3-24.

3.5.5. PAS-Hematoxylin staining

To analyze the cell count and structure of tissue sections, PAS-Hematoxylin (PAS-H) staining was performed. PAS stains glycogen-rich structures in tissues and Hematoxylin counterstains nucleic acids.

Protocol:

- Deparaffinize and rehydrate the tissue sections as described in section 3.5.4.
- Oxidize for 10 min by immersing the slides in 1% Periodic Acid solution
- Wash in distilled water for 3 min twice.
- Place in Schiff's reagent for 30 min in darkness.
- Wash in sulfurous water (10% Potassium metabisulfite, 0.1 M HCl in

- Milli-Q water) for 3 min twice.
- Wash in distilled water for 3 min twice.
 - Counterstain in Mayer's Hematoxylin for 1 min.
 - Rinse in running tap water to remove Hematoxylin excess.
 - Dehydrate the slides by immersing in the following sequence:
 - 70% Ethanol 2 min x2
 - 96% Ethanol 2 min x2
 - 100% Ethanol 3 min x2
 - Xylene 5 min x2
 - Mount with DPX mounting medium and analyze with an Optical microscope. Images were captured using Zeiss Axioskop microscope and processed using Photoshop.

3.5.6. TUNEL assay-*In situ* cell death detection

To detect and quantify cell apoptosis in tissue sections, TUNEL assay (In Situ Cell Death Detection Kit, Fluorescein, Roche Diagnostics) was performed as it detects DNA strand breaks generated during apoptosis by labeling the free 3'-OH termini with fluorescein-dUTP catalyzed by terminal deoxynucleotidyl transferase (TdT) enzyme.

Protocol:

- Deparaffinize and rehydrate the tissue sections as previously described.
- Wash in PBS for 2 min at RT.
- Immersing the slides in 0.5% Triton X-100 in PBS for 15 min for permeation.
- Wash in PBS for 2 min twice.
- Add 100 µl of background reducing solution (Dako) to each slide and incubate for 15 min at RT to remove the background.
- Rinse in PBS for 2 min.
- Add 5-10 µl of TUNEL reaction mixture (10% TdT enzyme solution in fluorescein-dUTP label solution) onto each section. Cover the slide with parafilm and incubate for 1 h at 37°C in a humid chamber.
- Wash in PBS for 5 min three times.

- Mount with 15 μ l DAPI (0.1 μ g/ml in Vectashield antifade mounting medium) and cover with a coverslip.
- Analyze the results with an epifluorescence microscope (Zeiss Axioskop).

3.5.7. Oocyte nuclei spreading

To study the events occurring during the first meiotic prophase in mice, chromosome spreads were prepared from fresh fetal and perinatal ovaries for females and frozen adult testis for males. The preparation of spermatocyte spread follows the same protocol as seen in section 3.3.3. The spread preparation for oocytes is described here.

Protocol:

- Dissect the females under a stereomicroscope (Nikon SMZ-1).
- Transfer ovaries in pairs from each female to one well containing 500 μ l of M2 medium (Sigma-Aldrich) in the first row of a 24-well plate. Repeat this for all the females.
- Add Collagenase (Sigma-Aldrich) to the M2 medium (Final concentration, 2.5 mg/ml) in the wells. Mix well by carefully pipetting.
- Incubate the ovaries in the collagenase for 30 min at 37°C.
- Transfer the ovaries to the wells in the second row containing 500 μ l of hypotonic buffer (30 mM Tris-HCl pH 8.2, 50 mM Sucrose, 17 mM Sodium Citrate, 5 mM EDTA, 0.5 mM DTT, 1x PI [Roche Diagnostics] in Milli-Q water) under the stereomicroscope.
- Incubate the ovaries for 30 min at RT.
- Transfer the ovaries to the wells in the third row containing 60 μ l of 100 mM sucrose under the stereomicroscope.
- Disaggregate the ovaries by pipetting under the stereo microscope to create a single-cell suspension.
- Distribute 10 μ l of the cell suspension onto 6 slides.
- Add 40 μ l of fixative solution (1% PFA, 5 mM Sodium Borate, 0.15% Triton X-100, 3 mM DTT, 1x PI in Milli-Q water, pH 9.2).
- Let the slides sit for 2 h in a closed humid chamber to fix the cells.
- Dry the slides under a fume hood for 20 min.

- Wash the slides four times in 0.4% Photoflo (Kodak) solution for 2 min. Samples of different genotypes were washed separately.
- Let the slides air dry and store at -80°C until use.

Immunostaining on the spreads was performed following previous protocol in section 3.3.5 and antibodies were indicated in Table 3-24.

Table 3-24. Antibodies used for immunostaining for mouse phenotyping

Antibody	Host	Dilution	Source
Anti-SYCP3	Mouse	1:200	Abcam
Anti-SYCP3	Rabbit	1:200	Abcam
Anti-SYCP1	Rabbit	1:200	Abcam
Anti-phospho-Histone H2A.X	Mouse	1:400	Millipore
Anti-MLH1	Mouse	1:50	BD Biosciences
RPA32 (4E4)	Rat	1:100	Cell signalling
Anti-RAD51 (ab-1)	Rabbit	1:100	Millipore
Anti-CXorf20	Rabbit	1:100	Abcam
Anti-Ubiquitin	Rabbit	1:50-100	Abcam
Cy3 anti-mouse	Goat	1:200-400	Jackson Immunoresearch
Cy3 anti-rat	Goat	1:200	Thermo Fisher
FITC anti-Rabbit	Goat	1:200	Jackson Immunoresearch
FITC anti-Mouse	Goat	1:200	Millipore
Alexa Fluor 594 anti-Rabbit	Donkey	1:200	Invitrogen

3.5.8. Follicle count and classification

To quantify the follicles in adult ovaries, the ovary was cut at 6-8 μm thickness and every 8-10 sections are mounted on one slide. Sections of 16-20 slides were cut per ovary, representing usually half of one wild-type ovary or half to the entire of one mutant ovary. One every two to three sections are counted per slide, and 5 slides were counted per ovary. Follicles were only counted if a visible oocyte nucleus was present. Follicles were classified into primordial follicles (with one layer of flat granulosa cells), primary follicles (with one layer of cuboid granulosa cells), secondary follicles (with more than one layer of granulosa cells), and antral follicles (with the antrum). The counting and classification were performed under the bright field microscope.

3.6. Microscopy, imaging process, and data analysis

3.6.1. Microscopy and image capture

PAS-Hematoxylin stained ovary sections were observed on a brightfield microscope Zeiss Axioskop and images were captured with a ProgRes Jenoptik camera using software ProgRes Capture Pro 2.7.7.

The fluorescent samples were examined by Zeiss Axiophot microscope and the images were captured with a Point Gray Research, Inc. camera with the ACO XY Software or ACOPT-Drecera (A.COLOMA Open microscopy). This setup was also applied to the image capture of PAS-Hematoxylin stained testis sections.

3.6.2. Image process and analysis

All the images were processed by Adobe Photoshop. Fluorescence intensity was quantified by ImageJ; fluorescence signals were counted manually or by ImageJ.

3.6.3. Statistical analysis

Data analysis and statistical inference were performed using GraphPad Prism 8 software.

Chapter 4

Results

4.1. Expression profile of candidate genes in mouse tissues

To identify candidate genes possibly involved in meiotic prophase I, we took advantage of several unannotated transcripts detected in 14 dpp wild-type mouse testis from our previous RNA sequencing analysis (Marcet-Ortega M. and Roig I., unpublished).

We first performed bioinformatic analysis to process these transcripts in collaboration with the Genome Assembly and Annotation team (Centre Nacional d'Anàlisi Genòmica, Barcelona). Briefly, all the transcripts were assembled, assessed for their protein-coding ability, and analyzed for their potential function, followed by the building of CDS of each transcript ensured with quality control. Consequently, a list of 104 putative novel non-annotated genes coding sequences for 203 transcripts and 160 proteins was obtained (Figure 4-1, Supplementary Table 1). Further, we continued the *in silico* analysis of these putative novel genes studying their homology within the animal kingdom and possible functionality of the predicted proteins with Gene Ontology (GO) term enrichment – statements of computational or experimental based gene function, etc. (Supplementary Table 1). It's worth noting that the RNA-seq transcripts were initially compared to *Mus musculus* genome assembly GRCm38.p4, while our study was ongoing, some of these unannotated genes were annotated as predicted genes according to the latest GRCm39.

To define the expression profile of these genes in mice, we performed RT-PCR with specific primers to each gene and total RNA from adult testis, adult ovary,

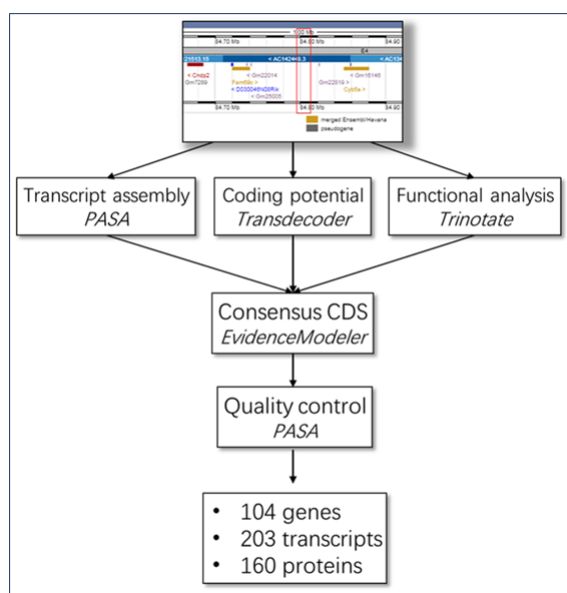


Figure 4-1. Finding novel putative gene strategy

The transcripts processing analysis was performed in collaboration with the Genome Assembly and Annotation Team from CNAG (Centro Nacional de Análisis Genómico, Spain). Transcripts were aligned by PASA (Program to Assemble Spliced Alignments), TransDecoder identified the coding regions, the functional annotations were analyzed by Trinotate. The consensus coding sequences were combined by EVM (EVIDENCEModeler).

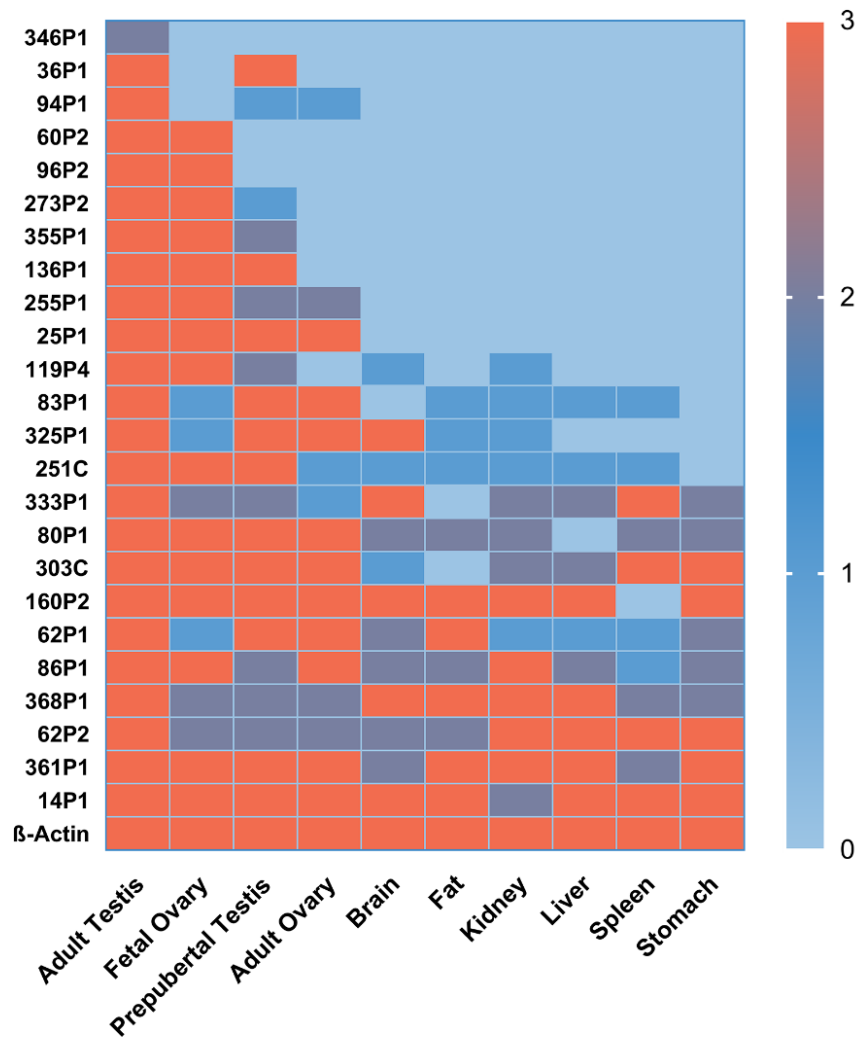
prepubertal testis (3-10 dpp), fetal ovary (16-18 dpc), brain, fat, kidney, liver, spleen and stomach. However, two significant difficulties caused the RT-PCR analysis in this panel of tissues was eventually only performed on 24 of the candidate genes (Figure 4-2). First, we could not design specific primers for most single-exon candidates (51 genes) or other multi-exon genes (7 genes). Second, after several attempts, RT-PCR failed to amplify any desired products for 22 genes. We also studied the expression of 11 single-exon genes in adult testis and fetal ovaries, 5 of which were detected in both tissues (Figure 4-3).

All 24 genes were expressed in adult testis, consistent with their origin from the 14 dpp mouse testis RNA library. Among them, fourteen were expressed in most or all of these six somatic tissues (14P1, 62P1, 62P2, 80P1, 83P1, 86P1, 119P4, 160P2, 251C, 303C, 325P1, 333P1, 361P1, and 368P1; Figure 4-2A). Ten were specifically expressed in the gonads, but not in any somatic tissues (25P1, 36P1, 60P2, 94P1, 96P2, 136P1, 255P1, 273P2, 346P1, and 355P1; Figure 4-2A). Notably, two of these ten gonad-specific genes (36P1 and 346P1) were exclusively expressed in the testis. Seven genes were preferentially expressed in both adult testis and fetal ovary (25P1, 60P2, 96P2, 136P1, 255P1, 273P2, and 355P1). Furthermore, the other gonad-specific gene (94P1) was not expressed in the fetal ovary but the adult testis and ovary (Figure 4-2).

To study the temporal expression pattern of the gonad-specific genes during spermatogenesis, we performed additional RT-PCR with total RNA from prepubertal mouse testis from 2 to 16 dpp (Figure 4-4). The analysis revealed that most of these gonad-specific genes started to express before 2 dpp, earlier than the onset of the first wave of spermatogenesis (during the second week after birth). However, 94P1, 60P2, and 273P2 genes were detectable much later at 10, 12, and 16 dpp, respectively, corresponding to the first meiotic prophase I (Soh et al. 2017). In agreement with what we found before (Figure 4-2), we failed to detect the expression of gene 346P1 in prepubertal testis, suggesting that this gene is expressed in post-meiotic cells (Figure 4-4).

In females, meiosis occurs in a semi-synchronous wave when oocytes enter prophase I during fetal development and arrest at the end of meiotic prophase I around two days after birth. In contrast, in males, meiosis occurs periodically and asynchronously after puberty, resulting in testis containing meiotic prophase I

A



B

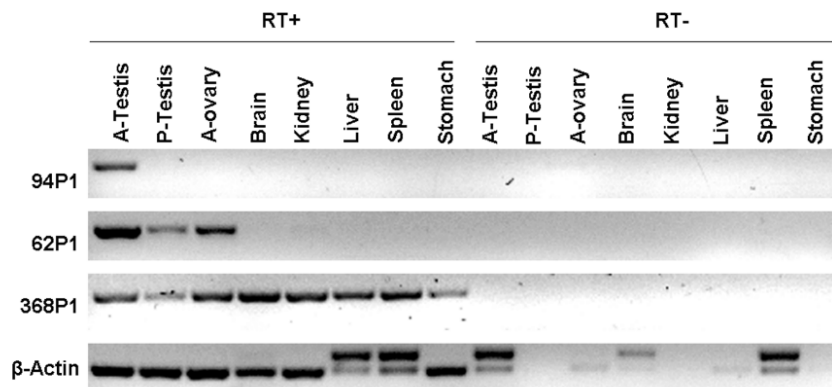


Figure 4-2. Expression profile of candidate genes in mouse tissues

(A) RT-PCR expression heatmap of 24 candidate genes in 10 different mouse tissues. RT-PCR in each tissue was repeated with samples from 3 different animals. Value: times of being detected. Prepubertal testis: 3-10 dpp; fetal ovary: 16-18 dpc; spermatogenesis-specific gene: 36P1 and 346P1; meiosis-specific gene: 25P, 60P2, 96P2, 136P1, 255P1, 273P2, and 355P1); gene 94P1 is absent in fetal ovary but present in adult ovary and testis. (B) Representative RT-PCR result. RT (+): experimental group; RT (-): minus RT control.

spermatocytes throughout adulthood. Therefore, expression of 25P1, 60P2, 96P2, 136P1, 255P1, 273P2, and 355P1 restricted to the adult testis and 18 dpc fetal ovary is compatible with the assumption that these genes are specifically expressed during meiotic prophase, and thus these could be meiosis-specific genes. For the other 19 genes that were also expressed in both adult testis and 18 dpc fetal ovary, we cannot exclude their possible involvement in meiosis in both sexes. Expression of 36P1 and 346P1 restricted to testis indicates that they are spermatogenesis-specific. Moreover, the fact that 36P1 was found in testis on day two after birth suggests that it might be involved in early spermatogenesis. Furthermore, the upregulation of the two meiosis-specific genes, 60P2 and 273P2, and one spermatogenesis-specific gene, 94P1, when meiosis commences in testis during the second week after birth (10-16 dpp) demonstrate that they might also have roles in meiosis, at least in males.

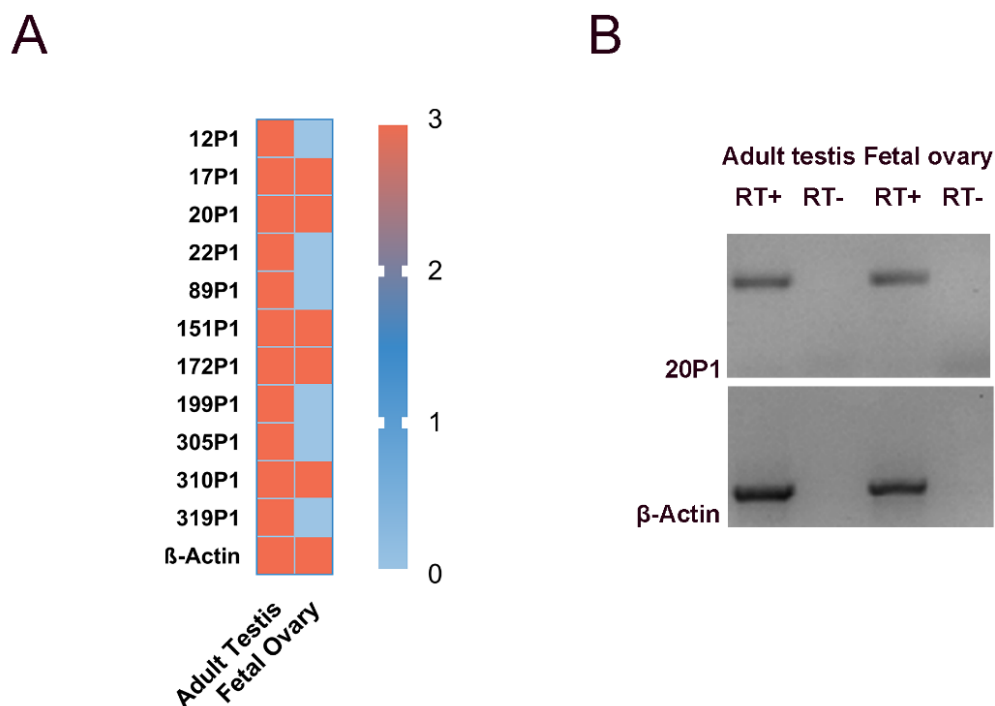


Figure 4-3. Expression of single-exon genes in mouse gonad tissues

(A) Expression heatmap of 11 single-exon candidate genes in mouse adult testis and fetal ovary by RT-PCR. Experiments were repeated with samples from 3 different animals. Value: times of being detected. Fetal ovary: 16-18 dpc. (B) Representative RT-PCR result; RT (+): experimental group; RT (-): minus RT control.

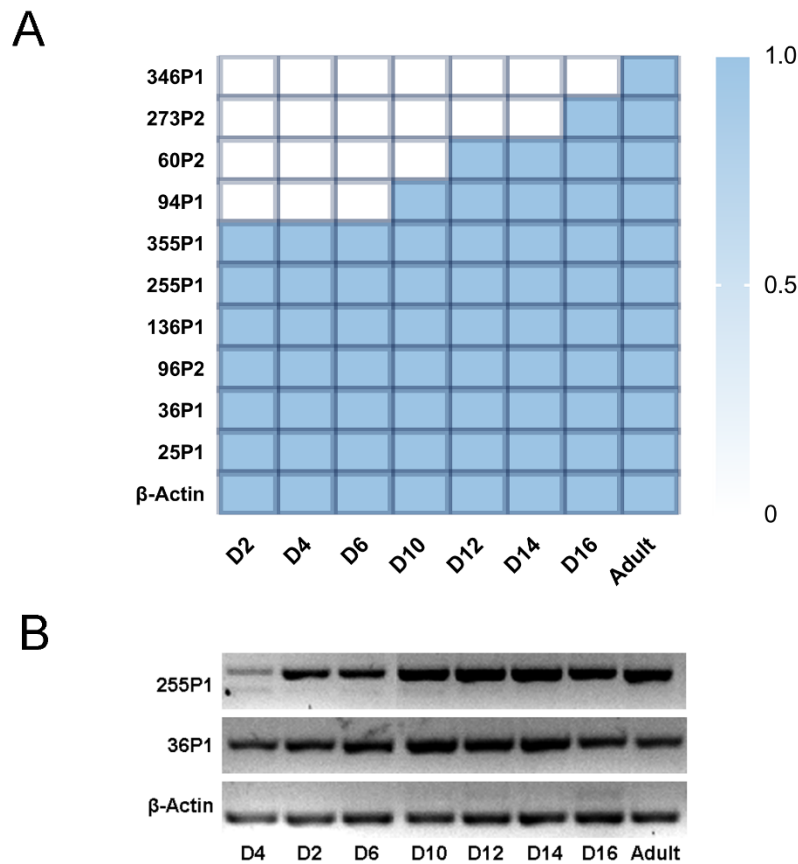


Figure 4-4. Expression pattern of gonad-specific genes during spermatogenesis

(A) Expression heatmap of gonad-specific genes in testis from 2 dpp, 4 dpp, 6 dpp, 10 dpp, 12 dpp, 14 dpp, 16 dpp, and adult mice by RT-PCR. Value: times of being detected. (B) Representative RT-PCR result.

4.2. Expression pattern of candidate genes in HEK 293T cells

Based on our expression profile analysis, we selected the 26 genes expressed in both adult testis and fetal ovaries (Figure 4-2 and 4-3) to further identify potential meiotic genes by examining their expression *in vitro*. For this purpose, we cloned the full-length coding sequence of each putative gene into the eukaryotic expression vectors, pEGFP-C₁, and pEGFP-N₁, to fuse the coded protein to an EGFP molecule. However, because of the inability of amplifying specific DNA by high-fidelity PCR, the difficulty of obtaining colonies containing a plasmid with the desired insertion, or no exact matches of some candidate genes found in the current genomic database, we ended with successfully introducing 12 of these putative genes to pEGFP-C₁ and/or -N₁ (Table 4-1).

To characterize the expression pattern *in vitro*, we transfected these 12 genes as

C- and/or N-terminal EGFP-tagged constructs under the control of the cytomegalovirus (CMV) promoter in HEK 293T cells and then observed their expression 24-48 h after transfection using inverted fluorescence microscopy. In those cases where C- and N-tagged plasmids were available, cells transfected with C-terminal EGFP-tagged gene displayed an identical expression pattern as those transfected with the same gene tagged with EGFP at the N-terminus. As seen in Figure 4-5A, strong EGFP signals were observed when the cells were transfected with the empty vector, indicating the delivered plasmids highly expressed EGFP in the cells. Similarly, EGFP-tagged 25P1, 96P2, 136P1, and 255P1 proteins were highly expressed in the transfected HEK 293T cells, localizing all over the cytoplasm and nucleus of the transfected cells (Figure 4-5A and Table 4-1).

Interestingly, for those less expressed proteins, we could observe they displayed a preferential location within the different cell compartments. Proteins from genes 62P1, 62P2, 273P2, 310P1, and 355P1 showed a preferential nuclear location. By contrast, the expression of genes 151P1 and 333P1 restrictedly resided in the cytoplasm. Furthermore, both of these two expression patterns were detected in cells transfected with the EGFP-tagged gene 20P1. (Figure 4-5A and Table 4-1).

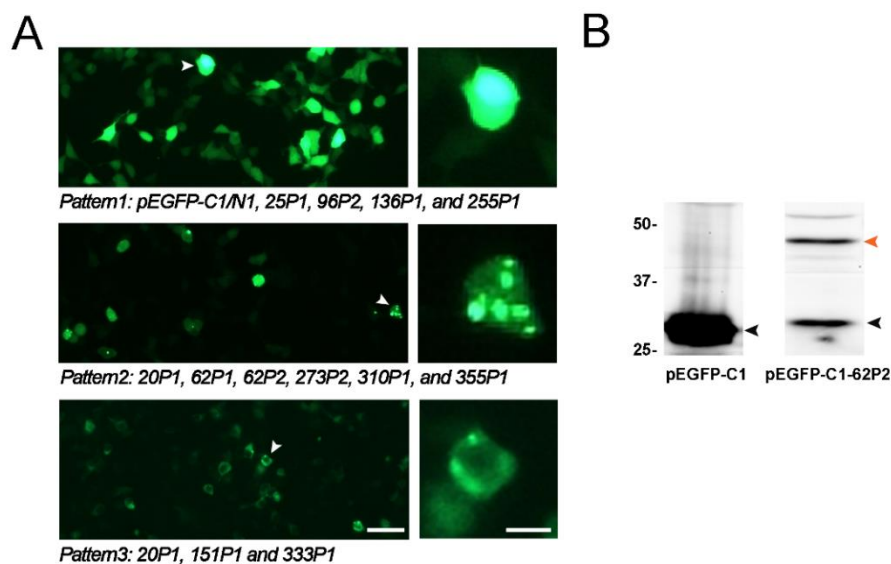


Figure 4-5. Expression of cloned genes in HEK 293T cells

(A) Representative images of the fluorescent signals of EGFP-tagged protein expressed under CMV. Pattern 1: whole-cell expression; pattern 2: nuclear enriched expression; pattern 3: prominent expression in the cytoplasm. Insets show magnification of the indicated cells. Scale bar (left panel), 40 μm ; scale bar (inset), 10 μm . (B) Representative images of EGFP-tagged protein in transfected HEK 293T cells detected by Western Blot. Arrows indicate the expected molecular weight of pEGFP-C1 (black), and pEGFP-C1-62P2 (orange).

Table 4-1. Characteristics of the cloned candidate proteins. Summarized data related with each cloned protein, including the expected protein molecular weight (MW), predicted motif searched by MyHits, NCBI-CDD, and MOTIF against multiple databases, overlap gene identified by BLAST/BLAT search against *Mus musculus* genome assembly GRChm39 (Ensembl), meiosis specificity determined by our RT-PCR results (section 4.1, N.A.: not available), vector plasmid used for cloning; repetition for mouse electroporation (EP), brief-expression pattern in HEK 293T cells and EP spermatocytes (spc), and the detection by WB in HEK 293T cells (HEK) or EP spc.

Name	Protein MW (kDa)	Predicted Motif	Overlap gene	Meiosis-specific	Cloning	EP times	Pattern in HEK293t cells	Pattern in EP spc	Protein detection by WB
20P1	35.4		Gm52969	N.A.	PEGFP-C1	3	Nuclear, cytoplasmic	Intense dots in nuclei	HEK
25P1	46.5	KRAB domain, Zinc finger domain array		Yes	PEGFP-C1/N1	3	Whole-cell	Big dot in cytoplasm/foci on SC	HEK
62P1	19.9			No	PEGFP-C1/N1	2	Nuclear	Telomeric signal/accumulation	HEK
62P2	27.8	Nup96 domain	Nup98	No	PEGFP-C1/N1	2	Nuclear	at XY	HEK
96P2	13.2		Cc2d2b	No	PEGFP-N1	1	Whole-cell	/	HEK
136P1	27.4		Gm11639, partially	No	PEGFP-C1/N1	1	Whole-cell	Telomeric signal/big dot in cytoplasm	HEK
151P1	17.4	Zinc finger domain		N.A.	PEGFP-C1/N1	2	Cytoplasmic	telomeric signal	HEK
255P1	46	BEN domain	Gm15262	Yes	PEGFP-C1/N1	1	Whole-cell	Patches at heterochromatin	HEK/EP spc
273P2	33.5	ANK domain	Gm49461, partially	No	PEGFP-C1/N1	2	Nuclear	telomeric signal	/
310P1	38.7	Zinc finger domain	Ortholog of ZNF660	N.A.	PEGFP-C1/N1	3	Nuclear	telomeric signal	HEK
333P1	41.3		partially Gm46430	No	PEGFP-C1	1	Cytoplasmic	telomeric signal	/
355P1	22.3	USP domain	Usp44	Yes	PEGFP-C1/N1	4	Nuclear	Foci on SC	HEK

After observing that the transfected cells expressed EGFP-tagged proteins under the microscope, we carried out immunoblotting with whole protein extracts from these transfected HEK 293T cells to further validate this expression. These experiments confirmed that all transfected cell lines expressed the expected molecular weight protein (Figure 4-5B). Unfortunately, we failed to detect any protein in cells transfected with the gene 333P1.

4.3. Expression pattern of candidate genes in mouse spermatocytes

Based on the expression analysis performed *in vitro*, we demonstrated that these plasmids, except for 333P1, codified for a protein and expressed the expected protein in a cellular environment. Thus, we decided to further characterize the expression pattern of these 12 candidate genes *in vivo* using these expression plasmids. To do so, we delivered the plasmids of EGFP-tagged genes, including our 12 candidate genes, SYCE3 (as a positive control), and two empty vectors, pEGFP-C1 and -N1 (as negative controls), into live mouse testes (16-18 dpp) by electroporation in collaboration with the lab of Dr. Alberto Pendas (CIC-CSIC, Salamanca, Spain). Plasmid DNAs were injected in the rete testis freed from the abdominal cavity and treated with multiple electric pulses for 1 h. 48 h later, we dissected the electroporated (EP) testes, performed spread and squash preparations, and immunostained them against GFP and the chromosomal axis marker, SYCP3. We examined the nuclear localization of the GFP signals in spermatocytes and their association with homolog chromosomes to assess their involvement in meiosis (Table 4-1).

As expected, SYCE3 signals co-localized with SYCP3 at the pachytene stage in both squashes and spread preparations suggesting that the electroporation technique allowed the successful expression of the EGFP-tagged genes in mouse spermatocytes. On the other hand, the negative controls, pEGFP-C1 and -N1, did not show any specific localization pattern or accumulation in any testicular cell type (Figure 4-6A). Apart from gene 96P2, the rest of the studied genes exhibited particular expression patterns in spermatocytes (see below).

We also performed a western blot analysis with extracts prepared from each electroporated testis to confirm the expression of these candidate genes at a protein level *in vivo*. However, we only detected the expression of C-terminal EGFP-tagged 255P and all the controls: pEGFP-C1, pEGFP-N1, and EGFP-tagged SYCE3 (Figure 4-6B).

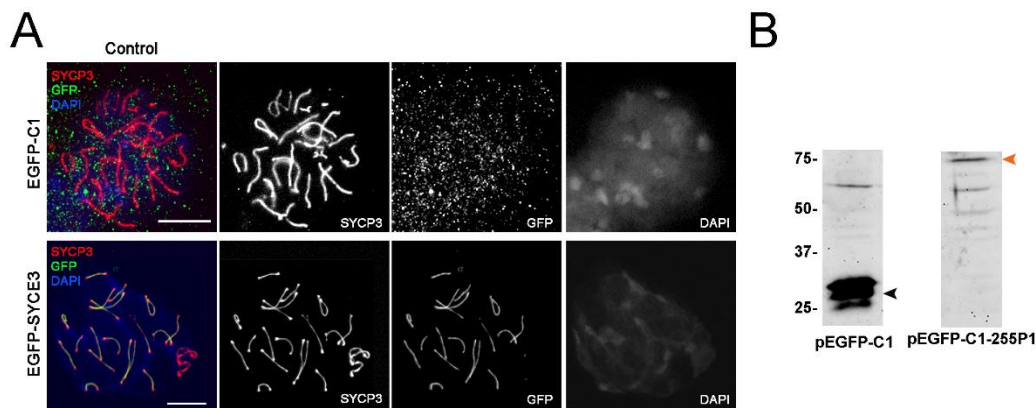


Figure 4-6. Expression of cloned genes in mouse testis

(A) Signals of pEGFP-C1 (negative-control) and EGFP-SYCE₃ (positive-control) in EP testis. Spermatocyte spread was stained against SYCP₃ (red) and GFP (green). DNA is counterstained with DAPI (blue). Scale bar, 10 μ m. (B) WB detection of EGFP-tagged protein in EP testis. Arrows indicate the expected molecular weight of pEGFP-C1 (black), and pEGFP-C1-255P1 (orange).

Below is a brief description of the expression pattern observed for each putative gene analyzed.

4.3.1. Gene 20P1

20P1 is a single-exon gene conserved across all the animals. It contains a histidine-rich region and a glutamine-rich region, a critical domain responsible for transcriptional activation of the mammalian transcription factors (Mitchell and Tjian 1989). Interestingly, the 20P1 overlaps with the predicted gene Gm52969 of the assembly version GRCm39 of the mouse genome (Table 4-1).

In the squash preparations in which the 3D conformation of the cells is preserved, 20P1 signals appeared like intense dots exclusively in some spermatocyte nuclei (Figure 4-7). We identified a similar pattern in spreads. Moreover, we could define

more precisely the localization of this protein. These protein aggregates were only

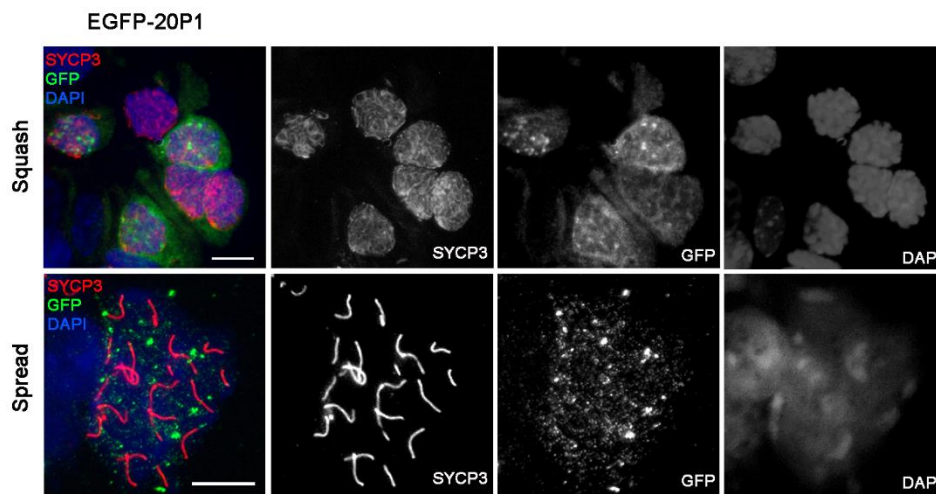


Figure 4-7. Expression pattern of EGFP-20P1 in mouse testis

Representative images of spermatocyte squash and spread stained against SYCP3 (red) and GFP (green). DNA is counterstained with DAPI (blue). Scale bar, 10 μm .

present in pachytene stage spermatocytes. However, these 20P1 dots were not exclusively associated with the SC since they did not always colocalize with the chromosome axes (Figure 4-7). This finding suggested that 20P1 may localize at the chromatin loops of pachytene spermatocytes.

4.3.2. Gene 25 P1

Gene 25P1 is meiosis-specifically expressed in mice and conserved across all animals. It has an N-terminal evolutionarily conserved Krueppel-associated box (KRAB) domain and an array of Zinc finger domains at the C-termini (Table 4-1). 25P1 protein probably belongs to the family of KRAB-containing proteins, characterized by the presence of a KRAB domain N-terminally located at a DNA-binding domain made of Zinc-finger repeats. It has been reported that when tethered to the template DNA by a DNA-binding domain, the KRAB domain functions as a transcriptional repressor (Urrutia 2003). Currently, known functions of the KRAB-containing proteins include transcriptional repression of RNA polymerase I, II, and III promoters, binding and splicing of RNA, and control of the nucleolus function (Urrutia 2003).

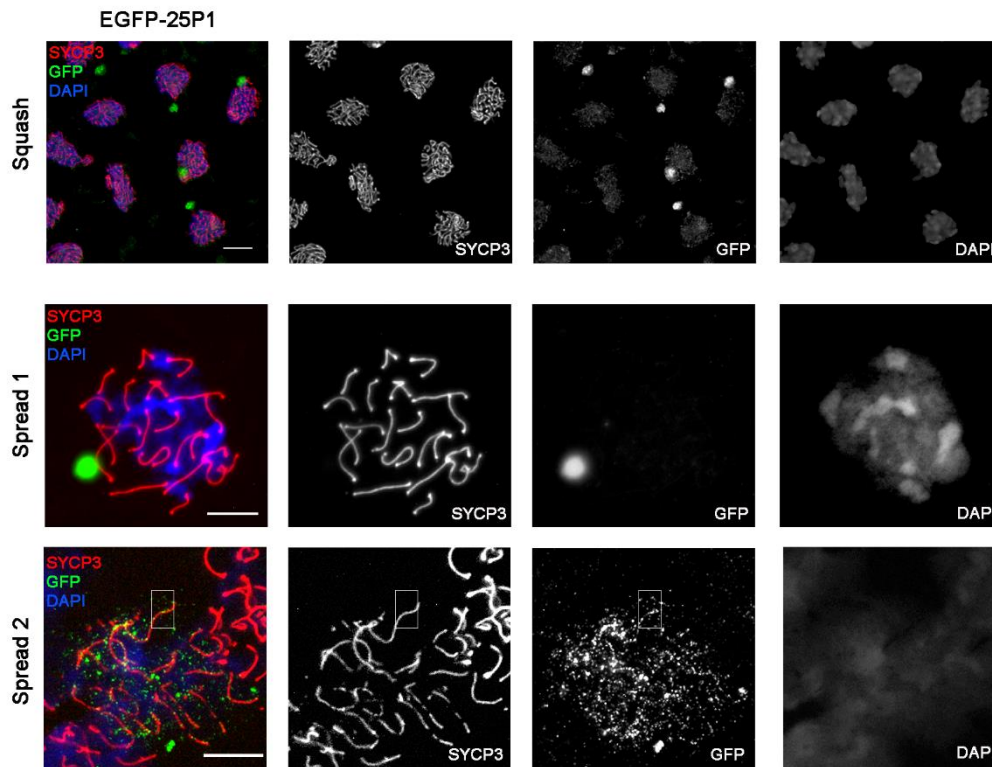


Figure 4-8. Expression pattern of EGFP-25P1 in mouse testis

Representative images of spermatocyte squash and spread stained against SYCP₃ (red) and GFP (green). DNA is counterstained with DAPI (blue). Foci-like signals along the chromosome in spread₂ were indicated (white rectangle). Scale bar, 10 μ m.

In the squash preparations, 25P₁ signals localized at the cytoplasm as a large dot and within the nucleus, at the chromosomal telomeric regions as foci in pachytene and diplotene spermatocytes (Figure 4-8). This dot-like pattern was also detected in spread preparations but without showing clear foci-like signals at telomeres (spread₁). Additionally, some weak foci-like 25P₁ signals were found along chromosomal axes in a minority of spermatocytes (spread₂).

4.3.3. Gene 62P₁ and 62P₂

62P₁ and 62P₂ are two isoforms encoding two proteins with a 71 amino acids difference at the C-terminus (Figure 4-9A). Both of them are widely expressed in a variety of mouse tissues and conserved across most mammals. These contain the nuclear pore complex protein 96 (Nup96) domain at the N-termini and overlap the gene *Nup98* (Table 4-1, Figure 4-9A), which encodes both nuclear protein 98 (NUP98) and NUP96. NUP98

and NUP96 are nucleoporins, which are the constituents of the nuclear pore complex (NPC), and contribute to nuclear transport. Growing evidence has shown that intranuclear nucleoporins, including NUP98, binds chromatin and regulate gene expression (Capitano, Montpetit, and Wozniak 2017).

In the 62P1 squash, foci-like signals were observed in spermatocytes, some of them coinciding with the ends of chromosomes, presumably the telomeres. In 62P2 squash, we could not detect the tagged protein in spermatocytes (Figure 4-9B).

In spreads, both 62P1 and 62P2 signals were found as foci at the chromosome ends and accumulated on the XY chromosomes. The 62P1 and 62P2 foci appeared at the end of chromosomes since the zygotene stage, and it persisted there until the diplotene stage. In contrast, the accumulations at the XY chromosomes were mainly found in diplotene spermatocytes for 61P1, but in pachytene spermatocytes for 62P2 (Figure 4-9B).

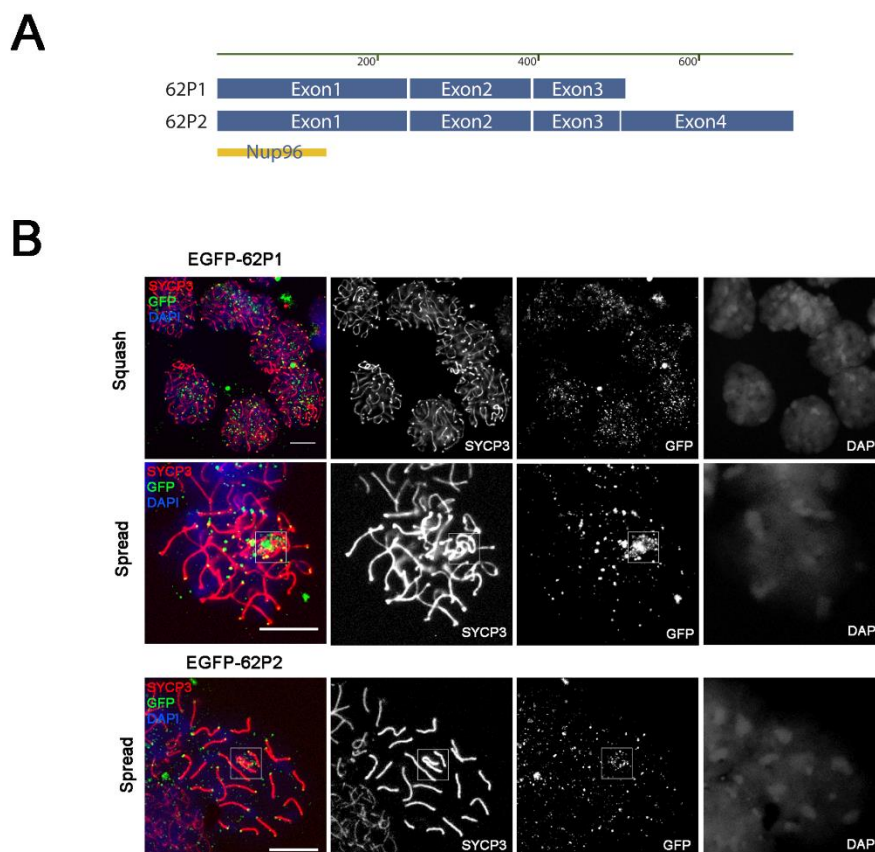


Figure 4-9. Expression pattern of EGFP-62P1 and 62P2 in mouse testis

(A) Schematic representation of 62P1 and 62P2 transcripts. Nup96: nuclear pore complex protein 96 domain. (B) Representative images of spermatocyte squash and spread stained against SYCP3 (red) and GFP (green). DNA is counterstained with DAPI (blue). Signal accumulation around XY chromosomes (white square). Scale bar, 10 μ m.

4.3.4. Gene 136P1

136P1 is a meiosis-specific gene. Part of it overlaps a predicted mouse gene GM11639 of the assembly version GRCm39 of the mouse genome, but no protein domains can be predicted based on its putative protein sequence (Table 4-1).

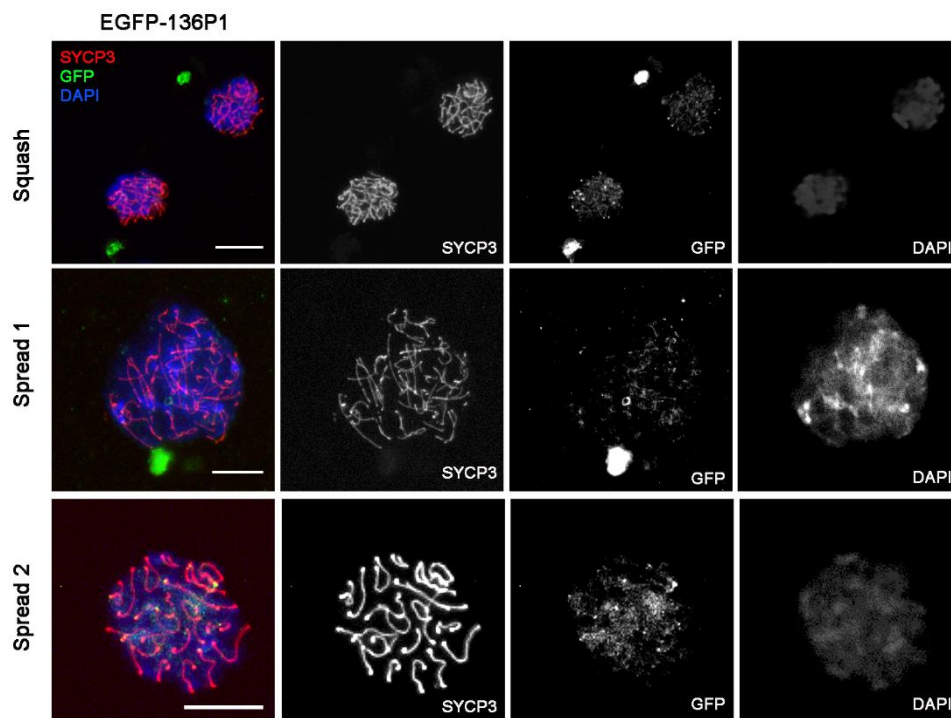


Figure 4-10. Expression pattern of EGFP-136P1 in mouse testis

Representative images of spermatocyte squash and spread stained against SYCP3 (red) and GFP (green). DNA is counterstained with DAPI (blue). Squash: representative cells exhibiting two localization patterns: spread 1: cell exhibiting only single dot-like signal in the cytoplasm. Spread 2: cell exhibiting only foci-like signals at telomeres. Scale bar, 10 μ m.

In squash preparations, 136P1 signals exhibit two localization patterns in spermatocytes, either formed foci at the telomeres, similar to 62P1/P2, or created a big cytoplasmic dot, like 25P1. In some cells, both patterns were observed (Figure 4-10). In spread preparations, both 136P1 patterns were found to occur at different stages from that of 25P1 (Figure 4-8) and 62P1/P2 (4-9B). The telomeric 136P1 foci were only present in late prophase spermatocytes. The cytoplasmic aggregates formed from leptotene until the diplotene stage, thus co-existing with the telomeric foci at late prophase in some cells (Figure 4-10). In addition, 136P1 foci at the telomeres were detected much less frequently

in the spread than in the squash preparations. This discrepancy might indicate that the spread preparation could cause a significant loss of $136P1$ protein from chromosomes.

4.3.5. Gene $151P1$

$151P1$ is a single-exon gene that is conserved in most mammals. It is predicted to contain an N-terminal Zinc finger domain based on its amino acid sequence.

In both squash and spread preparations, we only found $151P1$ as foci at the telomeres in very few spermatocytes at pachytene and diplotene stages (Figure 4-11).

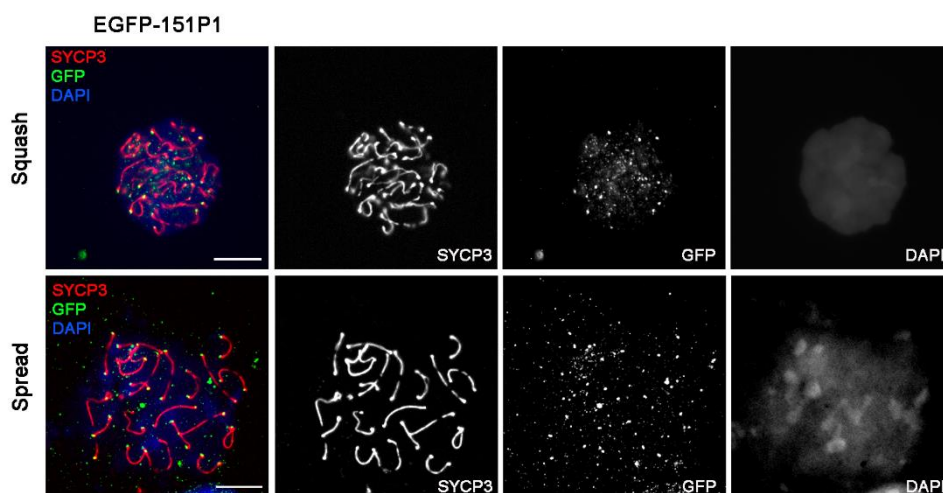


Figure 4-11. Expression pattern of EGFP- $151P1$ in mouse testis

Representative images of spermatocyte squash and spread stained against SYCP3 (red) and GFP (green). DNA is counterstained with DAPI (blue). Scale bar, 10 μm .

4.3.6. Gene $255P1$

$255P1$ is an X-linked gene specifically expressed during meiosis in mice. It overlaps a predicted mouse gene Gm15262 of the assembly version GRCm39 of the mouse genome. $255P1$ is conserved in *Rattus norvegicus* and contains two BEN domains (Table 4-1). The BEN domain is found in diverse animal proteins and is thought to mediate protein-DNA and protein-protein interactions during chromatin organization and transcription (Abhiman, Iyer, and Aravind 2008).

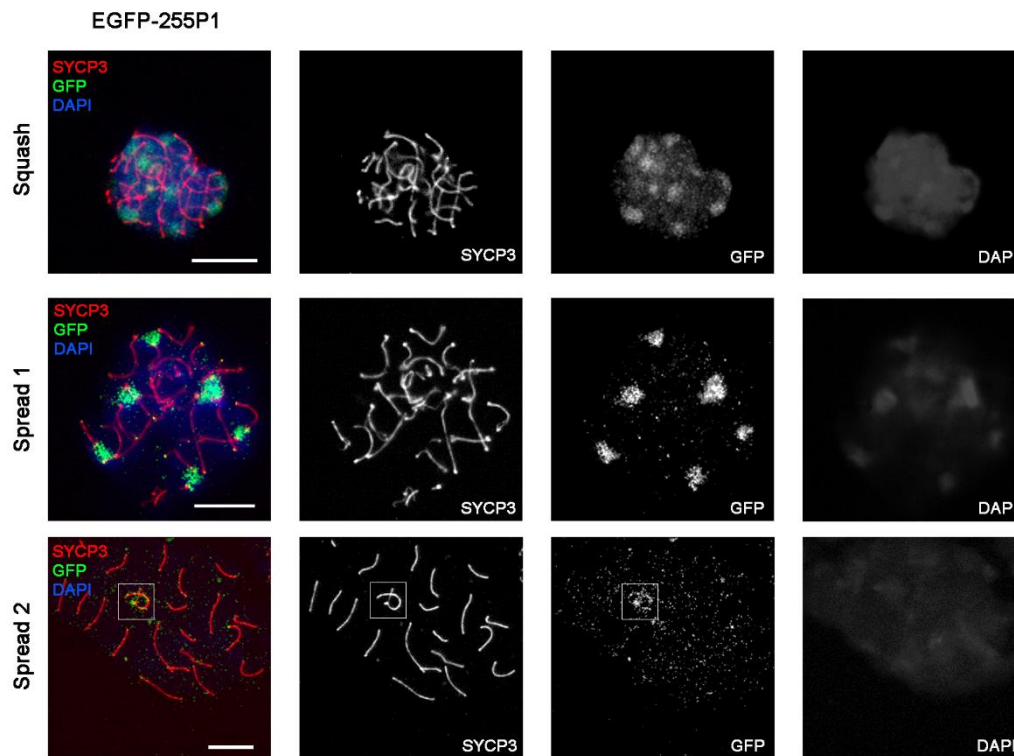


Figure 4-12. Expression pattern of EGFP-255P1 in mouse testis

Representative images of spermatocyte squash and spread stained against SYCP₃ (red) and GFP (green). DNA is counterstained with DAPI (blue). Squash: patch-like signals at the heterochromatic region. Spread 1: cell exhibiting clear foci signals at telomeres along with patch-like signals. Spread 2: cell exhibiting foci signals at the chromosomal telomeres and axes. Signal accumulation at XY chromosomes (white square). Scale bar, 10 μ m.

In squash preparations, 255P1 signals showed multiple patches coinciding with the heterochromatic regions, which were brightly stained by DAPI (Figure 4-12).

In spread preparations, 255P1 was frequently detected as foci residing at some telomeres rather than patch-like signals, which were occasionally observed. Moreover, a fainter signal along the autosomal axes in pachytene and diplotene spermatocytes could also be observed. Also, in most of the pachytene spermatocytes and some diplotene spermatocytes, abundant 255P1 foci were found along the XY chromosomes (Figure 4-12).

4.3.7. Gene 273P2

273P2 is a meiosis-specific putative gene that is conserved in rodents. Part of 273P2 overlaps the predicted gene Gm49461 of the assembly version GRCm39 of the mouse genome. 273P2 contains an ankyrin repeats (ANK) domain, one of the most

common protein-protein interaction motif (Table 4-1). Ankyrin repeats have been found in proteins of diverse cellular functions. For instance, mouse ANKRD31 – a component of DSB-promoting complex, regulates recombination initiation and is required for recombination between sex chromosomes in spermatocytes (Papanikos et al. 2019).

In squash preparations, strong 273P2 signals were observed all over the nuclei and cytoplasm of spermatocytes. In spread preparations, 273P2 signals were found as foci at the telomeres in a few spermatocytes (Figure 4-13).

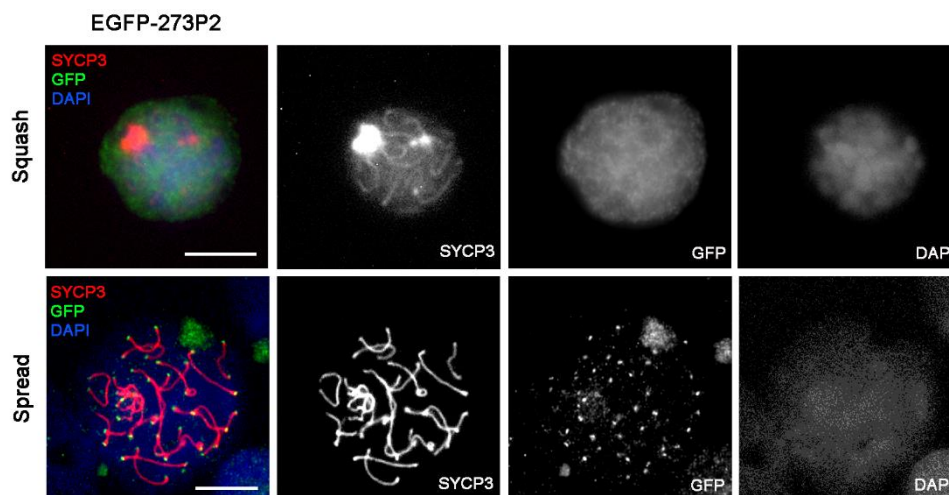


Figure 4-13. Expression pattern of EGFP-273P2 in mouse testis

Representative images of spermatocyte squash and spread stained against SYCP₃ (red) and GFP (green). DNA is counterstained with DAPI (blue). Scale bar, 10 μ m

4.3.8. Gene 310P1

310P1 is a single-exon gene conserved across all the animals. It is predicted to contain an array of Zinc finger domains and overlaps a pseudogene, ortholog of ZNF660, at the assembly version GRCm39 of the mouse genome (Table 4-1). Similar to 273P1, strong 310P1 signals were observed all over all spermatocyte compartments in squash preparations and were only detected as foci at the telomeres in a few spread spermatocytes (Figure 4-14).

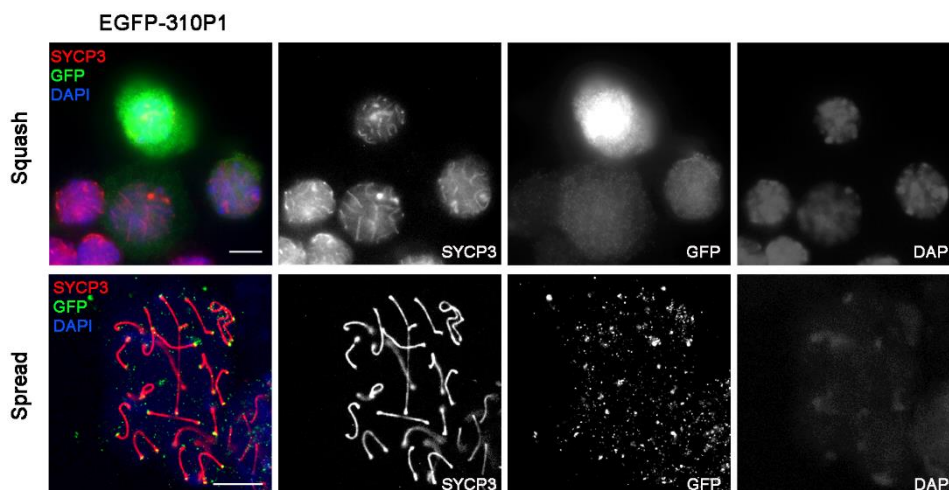


Figure 4-14. Expression pattern of EGFP-310P1 in mouse testis

Representative images of spermatocyte squash and spread stained against SYCP₃ (red) and GFP (green). DNA is counterstained with DAPI (blue). Scale bar, 10 μ m.

4.3.9. Gene 333P1

333P1 is universally expressed in many mouse tissues and is highly conserved across all animals. Part of it overlaps with a predicted gene Gm46430, assembly version GRCm39 of the mouse genome. However, our *in silico* analysis could not reveal any protein domain based on its predicted protein sequence (Table 4-1).

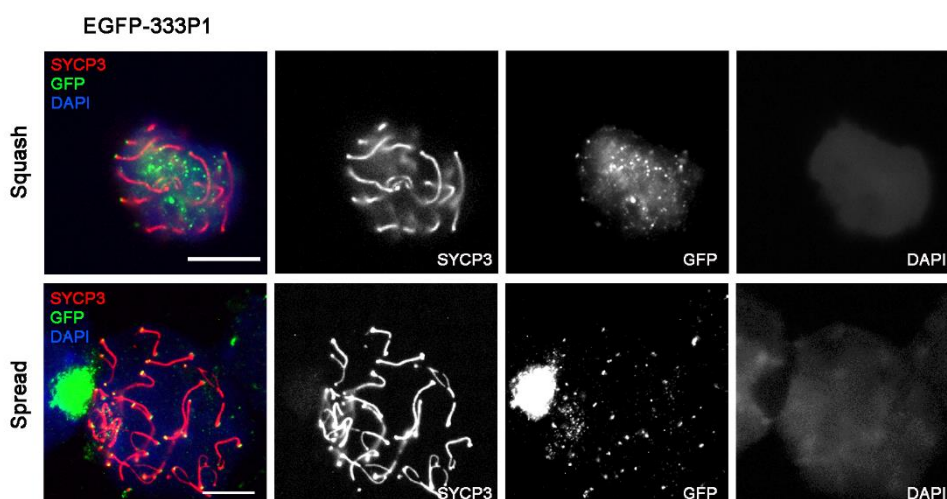


Figure 4-15. Expression pattern of EGFP-333P1 in mouse testis

Representative images of spermatocyte squash and spread stained against SYCP₃ (red) and GFP (green). DNA is counterstained with DAPI (blue). Scale bar, 10 μ m.

Similar to 151P1, we only found 310P1 as foci at the telomeres in a minority of spermatocytes in both squash and spread preparations (Figure 4-15).

4.3.10. Gene 355P1

355P1 is a meiosis-specific gene that is highly conserved across all animal species. It contains a ubiquitin-specific protease (USP) domain and overlaps with the C terminus of the ubiquitin carboxyl-terminal hydrolase 44 (*Usp44*) gene in the assembly version GRCm39 of the mouse genome (Table 4-1).

In squash preparations, 355P1 signals largely accumulated in some spermatocyte nuclei, seeming to align with chromosome axes partially. Interestingly, we confirmed that 355P1 formed foci-like signals colocalizing with SYCP3 in spermatocytes at all the meiotic prophase substages in spreads. 355P1 foci were first detected on the SYCP3-stained axes at leptotene. More foci were seen along the axes in a punctuated distribution at the zygotene stage. The SC axes were decorated with many 355P1 foci at the pachytene stage. In some cells, 355P1 foci formed a pattern of beads on a string along with the SCs. The number of 355P1 foci located on the chromosome axes decreased at the diplotene stage (Figure 4-16).

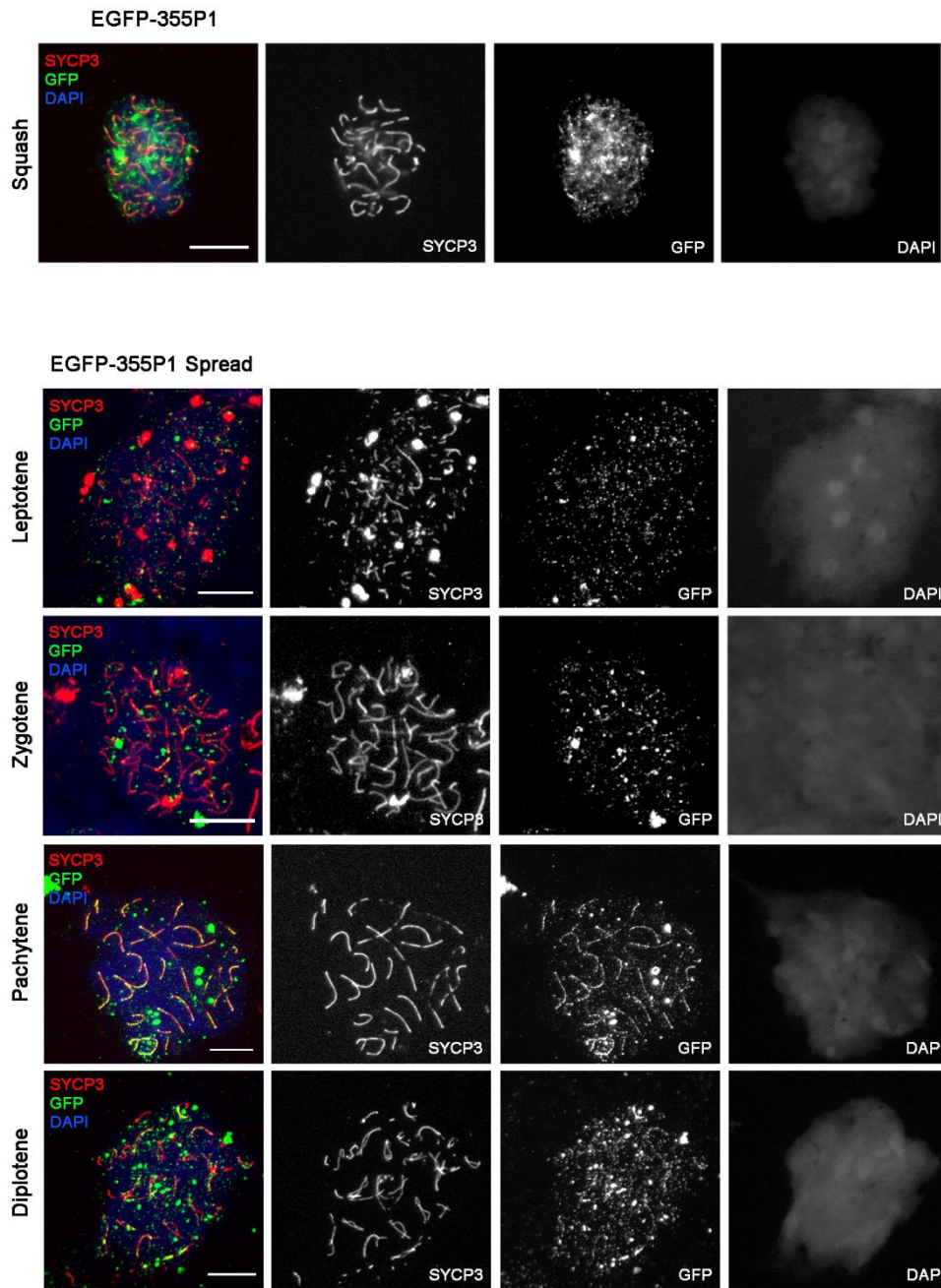


Figure 4-16. Expression pattern of EGFP-355P1 in mouse testis
 Representative images of spermatocyte squash and spread stained against SYCP₃ (red) and GFP (green). DNA is counterstained with DAPI (blue). Scale bar, 10 μ m.

4.4. Functional analysis of 255P1/BEND2 in meiosis

Based on the previous results, we hypothesized the gene 255P1 as a putative meiosis-specific gene that could have a role during the meiotic prophase. 255P1 is an X chromosome gene expressed during the meiotic prophase (section 4.1). It localizes at the heterochromatin of spermatocytes when electroporated to the testes of young mice (Figure 4-12). This localization is consistent with the known functions of the BEN domains-mediating protein and DNA interactions during chromatin restructuring and transcription (Abhiman, Iyer, and Aravind 2008). Interestingly, 255P1 overlaps with the predicted mouse gene *Gm15262*, which exhibits high homology with the human *BEND2* gene: both contain two BEN domains at the C termini, both express prominently in testis and share 28.1% of identity and 41.3% of similarity between their protein sequences (Figure 4-17A). Altogether, we speculated that 255P1 is a splice variant of *Gm15262*, the ortholog of human *BEND2*. Thus, henceforth, we will refer to *Gm15262* as mouse *Bend2* and 255P1 as a novel transcript *Bend2-208* after 7 annotated *Gm15262* (*Bend2*) transcripts

4.4.1. Localization of BEND2 in meiocytes

4.4.1.1. Study of BEND2 using commercially available antibodies

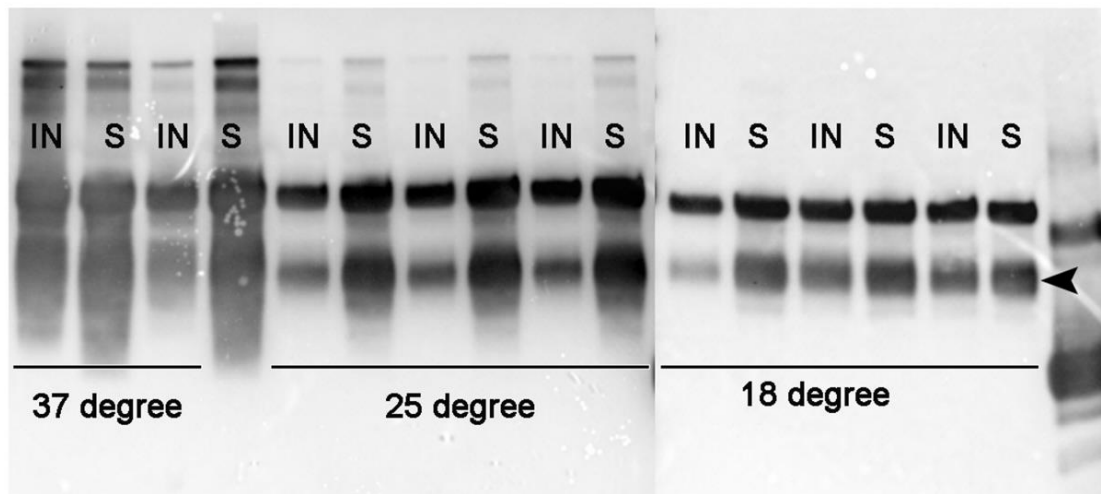
To gain insights into the possible functions of BEND2 in meiosis, we examined its localization in spermatocytes by immunofluorescence (IF). First, we tried a commercial polyclonal antibody raised against human BEND2 amino acids 415-559 (Abcam, ab204795). This oligopeptide has 56% similarity to mouse BEND2-202 amino acids 386-530 and BEND2-208 amino acids 63-207 (Figure 4-17A-B). Unfortunately, no specific staining was observed in the spread or squash preparations from either 16 dpp or adult mouse testis. However, we detected abundant BEND2 exclusively in nuclei of late prophase human spermatocytes from a non-infertile adult man (Figure 4-17C), suggesting this antibody is not appropriate for detecting the mouse BEND2. Thus, we decided to create a polyclonal serum to detect mouse BEND2.

deacetylase complex subunit SAP130 (Sin3-associated protein 130); BEN: BEN domain. (B) Protein sequence comparisons by CLUSTALW. Residues are identical (*); strongly conserved (:); weakly conserved (.). (C) Staining of human BEND2 in human spermatocytes. Human testis spread was stained with anti-human BEND2 antibody and SYCP3. Scale bar, 10 μ m.

4.4.1.2. BEND2 polyclonal antibody generation

To obtain a polyclonal serum, we cloned the full-length CDS of BEND2-208 into the bacterial expression vector pET-28a (+)-TEV, which was subsequently transformed to BL21(DE3) *E.coli* cells for protein expression. Since, to our knowledge, BEND2 C-term had not been produced in bacteria, we first performed a condition screen step to determine its optimal expression culture conditions. By comparing the amount and specificity of BEND2-208 protein expressed at different induction conditions (details of the method described in section 3.4.1.1 and 3.4.1.2), we determined that BEND2-208 was highly and more specifically expressed in *E.coli* cells after ON incubation at 18°C with 0.5mM IPTG induction (Figure 4-18A). Then, using this condition, we scaled up the expression culture to 4L and purified approximately 15 mg of recombinant BEND2-208 protein by IMAC. The purified BEND2-208 protein was further digested with TEVp and then loaded onto the HisTrap HP column. The flow-through containing His-tag-removed BEND2-208 protein was collected, dialyzed in PBS, and concentrated. Eventually, 0.9mg of recombinant BEND2-208 protein in PBS was obtained for animal immunization. The protein sequence of recombinant BEND2-208 protein was identified by Peptide Mass Fingerprinting (PMF) before injecting it to the animal as an antigen. Two rabbits were immunized for raising serums against BEND2-208, and after two rounds of boosters, we obtained a serum sample and checked the immune response by ELISA titration. Surprisingly high antibody responses were detected in both rabbit serums (Figure 4-18B). Based on these results, we decided to terminate the immunization and harvest the final serums. The polyclonal serum was further subjected to purification steps to remove serum proteins and enrich the fraction of immunoglobulins (IgG). Purified serum from both animals was confirmed to specifically react to target antigen by IF (shown below). In the end, the purified antiserum (mostly from Rb1886) was used for the following BEND2 detection analysis.

A



B

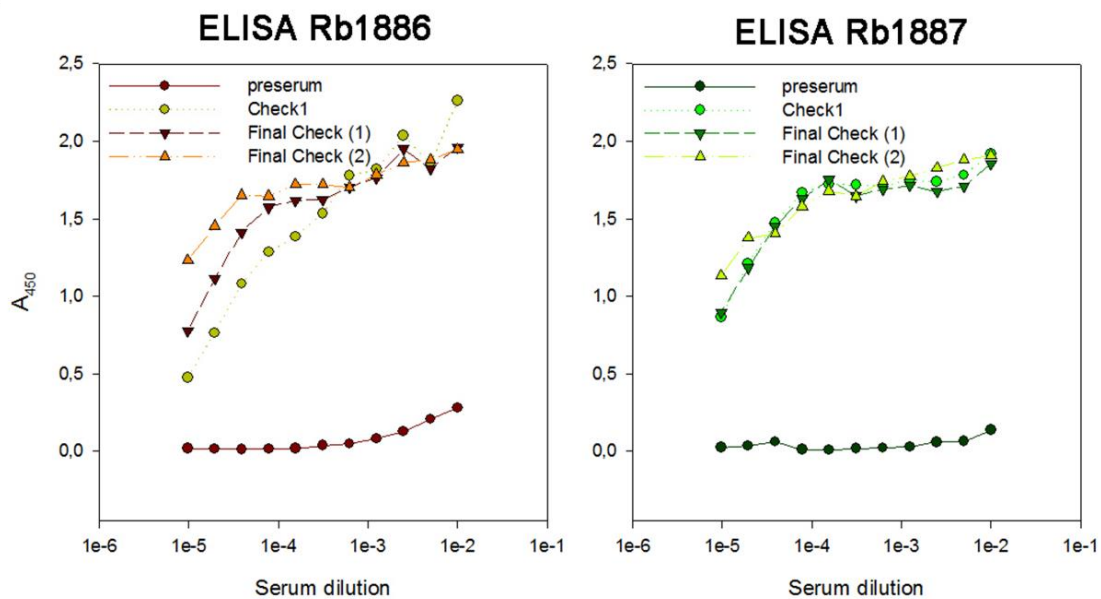


Figure 4-18. In-house BEND2-208 polyclonal antibody generation

(A) BEND2-208 protein expression levels under different induction conditions. Protein extracted from *E.coli* cells was detected by anti-His using WB. IN: insoluble fraction; S: soluble fraction. Replicate samples were loaded for each condition. Black arrowheads indicate the expected weight of BEND2-208 48.3 kDa. (B) BEND2 antibody ELISA titration. Serum from each rabbit was diluted serially from 1/100 to 1/102400. Preserum-serum before immunization; check1-serum after the second booster; final check (1)(2)-two aliquots from final serum.

4.4.2. Detection of BEND2 during spermatogenesis

Using our custom-made antibody, we examined BEND2 expression during spermatogenesis by staining against BEND2 and γ H2AX on PFA-fixed testis sections (Figure 4-19). BEND2 was abundantly detected in the nuclei of the periphery cells in tubules from stage V until XII-I (Figure 4-19A). This general nuclear staining first appeared in spermatogonia, then highly present in spermatocytes since pre-leptotene when meiosis initiates. This high level of BEND2 persisted in nuclei until early pachytene. In late pachytene and diplotene cells, little BEND2 remained in the nuclei of spermatocytes. (Figure 4-19B). Notably, this expression pattern of BEND2 in mouse testis is very similar to the reported human BEND2 expression in human testis (Uhlén et al. 2015).

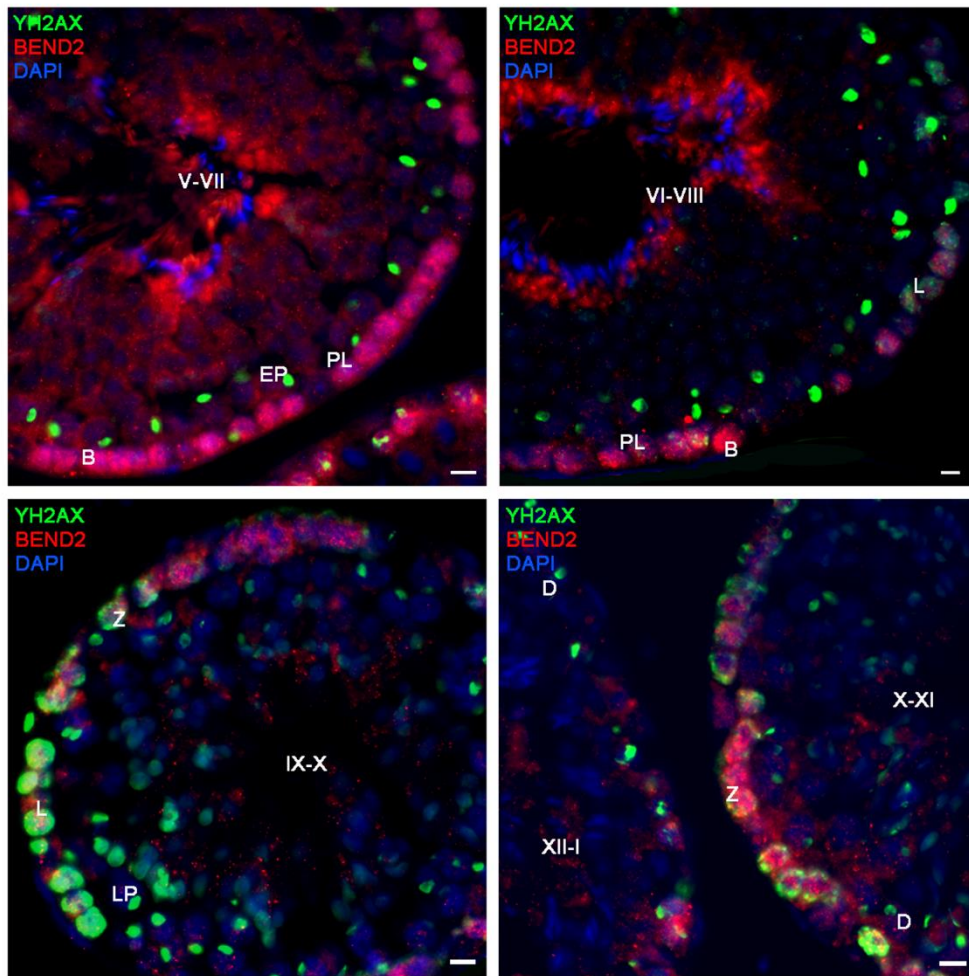
4.4.2.1. Detection of BEND2 in SPO11- and DMC1-deficient testis

We wondered if the localization of BEND2 in germ cells could be originated as a response to critical events of the meiotic prophase. To reveal this, BEND2 was examined in testis sections from recombination-defective mice lacking SPO11 or DMC1.

In SPO11-deficient testis, since no DSBs are formed at the onset of meiosis, spermatocytes cannot find their homologous partner, fail to synapse, and enter apoptosis at pachytene. BEND2 was also found extensively in nuclei of spermatogonia, leptotene, zygotene, and zygotene-like spermatocytes in these testes, as in wild-type mice (Figure 4-20). However, very occasionally, few BEND2 signals could be observed in some spermatocytes, presumably at a more advanced zygotene-like stage. This is also consistent with its reduced expression after early pachytene in wild type.

In the DMC1-deficient testis, spermatocytes cannot complete meiotic recombination. Thus, *Dmcr1*^{-/-} spermatocytes accumulate unrepaired DSBs and enter apoptosis at early pachytene (Pacheco et al. 2015). Plenty of BEND2 was detected in the nucleus of spermatogonia, leptotene, zygotene, and zygotene-like spermatocytes, resembling its expression in wild-type cells (Figure 4-20). Thus, the expression of BEND2 might be independent of either DSB formation or completion of recombination.

A



B

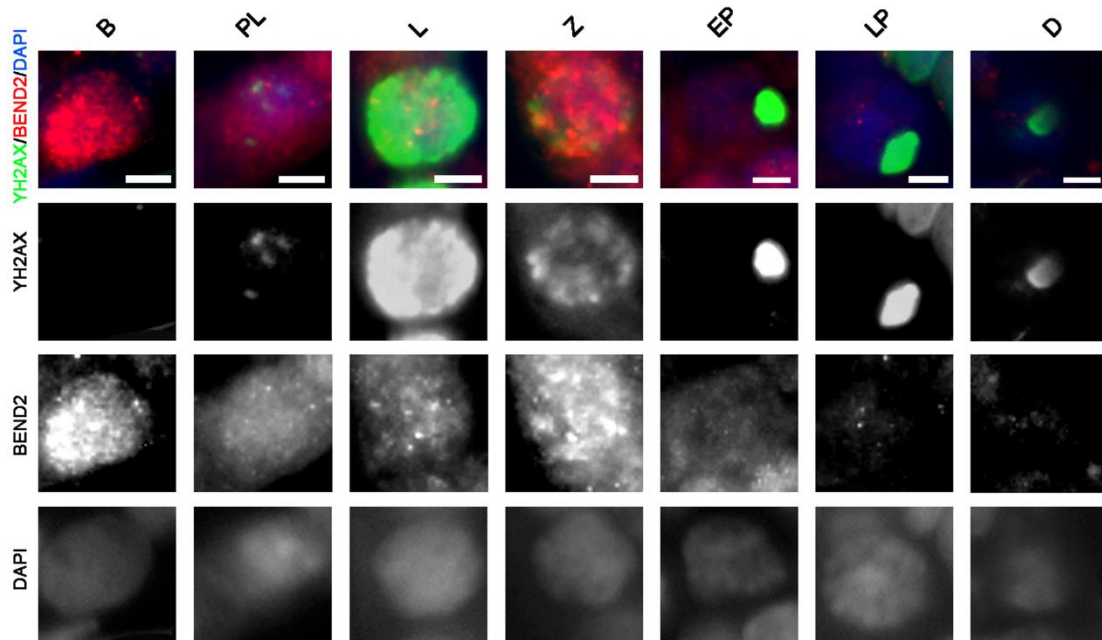
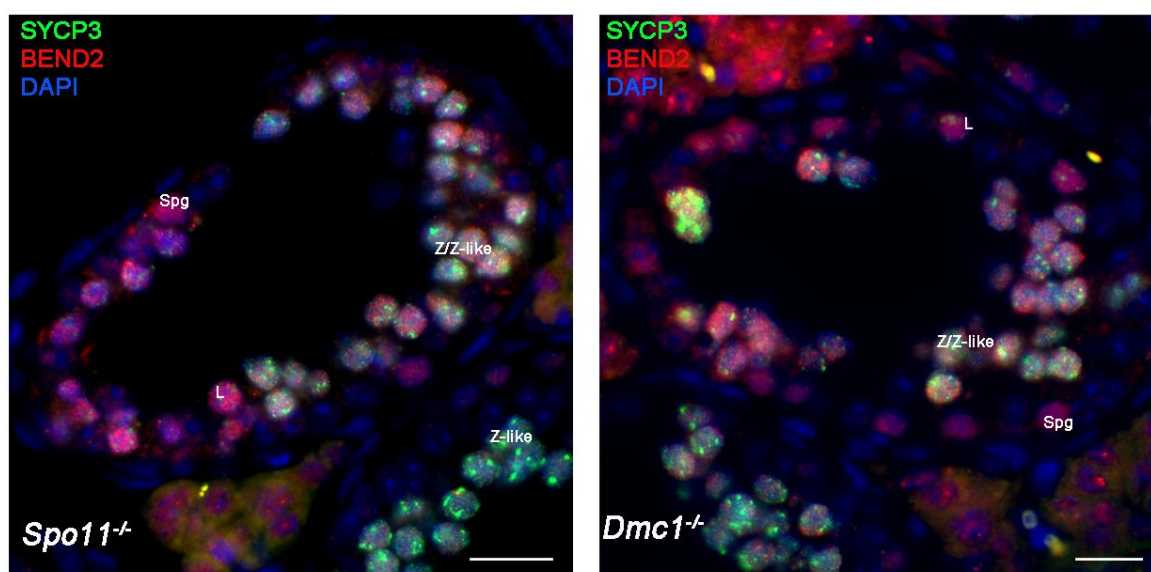


Figure 4-19. Expression of BEND2 during spermatogenesis

(A) BEND2 localization in wild-type mouse testis. Testis sections were treated with antigen retrieval using Tris-EDTA buffer and then stained with *in-house* BEND2 antibody (Rb1886) and γ H2AX antibody. Staging of the seminiferous epithelium is based on the localization of staged spermatocytes (indicated by the expression and localization of γ H2AX) and spermatid differentiation (indicated by DAPI). The tubule stage is indicated in uppercase roman numerals. Scale bar, 20 μ m. (B) Magnification of BEND2-positive cells from testis sections. Expression of BEND2 was characterized in cells along spermatogenesis from spermatogonia to late diplotene spermatocyte. B: B type spermatogonia; PL: pre-leptotene spermatocyte; L: leptotene spermatocyte; Z: zygotene spermatocyte; EP: early pachytene spermatocyte; LP: late pachytene spermatocyte; D: diplotene spermatocyte. Scale bar, 10 μ m.

**Figure 4-20. BEND2 localization in SPO11- and DMC1-deficient testis.**

Spo11^{-/-} and *Dmc1*^{-/-} testis sections were treated with antigen retrieval using Tris-EDTA buffer and then stained with *in-house* BEND2 antibody (Rb1886) and SYCP3 antibody. Spg: spermatogonia; L: leptotene spermatocyte; Z/Z-like: zygotene or zygotene-like spermatocyte. Z-like labeled cells showing few BEND2 signals. Scale bar, 50 μ m.

4.4.3. Phenotyping of *Bend2* mutant mice

4.4.3.1. Target disruption of *Bend2* gene

To address the meiotic functions of BEND2 in mice, we generated BEND2-deficient mice by CRISPR/Cas9. Part of exon 11 of *Bend2-202*, namely, exon4 of *Bend2-208* was targeted to be removed using a pair of gRNAs targeting opposite strands to disrupt one BEN domain (Figure 4-21). After microinjection and transfer of embryos, 17 pups were born. Among them, we identified two homozygous males (B39 and B41) and three heterozygous females (B45, B46, and B48) carrying desired mutations (Figure 4-21B) (sequence details in Supplementary Table 2). We crossed each of them with a wild-type B6 mouse and interbred the progenies to set up a breeding colony of each founder. No developmental abnormalities were observed during the growth of all the mutant progenies, and the segregation of the mutated allele followed the Mendelian ratio. Eventually, animals from at least F2 generation of B39 and B45 colonies were subjected to phenotyping analysis.

4.4.3.2. Analysis of spermatogenesis in *Bend2*^{-/y} male

Male *Bend2*^{-y} mice developed into adults without obvious differences in general physical appearance compared to their littermates. Male *Bend2*^{-y} mice were fertile. The size and weight of *Bend2*^{-y} testes were comparable to that of wild-type testes (Figure 4-22A). Performing RT-PCR and WB, we demonstrated the full-length *Bend2* mRNA and BEND2 protein were absent in *Bend2*^{-y} male testis (Figure 4-22B and C). By analyzing testis sections with IF, we confirmed that the staining of BEND2 observed in wild-type cells was undetectable in mutant cells (Figure 4-22D). These results suggest that BEND2 was successfully eliminated from mutant mouse testis, and its function was most likely removed. However, our RT-PCR also detected a smaller amplified DNA fragment in *Bend2*^{-y} testis. By sequencing this DNA fragment, we found there was an alternatively spliced mRNA in *Bend2*^{-y} testis, which was resulted from skipping exon 11 of *Bend2-202*. Moreover, a protein with a size corresponding to this alternative mRNA was found in both wild-type and *Bend2*^{-y} testis by WB (Figure 4-22B and C). Thus, we proposed that an

unannotated BEND2 isoform was likely present in mouse *Bend2*^{-y} testis.

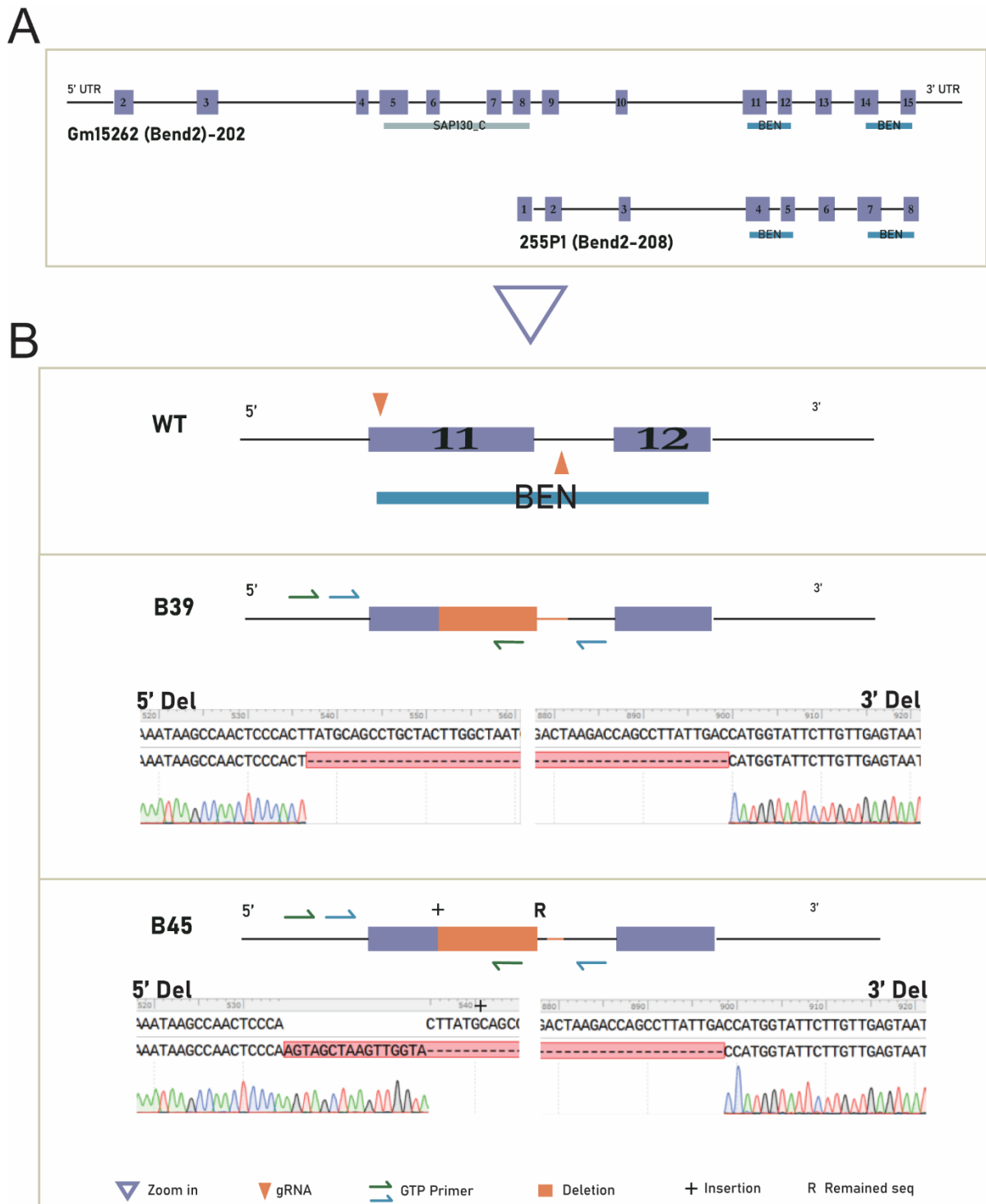


Figure 4-21. BEND2 mutation strategy

(A) Schematic representation of mouse *Gm15262* (*Bend2*)-202 and 255P1 (*Bend2*-208). The exons are shown as purple boxes. The predicted domains are labeled below the exons. SAP130_C: C-terminal domain of histone deacetylase complex subunit SAP130; BEN: BEN domain. (B) Schematic of target deletion. WT: magnification of C terminus of *Bend2* wild-type locus. A pair of gRNAs target at exon 11 (*Gm15262*)/exon 4 (255P1) within the BEN domain.

B39 and B45: disrupted *Bend2* loci from 2 founders. Sequence alignments of 5' and 3' end of deletions are shown. Notice that there are inserted and remained intronic sequences for B45 mutation. The locations of them are indicated in the schematic and their sequences of them are shown in supplementary Table 2. GTP (genotyping) primers represent BEND2 GTP Forward and BEND2 GTP Reverse wt (green), BEND2 GenoF, and BEND2 GenoR (blue), for genotyping PCR (Table 3-21).

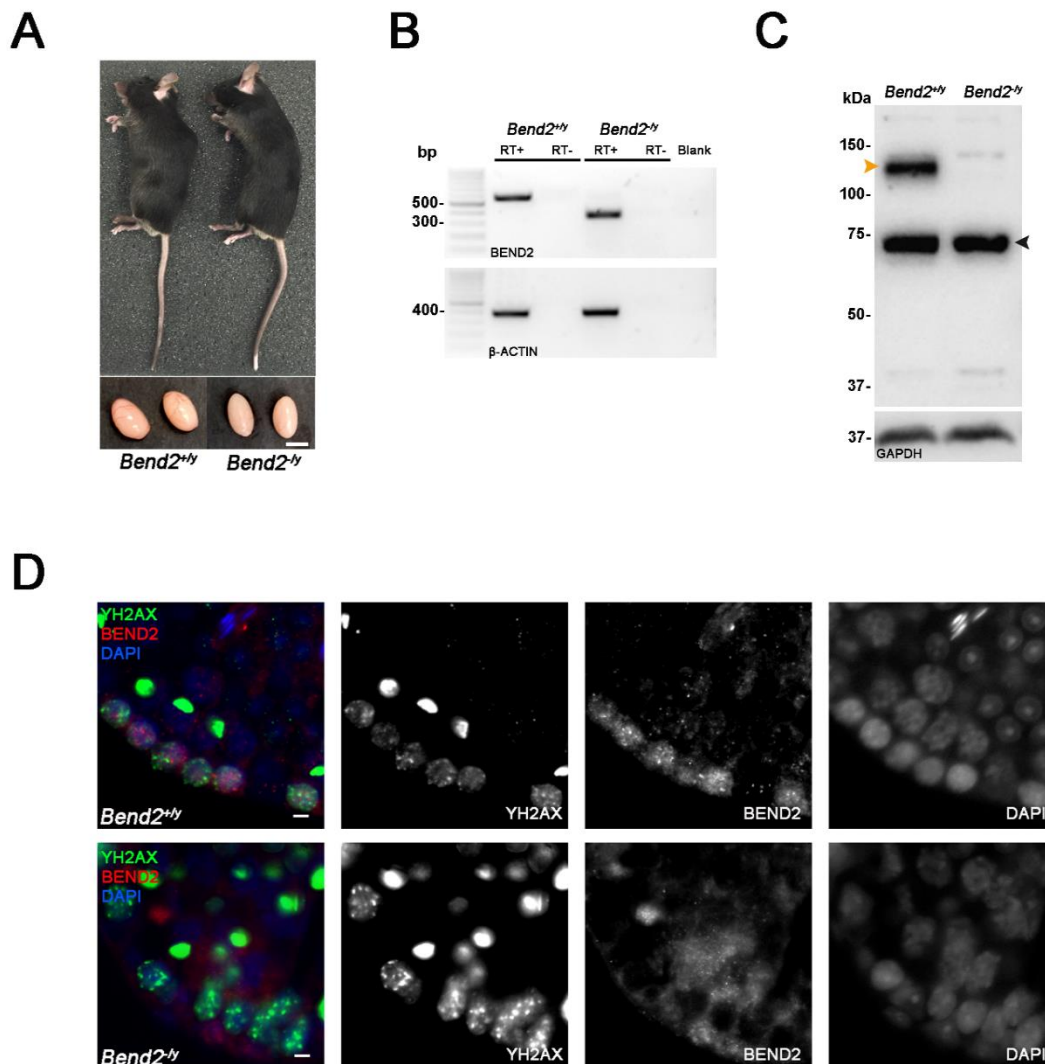


Figure 4-22. Disruption of BEND2 in *Bend2*^{-/-} mice.

(A) Mouse appearance and testis size. Scale bar, 5mm. (B) Detection of BEND2 in testis by RT-PCR. BEND2 GenoF and GenoR primers were used (locations indicated in Figure 4-21B) The expected size of the WT allele was 576bp. Sanger sequencing result showed that the amplified DNA in the mutated allele was 372bp, from an mRNA that resulted from skipping exon 11 of *Bend2*-202/exon 4 of *Bend2*-208. (C) Detection of BEND2 by WB. The full-length BEND2 protein band is indicated by orange arrow. An extra protein band ~75 kDa (black arrow) was also detected in both wild-type and mutant testes. (D) Detection of BEND2 by IF. Testis sections were treated with antigen retrieval using Tris-EDTA buffer before staining with BEND2 antibody (Rb 1886, 1:100) and SYCP3. Scale bar, 10 μ m.

Histological analysis of *Bend2*^{-/-} testes revealed cells at all the stages of spermatogenesis (Figure 4-23A). These results indicated that the full-length BEND2 might be dispensable for completing spermatogenesis. However, TUNEL assays showed a significant increase of apoptotic cells in *Bend2*^{-/-} testes compared to wild-type testes ($p < 0.0001$ t-test, Figure 4-23B and C), suggesting that the depletion of BEND2 caused a slight defect in spermatogenesis. We further examined the stage of these apoptotic cells and compared them to the ones observed in wild-type testes. *Bend2*^{-/-} mice presented comparable apoptotic spermatocytes (66.8 ± 9.7%, mean ± SD, N=4) than wild-type mice (52.5 ± 9.5%, mean ± SD, N=4, $p > 0.05$ One-Way ANOVA, Figure 4-23D).

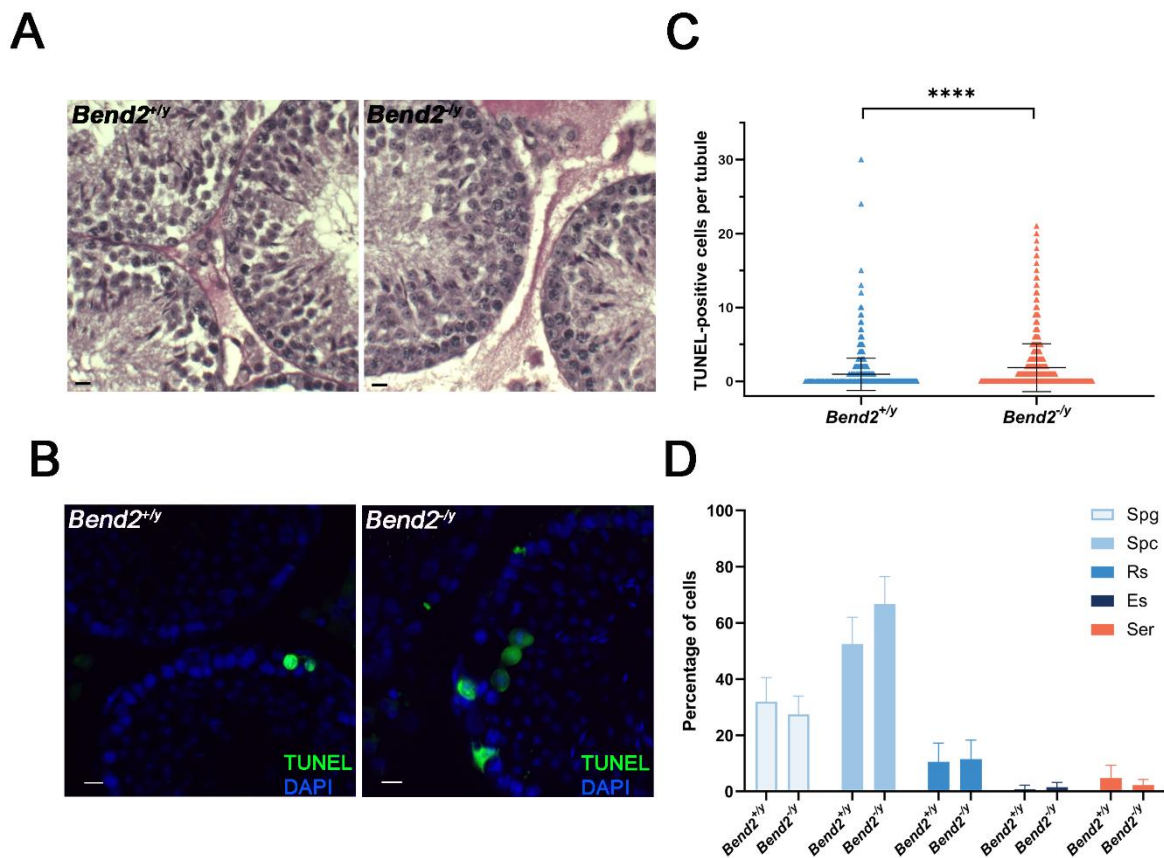


Figure 4-23. Spermatogenesis analysis in *Bend2*^{-/-} mice

(A) PAS-H stained mouse testis sections. Scale bar, 20 μ m. (B) Apoptosis detection on testis sections by TUNEL assay. Scale bar, 20 μ m. (C) Quantification of TUNEL-positive cells. The horizontal lines represent the mean \pm SD. N=1125 for *Bend2*^{+/y}; N=1195 for *Bend2*^{-/-}, **** $p < 0.0001$ t-test. (D) Classification of TUNEL-positive cells. The columns and error lines indicate the mean and SD. N=4, $p > 0.05$, One-Way ANOVA.

4.4.3.3. Analysis of synapsis and recombination in *Bend2*^{-/y} male

To examine the cause of the increased apoptosis in BEND2-deficient testes, we first assessed chromosome synapsis by immunolabelling surface-spread spermatocytes against SYCP3 (a marker of the AE) and SYCP1 (a marker of the SC transverse filament). SYCP3 began to form each developing chromosome axis in wild-type spermatocytes at leptotene. At zygotene, synapsis initiated as SYCP1 appeared at the synapsed region of the homologs. At pachytene, synapsis was completed as SYCP3 and SYCP1 completely colocalized. At diplotene, SCs disassembled, and SYCP1 were lost from separated SYCP3-labelled axes, but homologous chromosomes remained held together by chiasmata.

A similar synapsis progression was observed in *Bend2*^{-/y} spermatocytes (Figure 4-24A). However, the fraction of *Bend2*^{-/y} spermatocytes at the diplotene stage was significantly increased ($p=0.019$, One-Way ANOVA, Figure 4-24B) compared to wild-type mice. And the fraction of spermatocytes at the pachytene stage in *Bend2*^{-/y} mice ($48.6 \pm 6.8\%$, mean \pm SD, N=4,) appeared to be less than that in wild-type mice ($57.3 \pm 4.5\%$, mean \pm SD, N=4, $p=0.078$ One-Way ANOVA, Figure 4-24B). These results suggest that *Bend2*^{-/y} spermatocytes accumulate at the diplotene stage as there was a later block of the meiotic progression. Alternatively, this could also be explained if *Bend2*^{-/y} spermatocytes might exit pachytene faster than wild-type spermatocytes. Taken together, these results demonstrated that *Bend2*^{-/y} spermatocytes were able to complete synapsis and progress through meiotic prophase but following an altered timeline.

We next examined the meiotic recombination progress. During early meiosis, recombination initiates with SPO11-mediated DSB formation, leading to the phosphorylation of histone H2AX by ATM and thus triggering a series of DSB repair responses in the meiotic prophase (Bellani et al. 2005; Lange et al. 2011). In wild-type mice, YH2AX progressively disappeared from the autosomes while DSBs were repaired as prophase progressed. By pachytene, most YH2AX was associated with the sex body. From late pachytene, very few YH2AX patches could be observed on the autosomes, presumably corresponding to unrepaired DSBs (Figure 4-25A). In *Bend2*^{-/y} mice, there was a marked increase in the number of YH2AX patches from early pachytene until late diplotene (Figure 4-25B). This increase was significant at late pachytene ($p=0.0001$), early diplotene ($p=0.0007$), and late diplotene ($p=0.0222$) when compared to wild-type cells (t-

test, Figure 4-25B). These results indicated that in *Bend2*^{-/y} mice, there was a delay in DSB repair. Alternatively, the same results could be observed if more DSBs were formed during prophase in *Bend2*^{-/y} mice.

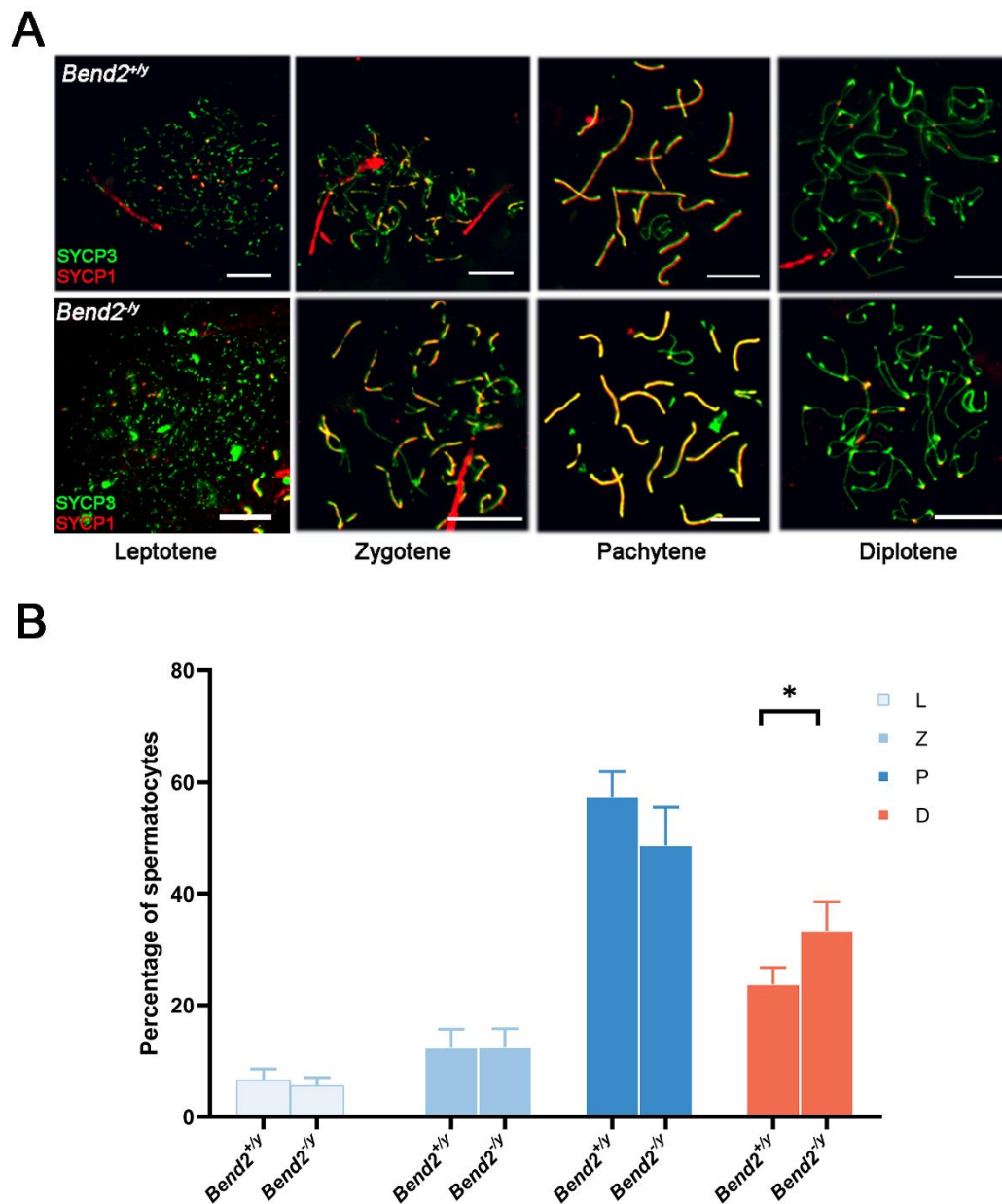


Figure 4-24. Meiotic progression of *Bend2*^{-/y} spermatocytes

(A) Chromosomal synapsis in spermatocytes. Representative images of SYCP3 and SYCP1 staining in spermatocyte nuclei from the stages shown. Scale bar, 10 μ m. (B) Meiotic prophase staging of spermatocytes. L: leptotene, Z: zygotene, P: pachytene, D: diplotene. The columns and lines indicate the mean and SD. N=4, * $p=0.019$, One-Way ANOVA.

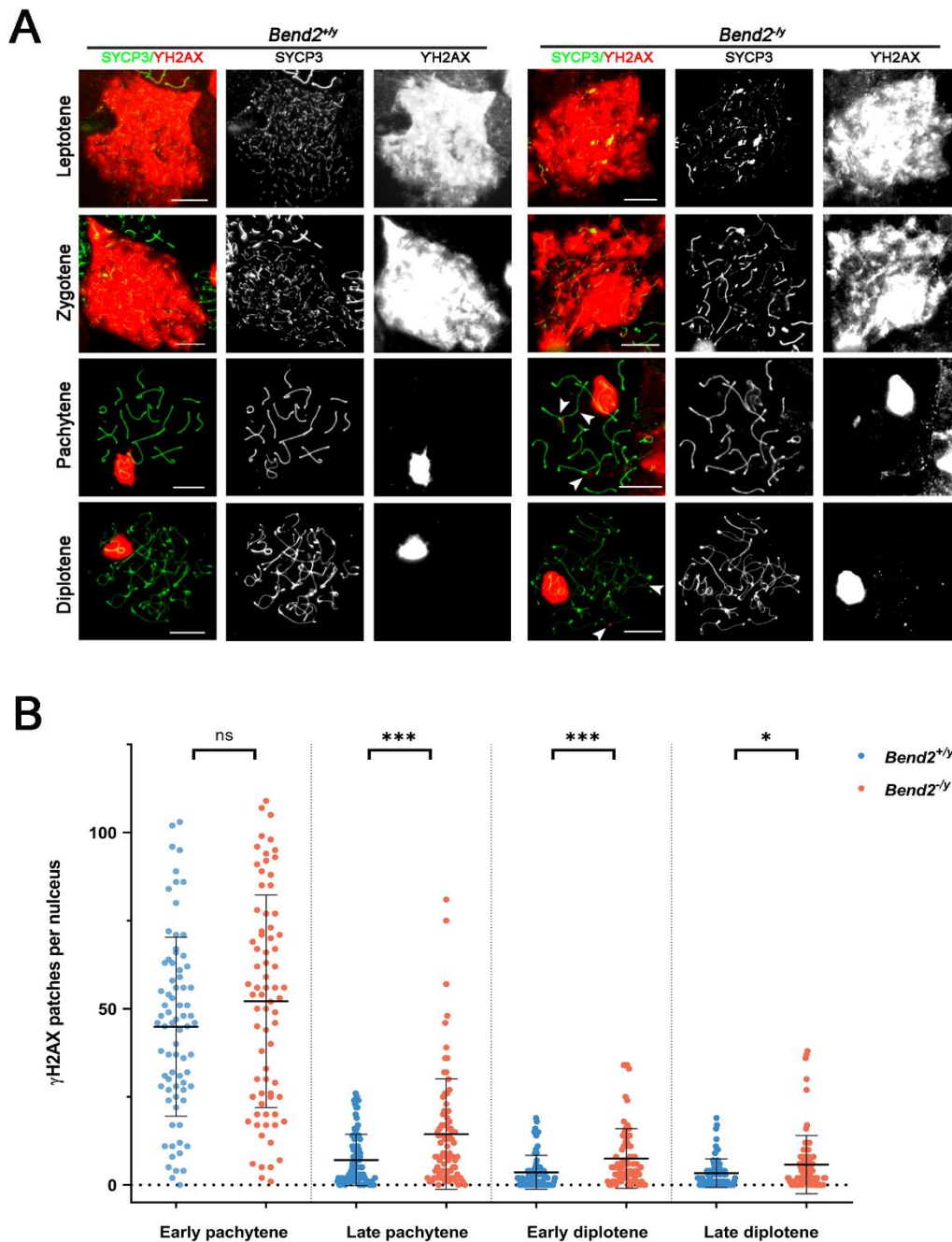


Figure 4-25. Examination of DSBs in *Bend2*^{-/y} spermatocytes

(A) Representative images of YH2AX staining in spermatocyte nuclei along meiotic prophase. Increased YH2AX signals are detected during late prophase in *Bend2*^{-/y} spermatocyte (white arrowheads). Scale bar, 10 μ m. (B) Quantification of YH2AX patches in spermatocyte nuclei per sub-stages. The patches were counted manually using the same method for every pair of control and mutant mice. The horizontal lines represent the mean and the vertical ones the SD. Number of analyzed nuclei from left to right: 76/74, 86/83, 73/75, and 78/81. *** $p=0.0001$ (late pachytene) and 0.0007 (early diplotene), * $p=0.0222$ t-test.

Once DSBs are resected, replication protein A (RPA) transiently binds to the nascent ssDNA overhangs, promoting the assembly of the recombinases RAD51 and DMC1 at DSBs sites (Moens et al. 2002). RAD51 and DMC1 replace RPA and form nucleoprotein filaments with the ssDNA, directing homology search and strand invasion (Brown and Bishop 2015; Hinch et al. 2020). These recombination intermediates can be visualized as foci on chromosome axes and thus used to monitor recombination progression (Baudat, Imai, and De Massy 2013).

In wild-type spermatocytes, the number of RPA foci peaked around early zygotene and progressively diminished as recombination proceeded (Figure 4-26). On the other hand, there were many RAD51 foci since leptotene. The number started to decline from early zygotene (Figure 4-27), consistent with previous studies (Moens et al. 2002; Pacheco et al. 2015). In *Bend2*^{-/y} mice, the spermatocytes had similar initial RPA and RAD51 foci numbers, suggesting that DSBs formation was not affected by the loss of *Bend2* (Figure 4-26B and 4-27B). While *Bend2*^{-/y} cells progressed, there was a tendency to accumulate more RPA foci and lose RAD51 foci at each stage. The differences became significant for RPA at late leptotene ($p=0.0015$ t-test, Figure 4-26B) and RAD51 at late zygotene and pachytene ($p=0.0428$ and 0.0002 respectively t-test, Figure 4-27B). These results indicated that there might be a subtle defect in the process of RAD51 replacing RPA.

As a result of homolog synapsis and recombination, at least one crossover per bivalent is generated to ensure accurate chromosome segregation at the first meiotic division (D Zickler and Kleckner 1999). We examined MLH1 foci, which becomes apparent at mid-late pachytene and marks most crossover-designated sites (L. K. Anderson et al. 1999). Although we detected a lower number of MLH1 foci in *Bend2*^{-/y} spermatocytes of (22.0 ± 2.3 , mean \pm SD, N=68) than in wild-type cells (22.5 ± 2.9 , mean \pm SD, N=74), the difference was not statistically significant ($p=0.2543$ t-test, Figure 4-28). Thus, based on these results, we concluded that crossover formation was not affected in *Bend2*^{-/y} spermatocytes.

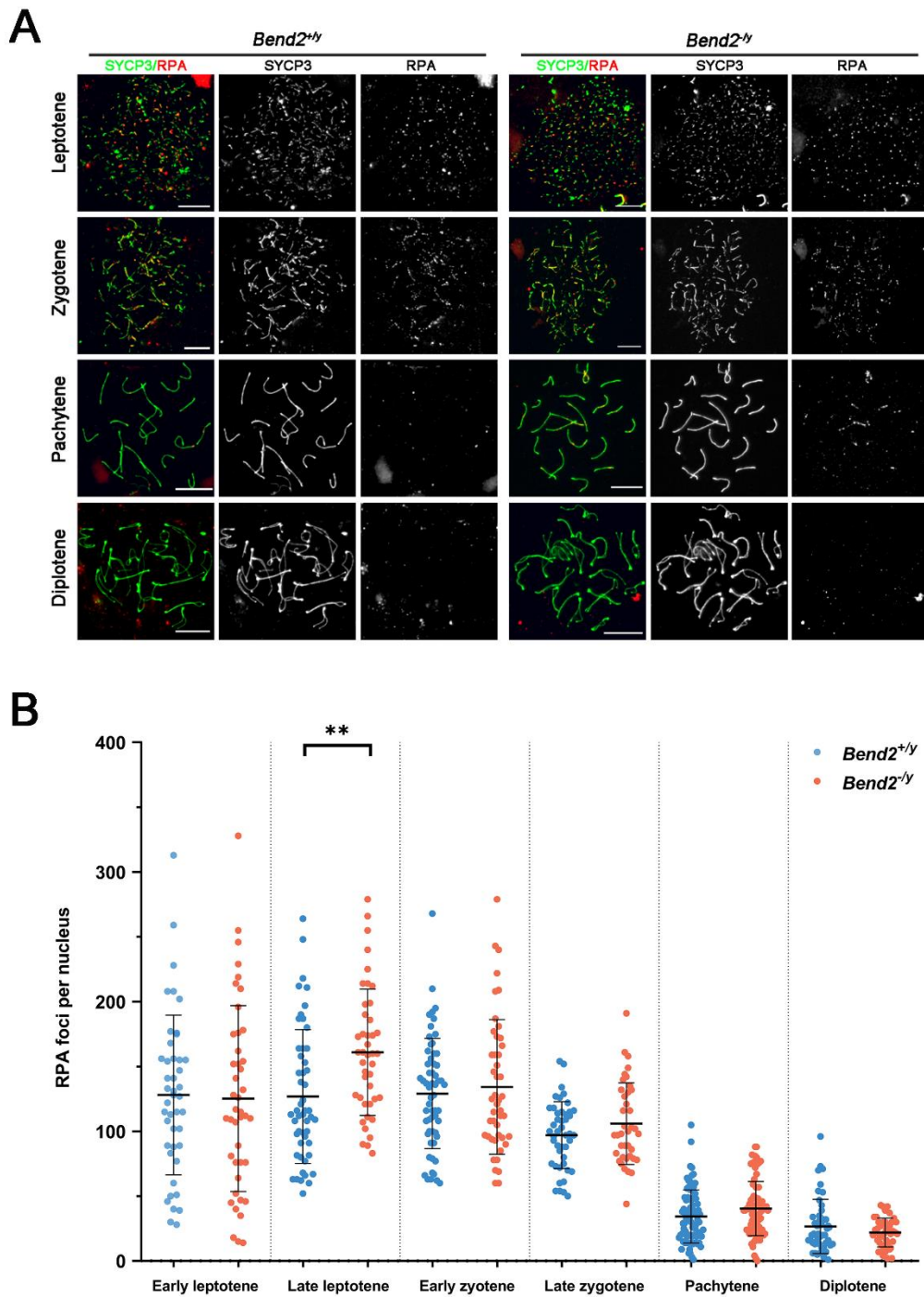


Figure 4-26. Examination of DSB repair-RPA in *Bend2*^{-/y} spermatocytes

(A) Representative images of RPA staining in spermatocyte nuclei during meiotic prophase. Scale bar, 10 μ m. (B) Quantification of RPA present in spermatocyte nuclei at the different sub-stages. Foci were counted using ImageJ with the same method for every *Bend2*^{+/y} and *Bend2*^{-/y} mice pair. The horizontal lines represent the mean and the vertical ones the SD. Number of analyzed nuclei from left to right (B): 44/43, 51/43, 59/46, 45/39, 81/77, and 48/43. ** $p=0.0015$ t-test.

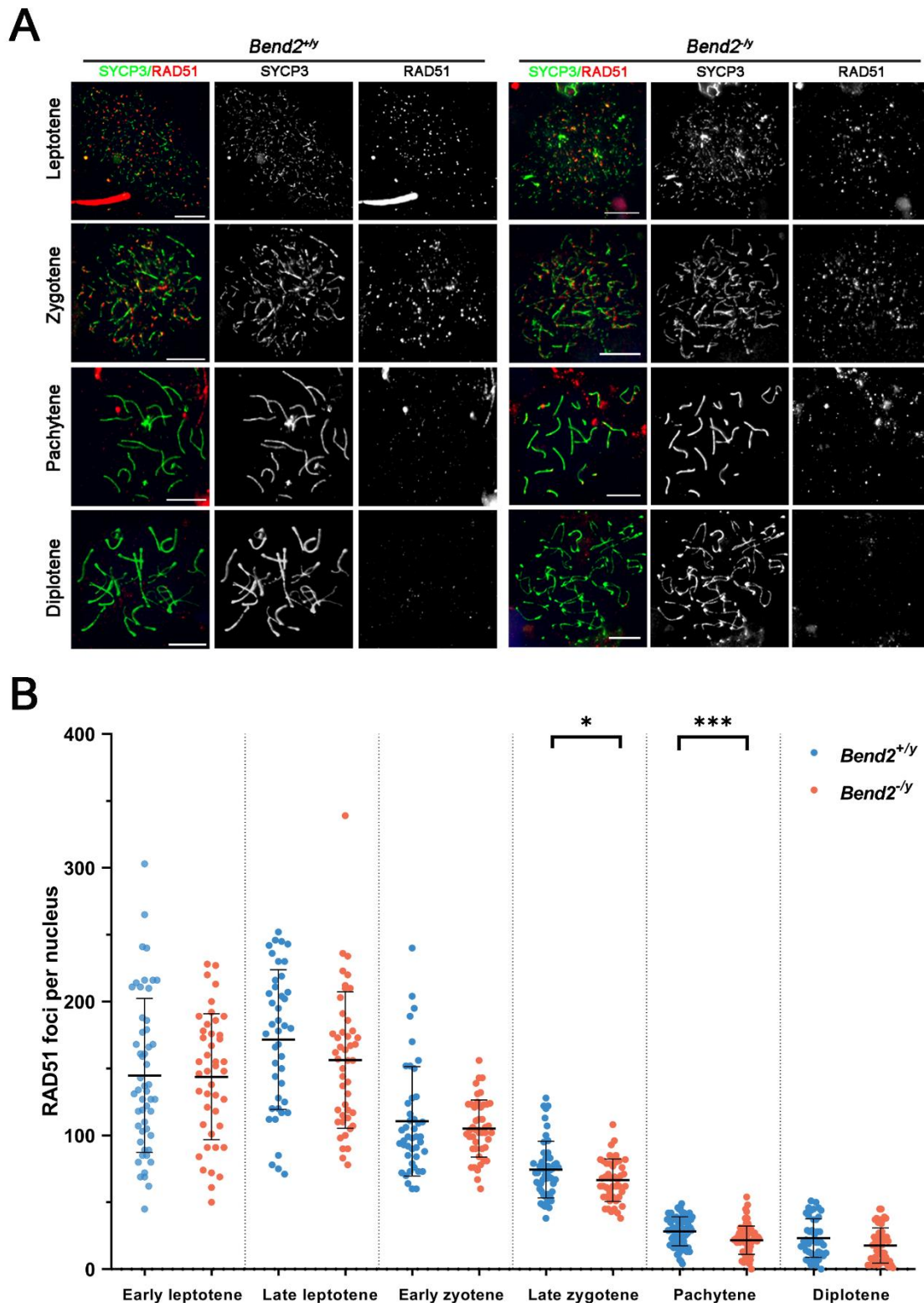


Figure 4-27. Examination of DSB repair-RAD51 in *Bend2^{-y}* spermatocytes

(A) Representative images of RAD51 staining in spermatocyte nuclei during meiotic prophase. Scale bar, 10 μ m. (B) Quantification of RAD51 present in spermatocyte nuclei at the different sub-stages. Foci were counted using ImageJ with the same method for every *Bend2^{+/y}* and *Bend2^{-y}* mice pair. The horizontal lines represent the mean and the vertical ones the SD. Number of analyzed nuclei from left to right (B): 52/43, 42/46, 44/46, 51/45, 77/73, and 45/49. * $p=0.0428$, *** $p=0.0002$ t-test.

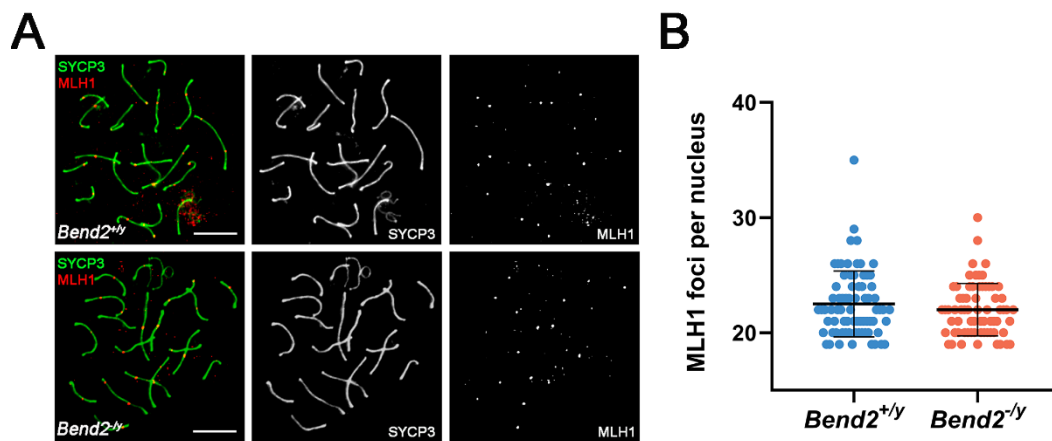


Figure 4-28. Examination of CO formation in *Bend2*^{-/-} spermatocytes

(A) Representative images of MLH1 in spermatocyte nuclei. Scale bars, 10 μ m. (B) Quantification of MLH1 foci in spermatocyte nuclei. Only spermatocytes containing ≥ 19 MLH1 foci/nucleus were counted. The horizontal lines represent the mean \pm SD. The nuclei analyzed were 74 for *Bend2*^{+/-} and 68 for *Bend2*^{-/-}, $p > 0.05$, Mann-Whitney test.

4.4.3.4. Analysis of oogenesis in *Bend2* female mutants

Female mutant mice develop normally in adults without apparent somatic defects too. *Bend2*^{-/-} mice were fertile. However, the litter size was significantly smaller than in wild-type females (Figure 4-29A). To investigate if the loss of BEND2 affected oogenesis, we performed histological analysis of whole ovaries of adult mice heterozygous (*Bend2*^{+/-}), homozygous (*Bend2*^{-/-}), as well as wild type. At 10-12 weeks of age (Figure 4-29B), we found one *Bend2*^{-/-} female had considerably small and malformed ovaries with complete absence of follicles. Other *Bend2*^{-/-} females had normal-sized ovaries with developing follicles but lacking primordial follicles (Figure 4-29B). These results suggested there might be a reduction in the oocyte pool in *Bend2*^{-/-} females.

To confirm this hypothesis, we further quantified the number of follicles found in 15 random non-consecutive sections per ovary and classified them into each follicle type. The results showed a significant reduction of the total number of follicles per section observed in both *Bend2*^{+/-} and *Bend2*^{-/-} ovaries compared to wild-type controls ($p = 0.0273$ and 0.0076 respectively t-test, Figure 4-30A). Moreover, we found a reduction

of the number of primordial follicles per ovary in *Bend2*^{+/-} (51.9.0 ± 33.1, mean ± SD, N=8) and *Bend2*^{-/-} (41.0 ± 58.9, mean ± SD, N=3) mice compared to wild-type mice (68.50 ± 17.2, mean ± SD, N=6, $p>0.05$ t-test Figure 4-30B). This tendency became more apparent when we examined the oocyte pool in females at an older age of 15-20 weeks (Figure 4-30D). At this age, we also found a substantial reduction of the follicle number per section in *Bend2*^{+/-} and *Bend2*^{-/-} ovaries ($p<0.0001$ both t-test, Figure 4-30C) than in wild-type ovaries. More importantly, the number of primordial follicles per ovary was significantly lower in *Bend2*^{+/-} and *Bend2*^{-/-} females ($p=0.0285$ and 0.0164 respectively t-test Figure 4-30D) than in wild-type females. Taken together, our results demonstrated that *Bend2* mutants have a reduced oocyte pool leading to quicker exhaustion of the ovarian reserve during adulthood.

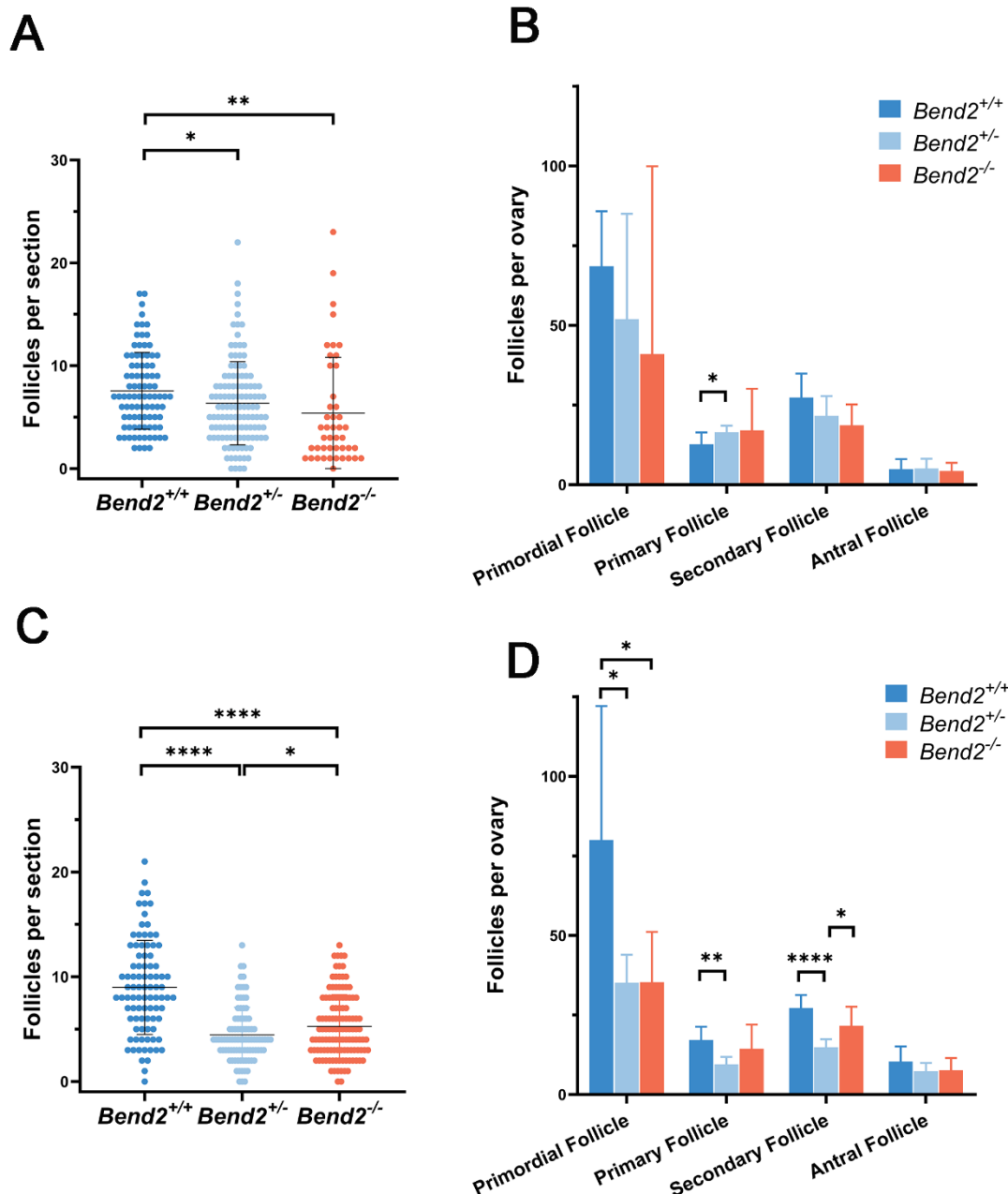


Figure 4-30. Follicle analysis in *Bend2* mutant females

Quantification of follicles from ovaries at 10-12 weeks of age (A) and 15-20 weeks of age (C). Follicles of 15 non-consecutive sections were counted from each ovary, representing between a twentieth and a tenth of the entire ovary. The horizontal lines represent the mean \pm SD. Number of counted sections (A): 90 for *Bend2*^{+/+}, 120 for *Bend2*^{+/-} and 45 for *Bend2*^{-/-}; number of counted sections (C): 90 for *Bend2*^{+/+}, 90 for *Bend2*^{+/-} and 120 for *Bend2*^{-/-}. * $p=0.0273$, ** $p=0.0076$ (A); **** $p<0.0001$, * $p=0.0463$ (C); t-test. Classification of follicles from ovaries at 10-12 weeks of age (B) and 15-20 weeks of age (D). Follicles of each ovary in (A)(C) were classified into different types. The columns and lines indicate the mean and SD. Number of analyzed ovaries \times total follicles per ovary (mean \pm SD), A and B: 6 \times (113.3 \pm 20.7) for *Bend2*^{+/+}, 8 \times (95.1 \pm 39.3) for *Bend2*^{+/-} and 3 \times (81 \pm 79.8) for *Bend2*^{-/-}; C and D: 6 \times (134.7 \pm 44.8) for *Bend2*^{+/+}, 6 \times (66.8 \pm 11.9) for *Bend2*^{+/-} and 8 \times (78.9 \pm 24.9) for *Bend2*^{-/-}. * $p=0.0283$ (A); * $p=0.0285$, * $p=0.0164$, ** $p=0.0027$, **** $p<0.0001$, * $p=0.0232$ (C); t-test.

4.4.3.5. Analysis of synapsis and recombination in *Bend2* mutant females

To investigate whether the reduced ovarian reserve in mutant adults was related to a defect during meiotic prophase, we examined the same synapsis and recombination markers described above (section 4.4.2.3) in wild-type, *Bend2*^{+/-}, and *Bend2*^{-/-} oocytes. According to our previous findings, we speculated that the deficiency of BEND2 preferably would cause defects during late prophase. Therefore, we performed this cytological analysis on spreads prepared from 18 dpc and 1 dpp ovaries, in which most oocytes should have reached the pachytene stage (Martínez-Marchal et al. 2020).

In wild-type ovaries, most oocytes at 18 dpc were at pachytene stages, a small fraction of them was still at the zygotene stage, and a minority at the leptotene stage (Figure 4-31B). At 1 dpp, most oocytes were at the pachytene and diplotene stages (Figure 4-31C). In *Bend2*^{+/-} and *Bend2*^{-/-} ovaries, zygotene and pachytene oocytes undergoing normal synapsis and diplotene oocytes undergoing desynapsis were observed at both 18 dpc and 1 dpp (Figure 4-31A-C). Although the difference was not significant, probably due to the inadequate number of analyzed animals or oocytes, a higher proportion of zygotene oocytes (38.5% ± 14.8%, mean ± SD, N=2) and a lower proportion of pachytene oocytes (58.5% ± 16.3%, mean ± SD, N=2) were shown in *Bend2*^{-/-} ovaries than in wild-type ovaries at 18 dpc (20.0% ± 4.2% for zygotene, 73.5% ± 5.0% for pachytene, mean ± SD, N=2 for both, *p*>0.05 One-Way ANOVA). Similarly, a higher proportion of pachytene oocytes (59.3% ± 22.0%, mean ± SD, N=3) and a lower proportion of diplotene oocytes (38.0% ± 19.2%, mean ± SD, N=3) were shown in *Bend2*^{-/-} ovaries than in wild-type ovaries at 1 dpp (40.7% ± 14.2% for pachytene, 57.0% ± 12.5%, mean ± SD, N=3 for both, *p*>0.05 One-Way ANOVA, Figure 4-31B and C). Overall, these results suggested a possible slower meiotic progression in BEND2-deficient oocytes without an apparent synapsis defect.

Consistent with the observation in *Bend2* male mutants, we also found increased levels of γH2AX in late prophase oocytes in *Bend2* mutant mice (Figure 4-32). In wild-type females, γH2AX patches could be detected along axes in most pachytene oocytes and even in many diplotene oocytes (Figure 4-32A-C). This is different from wild-type males, in which γH2AX can only be detected as very few patches in late pachytene cells and is almost undetectable in most diplotene cells (Figure 4-25), presumably because synapsis progresses faster than recombination in females than in males (Roig et

al. 2004). In *Bend2*^{-/-} females, higher levels of γH2AX were observed at all stages analyzed (early pachytene, 18 dpc and late pachytene, and diplotene, 1 dpp, Figure 4-32A-C). Many early pachytene *Bend2*^{-/-} oocytes exhibited an overall intense γH2AX signal reminiscent of wild-type zygotene cells (Figure 4-32A). To quantitatively compare these differences, we measured the mean γH2AX intensity in early pachytene oocytes and counted the γH2AX patches in late pachytene and diplotene oocytes. As expected, a substantial increase of γH2AX was present in *Bend2*^{-/-} oocytes at all the tested stages ($p=0.0288$ for early pachytene; $p<0.0001$ for late pachytene, early diplotene and late diplotene t-test, Figure 4-32B and C). Also, *Bend2*^{+/-} oocytes had a significant increase of γH2AX at early diplotene ($p=0.0086$ t-test, Figure 4-32C). Thus, like in *Bend2*^{-/-} mice, DSB repair was impaired or more DSBs were formed in *Bend2*^{-/-} mice.

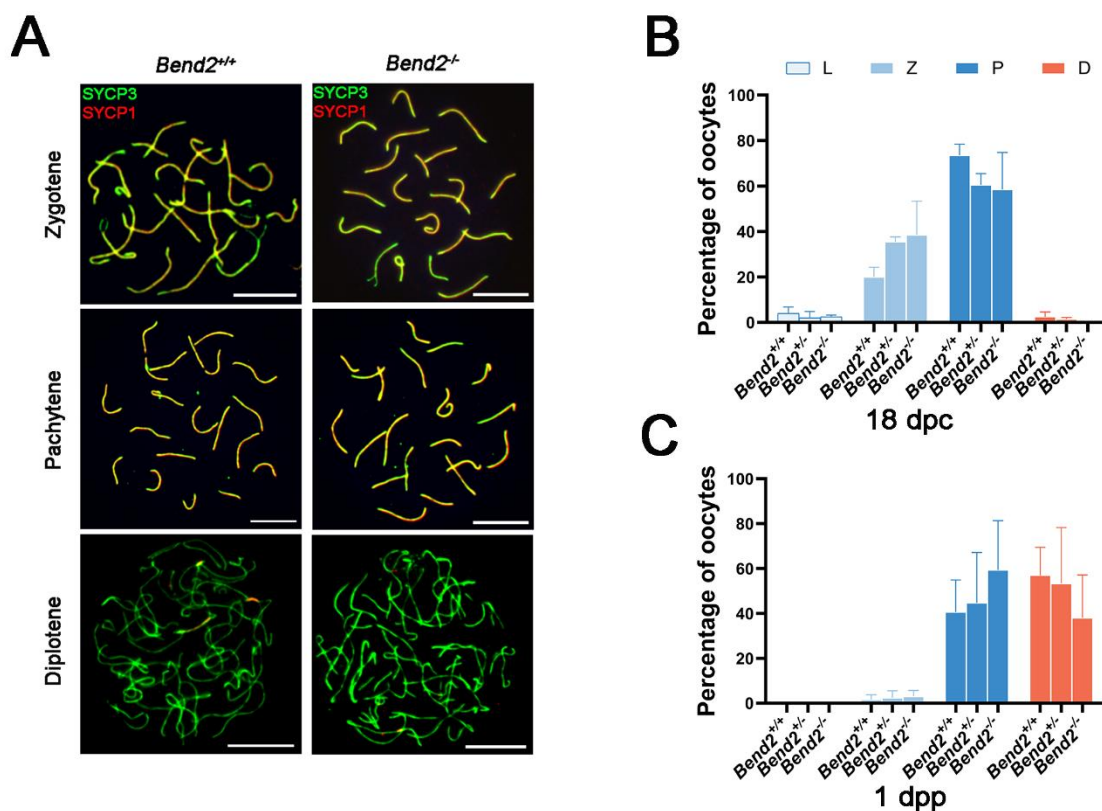


Figure 4-31. Meiotic progression of *Bend2* mutant oocytes

(A) Chromosomal synapsis in oocytes. Representative images of SYCP3 and SYCP1 staining in 18 dpc and 1 dpp oocyte nuclei are shown. Scale bar, 10 μ m. (B) Meiotic prophase staging of 18 dpc oocytes. (C) Meiotic prophase staging of 1 dpp oocytes. L: leptotene, Z: zygotene, P: pachytene, D: diplotene. The columns and lines indicate the mean and SD. The number of animals analyzed per genotype, 2 for 18 dpc and 3 for 1 dpp. $p>0.5$ for all the comparisons One-Way ANOVA.

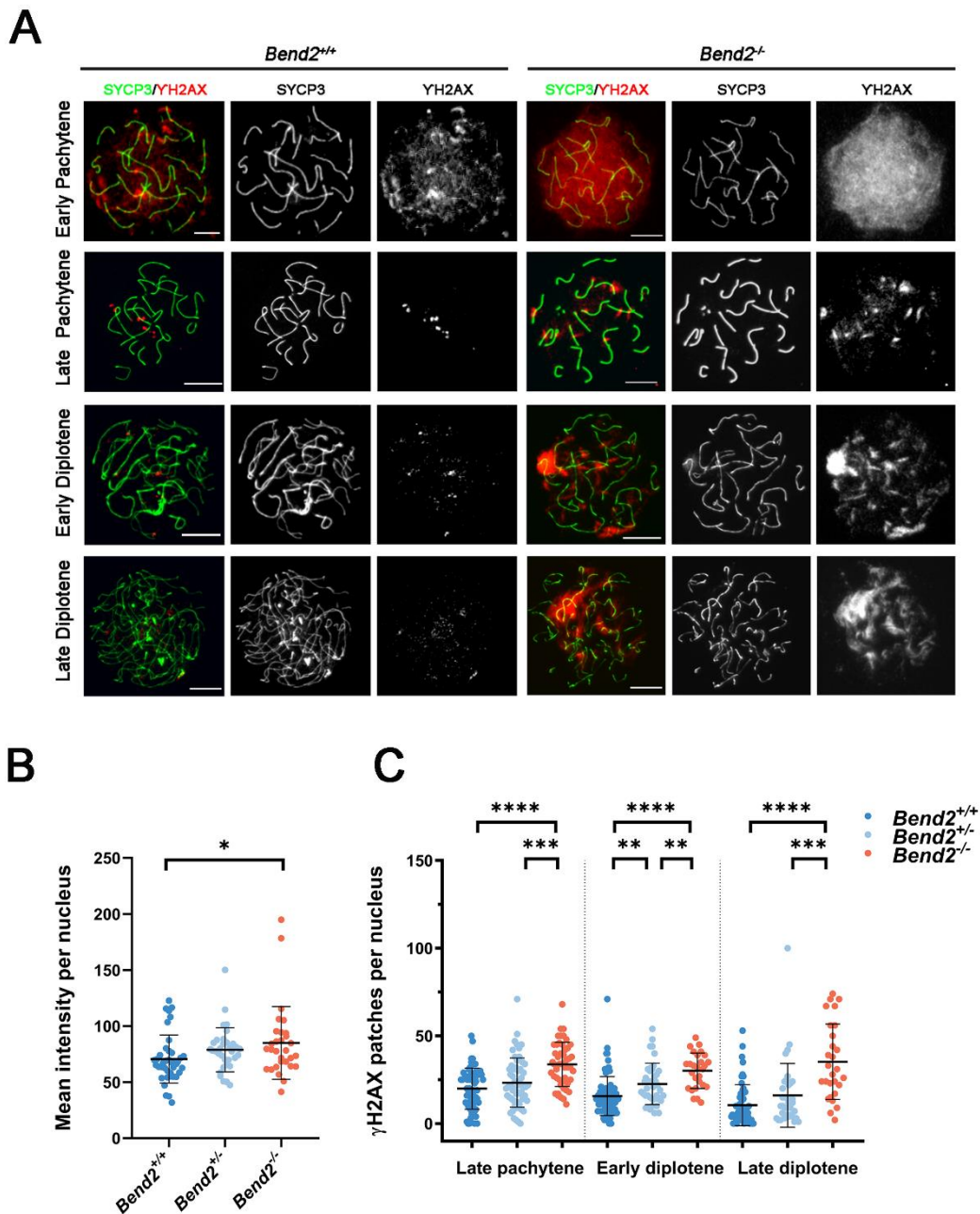


Figure 4-32. Examination of DSBs in *Bend2* mutant oocytes

(A) Representative images of γ H2AX staining in 18 dpc and 1 dpp oocyte nuclei at the pachytene and diplotene stage. Scale bar, 10 μ m. (B) Quantification of γ H2AX patches in oocyte nuclei at sub-stages. The mean intensity of γ H2AX staining in 18 dpc oocyte nuclei was measured by Image J. The patches of γ H2AX in 1 dpp oocyte nuclei were counted manually. The horizontal lines represent the mean \pm SD. The number of analyzed 18 dpc nuclei (B): 40 for *Bend2^{+/+}*, 33 for *Bend2^{+/-}*, 30 for *Bend2^{-/-}*. The number of analyzed 1dpp nuclei from left to right (C): 64/57/48, 81/40/27, and 57/37/28. * $p=0.0288$ (B); *** $p=0.0001$ (late pachytene), ** $p=0.002$ and ** $p=0.0086$ (early diplotene), *** $p=0.0003$ (late diplotene), **** $p<0.0001$; t-test.

We also analyzed the number of RPA and RAD51 foci in this wild-type, *Bend2^{+/-}* and *Bend2^{-/-}* oocytes. However, no differences were found despite a slight decrease in RPA

foci in *Bend2*^{-/-} oocytes (Figure 4-33) and a slight increase of RAD51 foci in only pachytene *Bend2*^{-/-} oocytes (Figure 4-34). These results suggest that the increased presence of YH2AX in *Bend2*^{-/-} oocytes may not be related to defective meiotic recombination but to other causes, like meiotic silencing of unsynapsed chromosomes (MSUC) or alternative DNA repair pathways.

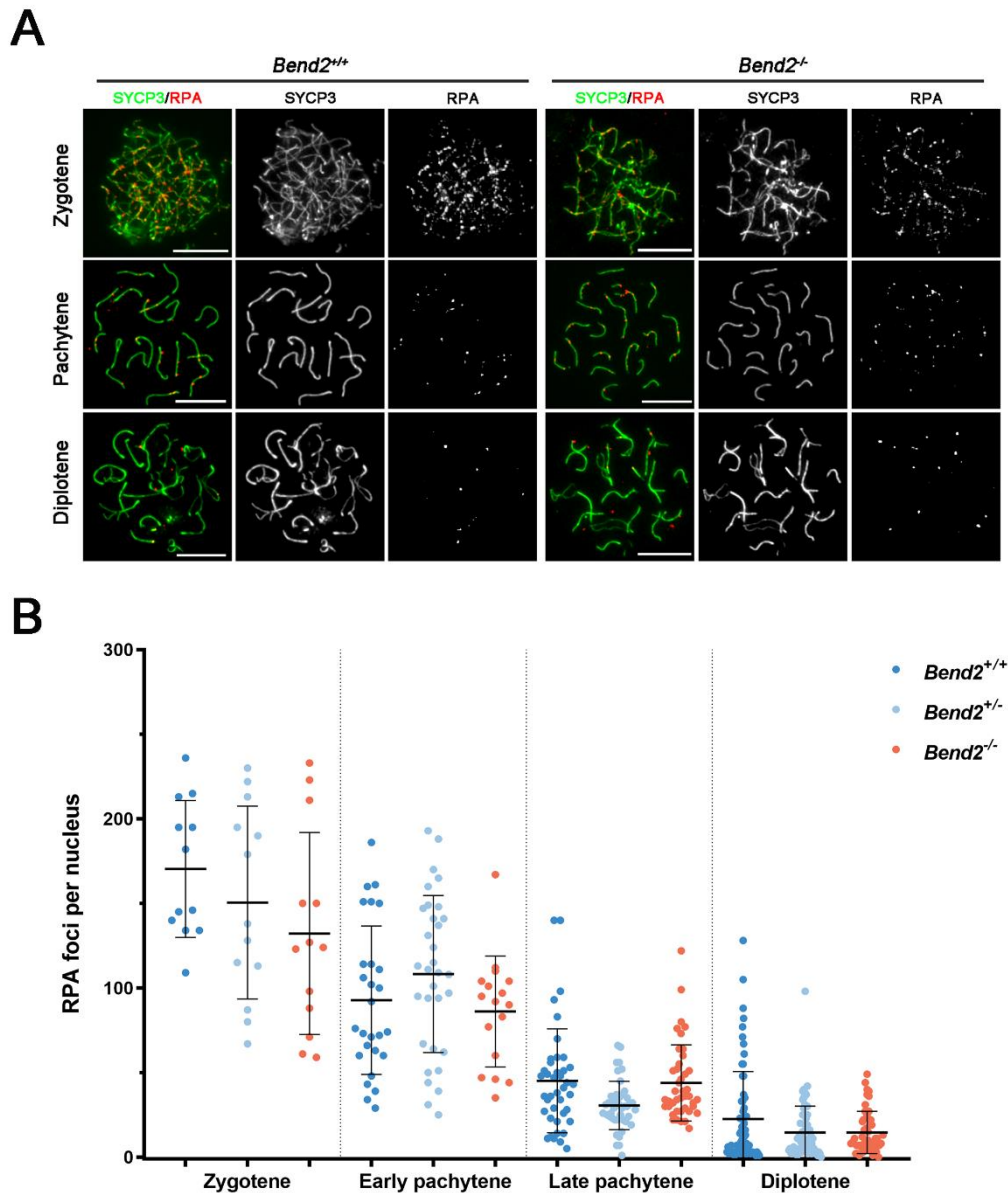


Figure 4-33. Examination of DSB repair-RPA in *Bend2* mutant oocytes

(A) Representative images of RPA staining in 18 dpc and 1 dpp oocyte nuclei from zygotene to diplotene stage. Scale bar, 10 μ m. (B) Quantification of RPA foci present in oocyte nuclei at sub-stages. Zygotene and early pachytene nuclei analyzed were from 18 dpc ovaries, and late pachytene and diplotene nuclei analyzed were from 1 dpp ovaries. Foci were counted manually. The horizontal lines represent the mean \pm SD. Number of analyzed nuclei from left to right (B): 12/13/13, 27/32/17, 41/43/42, and 65/67/49. $p > 0.5$ for all the comparisons t-test.

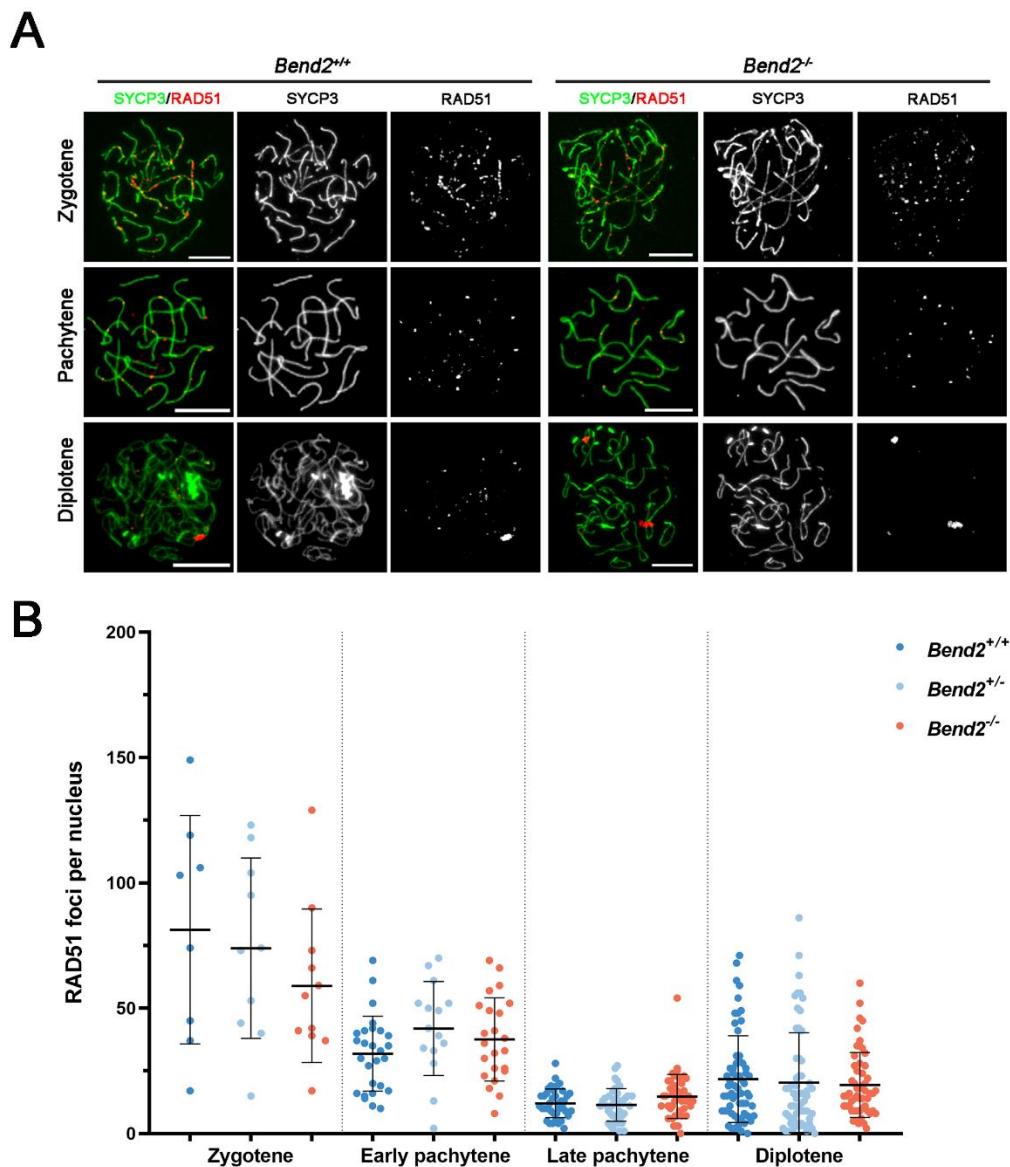


Figure 4-34. Examination of DSB repair-RAD51 in *Bend2* mutant oocytes

Representative images of RAD51 staining (A) in 18 dpc and 1 dpp oocyte nuclei from zygotene to diplotene stage. Scale bar, 10 μ m. Quantification of RAD51 foci (B) present in oocyte nuclei at sub-stages. Zygotene and early pachytene nuclei analyzed were from 18 dpc ovaries, and late pachytene and diplotene nuclei analyzed were from 1 dpp ovaries. Foci were counted manually. The horizontal lines represent the mean \pm SD. Number of analyzed nuclei from left to right (B): 8/10/11, 27/15/23, 38/39/46, and 62/60/55. $p > 0.5$ for all the comparisons t-test.

Interestingly, the number of MLH1 foci in late prophase oocytes was significantly lower in both *Bend2*^{-/-} and *Bend2*^{+/-} females than in wild-type females ($p = 0.006$ for *Bend2*^{-/-}, $p = 0.0106$ for *Bend2*^{+/-} t-test, Figure 4-35). These results show that the depletion of BEND2 in females did not affect the early recombination markers but caused a slight defect in crossover formation.

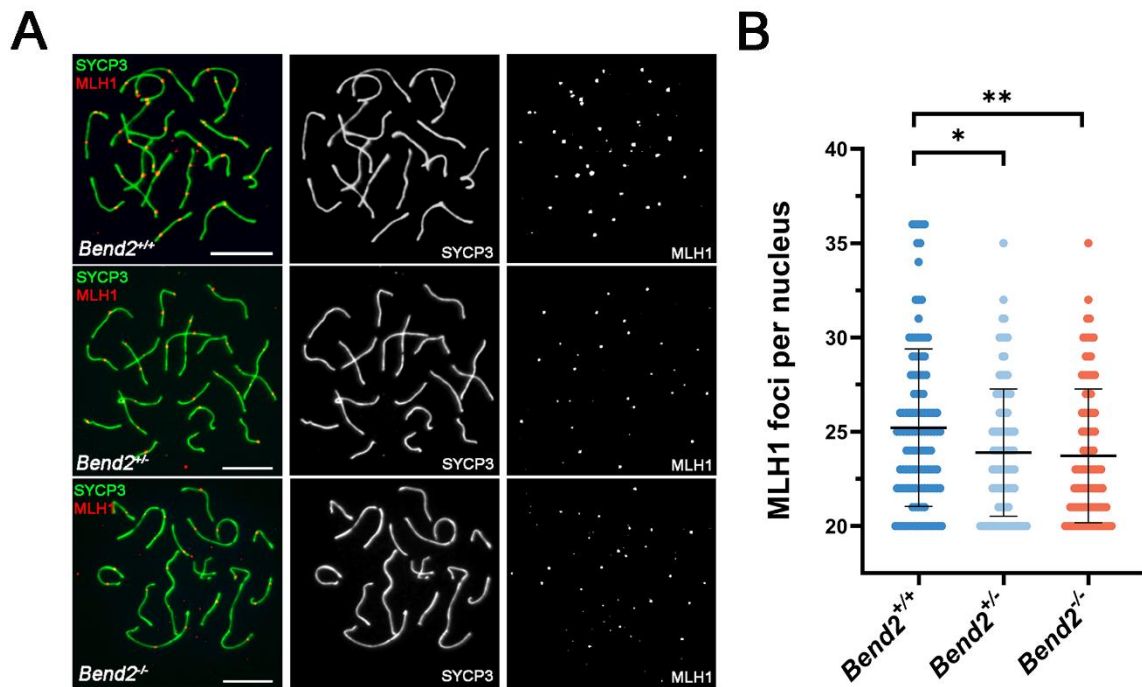


Figure 4-35. Examination of CO formation in *Bend2* mutant oocytes

(A) Representative images of MLH1 in 1 dpp oocyte nuclei. Scale bar, 10 μ m. (B) Quantification of MLH1 foci in 1 dpp oocyte nuclei. Only oocytes containing ≥ 20 MLH1 foci/nucleus were counted. The horizontal lines represent the mean \pm SD. Number of analysed nuclei: 120 for *Bend2*^{+/+}, 106 for *Bend2*^{+/-}, 95 for *Bend2*^{-/-}; * $p=0.0237$, ** $p=0.0057$; Mann-Whitney test.

4.5. Functional analysis of 355P1/USP44 in meiosis

On top of gene 255P1/BEND2, we also selected another putative meiotic gene, 355P1, and performed functional analysis to investigate its role in meiosis. 355P1 possessed several characteristics indicating its possible function in the meiotic prophase. First, it was meiosis-specifically expressed in testis and 18 dpc fetal ovaries but not present in the adult ovary (section 4.1), suggesting it might specifically be expressed during meiotic prophase in both genders. Second, when electroporated to mouse testis, 355P1 is closely associated with the SC, suggesting a meiotic function (section 4.3.9). Third, 355P1 contains an N-terminal USP domain, forming the largest family of deubiquitinating enzymes (DUBs)-the ubiquitin-specific proteases (USPs). DUBs cleave ubiquitin from proteins, thus reversing the effects of the ubiquitin-proteasome system (UPS) (Reyes-Turcu, Ventii, and Wilkinson 2009). The UPS has been demonstrated to be responsible for most protein turnover in the mammalian cells, and it is implicated in various aspects of meiotic prophase (Prasada Rao et al. 2017). Thus, we hypothesized that 355P1 could have a specific SC-related function during the meiotic prophase.

4.5.1. The distinction between 355P1 and USP44 in testis

Full-length 355P1 overlaps with the C-terminus of a known mouse gene *Usp44* (*Usp44-202* transcript), implying it might be a novel isoform of *Usp44* produced by an alternative transcript initiation site (Figure 4-36A). Thus, we questioned whether 355P1 was present in mouse testis alone or along with other *Usp44* transcripts. To address this issue, we carried out an *in-house* designed, template-switched-based 5' RACE analysis to detect all the mRNA transcription start points containing 355P1 sequences in mouse testis (Figure 4-36A and B). Our previous RT-PCR analysis showed that 355P1 was not expressed in the liver. Thus, we performed the 5' RACE analysis in the liver as a negative control. If 355P1 was expressed in mouse testis alone, we expected to detect only 355P1 mRNA in testis. If 355P1 was present with other splicing variants from USP44, we expected to identify 355P1 mRNA and at least another *Usp44* mRNA in the testis. Unexpectedly, we detected an mRNA of 355P1's size in both testis and liver (Figure 4-36C). Since 355P1 is not present in the liver, these RACE products were likely to result from unspecific amplification. We cloned the RACE products into a pEGFP vector and determined their sequences by Sanger sequencing to confirm this assumption. We found that these RACE products were unspecific amplification due to the mispriming of primers. Hence, we tried the 5' RACE analysis with a lower primer concentration and substituted the primer to avoid this unspecific amplification. However, we failed to detect any expected RACE products in the testis (Figure 4-36C).

Next, we used the RT-PCR to reveal the presence of 355P1 and the full-length *Usp44* (*Usp44-202*) in mouse testis. As 355P1 only overlaps with part of C-terminal *Usp44*, RT-PCR with a forward primer upstream 355p1 and a reverse primer within 355P1 would specifically detect *Usp44-202* (Figure 4-36A). Using these primers, we performed an RT-PCR analysis in prepubertal testis at different ages to determine the *Usp44* expression pattern during spermatogenesis. We compared it to our previous result of the expression pattern of 355P1 during spermatogenesis (section 4.1). We found that *Usp44-202* was undetectable in testis up to 16 dpp and abundantly present in adult testis. These results differed distinctly from that 355P1 could be detected as early as in the 2 dpp testis (Figure 4-36D). Therefore, we propose 355P1 as a possible novel meiosis-specific isoform of *Usp44* and will refer to 355P1 as *Usp44-203* after 2 annotated *Usp44* transcripts

henceforth.

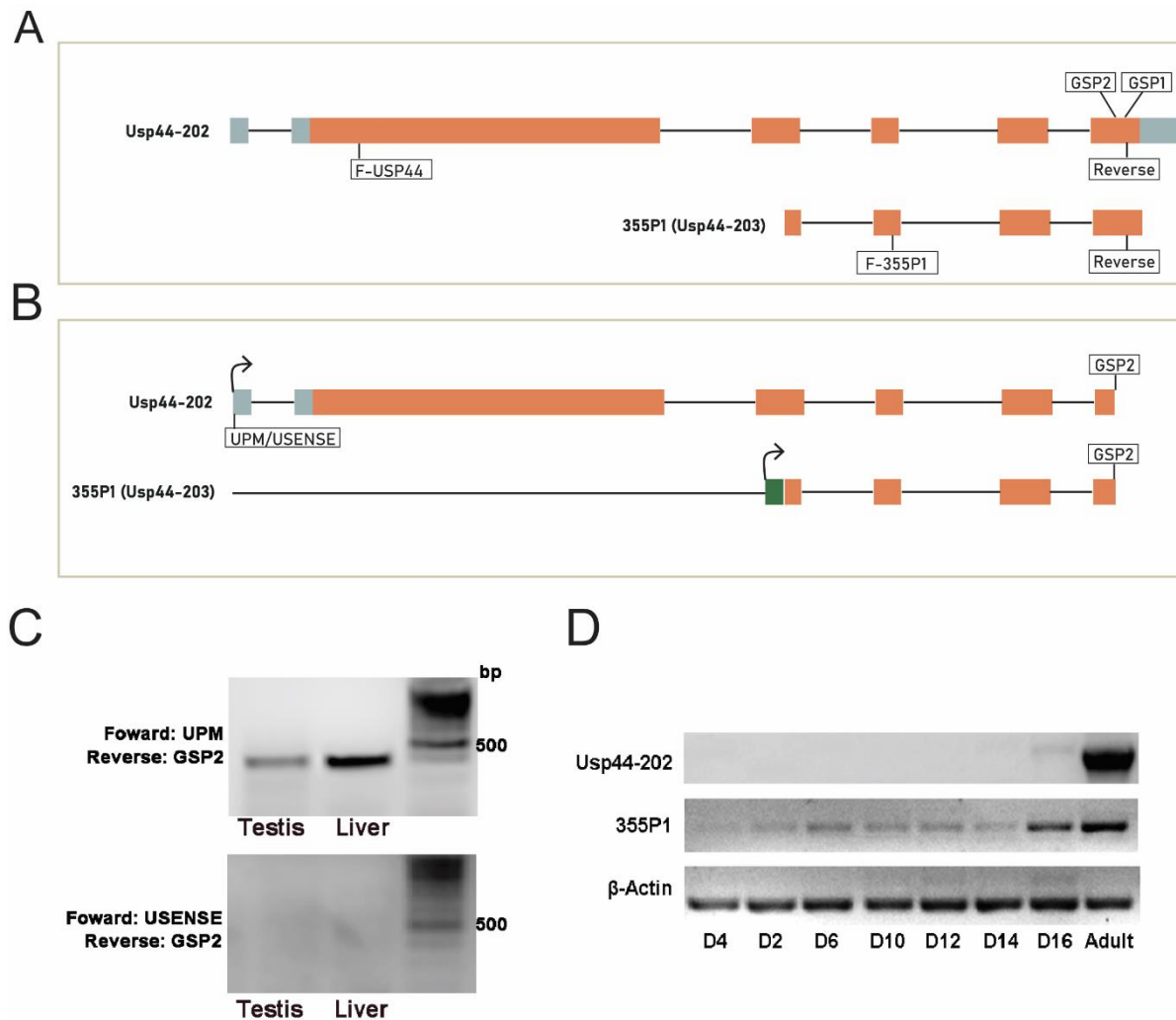


Figure 4-36. The distinction between 355P1 and mouse USP44

(A) Schematic representations of the mouse *Usp44* (transcript 202) and 355P1 (*Usp44-203*). Orange boxes indicate coding regions; grey boxes indicate non-coding regions. 355P1 overlaps the C terminus of *Usp44-202*, hence termed as *Usp44-203* following two annotated *Usp44* transcripts. The GSP1 and GSP2 primer locations used for 5' RACE RT-PCR are displayed at the coding region. (B) Schematics of expected transcriptions detected by 5' RACE. Arrows indicate transcription start points; the green box indicates a possible non-coding region of 355P1. (C) 5' RACE RT-PCR results. The liver is tested as a control. Two pairs of primers were tried, whose locations are indicated in (B). (D) Expression pattern during spermatogenesis. RT-PCR was performed in testes at different ages using primers indicated in (A): F-USP44 and Reverse for mouse USP44; F-355P1 and Reverse for 355P1.

4.5.2. Localization of USP44 in meiocytes

To gain insight into the function of USP44 in meiosis, we first tried to detect its cellular localization in spermatocytes using two different commercial antibodies against human USP44 or mouse USP44. Both failed to recognize USP44 either in spermatocytes

by IF or in testis by WB. Therefore, we also generated an *in-house* USP44 polyclonal antibody.

4.5.2.1. USP44 polyclonal antibody generation

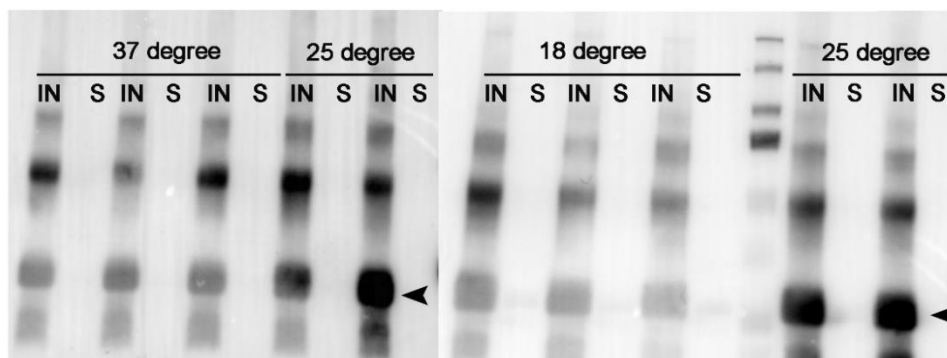
To obtain the polyclonal serum, we cloned the full-length CDS of *Usp44-203* into the bacterial expression vector pET-28a (+)-TEV and expressed the protein in BL21(DE3) *E. coli* cells. First, a condition screen step was performed to determine the optimal expression condition for USP44. We found that USP44 was highly expressed in *E. coli* cells after ON incubation at 25°C with 0.5mM IPTG induction. However, the expressed protein aggregated in inclusion bodies (IBs) (Figure 4-37A). Thus, after a 2L scale-up expression, we solubilized the IBs to release protein for purification and obtain ~8mg recombinant USP44 protein. Still, we could not remove the His-tag from the purified USP44 protein and eventually decided to use the remained 3.36 mg of His-tagged USP44 protein as antigen. Recombinant USP44's protein sequence was also confirmed by PMF analysis before injecting to animals. Two rabbits (Rb1888 and Rb889) were immunized for raising antiserum. High responses were detected in both rabbits by ELISA after the second and the third booster (Figure 4-37B). We terminated the immunization and harvested the final serum after the third booster. The polyclonal serum was further purified, and we tested the purified serum by IF. However, only the purified antiserum from Rb1889 detected USP44 in spermatocyte spreads. Thus, the purified antiserum from Rb1889 was used for the following USP44 detection analysis.

4.5.2.2. Characterization of USP44 in meiocytes

To characterize the expression and localization of USP44 in meiocytes, we performed IF in spermatocytes and 18 dpc oocyte spreads using the *in-house* USP44 polyclonal antibody. USP44 was first detected as continuous foci at synapsed chromosome axes in zygotene spermatocytes. More USP44 accumulated along with the SC until pachytene as chromosomes synapsed. USP44 coated the SC axis co-localizing with SYCP3. The general axis staining of USP44 became more apparent on autosomes until mid-late pachytene. Interestingly, no evident staining of USP44 was detected on

PAR or around sex chromosomes at pachytene (Figure 4-38A). During diplotene, as homologous chromosome desynapsed, USP44 mostly disappeared from the desynapsed axis and only remained at synapsed regions. (Figure 4-38A). In oocytes, a similar USP44 staining pattern was observed. USP44 appeared on synapsed axes from zygotene to diplotene as continuous foci or continuous axis staining. However, the general axis staining in females was most apparent during late-pachytene to early-diplotene, later than that in males. (Figure 4-38B).

A



B

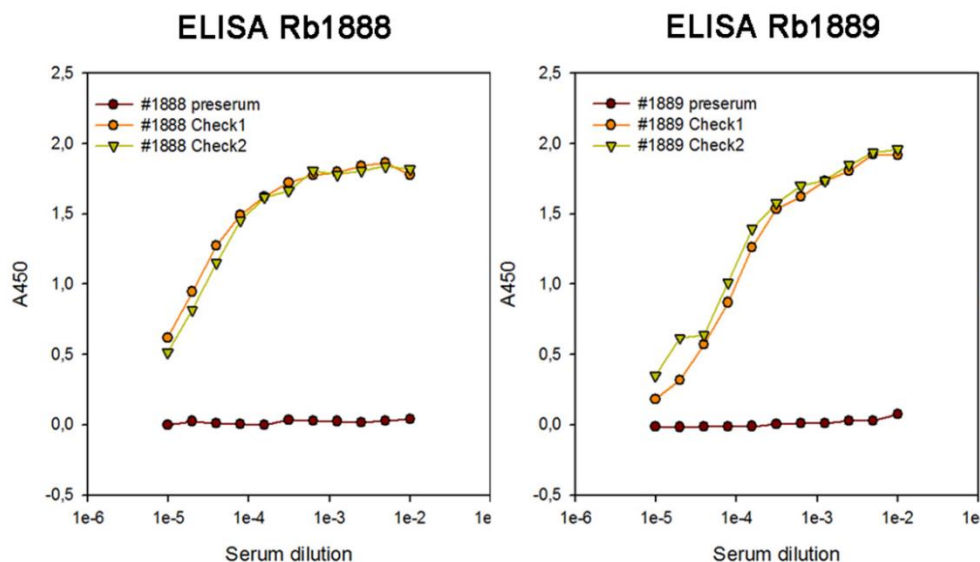


Figure 4-37. In-house USP44 polyclonal antibody generation

(A) USP44 protein expression levels under different induction conditions. Protein extracted from *E. coli* cells was detected by anti-His using WB. IN: insoluble fraction; S: soluble fraction. Replicate samples were loaded for each condition. Black arrowheads indicate the expected weight of 25.3 kDa. (B) USP44 antibody ELISA titration. Serum from each rabbit was diluted serially from 1/100 to 1/102400. Preserum-serum before immunization; check 1-serum after the second booster; check 2-serum after the third booster.

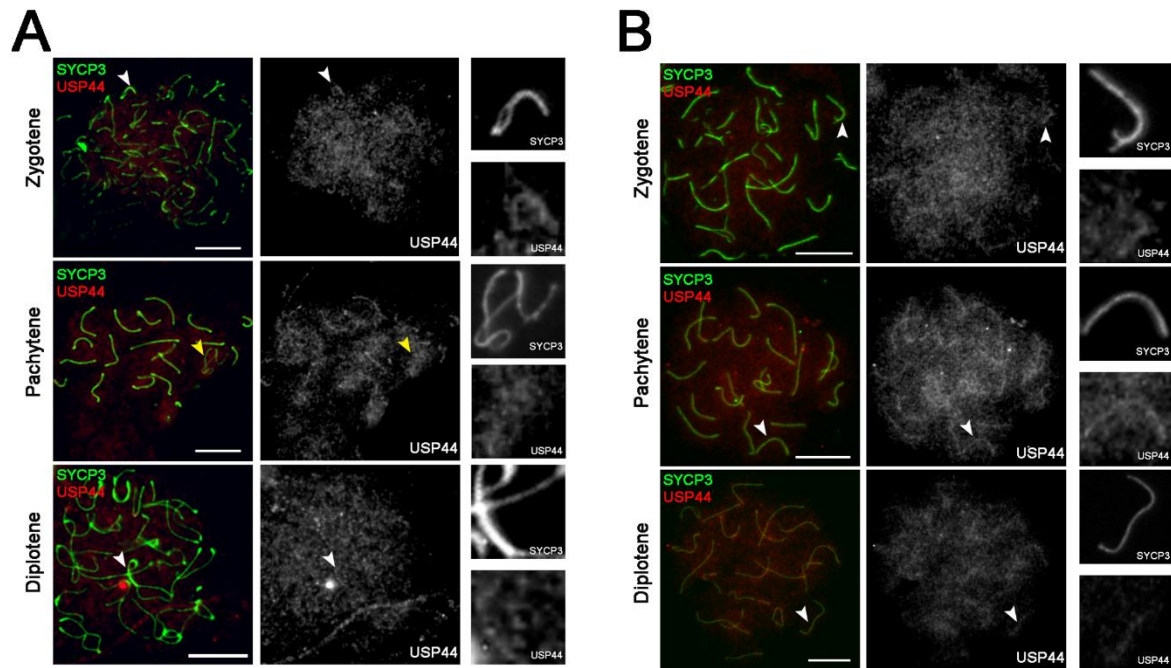


Figure 4-38. USP44 localization in meiocytes

(A) USP44 localization in wild-type spermatocytes. (B) USP44 localization in wild-type oocytes. Spermatocyte or oocyte spreads were stained with *in-house* USP44 antibody (Rb1889, 1:50-100) and SYCP3 antibodies. Arrowheads indicate inset areas: white-the synapsed autosomes; yellow-the XY chromosomes. Inserts magnify apparent axial USP44 staining on synapsed autosomes but not sex chromosomes. Scale bar, 10 μm .

4.5.2.3. Detection of USP44 in DMC1-deficient and SPO11-deficient testis

The localization of USP44 in meiocytes was closely associated with SC, suggesting its involvement in SC-related meiotic prophase events. Thus, to study if USP44 loading into the SC resulted from DSBs induction or recombination progression, we examined the localization of USP44 in *Spo11*^{-/-} and *Dmci*^{-/-} mouse spermatocytes. Both *Spo11*^{-/-} and *Dmci*^{-/-} spermatocytes displayed extensive synapsis defects, and the SC partially formed between non-homologous chromosomes. However, USP44 was not present at the synapsed axes of neither *Spo11*^{-/-} or *Dmci*^{-/-} spermatocytes (Figure 4-39). No other clear USP44 patterns were detected in these mutant cells either. These results suggest that the loading of USP44 onto the SC is dependent on DSB formation by SPO11 and DMC1-mediated homologous interactions.

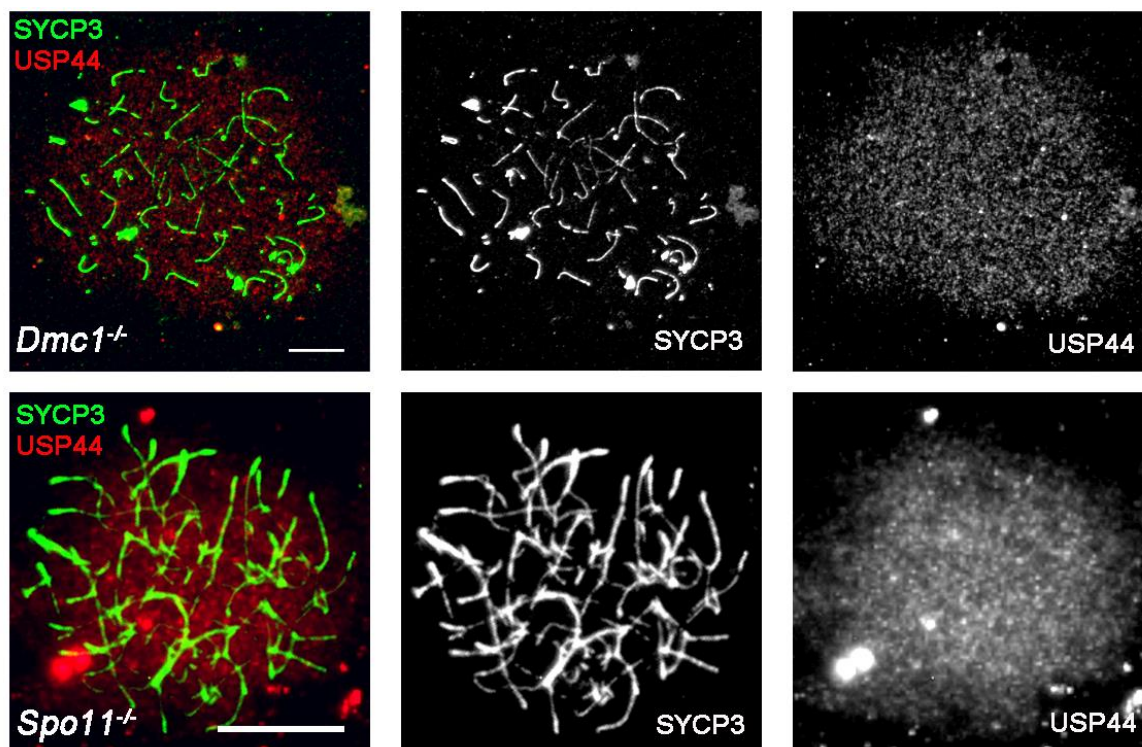


Figure 4-39. USP44 localization in SPO11- and DMC1-deficient spermatocytes. Representative images of spermatocytes containing synapsed chromosomes from *Dmc1*^{-/-} and *Spo11*^{-/-} mice stained with *in-house* USP44 antibody (Rb1889, 1:50-100) and SYCP3 antibody. Scale bar, 10 μ m.

4.5.3. Phenotyping of *Usp44* mutant mice

4.5.3.1. Target disruption of *Usp44* gene

To investigate the meiotic functions of USP44, we generated USP44-deficient mice by CRISPR/Cas9. Using a pair of gRNAs targeting opposite strands, we disrupted the functional USP domain by removing the whole exon 5 of *Usp44* that contains the active site of the USP domain (Figure 4-40). After microinjection and transfer of embryos, nine pups were born. Among them, we identified five heterozygous males (U₁, U₂, U₃, U₃₃, and U₃₄) and three heterozygous females (U₄, U₅, and U₃₅) carrying the desired deletion (Figure 4-40B, sequence details in supplementary Table 2). First, we crossed each U₁, U₃, and U₄ with a wild-type B6 mouse. Unfortunately, these three founders were mosaic as we did not identify any mice carrying the mutated allele among the 105 pups generated in 2-3 litters of progenies. We further crossed the other heterozygous founder

males and females (U₂, U₃₃, U₃₄, U₅, and U₃₅) with wild-type B6 mice and intercrossed the heterozygous progenies from each founder. Eventually, we set up one breeding colony for each U₂, U₃₃, and U₃₄ founder. No developmental abnormalities were observed during the growth of all the mutated progenies compared to their littermates. The segregation of the mutated allele followed the expected Mendelian ratio for U₃₃ and U₃₄ colonies. Nevertheless, in the U₂ colony, a loss of homozygous animals, especially mutant females, seemed to occur during embryonic development (genotypic ratio=1:2:0.5; $p=0.1437$, Chi-square). Animals from at least the F₂ generation of U₂ were subjected to phenotyping analysis.

4.5.3.2. Analysis of the relationship of USP44 with the UPS in meiotic prophase

The UPS has been found to regulate the major meiotic prophase events, including axis morphogenesis, homolog synapsis, and recombination in the mouse (Prasada Rao et al. 2017). Furthermore, ubiquitin was shown to have an axis-associated localization in mouse spermatocytes (Prasada Rao et al. 2017). USP44 is a deubiquitinase that can cleave ubiquitin and reverse its effects (Reyes-Turcu, Ventii, and Wilkinson 2009). Thus, to investigate if USP44 also participated in the UPS regulation of meiotic events, we examined the presence of ubiquitin in wild-type and *Usp44*^{-/-} spermatocytes. In wild-type spermatocytes, we could not obtain evident staining of ubiquitin along chromosome axes and only found the ubiquitin accumulation signals around sex chromosomes at the pachytene stage as described previously (Prasada Rao et al. 2017) (Figure 4-41A). In *Usp44*^{-/-} spermatocytes, the staining of ubiquitin on axes appeared to be more obvious, indicating an increase of ubiquitin level. Therefore, to confirm this, we measured the mean intensity of ubiquitin signals along chromosome axes in spermatocytes without synapsed XY and compared it between wild-type and *Usp44*^{-/-}. We found that there was a higher level of ubiquitin intensity in *Usp44*^{-/-} spermatocytes (12.87 ± 1.65 , Mean \pm SD, N=17), especially in these Z-like spermatocytes (abnormality description seen in section 4.5.3.4, 13.27 ± 1.70 , Mean \pm SD, N=11) than that in wild-type cells (12.69 ± 1.70 , Mean \pm SD, N=16). However, these differences were not significant ($p>0.05$ t-test Figure 4-41B). We also compared the mean intensity present in the whole nucleus if the ubiquitin localization was altered from chromatin axes to loops. However,

no difference was found (data not shown).

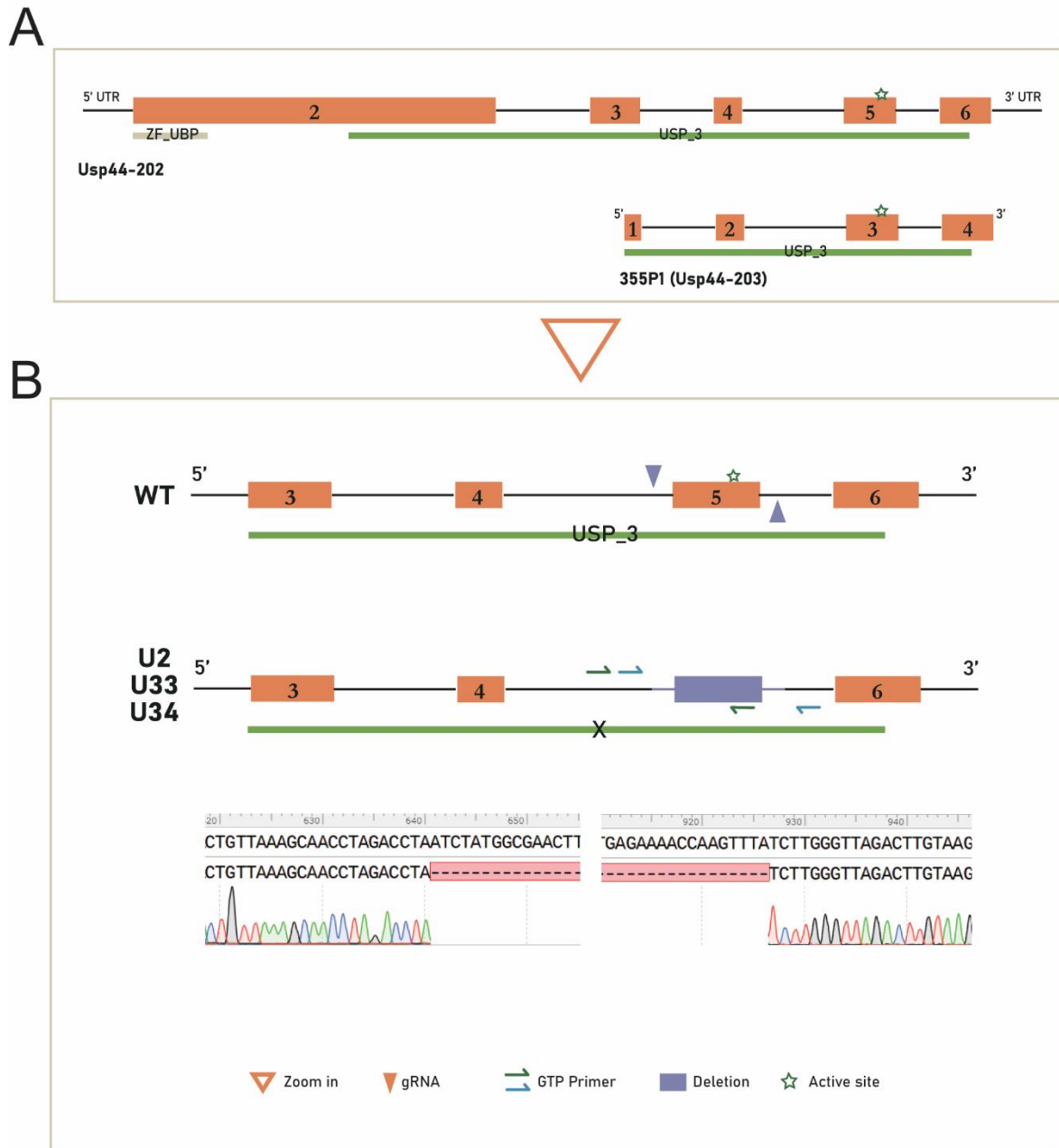


Figure 4-40. USP44 mutation strategy

(A) Schematic representation of mouse *Usp44* (transcript 202) and 355P1 (*Usp44-203*) gene loci. The exons are shown as orange boxes. The predicted domains are labeled below the exons. ZF_UBP: UBP-type Zinc finger domain, found only in a small subfamily of deubiquitinases; USP_3: USP domain profile. (B) Schematic of target deletion. WT: magnification of 355P1/*Usp44* wild-type locus. A pair of gRNAs target at exon 5 of *Usp44-202* within the USP_3 domain, containing an active site. U2, U33, and U34: disrupted *Usp44* loci from 3 founders. GTP primers represent USP44 GTP Forward and USP44 GTP Reverse Wildtype (green), USP44 GTP-F and USP44 GTP-R (blue) for genotyping PCR (Table 3-22).

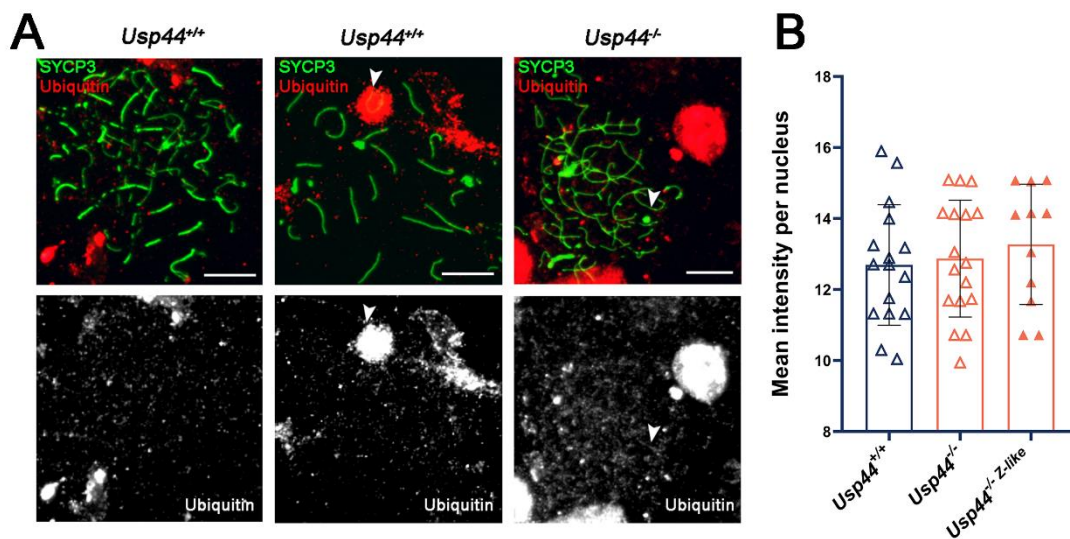


Figure 4-41. Presence of ubiquitin in *Usp44*^{-/-} spermatocytes

(A) ubiquitin staining in wild-type and *Usp44*^{-/-} spermatocyte nuclei. No clear ubiquitin staining was detected on chromosome axes in zygotene wild-type spermatocytes; ubiquitin accumulation was detected around the XY chromosomes in wild-type pachytene spermatocytes; relatively obvious ubiquitin axial staining was detected in *Usp44*^{-/-} Z-like spermatocytes. White arrowheads indicate ubiquitin staining around XY chromosome or along the axis. (B) Quantification of ubiquitin intensity. The columns and lines indicate the mean and SD. Number of analysed nuclei: 16 for *Usp44*^{+/+}, 17 for *Usp44*^{-/-}, 11 for *Usp44*^{-/-} Z-like spermatocytes. $p > 0.05$ t-test.

4.5.3.3. Analysis of spermatogenesis in *Usp44*^{-/-} males

The *Usp44*^{-/-} males normally developed into adulthood without obvious somatic defects (Figure 4-42A). *Usp44*^{-/-} normalized testes weight (TW/BW, 0.14% ± 0.04%, mean ± SD, N=3) was significantly smaller than wild type (0.67% ± 0.04%, mean ± SD, N=3, $p < 0.0001$ t-test, Figure 4-42A and B), suggesting *Usp44*^{-/-} males had an arrested spermatogenesis. The USP44 staining was absent at all the stages in mutant spermatocytes (Figure 4-42C), demonstrating the elimination of USP44 from mouse testis.

We further performed histological analysis of *Usp44*^{-/-} testis and found that spermatogenesis was severely impaired (Figure 4-43A). Most seminiferous tubules lacked sperm, spermatids, and/or spermatocytes, indicating spermatogenesis was halted in

Usp44^{-/-} mice. Interestingly, only very few tubules contained all spermatogenesis cell types including sperm. Moreover, TUNEL assays showed many of the remaining *Usp44*^{-/-} germ cells were undergoing apoptosis (Figure 4-43B). These observations indicated that USP44 is required to complete spermatogenesis, and *Usp44* mutants might be infertile.

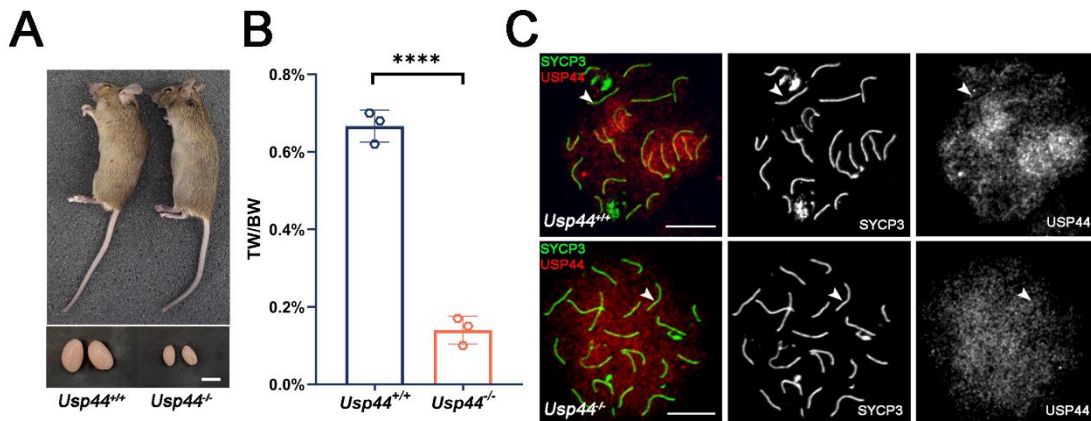


Figure 4-42. Disruption of USP44 in *Usp44*^{-/-} mice.

(A) Mouse appearance and testis size. Scale bar, 5 mm. (B) Comparison of the normalized testis weight. TW: testis weight, BW: body weight. The columns and lines indicate the mean and SD. *****p*<0.0001 t-test. (C) Detection of USP44 by IF. Spermatocyte spreads were stained with *in-house* USP44 antibody (Rb1889, 1:50-100) and SYCP3. White arrows indicate the presence (*Usp44*^{+/+}) or absence (*Usp44*^{-/-}) of USP44 staining on synapsed chromosomes. Scale bar, 10 μ m.

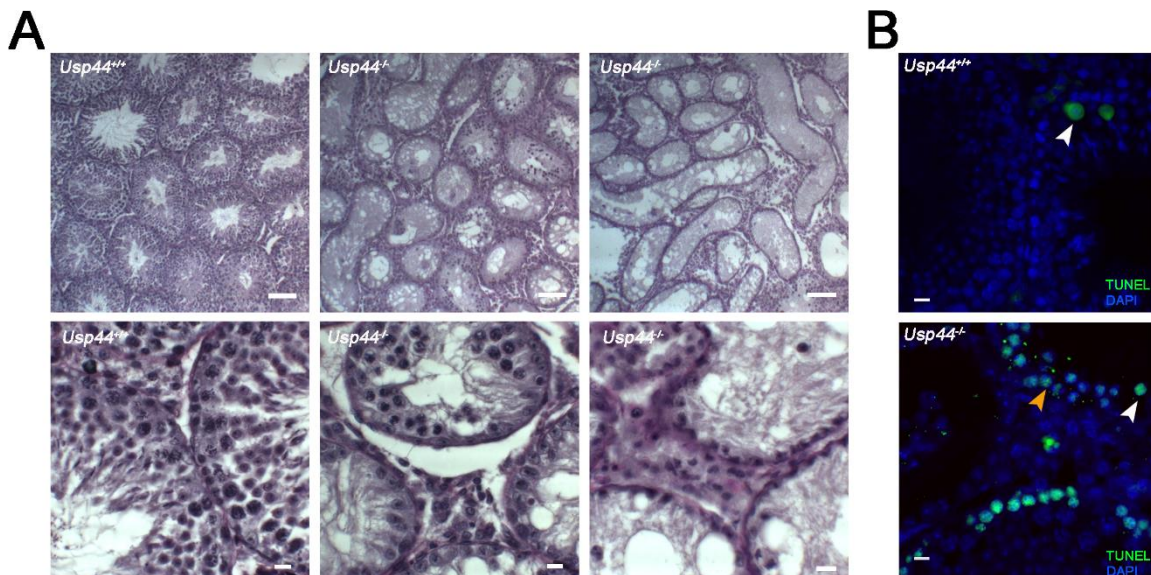


Figure 4-43. Spermatogenesis analysis in *Usp44*^{-/-} mice

(A) PAS-H stained mouse testis sections. Upper panel: an overview of several seminiferous tubules are shown; spermatogenesis is blocked in most *Usp44*^{-/-} tubules (middle); a more severe block is shown in most *Usp44*^{-/-} tubules (right). Lower panel: magnification of

individual tubules from the upper panel are shown. *Usp44*^{-/-} tubule lacks late prophase spermatocytes, round and elongating spermatids, and spermatozoa (middle). *Usp44*^{-/-} tubules lack most germ cells (right). Scale bar, 50 μm (upper panel) and 20 μm (lower panel). (B) Apoptosis detection on testis sections by TUNEL assay. Cells are undergoing apoptosis with strong TUNEL signals (white arrowheads), cells are entering apoptosis with fainter TUNEL signals and normal DAPI nuclear staining (orange arrow head). Scale bar, 20 μm.

4.5.3.4. Analysis of synapsis and recombination in *Usp44*^{-/-} males

To address the cause of defective spermatogenesis in *Usp44*^{-/-} males, we first examined the synapsis progression in *Usp44*^{-/-} spermatocytes by immunolabeling SYCP3 and SYCP1.

In *Usp44*^{-/-} spermatocytes, SYCP1 was first detected as foci at the developing axes marked by SYCP3 at leptotene, indicating SC formation start. As cells develop, only a minority of them progressed through zygotene and completed synapsis at pachytene (60.3% ± 3.8%, mean ± SEM, N=3 of wild type vs. 7.3% ± 7.3%, mean ± SEM, N=3 of *Usp44*^{-/-}, *p*=0.003 One-Way ANOVA, Figure 4-44B). Most *Usp44*^{-/-} spermatocytes could not complete synapsis. These abnormal spermatocytes displayed different extents of defects in homolog pairing and synapsis and accounted for more than half of the *Usp44*^{-/-} spermatocytes (Figure 4-44). We classified these aberrant spermatocytes in the following categories:

- Abnormal zygotene spermatocytes (16.7% ± 10.5%, Figure 4-44B) in which homolog axes barely paired even though they were fully formed; SYCP1 was mainly detected as foci along the axes of univalents or as short stretches at the synapsed non-homologous axes (Figure 4-44A).
- Zygotene-like (Z-like) spermatocytes (36.7% ± 18.3%, Figure 4-44B). These cells have all the axes developed in full length and exhibited some degree of synapsis but mostly between non-homologous chromosomes. SYCP1 was mostly assembled as short fragments (Figure 4-44A).
- Pachytene with limited asynapsis (7.7% ± 7.7%, Figure 4-44B). Synapsis was completed between most homologs in these cells but some SCs built between non-homolog partners (Figure 4-44A).

Nonetheless, a small fraction of *Usp44*^{-/-} spermatocytes managed to reach diplotene. However, these accounted for a much smaller proportion of spermatocytes

($5.3\% \pm 5.3\%$) than that in wild type ($24.0\% \pm 3.5\%$, $p=0.043$ One-Way ANOVA, Figure 44). Altogether, the deficiency of USP44 caused a severe defect in homolog pairing and synapsis in mouse spermatocytes, and meiotic progression was grossly altered in *Usp44*^{-/-} mice.

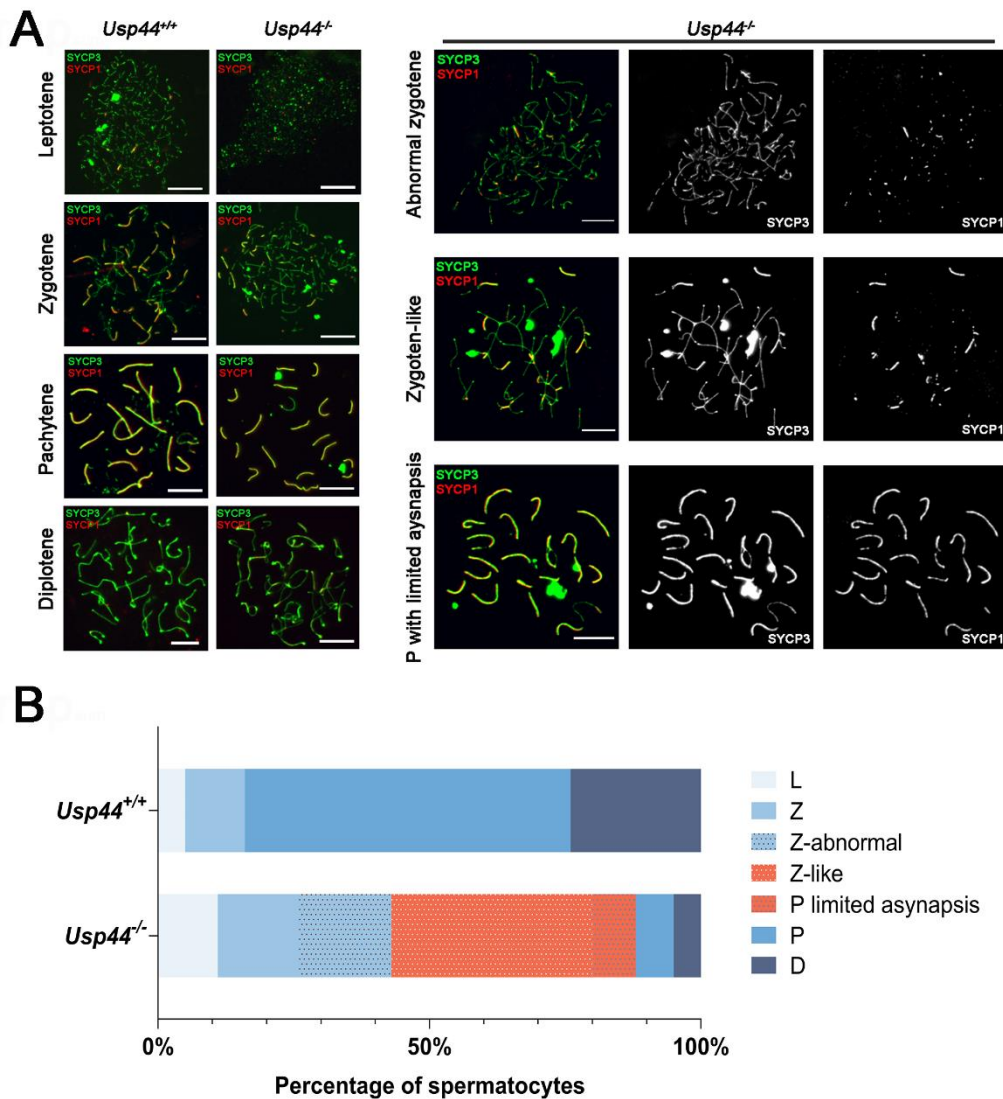


Figure 4-44. Meiotic progression of *Usp44*^{-/-} spermatocytes

(A) Chromosome synapsis in *Usp44*^{+/+} and *Usp44*^{-/-} spermatocytes. Representative images of wild-type spermatocytes and *Usp44*^{-/-} spermatocytes undergoing normal synapsis (left panel). Representative images of abnormal *Usp44*^{-/-} spermatocytes showing synaptic defects (right panel). Scale bar, 10 μ m. (B) Meiotic prophase staging of spermatocytes. L: leptotene, Z: zygotene, P: pachytene, D: diplotene, Z-abnormal: abnormal zygotene, Z-like: zygotene-like, P limited asynapsis: pachytene with limited asynapsis. The number of animals analyzed per genotype, 3.

Since USP44 loading onto the SCs is dependent on SPO11 and DMC1, we next investigated the progression of meiotic recombination in the *Usp44*^{-/-} mouse by examining DSB marker YH2AX and the recombination intermediates RPA and RAD51.

Interestingly, abundant YH2AX was detected in spermatocytes with synapsis defects (Figure 4-45). Z-like cells presented YH2AX flares on almost all the chromosomes. In pachytene cells with limited asynapsis, apart from relatively faint YH2AX patches along synapsed axes, YH2AX formed a sex body-like domain around these asynaptic chromosomes (Figure 4-45).

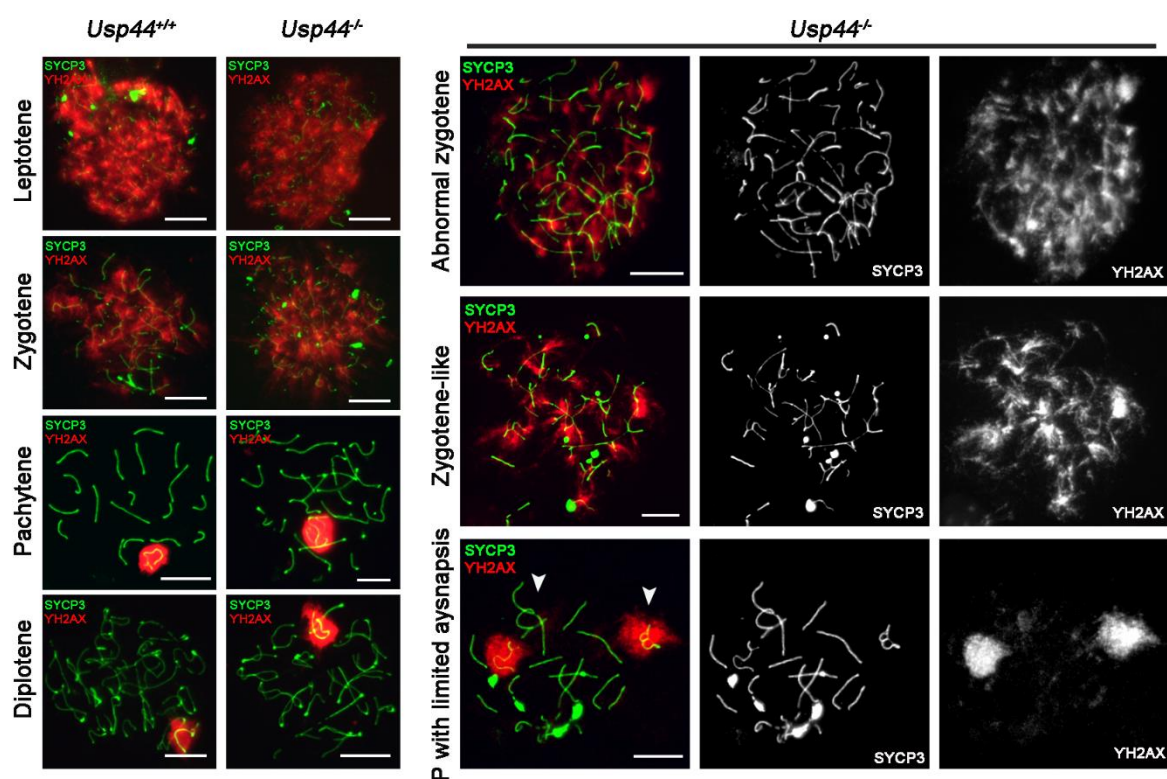


Figure 4-45. Examination of DSBs in *Usp44*^{-/-} spermatocytes

Representative images of YH2AX staining in wild-type and *Usp44*^{-/-} spermatocytes. YH2AX staining in *Usp44*^{-/-} abnormal zygotene, zygotene-like, and pachytene with limited asynapsis spermatocytes is shown on the right panel. Asynapsis in pachytene with limited asynapsis spermatocytes was indicated by white arrowheads. Scale bars, 10 μ m.

Similar to wild-type cells, multiple RPA and RAD51 foci were detected in *Usp44*^{-/-} spermatocytes since the leptotene stage (Figure 4-46), indicating that loading of RPA and RAD51 is independent of USP44. RPA and RAD51 foci gradually declined from

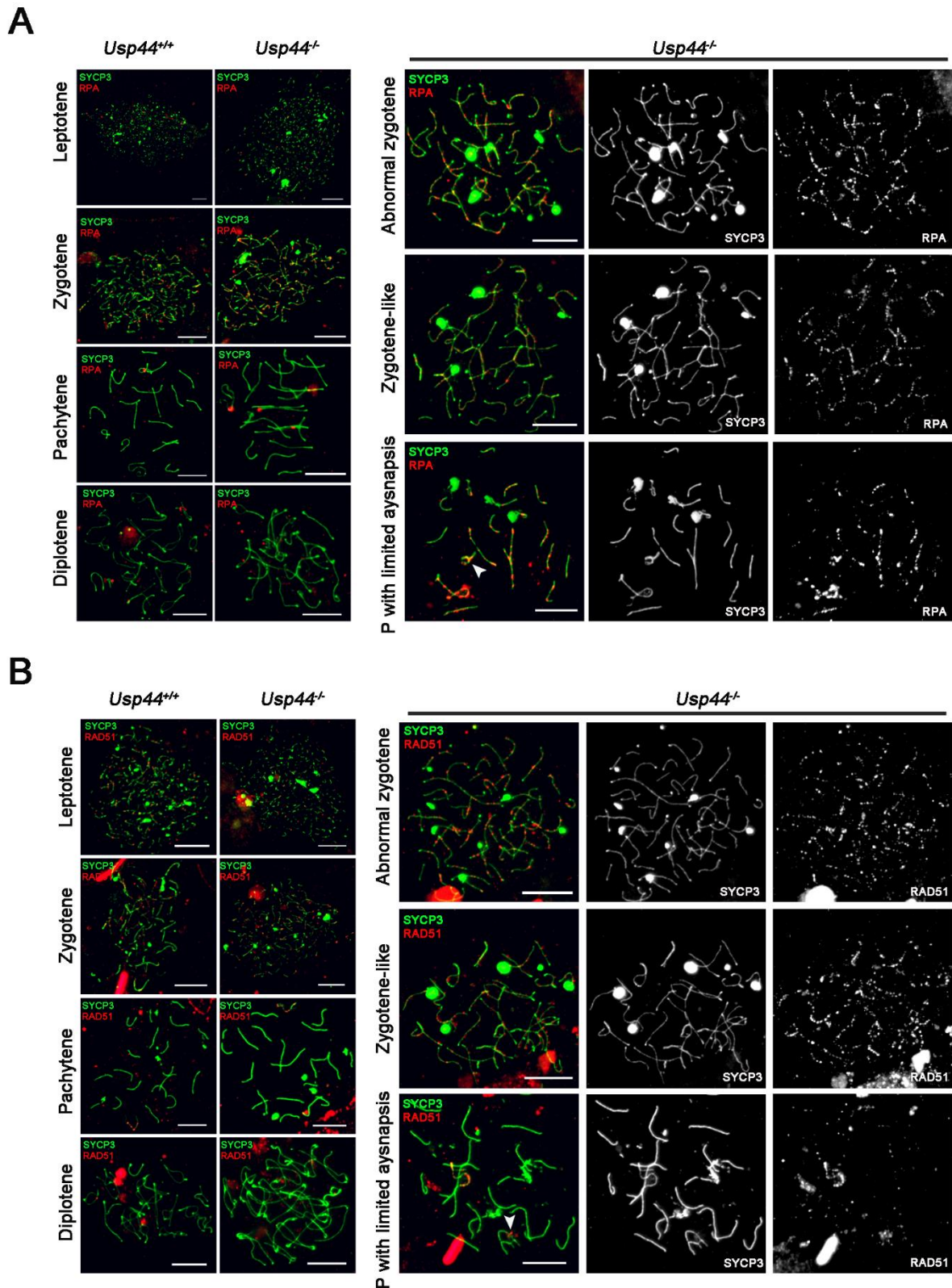


Figure 4-46. Examination of DSB repair in *Usp44^{-/-}* spermatocytes
 Representative images of RPA staining (A) and RAD51 staining (B) in wild-type and *Usp44^{-/-}* spermatocytes. RPA and RAD51 staining in *Usp44^{-/-}* abnormal zygotene, zygotene-like, and pachytene with limited asynapsis spermatocytes is shown on the right panel. Asynapsis in

pachytene with limited asynapsis spermatocytes is indicated by white arrowheads. Scale bars, 10 μm .

zygotene onwards in wild-type cells as recombination progressed. However, in *Usp44*^{-/-} abnormal zygotene and z-like spermatocytes, numerous RPA and RAD51 persisted on the axes, regardless of being unsynapsed or synapsed between homologs or not (Figure 4-46). In *Usp44*^{-/-} pachytene spermatocytes with limited asynapsis, the overall RPA, and RAD51 foci level was low because of the largely reduced foci number on properly synapsed chromosomes. However, a significant persistence of RPA and RAD51 foci could be observed on asynaptic chromosomes (Figure 4-46). In the *Usp44*^{-/-} cells that progressed to the diplotene stage, no noticeable difference was seen regarding the localization and number of RPA and RAD51 foci found (Figure 4-46). These results suggested that the recombination process was impaired in *Usp44*^{-/-} spermatocytes, resulting in unrepaired DSBs and persistent recombination intermediates. Although a defective synapsis could explain this defect, we cannot rule out any alteration of the recombination machinery downstream of RPA and RAD51 loading as the leading cause of the *Usp44*^{-/-} mouse phenotype.

Chapter 5

Discussion

5.1. Identification of meiotic genes essential for fertility

Meiosis is a highly specialized process essential in gamete formation in all sexually reproducing organisms. Meiotic errors and mutations could lead to consequences such as infertility and aneuploidy. Human infertility has become a major social and clinical problem worldwide. While genetic causes are already known to contribute a considerable proportion of infertility cases, many other uncovered genetic causes likely exist. Thus, identifying new genes involved in major meiotic events (e.g., recombination, synapsis, etc.) and studying their underlying functions is essential to increase our understanding of both the genetic regulation of meiosis and the origins of human infertility.

Our knowledge of meiotic genetic control in mammals has relied mainly on studies of mutations in mouse models. Fortunately, as most genes involved in conserved meiotic structures and processes usually exhibit similarities across diverse eukaryotes, many mammalian orthologs of model organisms genes, such as yeast, have been pinpointed and studied in mouse knock-outs (Handel and Schimenti 2010). However, it is also clear there are critical mammalian meiotic genes that do not have orthologs in yeast and vice versa. Various methods have been successfully applied to identify novel meiotic genes, such as front genetic screens, co-immunoprecipitation/mass spectrometry, or characterizing gene expression patterns by combining transcriptional profiling and cell-sorting technique (Bolcun-Filas and Schimenti 2012).

In this study, we performed a sequential screen to identify potential meiotic genes obtained from an *in silico* analysis of RNA sequencing data. First, we described the expression profile of candidate genes in a panel of mouse tissues by RT-PCR analysis. Then, we selected genes that were uniquely expressed in gonads undergoing meiotic prophase (adult testis and 18 dpc ovary). Subsequently, we constructed the EGFP-tagged gene plasmids; and transfected them into HEK 293T cells and live mouse testis. In the end, we validated the protein expressions in cells *in vitro* and characterized their localization in spermatocytes. Among these, several genes exhibited significant subcellular localization patterns in spermatocytes. We selected two genes of interest (*Bend2* and *Usp44*) to validate our strategy and further studied their functions by

examining their cellular localization and analyzing the phenotype of their mutant mice. Our preliminary phenotyping analysis showed that both genes were required for normal mouse gametogenesis. Their absence caused meiotic defects and alteration of mouse fertility (discussed in sections 5.2 and 5.3). Thus, these results validate our approach to identifying novel meiotic genes and successfully discovering essential genes required for mammalian fertility.

Mouse knock-out experiments have shown enormous value for identifying genes responsible for human infertility. Many genes were first found to be essential for spermatogenesis from studies in mouse knock-out models. Later, mutations of their human orthologs were identified in infertility patients, such as *KLHL10*, *SYCP3*, and *HSF2* (Miyamoto et al. 2003; W. Yan et al. 2004; Yuan et al. 2000; Mou et al. 2013).

Our study identifies two novel meiotic genes essential for mouse fertility, *Bend2*, and *Usp44*, which have known human orthologs. We found that the knock-out of *Bend2* in female mice leads to POI, a significant cause of human female infertility. In contrast, the mutation of *Usp44* leads to a meiotic arrest, which usually causes azoospermia or oligozoospermia and/or sperm aneuploidy in infertile humans. Thus, an intriguing question that can be addressed in the future is whether human *BEND2* and *USP44* have a role in infertility.

The discovery of new genetic infertility determinants in humans is critical for developing tests for clinical infertility diagnosis and screens for genetic abnormalities or unfavorable polymorphisms before performing ART (O'Flynn O'Brien, Varghese, and Agarwal 2010). Our discovery of these two mouse genes that impact meiosis and fertility provides valuable insights into not only the identification of novel genetic factors contributing to human infertility but also the development of new genetic techniques for human infertility diagnosis and treatment. However, further efforts are necessary to refine our findings and translate them into clinical studies, such as a more detailed characterization and validation of *Bend2* and *Usp44* gene functions in mouse models and the identification of their corresponding variants in human infertility patients, etc.

5.1.1. The efficiency of electroporation in live mouse testis

To identify genes whose protein showed characteristic meiotic localization in mouse spermatocytes (Shoji et al. 2005; Morimoto et al. 2012; Gómez-H et al. 2016), we used a well-established DNA electroporation technique to express the candidate genes fused with EGFP under an ectopic promoter in live mouse spermatocytes.

All the construct plasmids expressed proteins when transfected to HEK 293T cells based on the microscopy and WB analysis. However, the IF and WB analysis results in EP spermatocytes are not consistent. The GFP signals detected protein expression of almost all the candidate genes under the microscope. But, only one of them could be validated by WB analysis. Why was not the protein expression of the other EGFP-tagged genes revealed by WB analysis? Two reasons might be accounted for: first, the protein loading amount might not be enough. The amount of protein loaded for detection was relatively low because of the limited EP-testis remaining after spread and squash preparations. Secondly, *in vivo* protein expression by EP was not highly efficient. A previous study reported that 8.4% of the SYCP3-positive spermatocytes expressed the electroporated transcript (Shoji et al. 2005). In our hands, a similarly low efficiency was also observed. Spermatocytes displaying significant expression patterns (GFP-positive) comprised 1.6-7.0% of the SYCP3-positive spermatocytes in spreads, depending on the electroporated vector. This number varies from 4% to 34.6% when analyzed in squash preparations. Thus, a low expressed level of transfected genes together with insufficient protein loading results in failed protein detection in EP testis by WB.

5.2. Roles of BEND2 in meiotic prophase

BEND2 has two C-terminal BEN domains, marked by α -helical structure and conserved in a range of metazoan and viral proteins. BEN domain is suggested to mediate protein-DNA and protein-protein interactions during chromatin organization and transcription (Abhiman, Iyer, and Aravind 2008). So far, only a few BEN domain-containing proteins have been described. All of their functions link to transcriptional repression regardless of whether other characterized domains are contained or not, including mammalian BANP/SMAR1, NAC1, BEND3 and RBB and *Drosophila* mod(mdg4), BEND1 and BEND5 (Kaul-Ghanekar et al. 2004; Rampalli et al. 2005; L.

Korutla, Wang, and Mackler 2005; Laxminarayana Korutla et al. 2007; Sathyan et al. 2011; Gerasimova et al. 1995; Nègre et al. 2010; Dai et al. 2013; 2015; Xuan et al. 2012). BEND₁, BEND₅, and RBB are revealed to bind DNA through sequence-specific recognition (Dai et al. 2013; 2015; Xuan et al. 2012), and BEND₃ specifically binds heterochromatin (Sathyan et al. 2011). Additionally, several human BEND₂ fusion proteins have been identified in tumors, and the activation of BEND₂ is suggested to promote oncogenic activity (Sturm et al. 2016; Scarpa et al. 2017; Burford et al. 2018; Williamson et al. 2019). These data suggest BEND₂ might have a role in chromatin regulation and transcriptional regulation of gene expression.

5.2.1. The source of persistent DSBs in *Bend2* mutants

The disruption of BEND₂ results in grossly normal spermatogenesis in male mice, although with increased apoptosis. The synapsis process in spermatocytes is not affected, but the meiotic progression seems delayed with more cells at the diplotene stage. Unrepaired DSBs persist in spermatocytes since late pachytene, showing increased γ H2AX signals. However, recombination intermediates RPA and RAD51 are unaffected at most analyzed substages. A significant increase of RPA foci is only detected in late leptotene cells, and a decrease of RAD51 foci is found in late zygotene and pachytene cells. Intriguingly, the absence of BEND₂ causes more severe defects in female oogenesis with decreased ovarian reserve and subfertility. Adult female mice have a considerably reduced number of primordial follicles. Like males, synapsis in females is not affected either. Nonetheless, meiosis appears to progress faster. Persistent unrepaired DSBs are also found in female oocytes, exhibiting a high level of γ H2AX signals at pachytene and diplotene stages. No change of RPA and RAD51 foci were found in females. We also analyzed the female heterozygous mice for *Bend2*. Some are phenotypically similar to wild types, and others are more similar to mutant mice, overall displaying a midway phenotype between wildtypes and homozygote mutants.

The only common defect shown in both genders is the increased levels of γ H2AX present in late pachytene and diplotene spermatocytes and oocytes. These γ H2AX signals could indicate unrepaired DSBs due to defective recombination (Roig et

al., 2010) or some late-forming breaks during late prophase (Carofiglio et al. 2013). In the former case, we would expect some differences of early recombination intermediates (RPA and RAD51) in *Bend2* mutant cells, e.g., accumulations of RAD51 at the synapsed chromosomes in these mutant cells with a higher level of YH2AX presence. However, there is no difference in RPA and RAD51 foci numbers in *Bend2* mutant oocytes at all the counted stages. In mutant spermatocytes, the only differences are an increase of RPA foci in late leptotene and a decrease of RAD51 foci in late zygotene and pachytene. Thus, it seems that the recombination process is not that defective to trigger such a level of DSB persistence in the late prophase. This is consistent with observing roughly normal synapsis in mutant cells. Also, the expression of BEND2 is not altered in testis lacking DMC1 or SPO11, probably also indicating that BEND2 might not be highly required for SPO11-induced DSB repair and synapsis.

Alternatively, the presence of unrepaired damage at late prophase in *Bend2* mutant cells could be explained otherwise. This unrepaired DNA damage might not be the remaining unrepaired programmed DSBs formed at the onset of recombination, but some SPO11-independent DNA damage created during pachytene, as previously reported (Carofiglio et al. 2013). SPO11-independent DSBs have been identified in SPO11-deficient meiocytes in mice and indicated to be also present in wild-type cells (Carofiglio et al. 2013; Rinaldi et al. 2017). In SPO11-deficient zygotene-like oocytes, *de novo* RAD51 foci were generated, indicating spontaneous DSBs may arise in cells that should have reached the pachytene stage, coinciding with the observed YH2AX increase in pachytene *Bend2* mutant meiocytes. Moreover, in wild-type oocytes, one-third of pseudo-XY bodies are found to form on synapsed chromatin, accumulating mainly RAD51 and eliciting meiotic silencing. These pseudo-XY body sites are inferred to be where SPO11-independent damage persists (Carofiglio et al. 2013). In fact, we also found pseudo XY bodies on synapsed chromatin in 4.6% *Bend2* mutant oocytes and 1.5% wild-type oocytes at 1 dpp. Based on all of these observations, we hypothesize that the increased YH2AX signals during late prophase in *Bend2* mutant cells might represent mostly persistent SPO11-independent DSBs.

Further evidence needs to be found to validate this. For instance, to differentiate these SPO11-dependent or SPO11-independent YH2AX patches or pseudo XY bodies, the co-staining of RAD51 and DMC1 with YH2AX can help. Alternatively, to determine if

these pseudo XY bodies are truly silenced, RNA pol II could be examined.

5.2.2. Increased DSBs levels might be formed in *Bend2* mutants

Following this hypothesis, there are likely two causes for the persistence of these breaks. More SPO11-independent DSBs are formed in mutant cells leading to insufficient repair, or the repair pathway of these SPO11-independent DSBs is defective due to the lack of BEND2.

The formation of SPO11-independent DSBs has been linked to the LINE-1 (L1) retrotransposon activation (Malki et al. 2014; Carofiglio et al. 2013; Soper et al. 2008). L1 encodes two proteins: ORF1-a nucleic acid chaperone and ORF2, having endonuclease and reverse transcriptase activities. Both of them assemble into ribonucleoprotein complexes mediating transposition (Cost et al. 2002). The endonuclease activity of ORF2 is required for DSBs generation in the genome (Belgnaoui et al. 2006). An increased L1 expression caused by a mutation in *Mael*, a transposon-silencing factor, leads to SPO11-independent DNA damage and asynapsis in both spermatocytes and oocytes (Soper et al. 2008; Malki et al. 2014).

In wild-type oocytes and spermatocytes, a transient DNA demethylation (DdM) occurs at the onset of meiosis, triggering sustaining L1 expression until mid pachytene, followed by restored DNA methylation (DM) before meiotic division (Soper et al. 2008; Van Der Heijden and Bortvin 2009). Although the precise DdM mechanism is still unknown, it has been suggested to be caused by a downregulation of the methyltransferase DNMT1 in B-type spermatogonia and preleptotene spermatocytes (Jue, Bestor, and Trasler 1995; Van Der Heijden and Bortvin 2009). Interestingly, a noticeable reduction of DNMT1 mRNA and protein is exhibited in B-type spermatogonia and preleptotene, leptotene, and zygotene spermatocytes (Jue, Bestor, and Trasler 1995), concomitant with the high-level BEND2 expression in wild-type spermatocytes.

Then it is reasonable to speculate that BEND2 might be required for regulating the transient DdM of L1, probably through repressing DdM in parallel with the downregulation of DNMT1. Alternatively, BEND2 might support the *de novo* DM, as the methyltransferase activity proposed to be responsible for the restoration of DM is also

detected in cells at the same stages when BEND2 is highly expressed (B-type spermatogonia and preleptotene to zygotene spermatocytes) (La Salle and Trasler 2006; Van Der Heijden and Bortvin 2009). In any case, we hypothesize the depletion of BEND2 would cause increased L1 expression. A direct way to validate this could be by examining L1 expression in *Bend2* mutant meiocytes by IF and WB.

In *Bend2* mutant females, the increased DSBs, the decreased ovarian reserve, and the reduced CO numbers could be interpreted with elevated L1 activity. This is because that L1-ORF2 endonuclease activity can contribute to late oocyte attrition occurring in the perinatal and early postnatal period, triggered by unrepaired DNA breaks; (Malki et al. 2014; Hunter 2017; Tharp, Malki, and Bortvin 2020). Also, the L1-reverse transcriptase activity could interfere with CO formation. It has been shown that elevated L1 activity leads to reduced CO numbers and chromosome segregation defects in mouse oocytes, which is reverse transcriptase dependent (Malki et al. 2014).

It is intriguing why *Bend2* male mutants' defects were less severe, in terms of increased γ H2AX levels and apoptosis, but CO formation and spermatogenesis were not affected. One possibility could be that the damage caused by the elevated L1 expression was more negligible in spermatocytes than in oocytes. Indeed, the *de novo* RAD51 foci, which may indicate DSBs arising from ORF2 mediated endonuclease activity, are only detected in SPO11-deficient oocytes but not in the *Spo11*^{-/-} spermatocytes (Carofiglio et al. 2013). It's likely that, although L1 DdM occurs at the onset of meiosis in both males and females (Van Der Heijden and Bortvin 2009), the DdM levels might be lower in males than females. Supporting the idea that L1 activation is higher in the oocytes than the spermatocytes, L1 activity contributes to massive wild-type oocyte elimination, but it does not cause the same effects in spermatogenesis (Hunter 2017). Also, we observed a trend of increased RAD51 in pachytene mutant oocytes but not in spermatocytes, indicating there might be more unrepaired SPO11-independent DSBs in females. Thus, the increase of L1 activity might be lower in *Bend2* mutant males than females due to the derepression of DdM or defective *de novo* DM, leading to milder consequences.

Asynapsis is found in a significant percentage of mutant oocytes with increased L1 levels due to the lack of transposon silencing protein MAEL (Malki et al. 2014; Soper et al. 2008). However, we did not observe obvious asynapsis in *Bend2* mutant meiocytes. This difference suggests that the roles of MAEL and BEND2 in DdM, or *de novo* DM, are

likely different, and BEND2 deletion could cause a milder elevation of L1. Further examination could be performed to test if minor asynapsis exist in *Bend2* mutant oocytes by staining MSUC markers like HORMAD1 or BRCA1 (Wojtasz et al. 2009; Kouznetsova et al. 2009).

It's worth noting that there might be another explanation for the difference between *Bend2* mutant female and male phenotypes. Our WB results (section 4.4.2.1) showed that there was an unexpected protein present in both *Bend2* wild-type and mutant testes, which might correspond to the alternative spliced transcript detected in *Bend2*^{-/y} male testis by RT-PCR that skips exon 11. However, we have never detected this transcript in wild-type testis by RT-PCR. This might indicate that this alternatively spliced transcript is expressed at lower levels than the full-length one in testis. This could favor the amplification of the full-length transcript by RT-PCR in wild-type testis and the one skipping exon 11 in the mutant testis.

Thus, we propose that, apart from the full-length BEND2 protein we mutated, there might be another BEND2 protein present in male testis, which might be sufficient to perform most BEND2 functions. Furthermore, it's possible this protein is testis-specific and does not exist in female ovary. Thus, our mutation could cause a more complete loss of BEND2 function in females, leading to a more severe phenotype, compared to male mutants. Further sequence examination of this protein in testis and ovary need to be performed to address this issue.

5.2.3. DSB repair might be impaired in *Bend2* mutants

An alternative explanation to interpret the persistent DSBs in *Bend2* mutants is that the repair of wild-type levels of SPO11-independent DSBs is defective due to the deletion of BEND2. As discussed above, there are fewer SPO11-independent breaks in spermatocytes but more in oocytes (Malki et al. 2014). Thus, it would make sense that the repair defects due to the absence of BEND2 caused more severe consequences in oocytes rather than in spermatocytes.

Then, the next question is how BEND2 would participate in the repair of these breaks in mice? A possible answer is BEND2 might mediate the shift in DNA damage

response in spermatocytes.

It has been reported that apart from the principal MR DNA repair pathway, other “somatic” DSB repair pathways, such as non-homologous end joining (NHEJ) or inter-sister homologous recombination (IS-HR), can also be used in normal meiosis (Ahmed et al. 2010; Goedecke et al. 1999; Enguita-Marruedo et al. 2019). NHEJ is suggested to respond to both endogenous or exogenous DNA damage during late meiotic prophase in collaboration with late IS-HR response (Enguita-Marruedo et al. 2019). From mid pachytene, NHEJ should respond to newly formed breaks that are not resected. Later, an IS-HR response, using only RAD51, should help repair the remaining DSBs. The later IS-HR repair uses the sister chromatid as a template, thus facilitating DSB repair at the diplotene stage when repair with IH-MR is complicated due to chromosome desynapsis (Enguita-Marruedo et al. 2019). Hints about the use of alternative methods to repair meiotic DSBs, including the use of IS-HR, have also been found in *Trip13* mutant oocytes (Rinaldi et al. 2017; Martínez-Marchal et al. 2020).

One proposed mechanism that regulates the shift in DNA damage response from the early IH-MR mediated massive response to this later combined response is related to the changes of chromatin configuration and transcriptional activity as in somatic cells (Aymard et al. 2014; Enguita-Marruedo et al. 2019). Since BEND2 is functionally related to chromatin organization and transcription, and it is highly expressed during early meiotic prophase before mid pachytene, it's possible BEND2 may play a role in mediating the DNA damage repair pathway choice occurring at mid pachytene. As a result, the depletion of BEND2 might cause the delay of the shift or a failure to activate these alternative pathways to repair DSBs.

Apart from the impaired repair of SPO11-independent DSBs in *Bend2* mutant meiocytes as discussed above, other pieces of evidence could also support this assumption. If the *Bend2* mutant cells cannot activate the alternative repair pathways (such as NHEJ or IS-HR), it is possible that mutant spermatocytes exit pachytene faster and eventually present more unrepaired breaks. However, *Bend2* mutant oocytes seem to take longer to complete pachytene than wild-type oocytes. Because synapsis is completed earlier relative to the recombination in oocytes, compared to spermatocytes (Koubova et al. 2014b), probably, the shift to late DNA damage response might also occur later in oocytes, from late pachytene onwards. Thus, *Bend2* mutant oocytes may skip NHEJ at

diplotene and have less time for MR than spermatocytes, leading to more unrepaired breaks. Also, these late repair pathways (NHEJ and IS-HR) are likely to be necessary for spermatocytes to repair DSBs at non-PAR regions of XY chromosomes. As this is not the case in females, it is not surprising that the mechanisms of repair pathway choice might be less well regulated or differently regulated in oocytes. Thus, the disrupted pathway activation due to the absence of BEND2 might cause distinct consequences in males and females, like the phenotypes we revealed.

L1 activity contributes to wild-type early oocyte attrition during fetal development (Hunter 2017). Recently, a Caspase 9 (CASP9)-dependent apoptosis pathway is suggested to be responsible for eliminating these oocytes with increased L1 activity (X. Liu, Castle, and Taketo 2019). The oocyte loss in fetal ovaries was prevented by CASP9 deficiency. Cultured *Casp9*^{-/-} oocytes exhibit higher levels of L1 expression and persistent γH2AX at pachytene stage with no difference of RAD51 foci and synapsis compared to control, most of which are similar to the observations in *Bend2* mutant oocytes. These *Casp9*^{-/-} oocytes are eliminated later in postnatal development by CASP9-independent mechanisms (X. Liu, Castle, and Taketo 2019). Thus, another possible role of BEND2 in this CASP9-dependent apoptosis in early meiotic prophase could be speculated.

Finally, whether these observed increased γH2AX signals during late meiotic prophase are mostly SPO11-independent or not, we cannot rule out that BEND2 might be required for SPO11-induced DSBs repair. As discussed above, more evidence needs to be found to confirm this hypothesis.

5.3. USP44 as a novel meiotic gene

5.3.1. Ubiquitination and deubiquitination protein regulation

This study also identified another new player in the meiotic prophase, USP44. USP44 is a deubiquitinating enzyme belonging to the largest DUB family-the USP. DUBs counterbalance ubiquitination, a post-translational modification that regulates the protein's stability, function, and localization, reversibly (Suresh et al. 2015; Reyes-Turcu,

Ventii, and Wilkinson 2009).

The ubiquitination process entails the conjugation of an oligopeptide, ubiquitin, to the target protein. This process requires ATP hydrolysis to provide the energy and sequential actions of three ubiquitin ligases, E1, E2, and E3, with distinct biochemical activities (Callis 2014). Target protein could be attached to a single ubiquitin (monoubiquitination) or a ubiquitin chain (polyubiquitination) internally linked via the lysine residue. Ubiquitinated proteins have proteolytic and non-proteolytic fates, giving diverse outcomes (Callis 2014; Suresh et al. 2015). For instance, monoubiquitin mainly regulates proteins for DNA repair and receptor endocytosis. K48-linked polyubiquitin chains usually channel target proteins for proteasome-mediated degradation. And K63-linked polyubiquitin chains likely modulate the localization, activity, and function of target proteins in signaling pathways (Callis 2014; J. Choi et al. 2010; Suresh et al. 2015).

DUBs regulate this system through disassembling ubiquitin-substrate, editing ubiquitin-ubiquitin links, activating and recycling ubiquitin (Reyes-Turcu, Ventii, and Wilkinson 2009). It is known that wherever there is ubiquitination, DUBs exist to regulate the process (Suresh et al. 2015). Although the roles of ubiquitination have been implicated in various aspects of meiotic prophase (Bolaños-Villegas et al. 2018; Jahns et al. 2014; Bose et al. 2014; Qiao et al. 2014; L. Zhang, Wang, et al. 2014; Prasada Rao et al. 2017), little is known about how DUBs are involved in meiotic prophase.

5.3.2. Roles of USP44 in mammals

We propose that the 355p1 gene we identified is likely to be a novel testis splicing isoform from the mouse *Usp44* gene (*Usp44-203*), based on their different expression patterns during spermatogenesis. In support of this assumption, expression profile analyses of mouse and human *USP44* in a set of diverse tissues, including the ones we tested, show that both mouse and human *USP44* genes are highly expressed in more tissues than 355P1 (J. Choi et al. 2010; Y. Zhang, van Deursen, and Galardy 2011). Moreover, human *USP44* has been found to have several transcription initiation sites, some of them being only active in certain specific cells types or tissues, including testis (Tropel et al. 2017). Therefore, 355P1 might result from a testis-specific transcription initiation site

within the mouse *Usp44* loci. Compared to 355P1, the full-length mouse or human USP44 contains one more ZnF-UBP domain. This domain has been found in a subset of USPs. It is suggested to regulate the activity of the corresponding USP and act as a sensor of the free ubiquitin pool by binding to the ubiquitin C-terminus (Bonnet et al. 2008).

The function of the mouse USP44 is poorly studied (Vasmatzis et al. 2012). In contrast, human USP44, with a high homology degree to mouse USP44, has been demonstrated to participate in a variety of cellular processes through reversing ubiquitination, including stem cell differentiation (Fuchs et al. 2013), DDR (Mosbech et al. 2013), mitotic SAC regulation (Stegmeier et al. 2007), gene repression (Lan et al. 2016), immune response (H. Y. Zhang et al. 2020) and tumorigenesis (Y. Zhang, van Deursen, and Galardy 2011; Vasmatzis et al. 2012; T. Liu et al. 2015; Park et al. 2019).

USP44 plays an important role in mitosis and cell proliferation via regulating the mitotic SAC (Vasmatzis et al. 2012). USP44 deubiquitinates anaphase-promoting complex (APC) coactivator CDC20 to stabilize the APC inhibitory MAD2–CDC20 complex *in vitro* and *in vivo* (Stegmeier et al. 2007; Y. Zhang, van Deursen, and Galardy 2011). USP44 also plays positive and negative roles in tumorigenesis and cancer aggressiveness (Y. Zhang, van Deursen, and Galardy 2011; Vasmatzis et al. 2012; Lan et al. 2016; Park et al. 2019; T. Liu et al. 2015). Furthermore, not only can USP44 directly function via deubiquitylating target protein, but it can also play diverse roles by forming complexes with distinct partners (Lan et al. 2016). For instance, USP44 acts as an integral subunit of the nuclear receptor co-repressor (N-CoR) complex. It contributes to N-CoR mediated transcriptional repression through its deubiquitylation of histone H2B (Lan et al. 2016). It also forms a complex with CETN2 independently of the N-CoR complex *in vitro*, and the USP44-CETN2 complex is proposed to play other vital roles in preventing mitotic chromosome missegregation (Lan et al. 2016; Y. Zhang, van Deursen, and Galardy 2011). Indeed, it has been accepted that DUBs must associate with multi-protein complexes to exert their physiological functions. This can help colocalize substrates and the DUB and allow a sequential ubiquitination and deubiquitination cycle to regulate these pathways (Reyes-Turcu, Ventii, and Wilkinson 2009).

Interestingly, histone H2A and H2B seem to be essential interactors of USP44. This was first identified in proteomic analysis and further validated in several functional studies (Lan et al. 2016; Mosbech et al. 2013; Fuchs et al. 2013; Sowa et al. 2009). USP44

downregulates the monoubiquitylation of histone H2B, catalyzed by E3 ligase RNF20 and required for efficient human and mouse embryonic stem cells differentiation (Fuchs et al. 2013). The DDR signaling regulates the DSB repair pathway choice. The E3 ubiquitin ligases RNF 8 and RNF168 transduce the DDR signal by ubiquitinating the histone H2A. Consequently, the DDR proteins 53BP1 and RAP80 are recruited to the DSB sites, suppressing HR and promoting NHEJ DSB repair (Nakada 2016). USP44 and other DUBs counteract H2A ubiquitination and thus restrict the assembly of 53BP1 and RAP80 (Mosbech et al. 2013). Therefore, the restriction of 53BP1 and RAP80 recruitment enabled by DUBs is proposed to promote HR and suppress NHEJ in an early DDR phase (Nakada 2016).

MR repair, a particular kind of HR, is fundamentally biased in meiosis. The mechanism is poorly understood and likely to be achieved both by inhibiting other non-HR repair pathways and promoting IH bias (Denise Zickler and Kleckner 2015; Brown and Bishop 2015). In fact, NHEJ repair has been suggested to be repressed during early prophase and active at the later stages in mouse spermatocytes (Ahmed et al. 2010; Enguita-Marruedo et al. 2019). Also, H2A can be ubiquitinated by several ligases in mouse spermatocytes (An et al. 2010; Hasegawa et al. 2015; Luo et al. 2015). This modification has been suggested to be linked to the transcriptional silencing of meiotic chromatin (Baarends et al. 2005). USP44 is likely to be involved in the early events of IH-MR, such as strand exchange, based on the phenotype of the *Usp44*^{-/-} mice (discussed below). Therefore, a similar role of USP44 in regulating DSB repair in meiosis as in mitosis could be hypothesized and need to be further investigated through answering, first, if USP44 could reverse the ubiquitination of H2A in spermatocytes. Second, if this ubiquitination of H2A is related to the DDR protein recruitment or other processes related to the DSB repair pathway choice.

It is worth noting that USP44 can also be phosphorylated and dephosphorylated (Visconti et al. 2012), as well as ubiquitinated. However, the ubiquitination of USP44 seems to require its ZNF domain (J. Choi et al. 2010), which is absent in the novel *Usp44* isoform expressed during meiotic prophase (*Usp44-203*).

5.3.3. Roles of USP44 in meiosis

This work shows that USP44 is required for homolog pairing, synapsis, and DSB repair in meiotic prophase. The disruption of USP44 results in meiotic failure and defective spermatogenesis. Our analysis reveals that *Usp44*^{-/-} spermatocytes display severe defects during meiotic prophase I. Homologous axes develop similarly to wild-type ones, but homologous chromosomes cannot pair. Synapsis can hardly be completed between the homologs but frequently form between non-homologous chromosomes. Plenty of DSBs are generated given the number of RPA and RAD51 foci during the early prophase, but these cannot be repaired. Consequently, most spermatocytes are arrested at prophase I before entering apoptosis with persistent DSBs, RPA, RAD51, and extensive asynapsis. Only a minority of cells can progress to the diplotene stage or even form sperm.

The extensive asynapsis in *Usp44* mutant spermatocytes likely results from impaired DSB repair. In mouse mutants lacking CR components of the SC (e.g., SYCP1, SYCE1, SYCE3, TEX12, or SIX6OS1) (Figure 1-3), despite failing to complete synapsis and presenting impaired recombination, most homologous axes pair and align along their entire length (Hamer et al. 2008; Bolcun-Filas et al. 2009; Schramm et al. 2011; F. A. T. De Vries et al. 2005; Gómez-H et al. 2016). contrasting to the widely unpaired homologs found in *Usp44*^{-/-} mutants. *Usp44* mutants are also clearly different from mice defective in late recombination processes, e.g., mutants lacking ZMM protein CNDT1, HFM1, RNF212, or HEI10 (Guiraldelli et al. 2013; Reynolds et al. 2013; Qiao et al. 2014; Holloway et al. 2014)(Figure 1-5), in which CO formation is primarily affected, but the early stages of meiotic recombination occur typically with no, or minimal, synapsis defects.

In *Usp44*^{-/-} spermatocytes, recombination initiation seems not to be affected, as evidenced by the presence of γH2AX staining and numerous RPA and RAD51 foci at the leptotene stage. However, both RPA and RAD51 foci accumulate on both synapsed and unsynapsed chromosomes in these late zygotene-like cells, in sharp contrast to the gradual decrease in foci numbers that occur throughout zygotene in wild-type cells. Mouse spermatocytes lacking DSB resection factors, e.g., *Nbs1*^{-/-}, (B. Zhang et al. 2020) or recombinase recruiter and stabilizers, e.g., MEILB2, BRCA2, BRME1, or MEIOB (J. Zhang et al. 2019; 2020; Takemoto et al. 2020; Felipe-Medina et al. 2020; Sharan et al. 2004;

Souquet et al. 2013) (Figure 1-5), exhibit dramatically reduced RAD51 foci at zygotene stage, or even since leptotene stage. Thus, our observations allow us to conclude that DSB resection and recombinase recruitment are likely not majorly impaired in *Usp44*^{-/-} spermatocytes. Unfortunately, we couldn't investigate another important recombinase, DMC1, in mutant cells due to the unavailability of appropriate antibodies.

In the end, the phenotype of *Usp44* mutants is strikingly similar to those of *Dmcl*, *Hop2/Mnd1*, and *Msh4/5* mutant mice (K. Yoshida et al. 1998; Pittman et al. 1998; S. S. De Vries et al. 1999; Barchi et al. 2005; Kneitz et al. 2000; Petukhova, Romanienko, and Camerini-Otero 2003; Pezza et al. 2014). DMC1, together with RAD51, binds to ssDNA forming nucleofilament and then carries out homology search and strand exchange (Brown and Bishop 2015). HOP2-MND1 complex stabilizes the filament and promotes the activity of recombinases (Pezza et al. 2007; Petukhova et al. 2005; Chi et al. 2007) (Figure 1-5). Subsequently, unstable nascent D-loops are formed, further bound and stabilized by MMR protein MSH4 and MSH5, thus promoting CO formation via dHJs (Hunter 2015).

Like *Usp44*^{-/-} spermatocytes, *Dmcl*, *Hop2/Mnd1*, and *Msh4/5* mutant spermatocytes all exhibit profound meiotic defects, including impaired pairing and synapsis, the persistence of RAD51, and failed DSB repair (Pittman et al. 1998; K. Yoshida et al. 1998; S. S. De Vries et al. 1999; Petukhova, Romanienko, and Camerini-Otero 2003). A unique observation in *Usp44* mutants is that a fraction of mutant spermatocytes could complete synapsis and DSB repair. Something that is also surprisingly found in *Mnd1* mutants spermatocytes (Pezza et al. 2014). A fraction (23%) of *Mnd1*^{-/-} spermatocytes at the zygotene/pachytene-like stage exhibits extensive homologous synapsis (80-100% synapsis) with most DSBs repaired. Likewise, in our data, pachytene cells with limited asynapsis and complete synapsis account for around 28% of both late zygotene-like and pachytene cells.

HOP2-MND1 complex has an essential role in promoting DMC1/RAD51-mediated homology search and strand exchange (Chi et al. 2007; Petukhova et al. 2005; Brown and Bishop 2015). Thus, the absence of this complex in *Mnd1* mutants leads to deficient strand invasion, which leads to failure to complete synapsis. Interestingly, it is thought that HOP2 can function alone as a recombinase to promote strand exchange and DSB repair in the absence of MND1, resulting in a population of *Mnd1* mutant

spermatocytes with extensive synapsis and most DSB repaired (Pezza et al. 2014).

Under this assumption, we hypothesize that if the observations in *Usp44* mutants were also caused by deficient strand invasion, which is partially rescued by HOP2's recombinase activity, USP44 would be related to MND1 itself or the formation/activity of the HOP2-MND1 complex. Since *Usp44*^{-/-} mutants displayed cells more advanced such as diplotene spermatocytes and spermatids than *Mnd1*^{-/-} mutants, we hypothesize an inefficient function of HOP2-MND1 caused by USP44 disruption would be favored rather than the complete absence of HOP2-MND1 complex activity. However, MND1 is poorly studied, and there is no information on how HOP2-MND1 is regulated *in vivo*. A recent study identifies that the expression of MND1 is highly correlated with ubiquitin-conjugating enzyme-E2C (UBE2C) in cancers (Dastsooz et al. 2019). UBE2C is also known as a mitotic SAC regulator (Jia-hao Wang et al. 2019). Thus, it would be interesting to explore if MND1 is ubiquitinated during meiosis, its effect on the activity of the HOP2-MND1 complex and if USP44 regulates the MND1 ubiquitination status during meiosis.

Nonetheless, we cannot rule out that the small population of *Usp44*^{-/-} spermatocytes that could complete synapsis and DSB repair and even progress to the diplotene stage might be attributed to the mixed genetic background of the *Usp44* mutant mice.

So far, we have no information on how the absence of USP44 may affect DMC1 function due to the unavailability of specific antibodies. RAD51 is suggested to enhance DMC1 assembly and stabilization with other recombinase cofactors (Brown and Bishop 2015). Also, DMC1 foci numbers are similarly altered as RAD51 in *Hop2/Mnd1* and *Msh4/5* mutant mice (Pittman et al. 1998; K. Yoshida et al. 1998; S. S. De Vries et al. 1999; Petukhova, Romanienko, and Camerini-Otero 2003). Thus, it is likely that DMC1 will also show persistence in *Usp44* mutant cells before the arrest. Still and all, further examination of DMC1 is necessary to be performed in *Usp44* mutants spermatocytes. Moreover, it will be fascinating if DMC1 is altered differently from RAD51.

Since we observed accumulation of RAD51 at the late zygotene-like stage, in principle, it could be possible that the impaired synapsis and DSB repair from *Usp44* mutant cells resulted from deficient removal of RAD51 and DMC1. Indeed, there is some evidence that might favor this possibility. The UPS has been shown to regulate the

turnover of both RAD51 and DMC1 in mice. The E3 ligase HEI10 mediated UPS pathway is responsible for the turnover of RAD51, and the turnover of DMC1 is involved in other branches of the UPS (Prasada Rao et al. 2017). Moreover, RAD51 also can be regulated by other ubiquitin ligases for different fates. RAD51 has been identified to bear multiple ubiquitination target sites. Also, FBH1-mediated ubiquitination of RAD51 regulates the subcellular localization of RAD51 rather than its degradation (Chu et al. 2015). The E3 ligase RFWD3 can ubiquitinate both RPA and RAD51 and promote their removal from DSB sites, facilitating the progression of HR repair in human cell lines (Inano et al. 2017). Thus, it is likely that ubiquitination events regulate RAD51 and DMC1's turnover in meiosis. As DUBs function wherever there is ubiquitination, the roles of USP44 in regulating these potential ubiquitination processes will be appealing to pursue in future studies.

Overall, our preliminary characterization of the *Usp44* mutant spermatocytes makes us conclude that USP44 is presumably involved in strand invasion or D-loop formation/stabilization during meiosis. The depletion of USP44 leads to failed homology search and homologous interaction, consequently incomplete synapsis and DSB repair. Moreover, future investigations are required to uncover the precise functions of USP44 in the meiotic prophase. Indeed, the phenotypes of female USP44 mutants still need to be studied. Also, cytological analysis of more early recombination markers needs to be examined to support the hypothesis discussed above, for instance, DMC1, MSH4/MSH5. It is also attractive to investigate the final fate of the fully-synapsed spermatocytes. How many of these cells could reach the mid-late pachytene stage as H1t positive, and how many of these H1t-positive cells could have a standard number of MLH1 foci. It is possible that even though some *Usp44*^{-/-} cells could progress to late prophase, they might have a deficiency in the CO-forming pathway. Identification of specific target proteins for USP44 is also essential. Several methods could be used to achieve this, including *in vitro* interaction studies using immunoprecipitation assay (Park et al. 2019) and proteomic approaches (Sowa et al. 2009). A start point could be from some target proteins of human USP44 that have been identified but not studied in meiosis, including RNA Polymerase II Subunit G (Sowa et al. 2009), or PSMC proteasomes (Lan et al. 2016). In any case, we are still far from understanding how the absence of USP44 results in the phenotype described here, and more studies are required to reveal the USP44 function in meiosis.

Nonetheless, the data provided here clearly shows that USP44 is indispensable to complete meiosis in spermatocytes and mammalian spermatogenesis.

Chapter 6

Conclusions

1. Our approach has proved useful to identify novel meiotic genes required for mammalian gametogenesis.
2. The validation of our approach provided by the phenotype of *Bend2* and *Usp44* mutant mice suggests that other relevant genes for mammalian gametogenesis are among the list of presumed genes studied.
3. Using our approach, we successfully identified two novel meiotic genes, *Bend2* and *Usp44*, essential for mouse fertility, thus providing new insights into understanding and diagnosing human infertility.
4. BEND2 is highly expressed in nuclei of spermatogonia and spermatocytes from pre-leptotene to early pachytene stage. This expression is independent of either DSB formation or completion of recombination.
5. BEND2 is dispensable for completing spermatogenesis. However, the deletion of BEND2 causes increased apoptosis in testicular cells.
6. BEND2 is required for establishing a normal ovarian reserve. The deficiency of BEND2 leads to a significant loss of primordial follicles and primary ovarian insufficiency in adult mice.
7. BEND2 is dispensable for completing synapsis in both spermatocytes and oocytes. However, meiotic prophase progression is altered in the absence of BEND2.
8. BEND2 is required for sufficient DSB repair. In the absence of BEND2, unrepaired DSBs persist since pachytene in spermatocytes and oocytes. However, the early recombination process is mainly unaffected.

9. BEND2 is indispensable for normal CO formation in females but not in males.
10. USP44 is preferentially loaded at synapsed chromosome axes during meiotic prophase, likely dependent on SPO11-induced DSB formation and DMC1-mediated homologous interactions.
11. USP44 is required for male fertility since its deletion causes meiotic arrest in most seminiferous tubules.
12. USP44 is required for standard homolog pairing and synapsis in males. In the absence of USP44, meiotic progression is grossly altered, and only a small proportion of spermatocytes progress to the diplotene stage.
13. USP44 is required for homologous recombination in males. Without USP44, most spermatocytes are arrested at mid-stages of prophase I before entering apoptosis with persistent DSBs, RPA, and RAD51.

References

- Abhiman, Saraswathi, Lakshminarayan M. Iyer, and L. Aravind. 2008. "BEN: A Novel Domain in Chromatin Factors and DNA Viral Proteins." *Bioinformatics (Oxford, England)* 24 (4): 458. <https://doi.org/10.1093/BIOINFORMATICS/BTN007>.
- Abreu, Carla M., Rohit Prakash, Peter J. Romanienko, Ignasi Roig, Scott Keeney, and Maria Jasin. 2018. "Shu Complex SWS1-SWSAP1 Promotes Early Steps in Mouse Meiotic Recombination." *Nature Communications* 9 (1): 3961. <https://doi.org/10.1038/s41467-018-06384-x>.
- Adelman, Carrie A., and John H.J. Petrini. 2008. "ZIP4H (TEX11) Deficiency in the Mouse Impairs Meiotic Double Strand Break Repair and the Regulation of Crossing Over." *PLoS Genetics* 4 (3): e1000042. <https://doi.org/10.1371/journal.pgen.1000042>.
- Ahmed, Emad A., Marielle E.P. Philippens, Henk B. Kal, Dirk G. de Rooij, and Peter de Boer. 2010. "Genetic Probing of Homologous Recombination and Non-Homologous End Joining during Meiotic Prophase in Irradiated Mouse Spermatocytes." *Mutation Research - Fundamental and Molecular Mechanisms of Mutagenesis* 688 (1–2): 12–18. <https://doi.org/10.1016/j.mrfmmm.2010.02.004>.
- Allen, J. W., D. J. Dix, B. W. Collins, B. A. Merrick, C. He, J. K. Selkirk, P. Poorman-Allen, M. E. Dresser, and E. M. Eddy. 1996. "HSP70-2 Is Part of the Synaptonemal Complex in Mouse and Hamster Spermatocytes." *Chromosoma* 104 (6): 414–21. <https://doi.org/10.1007/BF00352265>.
- Alsheimer, M., A. Baier, S. Schramm, W. Schütz, and R. Benavente. 2010. "Synaptonemal Complex Protein SYCP3 Exists in Two Isoforms Showing Different Conservation in Mammalian Evolution." *Cytogenetic and Genome Research* 128 (1–3): 162–68. <https://doi.org/10.1159/000303341>.
- An, Jee Young, Eun A. Kim, Yonghua Jiang, Adriana Zakrzewska, Dong Eun Kim, Min Jae Lee, Inhee Mook-Jung, Yi Zhang, and Yong Tae Kwon. 2010. "UBR2 Mediates Transcriptional Silencing during Spermatogenesis via Histone Ubiquitination." *Proceedings of the National Academy of Sciences of the United States of America* 107 (5): 1912. <https://doi.org/10.1073/PNAS.0910267107>.
- Anand, Roopesh, Arti Jasrotia, Diana Bundschuh, Sean Michael Howard, Lepakshi Ranjha, Manuel Stucki, and Petr Cejka. 2019. "NBS1 Promotes the Endonuclease Activity of the MRE11-RAD50 Complex by Sensing CtIP Phosphorylation." *The EMBO Journal* 38 (7): e101005. <https://doi.org/10.15252/embj.2018101005>.
- Anderson, Carol M., Ashwini Oke, Phoebe Yam, Tangna Zhuge, and Jennifer C. Fung. 2015. "Reduced Crossover Interference and Increased ZMM-Independent Recombination in the Absence of Tel1/ATM." *PLoS Genetics* 11 (8): e1005478. <https://doi.org/10.1371/journal.pgen.1005478>.
- Anderson, Ericka L., Andrew E. Baltus, Hermien L. Roepers-Gajadien, Terry J. Hassold, Dirk G. De Rooij, Ans M.M. Van Pelt, and David C. Page. 2008. "Stra8 and Its Inducer, Retinoic Acid, Regulate Meiotic Initiation in Both Spermatogenesis and Oogenesis in Mice." *Proceedings of the National Academy of Sciences of the United States of America* 105 (39): 14976–80. <https://doi.org/10.1073/pnas.0807297105>.
- Anderson, Lorinda K., Aaron Reeves, Lisa M. Webb, and Terry Ashley. 1999. "Distribution of Crossing over on Mouse Synaptonemal Complexes Using Immunofluorescent Localization of MLH1 Protein." *Genetics* 151 (4): 1569–79. <https://doi.org/10.1093/genetics/151.4.1569>.
- Anderson, R, T K Copeland, H Scholer, J Heasman, and C Wylie. 2000. "The Onset of Germ Cell Migration in the Mouse Embryo." *Mechanisms of Development* 91 (1–2): 61–68. [https://doi.org/10.1016/s0925-4773\(99\)00271-3](https://doi.org/10.1016/s0925-4773(99)00271-3).

- Arora, Charanjit, Kehkooi Kee, Shohreh Maleki, and Scott Keeney. 2004. "Antiviral Protein Ski8 Is a Direct Partner of Spo11 in Meiotic DNA Break Formation, Independent of Its Cytoplasmic Role in RNA Metabolism." *Molecular Cell* 13 (4): 549–59. [https://doi.org/10.1016/S1097-2765\(04\)00063-2](https://doi.org/10.1016/S1097-2765(04)00063-2).
- Aymard, François, Beatrix Bugler, Christine K. Schmidt, Emmanuelle Guillou, Pierre Caron, Sébastien Briois, Jason S. Iacovoni, et al. 2014. "Transcriptionally Active Chromatin Recruits Homologous Recombination at DNA Double-Strand Breaks." *Nature Structural & Molecular Biology* 2014 21:4 21 (4): 366–74. <https://doi.org/10.1038/nsmb.2796>.
- Baarends, Willy M., Evelyne Wassenaar, Roald van der Laan, Jos Hoogerbrugge, Esther Sleddens-Linkels, Jan H. J. Hoeijmakers, Peter de Boer, and J. Anton Grootegoed. 2005. "Silencing of Unpaired Chromatin and Histone H2A Ubiquitination in Mammalian Meiosis." *Molecular and Cellular Biology* 25 (3): 1041–53. <https://doi.org/10.1128/mcb.25.3.1041-1053.2005>.
- Baier, Andrea, Manfred Alsheimer, and Ricardo Benavente. 2007. "Synaptonemal Complex Protein SYCP3: Conserved Polymerization Properties among Vertebrates." *Biochimica et Biophysica Acta - Proteins and Proteomics* 1774 (5): 595–602. <https://doi.org/10.1016/j.bbapap.2007.03.008>.
- Baker, Scan M., Annemieke W. Plug, Tomas A. Prolla, C. Eric Bronner, Allie C. Harris, Xiang Yao, Donna Marie Christie, et al. 1996. "Involvement of Mouse Mlh1 in DNA Mismatch Repair and Meiotic Crossing Over." *Nature Genetics* 13 (3): 336–42. <https://doi.org/10.1038/ng0796-336>.
- Baker, T G. 1963. "A QUANTITATIVE AND CYTOLOGICAL STUDY OF GERM CELLS IN HUMAN OVARIES." *Proceedings of the Royal Society of London. Series B, Biological Sciences* 158 (October): 417–33. <https://doi.org/10.1098/rspb.1963.0055>.
- Baltus, Andrew E., Douglas B. Menke, Yueh Chiang Hu, Mary L. Goodheart, Anne E. Carpenter, Dirk G. De Rooij, and David C. Page. 2006. "In Germ Cells of Mouse Embryonic Ovaries, the Decision to Enter Meiosis Precedes Premeiotic DNA Replication." *Nature Genetics* 38 (12): 1430–34. <https://doi.org/10.1038/ng1919>.
- Bannister, Laura A., Laura G. Reinholdt, Robert J. Munroe, and John C. Schimenti. 2004. "Positional Cloning and Characterization of Mouse Mei8, a Disrupted Allele of the Meiotic Cohesin Rec8." *Genesis* 40 (3): 184–94. <https://doi.org/10.1002/gene.20085>.
- Barchi, Marco, Shantha Mahadevaiah, Monica Di Giacomo, Frédéric Baudat, Dirk G. de Rooij, Paul S. Burgoyne, Maria Jasin, and Scott Keeney. 2005. "Surveillance of Different Recombination Defects in Mouse Spermatocytes Yields Distinct Responses despite Elimination at an Identical Developmental Stage." *Molecular and Cellular Biology* 25 (16): 7203–15. <https://doi.org/10.1128/mcb.25.16.7203-7215.2005>.
- Barchi, Marco, Ignasi Roig, Monica Di Giacomo, Dirk G. De Rooij, Scott Keeney, and Maria Jasin. 2008. "ATM Promotes the Obligate XY Crossover and Both Crossover Control and Chromosome Axis Integrity on Autosomes." *PLoS Genetics* 4 (5): e1000076. <https://doi.org/10.1371/journal.pgen.1000076>.
- Barlow, Andrew L., Fiona E. Benson, Stephen C. West, and Maj A. Hultén. 1997. "Distribution of the Rad51 Recombinase in Human and Mouse Spermatocytes." *EMBO Journal* 16 (17): 5207–15. <https://doi.org/10.1093/emboj/16.17.5207>.
- Baudat, Frédéric, Yukiko Imai, and Bernard De Massy. 2013. "Meiotic Recombination in Mammals: Localization and Regulation." *Nature Reviews Genetics*. <https://doi.org/10.1038/nrg3573>.
- Baudat, Frédéric, Katia Manova, Julie Pui Yuen, Maria Jasin, and Scott Keeney. 2000. "Chromosome

- Synapsis Defects and Sexually Dimorphic Meiotic Progression in Mice Lacking Spo11.” *Molecular Cell* 6 (5): 989–98. [https://doi.org/10.1016/S1097-2765\(00\)00098-8](https://doi.org/10.1016/S1097-2765(00)00098-8).
- Beke, Artur. 2019. “Genetic Causes of Female Infertility.” *Experientia Supplementum* (2012) 111: 367–83. https://doi.org/10.1007/978-3-030-25905-1_17.
- Belgnaoui, S. Mehdi, Roger G. Gosden, O. John Semmes, and Abdelali Haoudi. 2006. “Human LINE-1 Retrotransposon Induces DNA Damage and Apoptosis in Cancer Cells.” *Cancer Cell International* 6 (13). <https://doi.org/10.1186/1475-2867-6-13>.
- Bellani, Marina A., Peter J. Romanienko, Damian A. Cairatti, and R. Daniel Camerini-Otero. 2005. “SPO11 Is Required for Sex-Body Formation, and Spo11 Heterozygosity Rescues the Prophase Arrest of *Atm*^{-/-} Spermatocytes.” *Journal of Cell Science* 118 (15): 3233–45. <https://doi.org/10.1242/jcs.02466>.
- Bellve, A. R., J. C. Cavicchia, C. F. Millette, D. A. O’Brien, Y. M. Bhatnagar, and M. Dym. 1977. “Spermatogenic Cells of the Prepuberal Mouse. Isolation and Morphological Characterization.” *Journal of Cell Biology* 74 (1): 68–85. <https://doi.org/10.1083/jcb.74.1.68>.
- Berchowitz, Luke, and Gregory Copenhagen. 2010. “Genetic Interference: Dont Stand So Close to Me.” *Current Genomics* 11 (2): 91–102. <https://doi.org/10.2174/138920210790886835>.
- Bergerat, Agnès, Bernard De Massy, Danielle Gadelle, Paul Christophe Varoutas, Alain Nicolas, and Patrick Forterre. 1997. “An Atypical Topoisomerase II from Archaea with Implications for Meiotic Recombination.” *Nature* 386 (6623): 414–17. <https://doi.org/10.1038/386414a0>.
- Bettegowda, Anilkumar, and Miles F. Wilkinson. 2010. “Transcription and Post-Transcriptional Regulation of Spermatogenesis.” *Philosophical Transactions of the Royal Society B: Biological Sciences* 365 (1546): 1637–51. <https://doi.org/10.1098/rstb.2009.0196>.
- Bhalla, Needhi, and Abby F. Dernburg. 2005. “Cell Biology: A Conserved Checkpoint Monitors Meiotic Chromosome Synapsis in *Caenorhabditis Elegans*.” *Science* 310 (5754): 1683–86. <https://doi.org/10.1126/science.1117468>.
- Bhattacharyya, Tanmoy, Michael Walker, Natalie R. Powers, Catherine Brunton, Alexander D. Fine, Petko M. Petkov, and Mary Ann Handel. 2019. “Prdm9 and Meiotic Cohesin Proteins Cooperatively Promote DNA Double-Strand Break Formation in Mammalian Spermatocytes.” *Current Biology* 29 (6): 1002-1018.e7. <https://doi.org/10.1016/j.cub.2019.02.007>.
- Bisig, C. Gaston, Michel F. Guiraldelli, Anna Kouznetsova, Harry Scherthan, Christer Höög, Dean S. Dawson, and Roberto J. Pezza. 2012. “Synaptonemal Complex Components Persist at Centromeres and Are Required for Homologous Centromere Pairing in Mouse Spermatocytes.” *PLoS Genetics* 8 (6): e1002701. <https://doi.org/10.1371/journal.pgen.1002701>.
- Boekhout, Michiel, Mehmet E. Karasu, Juncheng Wang, Laurent Acquaviva, Florencia Pratto, Kevin Brick, Diana Y. Eng, et al. 2019. “REC114 Partner ANKRD31 Controls Number, Timing, and Location of Meiotic DNA Breaks.” *Molecular Cell* 74 (5): 1053-1068.e8. <https://doi.org/10.1016/j.molcel.2019.03.023>.
- Bolaños-Villegas, Pablo, Wanyue Xu, Marina Martínez-García, Mónica Pradillo, and Yingxiang Wang. 2018. “Insights Into the Role of Ubiquitination in Meiosis: Fertility, Adaptation and Plant Breeding.” *The Arabidopsis Book* 16 (January): e0187. <https://doi.org/10.1199/tab.0187>.
- Bolcun-Filas, Ewelina, Yael Costa, Robert Speed, Mary Taggart, Ricardo Benavente, Dirk G. De Rooij, and Howard J. Cooke. 2007. “SYCE2 Is Required for Synaptonemal Complex Assembly, Double Strand Break Repair, and Homologous Recombination.” *Journal of Cell Biology* 176 (6): 741–47. <https://doi.org/10.1083/jcb.200610027>.

- Bolcun-Filas, Ewelina, and Mary Ann Handel. 2018. "Meiosis: The Chromosomal Foundation of Reproduction." *Biology of Reproduction*. Oxford University Press. <https://doi.org/10.1093/biolre/iory021>.
- Bolcun-Filas, Ewelina, Vera D. Rinaldi, Michelle E. White, and John C. Schimenti. 2014. "Reversal of Female Infertility by Chk2 Ablation Reveals the Oocyte DNA Damage Checkpoint Pathway." *Science* 343 (6170): 533–36. <https://doi.org/10.1126/science.1247671>.
- Bolcun-Filas, Ewelina, and John C Schimenti. 2012. "Genetics of Meiosis and Recombination in Mice." In *International Review of Cell and Molecular Biology*, 298:179–227. <https://doi.org/10.1016/B978-0-12-394309-5.00005-5>.
- Bolcun-Filas, Ewelina, Robert Speed, Mary Taggart, Corinne Grey, Bernard De Massy, Ricardo Benavente, and Howard J. Cooke. 2009. "Mutation of the Mouse Syce1 Gene Disrupts Synapsis and Suggests a Link between Synaptonemal Complex Structural Components and DNA Repair." *PLoS Genetics* 5 (2): e1000393. <https://doi.org/10.1371/journal.pgen.1000393>.
- Bonnet, Jacques, Christophe Romier, László Tora, and Didier Devys. 2008. "Zinc-Finger UBPs: Regulators of Deubiquitylation." *Trends in Biochemical Sciences* 33 (8): 369–75. <https://doi.org/10.1016/J.TIBS.2008.05.005>.
- Börner, G. Valentin, Nancy Kleckner, and Neil Hunter. 2004. "Crossover/Noncrossover Differentiation, Synaptonemal Complex Formation, and Regulatory Surveillance at the Leptotene/Zygotene Transition of Meiosis." *Cell* 117 (1): 29–45. [https://doi.org/10.1016/S0092-8674\(04\)00292-2](https://doi.org/10.1016/S0092-8674(04)00292-2).
- Borum, Kirstine. 1961. "Oogenesis in the Mouse: A Study of the Meiotic Prophase." *Experimental Cell Research* 24 (3): 495–507. [https://doi.org/10.1016/0014-4827\(61\)90449-9](https://doi.org/10.1016/0014-4827(61)90449-9).
- Bose, R, • S S Wing, G Manku, M Culty, Rohini Bose, Gurpreet Manku, Martine Culty, Simon S Wing, and P Sutovsky. 2014. "Ubiquitin–Proteasome System in Spermatogenesis." *Advances in Experimental Medicine and Biology* 759: 181–213. https://doi.org/10.1007/978-1-4939-0817-2_9.
- Bowles, Josephina, Deon Knight, Christopher Smith, Dagmar Wilhelm, Joy Richman, Satoru Mamiya, Kenta Yashiro, et al. 2006. "Retinoid Signaling Determines Germ Cell Fate in Mice." *Science* 312 (5773): 596–600. <https://doi.org/10.1126/science.1125691>.
- Brick, Kevin, Fatima Smagulova, Pavel Khil, R. Daniel Camerini-Otero, and Galina V. Petukhova. 2012. "Genetic Recombination Is Directed Away from Functional Genomic Elements in Mice." *Nature* 485 (7400): 642–45. <https://doi.org/10.1038/nature11089>.
- Brieño-Enríquez, Miguel A., Stefannie L. Moak, Melissa Toledo, Joshua J. Filter, Stephen Gray, José L. Barbero, Paula E. Cohen, and J. Kim Holloway. 2016. "Cohesin Removal along the Chromosome Arms during the First Meiotic Division Depends on a NEK1-PP1γ-WAPL Axis in the Mouse." *Cell Reports* 17 (4): 977–86. <https://doi.org/10.1016/j.celrep.2016.09.059>.
- Brown, M. Scott, and Douglas K. Bishop. 2015. "DNA Strand Exchange and RecA Homologs in Meiosis." *Cold Spring Harbor Perspectives in Biology* 7 (1). <https://doi.org/10.1101/cshperspect.a016659>.
- Burford, Anna, Alan Mackay, Sergey Popov, Maria Vinci, Diana Carvalho, Matthew Clarke, Elisa Izquierdo, et al. 2018. "Tumor BEN FUSTION The Ten-Year Evolutionary Trajectory of a Highly Recurrent Paediatric High Grade Neuroepithelial Tumour with MN1:BEND2 Fusion." *Scientific Reports* 8 (1): 1–10. <https://doi.org/10.1038/s41598-018-19389-9>.
- Burgoyne, Paul S., Shantha K. Mahadevaiah, and James M.A. Turner. 2009. "The Consequences of

- Asynapsis for Mammalian Meiosis." *Nature Reviews Genetics*. Nat Rev Genet. <https://doi.org/10.1038/nrg2505>.
- Burke, Brian. 2018. "LINC Complexes as Regulators of Meiosis." *Current Opinion in Cell Biology*. Elsevier Ltd. <https://doi.org/10.1016/j.ceb.2018.01.005>.
- Cahoon, Cori K., and R. Scott Hawley. 2016. "Regulating the Construction and Demolition of the Synaptonemal Complex." *Nature Structural and Molecular Biology*. Nature Publishing Group. <https://doi.org/10.1038/nsmb.3208>.
- Callis, Judy. 2014. "The Ubiquitination Machinery of the Ubiquitin System." *The Arabidopsis Book 12*: e0174. <https://doi.org/10.1199/tab.0174>.
- Cannavo, Elda, and Petr Cejka. 2014. "Sae2 Promotes DsDNA Endonuclease Activity within Mre11-Rad50-Xrs2 to Resect DNA Breaks." *Nature* 514 (7520): 122–25. <https://doi.org/10.1038/nature13771>.
- Capitano, Juliana S, Ben Montpetit, and Richard W Wozniak. 2017. "Human Nup98 Regulates the Localization and Activity of DExH/D-Box Helicase DHX9." *ELife* 6 (February). <https://doi.org/10.7554/eLife.18825>.
- Carballo, Jesús A., Anthony L. Johnson, Steven G. Sedgwick, and Rita S. Cha. 2008. "Phosphorylation of the Axial Element Protein Hop1 by Mec1/Tel1 Ensures Meiotic Interhomolog Recombination." *Cell* 132 (5): 758–70. <https://doi.org/10.1016/j.cell.2008.01.035>.
- Carballo, Jesús A., Silvia Panizza, Maria Elisabetta Serrentino, Anthony L. Johnson, Marco Geymonat, Valérie Borde, Franz Klein, and Rita S. Cha. 2013. "Budding Yeast ATM/ATR Control Meiotic Double-Strand Break (DSB) Levels by Down-Regulating Rec114, an Essential Component of the DSB-Machinery." *PLoS Genetics* 9 (6). <https://doi.org/10.1371/journal.pgen.1003545>.
- Carney, James P., Richard S. Maser, Heidi Olivares, Elizabeth M. Davis, Michelle Le Beau, John R. Yates, Lara Hays, William F. Morgan, and John H.J. Petrini. 1998. "The HMre11/HRad50 Protein Complex and Nijmegen Breakage Syndrome: Linkage of Double-Strand Break Repair to the Cellular DNA Damage Response." *Cell* 93 (3): 477–86. [https://doi.org/10.1016/S0092-8674\(00\)81175-7](https://doi.org/10.1016/S0092-8674(00)81175-7).
- Carofiglio, Fabrizia, Akiko Inagaki, Sandra de Vries, Evelyne Wassenaar, Sam Schoenmakers, Christie Vermeulen, Wiggert A. van Cappellen, et al. 2013. "SPO11-Independent DNA Repair Foci and Their Role in Meiotic Silencing." *PLoS Genetics* 9 (6): e1003538. <https://doi.org/10.1371/journal.pgen.1003538>.
- Cartagena-Lirola, Hugo, Ilaria Guerini, Nicola Manfrini, Giovanna Lucchini, and Maria Pia Longhese. 2008. "Role of the *Saccharomyces Cerevisiae* Rad53 Checkpoint Kinase in Signaling Double-Strand Breaks during the Meiotic Cell Cycle." *Molecular and Cellular Biology* 28 (14): 4480–93. <https://doi.org/10.1128/mcb.00375-08>.
- Cherry, Sheila M., Carrie A. Adelman, Jan W. Theunissen, Terry J. Hassold, Patricia A. Hunt, and John H.J. Petrini. 2007. "The Mre11 Complex Influences DNA Repair, Synapsis, and Crossing Over in Murine Meiosis." *Current Biology* 17 (4): 373–78. <https://doi.org/10.1016/j.cub.2006.12.048>.
- Chi, Peter, Joseph San Filippo, Michael G. Sehorn, Galina V. Petukhova, and Patrick Sung. 2007. "Bipartite Stimulatory Action of the Hop2-Mnd1 Complex on the Rad51 Recombinase." *Genes and Development* 21 (14): 1747–57. <https://doi.org/10.1101/gad.1563007>.
- Chiquoine, A. Duncan. 1954. "The Identification, Origin, and Migration of the Primordial Germ Cells in the Mouse Embryo." *The Anatomical Record* 118 (2): 135–46. <https://doi.org/10.1002/ar.1091180202>.

- Choi, Jong-Ho, Suresh Ramakrishna, Kwang-Hyun Baek, Woong-Shick Ahn, Hey-Jin Lee, Bharathi Suresh, and Jin-Young Kim. 2010. "K48- and K63-Linked Polyubiquitination of Deubiquitinating Enzyme USP44." *Cell Biology International* 34 (8): 799–808. <https://doi.org/10.1042/cbi20090144>.
- Choi, Youngsok, Daniel J Ballow, Yun Xin, and Aleksandar Rajkovic. 2008. "Lim Homeobox Gene, Lhx8, Is Essential for Mouse Oocyte Differentiation and Survival." *Biology of Reproduction* 79 (3): 442–49. <https://doi.org/10.1095/biolreprod.108.069393>.
- Choi, Youngsok, Daniel Yuan, and Aleksandar Rajkovic. 2008. "Germ Cell-Specific Transcriptional Regulator Sohlh2 Is Essential for Early Mouse Folliculogenesis and Oocyte-Specific Gene Expression." *Biology of Reproduction* 79 (6): 1176–82. <https://doi.org/10.1095/biolreprod.108.071217>.
- Chu, Wai Kit, Miranda J. Payne, Petra Beli, Katsuhiko Hanada, Chunaram Choudhary, and Ian D. Hickson. 2015. "FBH1 Influences DNA Replication Fork Stability and Homologous Recombination through Ubiquitylation of RAD51." *Nature Communications* 6 (1): 1–9. <https://doi.org/10.1038/ncomms6931>.
- Chuang, Chi Ning, Yun Hsin Cheng, and Ting Fang Wang. 2012. "Mek1 Stabilizes Hop1-Thr318 Phosphorylation to Promote Interhomolog Recombination and Checkpoint Responses during Yeast Meiosis." *Nucleic Acids Research* 40 (22): 11416–27. <https://doi.org/10.1093/nar/gks920>.
- Cloud, Veronica, Yuen Ling Chan, Jennifer Grubb, Brian Budke, and Douglas K. Bishop. 2012. "Rad51 Is an Accessory Factor for Dmc1-Mediated Joint Molecule Formation during Meiosis." *Science* 337 (6099): 1222–25. <https://doi.org/10.1126/science.1219379>.
- Cloutier, J. M., S. K. Mahadevaiah, E. Ellnati, A. Tóth, and James Turner. 2016. "Mammalian Meiotic Silencing Exhibits Sexually Dimorphic Features." *Chromosoma* 125 (2): 215–26. <https://doi.org/10.1007/s00412-015-0568-z>.
- Cloutier, Jeffrey M., Shantha K. Mahadevaiah, Elias Ellnati, André Nussenzweig, Attila Tóth, and James M. A. Turner. 2015. "Histone H2AFX Links Meiotic Chromosome Asynapsis to Prophase I Oocyte Loss in Mammals." *PLOS Genetics* 11 (10): e1005462. <https://doi.org/10.1371/journal.pgen.1005462>.
- Cole, Francesca, Liisa Kauppi, Julian Lange, Ignasi Roig, Raymond Wang, Scott Keeney, and Maria Jasin. 2012. "Homeostatic Control of Recombination Is Implemented Progressively in Mouse Meiosis." *Nature Cell Biology* 14 (4): 424–30. <https://doi.org/10.1038/ncb2451>.
- Cooper, Tim J., Kayleigh Wardell, Valerie Garcia, and Matthew J. Neale. 2014. "Homeostatic Regulation of Meiotic DSB Formation by ATM/ATR." *Experimental Cell Research*. Academic Press Inc. <https://doi.org/10.1016/j.yexcr.2014.07.016>.
- Cordeiro, Marília H., So Youn Kim, Katherine Ebbert, Francesca E. Duncan, João Ramalho-Santos, and Teresa K. Woodruff. 2015. "Geography of Follicle Formation in the Embryonic Mouse Ovary Impacts Activation Pattern during the First Wave of Folliculogenesis." *Biology of Reproduction* 93 (4): 1–10. <https://doi.org/10.1095/biolreprod.115.131227>.
- Cost, Gregory J., Qinghua Feng, Alain Jacquier, and Jef D. Boeke. 2002. "Human L1 Element Target-Primed Reverse Transcription in Vitro." *EMBO Journal* 21 (21): 5899–5910. <https://doi.org/10.1093/emboj/cdf592>.
- Costa, Yael, Robert Speed, Rupert Öllinger, Manfred Aisheimer, Colin A. Semple, Philippe Gautier, Klio Maratou, et al. 2005. "Two Novel Proteins Recruited by Synaptonemal Complex Protein 1 (SYCP1) Are at the Centre of Meiosis." *Journal of Cell Science* 118 (12): 2755–62.

- <https://doi.org/10.1242/jcs.02402>.
- Dai, Qi, Aiming Ren, Jakub O. Westholm, Artem A. Serganov, Dinshaw J. Patel, and Eric C. Lai. 2013. "The BEN Domain Is a Novel Sequence-Specific DNA-Binding Domain Conserved in Neural Transcriptional Repressors." *Genes & Development* 27 (6): 602. <https://doi.org/10.1101/GAD.213314.113>.
- Dai, Qi, Aiming Ren, Jakub O. Westholm, Hong Duan, Dinshaw J. Patel, and Eric C. Lai. 2015. "BEND1 Common and Distinct DNA-Binding and Regulatory Activities of the BEN-Solo Transcription Factor Family." *Genes and Development* 29 (1): 48–62. <https://doi.org/10.1101/gad.252122.114>.
- Dastsooz, Hassan, Matteo Cereda, Daniela Donna, and Salvatore Oliviero. 2019. "A Comprehensive Bioinformatics Analysis of UBE2C in Cancers." *International Journal of Molecular Sciences* 20 (9). <https://doi.org/10.3390/ijms20092228>.
- Davies, Michael J, Vivienne M Moore, Kristyn J Willson, Phillipa Van Essen, Kevin Priest, Heather Scott, Eric A Haan, and Annabelle Chan. 2012. "Reproductive Technologies and the Risk of Birth Defects." *The New England Journal of Medicine* 366 (19): 1803–13. <https://doi.org/10.1056/NEJMoa1008095>.
- Davies, Owen R., Joseph D. Maman, and Luca Pellegrini. 2012. "Structural Analysis of the Human SYCE2-TEX12 Complex Provides Molecular Insights into Synaptonemal Complex Assembly." *Open Biology* 2 (JULY). <https://doi.org/10.1098/rsob.120099>.
- Desai-Mehta, Ami, Karen M. Cerosaletti, and Patrick Concannon. 2001. "Distinct Functional Domains of Nibrin Mediate Mre11 Binding, Focus Formation, and Nuclear Localization." *Molecular and Cellular Biology* 21 (6): 2184–91. <https://doi.org/10.1128/mcb.21.6.2184-2191.2001>.
- Dissen, G A, C Romero, A N Hirshfield, and S R Ojeda. 2001. "Nerve Growth Factor Is Required for Early Follicular Development in the Mammalian Ovary." *Endocrinology* 142 (5): 2078–86. <https://doi.org/10.1210/endo.142.5.8126>.
- Dokshin, Gregoriy A., Andrew E. Baltus, John J. Eppig, and David C. Page. 2013. "Oocyte Differentiation Is Genetically Dissociable from Meiosis in Mice." *Nature Genetics* 45 (8): 877–83. <https://doi.org/10.1038/ng.2672>.
- Durlinger, Alexandra L.L., Maria J.G. Gruijters, Piet Kramer, Bas Karels, Holly A. Ingraham, Mark W. Nachtigal, Jan Th J. Uilenbroek, J. Anton Grootegoed, and Axel P.N. Themmen. 2002. "Anti-Müllerian Hormone Inhibits Initiation of Primordial Follicle Growth in the Mouse Ovary." *Endocrinology* 143 (3): 1076–84. <https://doi.org/10.1210/ENDO.143.3.8691>.
- Duroc, Yann, Rajeev Kumar, Lepakshi Ranjha, Céline Adam, Raphaël Guérois, Khan Md Muntaz, Marie Claude Marsolier-Kergoat, et al. 2017. "Concerted Action of the MutL β Heterodimer and Mer3 Helicase Regulates the Global Extent of Meiotic Gene Conversion." *ELife* 6 (January): e21900. <https://doi.org/10.7554/eLife.21900>.
- Edelmann, Winfried, Paula E. Cohen, Michael Kane, Kirkland Lau, Bernice Morrow, Samuel Bennett, Asad Umar, et al. 1996. "Meiotic Pachytene Arrest in MLH1-Deficient Mice." *Cell* 85 (7): 1125–34. [https://doi.org/10.1016/S0092-8674\(00\)81312-4](https://doi.org/10.1016/S0092-8674(00)81312-4).
- Edelmann, Winfried, Paula E. Cohen, Burkhard Kneitz, Nena Winand, Marie Lia, Joerg Heyer, Richard Kolodner, Jeffrey W. Pollard, and Raju Kucheralapati. 1999. "Mammalian MutS Homologue 5 Is Required for Chromosome Pairing in Meiosis." *Nature Genetics* 21 (1): 123–27. <https://doi.org/10.1038/5075>.
- Edson, Mark A, Ankur K Nagaraja, and Martin M Matzuk. 2009. "The Mammalian Ovary from Genesis

- to Revelation." *Endocrine Reviews* 30 (6): 624–712. <https://doi.org/10.1210/er.2009-0012>.
- Ellnati, Elias, Agata P. Zielinska, Afshan McCarthy, Nada Kubikova, Valdone Maciulyte, Shantha Mahadevaiah, Mahesh N. Sangrithi, et al. 2020. "The BCL-2 Pathway Preserves Mammalian Genome Integrity by Eliminating Recombination-Defective Oocytes." *Nature Communications* 11 (1): 1–10. <https://doi.org/10.1038/s41467-020-16441-z>.
- Ellermeier, Chad, Emily C. Higuchi, Naina Phadnis, Laerke Holm, Jennifer L. Geelhood, Genevieve Thon, and Gerald R. Smith. 2010. "RNAi and Heterochromatin Repress Centromeric Meiotic Recombination." *Proceedings of the National Academy of Sciences of the United States of America* 107 (19): 8701–5. <https://doi.org/10.1073/pnas.0914160107>.
- Endoh, Mitsuhiro, Takaho A. Endo, Jun Shinga, Katsuhiko Hayashi, Anca Farcas, Kit Wan Ma, Shinsuke Ito, et al. 2017. "PCGF6-PRC1 Suppresses Premature Differentiation of Mouse Embryonic Stem Cells by Regulating Germ Cell-Related Genes." *ELife* 6 (March). <https://doi.org/10.7554/eLife.21064>.
- Enguita-Marruedo, Andrea, Marta Martín-Ruiz, Eva García, Ana Gil-Fernández, María Teresa Parra, Alberto Viera, Julio S. Rufas, and Jesús Page. 2019. "Transition from a Meiotic to a Somatic-like DNA Damage Response during the Pachytene Stage in Mouse Meiosis." *PLoS Genetics* 15 (1). <https://doi.org/10.1371/JOURNAL.PGEN.1007439>.
- Extavour, Cassandra G, and Michael Akam. 2003. "Mechanisms of Germ Cell Specification across the Metazoans: Epigenesis and Preformation." *Development* 130 (24): 5869 LP – 5884. <https://doi.org/10.1242/dev.00804>.
- Fechner, Patricia Y, Marsha L Davenport, Rebecca L Qualy, Judith L Ross, Daniel F Gunther, Erica A Eugster, Carol Huseman, Anthony J Zagar, and Charmian A Quigley. 2006. "Differences in Follicle-Stimulating Hormone Secretion between 45,X Monosomy Turner Syndrome and 45,X/46,XX Mosaicism Are Evident at an Early Age." *The Journal of Clinical Endocrinology and Metabolism* 91 (12): 4896–4902. <https://doi.org/10.1210/jc.2006-1157>.
- Felipe-Medina, Natalia, Sandrine Caburet, Fernando Sánchez-Sáez, Yazmine B. Condezo, Dirk de Rooij, Laura Gómez-H, Rodrigo García-Valiente, et al. 2020. "A Missense in HSF2BP Causing Primary Ovarian Insufficiency Affects Meiotic Recombination by Its Novel Interactor C19orf57/Brme1." *ELife* 9 (August): 1–93. <https://doi.org/10.7554/ELIFE.56996>.
- Feng, Jianrong, Shijuan Fu, Xuan Cao, Hao Wu, Jing Lu, Ming Zeng, Lin Liu, Xue Yang, and Yuequan Shen. 2017. "Synaptonemal Complex Protein 2 (SYCP2) Mediates the Association of the Centromere with the Synaptonemal Complex." *Protein & Cell* 8 (7): 538–43. <https://doi.org/10.1007/s13238-016-0354-6>.
- Fernandez-Capetillo, Oscar, Shantha K. Mahadevaiah, Arkady Celeste, Peter J. Romanienko, R. Daniel Camerini-Otero, William M. Bonner, Katia Manova, Paul Burgoyne, and André Nussenzweig. 2003. "H2AX Is Required for Chromatin Remodeling and Inactivation of Sex Chromosomes in Male Mouse Meiosis." *Developmental Cell* 4 (4): 497–508. [https://doi.org/10.1016/S1534-5807\(03\)00093-5](https://doi.org/10.1016/S1534-5807(03)00093-5).
- Finsterbusch, Friederike, Ramya Ravindranathan, Ihsan Dereli, Marcello Stanzione, Daniel Tränkner, and Attila Tóth. 2016. "Alignment of Homologous Chromosomes and Effective Repair of Programmed DNA Double-Strand Breaks during Mouse Meiosis Require the Minichromosome Maintenance Domain Containing 2 (MCMDC2) Protein." *PLoS Genetics* 12 (10): e1006393. <https://doi.org/10.1371/journal.pgen.1006393>.
- Fowler, Kyle R., Randy W. Hyppa, Gareth A. Cromie, and Gerald R. Smith. 2018. "Physical Basis for Long-Distance Communication along Meiotic Chromosomes." *Proceedings of the National*

- Academy of Sciences of the United States of America* 115 (40): E9333–42.
<https://doi.org/10.1073/pnas.1801920115>.
- Fraune, Johanna, Céline Brochier-Armanet, Manfred Alsheimer, Jean Nicolas Volff, Katharina Schücker, and Ricardo Benavente. 2016. “Evolutionary History of the Mammalian Synaptonemal Complex.” *Chromosoma*. Springer Science and Business Media Deutschland GmbH. <https://doi.org/10.1007/s00412-016-0583-8>.
- Fraune, Johanna, Sabine Schramm, Manfred Alsheimer, and Ricardo Benavente. 2012. “The Mammalian Synaptonemal Complex: Protein Components, Assembly and Role in Meiotic Recombination.” *Experimental Cell Research* 318 (12): 1340–46.
<https://doi.org/10.1016/j.yexcr.2012.02.018>.
- Fuchs, Gilad, Efrat Shema, Rita Vesterman, Eran Kotler, Zohar Wolchinsky, Lior Golomb, Ariel Pribluda, et al. 2013. “RNF20 and USP44 Regulate Stem Cell Differentiation by Modulating H2B Monoubiquitylation” 46 (5): 662–73. <https://doi.org/10.1016/j.molcel.2012.05.023>.RNF20.
- Fukuda, Tomoyuki, Katrin Daniel, Lukasz Wojtasz, Attila Toth, and Christer Höög. 2010. “A Novel Mammalian HORMA Domain-Containing Protein, HORMAD1, Preferentially Associates with Unsynapsed Meiotic Chromosomes.” *Experimental Cell Research* 316 (2): 158–71.
<https://doi.org/10.1016/j.yexcr.2009.08.007>.
- Fukuda, Tomoyuki, Nanaho Fukuda, Ana Agostinho, Abrahan Hernández-Hernández, Anna Kouznetsova, and Christer Höög. 2014. “STAG3-Mediated Stabilization of REC8 Cohesin Complexes Promotes Chromosome Synapsis during Meiosis.” *EMBO Journal* 33 (11): 1243–55.
<https://doi.org/10.1002/emj.201387329>.
- Fukuda, Tomoyuki, Florencia Pratto, John C. Schimenti, James M.A. Turner, R. Daniel Camerini-Otero, and Christer Höög. 2012. “Phosphorylation of Chromosome Core Components May Serve as Axis Marks for the Status of Chromosomal Events during Mammalian Meiosis.” *PLoS Genetics* 8 (2). <https://doi.org/10.1371/journal.pgen.1002485>.
- Fung, Jennifer C., Beth Rockmill, Michael Odell, and G. Shirleen Roeder. 2004. “Imposition of Crossover Interference through the Nonrandom Distribution of Synapsis Initiation Complexes.” *Cell* 116 (6): 795–802. [https://doi.org/10.1016/S0092-8674\(04\)00249-1](https://doi.org/10.1016/S0092-8674(04)00249-1).
- Gandhi, Rita, Peter J. Gillespie, and Tatsuya Hirano. 2006. “Human Wapl Is a Cohesin-Binding Protein That Promotes Sister-Chromatid Resolution in Mitotic Prophase.” *Current Biology : CB* 16 (24): 2406–17. <https://doi.org/10.1016/J.CUB.2006.10.061>.
- Gao, Jinmin, and Monica P. Colaiácovo. 2018. “Zipping and Unzipping: Protein Modifications Regulating Synaptonemal Complex Dynamics.” *Trends in Genetics*. Elsevier Ltd.
<https://doi.org/10.1016/j.tig.2017.12.001>.
- Garcia, Valerie, Stephen Gray, Rachal M. Allison, Tim J. Cooper, and Matthew J. Neale. 2015. “Tel1ATM-Mediated Interference Suppresses Clustered Meiotic Double-Strand-Break Formation.” *Nature* 520 (7545): 114–18. <https://doi.org/10.1038/nature13993>.
- Garcia, Valerie, Sarah E.L. Phelps, Stephen Gray, and Matthew J. Neale. 2011. “Bidirectional Resection of DNA Double-Strand Breaks by Mre11 and Exo1.” *Nature* 479 (7372): 241–44.
<https://doi.org/10.1038/nature10515>.
- Geisinger, Adriana, and Ricardo Benavente. 2017. “Mutations in Genes Coding for Synaptonemal Complex Proteins and Their Impact on Human Fertility.” *Cytogenetic and Genome Research*. S. Karger AG. <https://doi.org/10.1159/000453344>.
- Gerasimova, Tatiana I., David A. Gdula, Denis V. Gerasimov, Olga Simonova, and Victor G. Corces.

1995. "A *Drosophila* Protein That Imparts Directionality on a Chromatin Insulator Is an Enhancer of Position-Effect Variegation." *Cell* 82 (4): 587–97. [https://doi.org/10.1016/0092-8674\(95\)90031-4](https://doi.org/10.1016/0092-8674(95)90031-4).
- Gerton, Jennifer L., and R. Scott Hawley. 2005. "Homologous Chromosome Interactions in Meiosis: Diversity amidst Conservation." *Nature Reviews Genetics* 6 (6): 477–87. <https://doi.org/10.1038/nrg1614>.
- Giacomo, Monica Di, Marco Barchi, Frédéric Baudat, Winfried Edelmann, Scott Keeney, and Maria Jasin. 2005. "Distinct DNA-Damage-Dependent and -Independent Responses Drive the Loss of Oocytes in Recombination-Defective Mouse Mutants." *Proceedings of the National Academy of Sciences of the United States of America* 102 (3): 737–42. <https://doi.org/10.1073/pnas.0406212102>.
- Ginsburg, M., M. H.L. Snow, and A. McLaren. 1990. "Primordial Germ Cells in the Mouse Embryo during Gastrulation." *Development* 110 (2): 521–28. <https://doi.org/10.1242/dev.110.2.521>.
- Goedecke, Wolfgang, Maureen Eijpe, Hildo H. Offenbergh, Mirjam Van Aalderen, and Christa Heyting. 1999. "Mre11 and Ku70 Interact in Somatic Cells, but Are Differentially Expressed in Early Meiosis." *Nature Genetics* 23 (2): 194–98. <https://doi.org/10.1038/13821>.
- Gómez-H, Laura, Natalia Felipe-Medina, Manuel Sánchez-Martín, Owen R. Davies, Isabel Ramos, Ignacio García-Tuñón, Dirk G. De Rooij, et al. 2016. "C14ORF39/SIX6OS1 Is a Constituent of the Synaptonemal Complex and Is Essential for Mouse Fertility." *Nature Communications* 7 (1): 1–16. <https://doi.org/10.1038/ncomms13298>.
- Gray, Stephen, and Paula E. Cohen. 2016. "Control of Meiotic Crossovers: From Double-Strand Break Formation to Designation." *Annual Review of Genetics* 50 (1): 175–210. <https://doi.org/10.1146/annurev-genet-120215-035111>.
- Grey, Corinne, Frédéric Baudat, and Bernard de Massy. 2018. "PRDM9, a Driver of the Genetic Map." *PLoS Genetics*. NLM (Medline). <https://doi.org/10.1371/journal.pgen.1007479>.
- Grishaeva, Tatiana M, and Yuri F Bogdanov. 2014. "Conservation and Variability of Synaptonemal Complex Proteins in Phylogenesis of Eukaryotes." <https://doi.org/10.1155/2014/856230>.
- Griswold, Michael D. 1998. "The Central Role of Sertoli Cells in Spermatogenesis." *Seminars in Cell and Developmental Biology* 9 (4): 411–16. <https://doi.org/10.1006/scdb.1998.0203>.
- . 2016. "Spermatogenesis: The Commitment to Meiosis." *Physiological Reviews* 96 (1): 1–17. <https://doi.org/10.1152/physrev.00013.2015>.
- Guiraldelli, Michel F., Craig Eyster, Joseph L. Wilkerson, Michael E. Dresser, and Roberto J. Pezza. 2013. "Mouse HFM1/Mer3 Is Required for Crossover Formation and Complete Synapsis of Homologous Chromosomes during Meiosis." *PLoS Genetics* 9 (3): e1003383. <https://doi.org/10.1371/journal.pgen.1003383>.
- Guiraldelli, Michel F., Anna Felberg, Luciana P. Almeida, Aniruddha Parikh, Rodrigo O. de Castro, and Roberto J. Pezza. 2018. "SHOC1 Is a ERCC4-(HhH)2-like Protein, Integral to the Formation of Crossover Recombination Intermediates during Mammalian Meiosis." *PLoS Genetics* 14 (5). <https://doi.org/10.1371/journal.pgen.1007381>.
- Günesdogan, Ufuk, and M Azim Surani. 2016. "Developmental Competence for Primordial Germ Cell Fate." *Current Topics in Developmental Biology* 117: 471–96. <https://doi.org/10.1016/bs.ctdb.2015.11.007>.
- Hamer, Geert, Katarina Gell, Anna Kouznetsova, Ivana Novak, Ricardo Benavente, and Christer Höög.

2006. "Characterization of a Novel Meiosis-Specific Protein within the Central Element of the Synaptonemal Complex." *Journal of Cell Science* 119 (19): 4025–32. <https://doi.org/10.1242/jcs.03182>.
- Hamer, Geert, Hong Wang, Ewelina Bolcun-Filas, Howard J. Cooke, Ricardo Benavente, and Christer Höög. 2008. "Progression of Meiotic Recombination Requires Structural Maturation of the Central Element of the Synaptonemal Complex." *Journal of Cell Science* 121 (15): 2445–51. <https://doi.org/10.1242/jcs.033233>.
- Handel, Mary Ann. 2004. "The XY Body: A Specialized Meiotic Chromatin Domain." *Experimental Cell Research*. Academic Press Inc. <https://doi.org/10.1016/j.yexcr.2004.03.008>.
- Handel, Mary Ann, and John J. Eppig. 1997. "10 Sexual Dimorphism in the Regulation of Mammalian Meiosis." *Current Topics in Developmental Biology* 37 (C): 333–58. [https://doi.org/10.1016/S0070-2153\(08\)60179-9](https://doi.org/10.1016/S0070-2153(08)60179-9).
- Handel, Mary Ann, and John C. Schimenti. 2010. "Genetics of Mammalian Meiosis: Regulation, Dynamics and Impact on Fertility." *Nature Reviews Genetics*. Nature Publishing Group. <https://doi.org/10.1038/nrg2723>.
- Hartmann, Michaelyn, James Umbanhowar, and Jeff Sekelsky. 2019. "Centromere-Proximal Meiotic Crossovers in *Drosophila Melanogaster* Are Suppressed by Both Highly-Repetitive Heterochromatin and Proximity to the Centromere." <https://doi.org/10.1534/genetics.119.302509>.
- Hasegawa, Kazuteru, and Yumiko Saga. 2012. "Retinoic Acid Signaling in Sertoli Cells Regulates Organization of the Blood-Testis Barrier through Cyclical Changes in Gene Expression." *Development (Cambridge, England)* 139 (23): 4347–55. <https://doi.org/10.1242/dev.080119>.
- Hasegawa, Kazuteru, Ho Su Sin, So Maezawa, Tyler J. Broering, Andrey V. Kartashov, Kris G. Alavattam, Yosuke Ichijima, et al. 2015. "SCML2 Establishes the Male Germline Epigenome through Regulation of Histone H2A Ubiquitination." *Developmental Cell* 32 (5): 574. <https://doi.org/10.1016/J.DEVCEL.2015.01.014>.
- Heemst, Diana Van, and Christa Heyting. 2000. "Sister Chromatid Cohesion and Recombination in Meiosis." *Chromosoma*. Chromosoma. <https://doi.org/10.1007/s004120050408>.
- Heijden, Godfried W Van Der, and Alex Bortvin. 2009. "Transient Relaxation of Transposon Silencing at the Onset of Mammalian Meiosis." <https://doi.org/10.4161/epi.4.2.7783>.
- Henderson, Kiersten A., and Scott Keeney. 2004. "Tying Synaptonemal Complex Initiation to the Formation and Programmed Repair of DNA Double-Strand Breaks." *Proceedings of the National Academy of Sciences of the United States of America* 101 (13): 4519–24. <https://doi.org/10.1073/PNAS.0400843101>.
- Hermo, Louis, R. Marc Pelletier, Daniel G. Cyr, and Charles E. Smith. 2010. "Surfing the Wave, Cycle, Life History, and Genes/Proteins Expressed by Testicular Germ Cells. Part 2: Changes in Spermatid Organelles Associated with Development of Spermatozoa." *Microscopy Research and Technique* 73 (4): 279–319. <https://doi.org/10.1002/jemt.20787>.
- Hernández-Hernández, Abrahan, Sergej Masich, Tomoyuki Fukuda, Anna Kouznetsova, Sara Sandin, Bertil Daneholt, and Christer Höög. 2016. "The Central Element of the Synaptonemal Complex in Mice Is Organized as a Bilayered Junction Structure." *Journal of Cell Science* 129 (11): 2239–49. <https://doi.org/10.1242/jcs.182477>.
- Herold, Julia, Stefan Kurtz, and Robert Giegerich. 2008. "Efficient Computation of Absent Words in Genomic Sequences." *BMC Bioinformatics* 9: 1–9. <https://doi.org/10.1186/1471-2105-9-167>.

- Higgins, James D., Julien Vignard, Raphael Mercier, Alice G. Pugh, F. Chris H. Franklin, and Gareth H. Jones. 2008. "AtMSH5 Partners AtMSH4 in the Class I Meiotic Crossover Pathway in Arabidopsis Thaliana, but Is Not Required for Synapsis." *Plant Journal* 55 (1): 28–39. <https://doi.org/10.1111/j.1365-313X.2008.03470.x>.
- Hillers, Kenneth J. 2004. "Crossover Interference." *Current Biology : CB*. Curr Biol. <https://doi.org/10.1016/j.cub.2004.11.038>.
- Hinch, Anjali Gupta, Philipp W. Becker, Tao Li, Daniela Moralli, Gang Zhang, Clare Bycroft, Catherine Green, et al. 2020. "The Configuration of RPA, RAD51, and DMC1 Binding in Meiosis Reveals the Nature of Critical Recombination Intermediates." *Molecular Cell* 79 (4): 689–701.e10. <https://doi.org/10.1016/J.MOLCEL.2020.06.015>.
- Hochwagen, Andreas, and Angelika Amon. 2006. "Checking Your Breaks: Surveillance Mechanisms of Meiotic Recombination." *Current Biology*. Elsevier. <https://doi.org/10.1016/j.cub.2006.03.009>.
- Holloway, J. Kim, James Booth, Winfried Edelmann, Clare H. McGowan, and Paula E. Cohen. 2008. "MUS81 Generates a Subset of MLH1-MLH3-Independent Crossovers in Mammalian Meiosis." *PLoS Genetics* 4 (9): e1000186. <https://doi.org/10.1371/journal.pgen.1000186>.
- Holloway, J. Kim, Meisha A. Morelli, Peter L. Borst, and Paula E. Cohen. 2010. "Mammalian BLM Helicase Is Critical for Integrating Multiple Pathways of Meiotic Recombination." *Journal of Cell Biology* 188 (6): 779–89. <https://doi.org/10.1083/jcb.200909048>.
- Holloway, J Kim, Xianfei Sun, Rayka Yokoo, Anne M Villeneuve, and Paula E Cohen. 2014. "Mammalian CNTD1 Is Critical for Meiotic Crossover Maturation and Deselection of Excess Precrossover Sites." *The Journal of Cell Biology* 205 (5): 633–41. <https://doi.org/10.1083/jcb.201401122>.
- Humphries, Neil, Wing-Kit Leung, Bilge Argunhan, Yaroslav Terentyev, Martina Dvorackova, and Hideo Tsubouchi. 2013. "The Ecm11-Gmc2 Complex Promotes Synaptonemal Complex Formation through Assembly of Transverse Filaments in Budding Yeast." *PLOS Genetics* 9 (1): e1003194. <https://doi.org/10.1371/JOURNAL.PGEN.1003194>.
- Hunter, Neil. 2015. "Meiotic Recombination: The Essence of Heredity." *Cold Spring Harbor Perspectives in Biology* 7 (12). <https://doi.org/10.1101/cshperspect.a016618>.
- . 2017. "Oocyte Quality Control: Causes, Mechanisms, and Consequences." *Cold Spring Harbor Symposia on Quantitative Biology* 82: 235–47. <https://doi.org/10.1101/sqb.2017.82.035394>.
- Ichijima, Yosuke, Misako Ichijima, Zhenkun Lou, André Nussenzweig, R. Daniel Camerini-Otero, Junjie Chen, Paul R. Andreassen, and Satoshi H. Namekawa. 2011. "MDC1 Directs Chromosome-Wide Silencing of the Sex Chromosomes in Male Germ Cells." *Genes and Development* 25 (9): 959–71. <https://doi.org/10.1101/gad.2030811>.
- Imai, Yukiko, Frédéric Baudat, Miguel Taillepierre, Marcello Stanzione, Attila Toth, and Bernard de Massy. 2017. "The PRDM9 KRAB Domain Is Required for Meiosis and Involved in Protein Interactions." *Chromosoma* 126 (6): 681–95. <https://doi.org/10.1007/s00412-017-0631-z>.
- Inano, Shojiro, Koichi Sato, Yoko Katsuki, Wataru Kobayashi, Hiroki Tanaka, Kazuhiro Nakajima, Shinichiro Nakada, et al. 2017. "RFWD3-Mediated Ubiquitination Promotes Timely Removal of Both RPA and RAD51 from DNA Damage Sites to Facilitate Homologous Recombination." *Molecular Cell* 66 (5): 622–634.e8. <https://doi.org/10.1016/J.MOLCEL.2017.04.022/ATTACHMENT/861664DA-3A09-4B93-99CC-4B95FE94DB5D/MMC1.PDF>.
- Ishiguro, Kei ichiro. 2019. "The Cohesin Complex in Mammalian Meiosis." *Genes to Cells*. Blackwell

- Publishing Ltd. <https://doi.org/10.1111/gtc.12652>.
- Ishiguro, Kei Ichiro, Jihye Kim, Sally Fujiyama-Nakamura, Shigeaki Kato, and Yoshinori Watanabe. 2011. "A New Meiosis-Specific Cohesin Complex Implicated in the Cohesin Code for Homologous Pairing." *EMBO Reports* 12 (3): 267–75. <https://doi.org/10.1038/embor.2011.2>.
- Ishiguro, Kei Ichiro, Jihye Kim, Hiroki Shibuya, Abraham Hernández-Hernández, Aussie Suzuki, Tatsuo Fukagawa, Go Shioi, et al. 2014. "Meiosis-Specific Cohesin Mediates Homolog Recognition in Mouse Spermatocytes." *Genes and Development* 28 (6): 594–607. <https://doi.org/10.1101/gad.237313.113>.
- Ishishita, Satoshi, Yoichi Matsuda, and Kazuhiro Kitada. 2014. "Genetic Evidence Suggests That Spata22 Is Required for the Maintenance of Rad51 Foci in Mammalian Meiosis." *Scientific Reports* 4 (August). <https://doi.org/10.1038/srep06148>.
- Jaffe, Laurinda A., and Jeremy R. Egbert. 2017. "Regulation of Mammalian Oocyte Meiosis by Intercellular Communication Within the Ovarian Follicle." *Annual Review of Physiology*. NIH Public Access. <https://doi.org/10.1146/annurev-physiol-022516-034102>.
- Jahns, Marina Tagliaro, Daniel Vezon, Aurélie Chambon, Lucie Pereira, Matthieu Falque, Olivier C. Martin, Liudmila Chelysheva, and Mathilde Grelon. 2014. "Crossover Localisation Is Regulated by the Neddylation Posttranslational Regulatory Pathway." *PLOS Biology* 12 (8): e1001930. <https://doi.org/10.1371/JOURNAL.PBIO.1001930>.
- Jensen, Ryan B., Aura Carreira, and Stephen C. Kowalczykowski. 2010. "Purified Human BRCA2 Stimulates RAD51-Mediated Recombination." *Nature* 467:7316 467 (7316): 678–83. <https://doi.org/10.1038/nature09399>.
- Jessop, Lea, Beth Rockmill, G. Shirleen Roeder, and Michael Lichten. 2006. "Meiotic Chromosome Synapsis-Promoting Proteins Antagonize the Anti-Crossover Activity of Sgs1." *PLoS Genetics* 2 (9): e155. <https://doi.org/10.1371/journal.pgen.0020155>.
- Jordan, Philip W., Jesse Karppinen, and Mary A. Handel. 2012. "Polo-like Kinase Is Required for Synaptonemal Complex Disassembly and Phosphorylation in Mouse Spermatocytes." *Journal of Cell Science* 125 (21): 5061–72. <https://doi.org/10.1242/jcs.105015>.
- Joshi, Neeraj, M. Scott Brown, Douglas K. Bishop, and G. Valentin Börner. 2015. "Gradual Implementation of the Meiotic Recombination Program via Checkpoint Pathways Controlled by Global DSB Levels." *Molecular Cell* 57 (5): 797–811. <https://doi.org/10.1016/j.molcel.2014.12.027>.
- Joyce, Eric F., Michael Pedersen, Stanley Tiong, Sanese K. White-Brown, Anshu Paul, Shelagh D. Campbell, and Kim S. McKim. 2011. "Drosophila ATM and ATR Have Distinct Activities in the Regulation of Meiotic DNA Damage and Repair." *Journal of Cell Biology* 195 (3): 359–67. <https://doi.org/10.1083/jcb.201104121>.
- Jue, K., T. H. Bestor, and J. M. Trasler. 1995. "Regulated Synthesis and Localization of DNA Methyltransferase during Spermatogenesis." *Biology of Reproduction* 53 (3): 561–69. <https://doi.org/10.1095/biolreprod53.3.561>.
- Kagey, Michael H., Jamie J. Newman, Steve Bilodeau, Ye Zhan, David A. Orlando, Nynke L. Van Berkum, Christopher C. Ebmeier, et al. 2010. "Mediator and Cohesin Connect Gene Expression and Chromatin Architecture." *Nature* 467 (7314): 430–35. <https://doi.org/10.1038/NATURE09380>.
- Kaul-Ghanekar, Ruchika, Archana Jalota, L. Pavithra, Philip Tucker, and Samit Chattopadhyay. 2004. "SMAR1 and Cux/CDP Modulate Chromatin and Act as Negative Regulators of the TCR β

- Enhancer (E β).” *Nucleic Acids Research* 32 (16): 4862–75. <https://doi.org/10.1093/nar/gkh807>.
- Kauppi, Liisa, Marco Barchi, Julian Lange, Frédéric Baudat, Maria Jasin, and Scott Keeney. 2013. “Numerical Constraints and Feedback Control of Double-Strand Breaks in Mouse Meiosis.” *Genes and Development* 27 (8): 873–86. <https://doi.org/10.1101/gad.213652.113>.
- Keeney, S., and M. J. Neale. 2006. “Initiation of Meiotic Recombination by Formation of DNA Double-Strand Breaks: Mechanism and Regulation.” *Biochemical Society Transactions*. Biochem Soc Trans. <https://doi.org/10.1042/BST0340523>.
- Keeney, Scott. 2001. “Mechanism and Control of Meiotic Recombination Initiation.” *Current Topics in Developmental Biology*. Academic Press Inc. [https://doi.org/10.1016/s0070-2153\(01\)52008-6](https://doi.org/10.1016/s0070-2153(01)52008-6).
- . 2008. “Spo11 and the Formation of DNA Double-Strand Breaks in Meiosis.” *Genome Dynamics and Stability*. Springer, Berlin, Heidelberg. https://doi.org/10.1007/7050_2007_026.
- Keeney, Scott, Craig N. Giroux, and Nancy Kleckner. 1997. “Meiosis-Specific DNA Double-Strand Breaks Are Catalyzed by Spo11, a Member of a Widely Conserved Protein Family.” *Cell* 88 (3): 375–84. [https://doi.org/10.1016/S0092-8674\(00\)81876-0](https://doi.org/10.1016/S0092-8674(00)81876-0).
- Kerr, Jeffrey B., Michelle Myers, and Richard A. Anderson. 2013. “The Dynamics of the Primordial Follicle Reserve.” *Reproduction*. BioScientifica. <https://doi.org/10.1530/REP-13-0181>.
- Kidane, Dawit, Alan S. Jonason, Timothy S. Gorton, Ivailo Mihaylov, Jing Pan, Scott Keeney, Dirk G. De Rooij, et al. 2010. “DNA Polymerase B Is Critical for Mouse Meiotic Synapsis.” *EMBO Journal* 29 (2): 410–23. <https://doi.org/10.1038/emboj.2009.357>.
- Kim, Yumi, Scott C. Rosenberg, Christine L. Kugel, Nora Kostow, Ofer Rog, Vitaliy Davydov, Tiffany Y. Su, Abby F. Dernburg, and Kevin D. Corbett. 2014. “The Chromosome Axis Controls Meiotic Events through a Hierarchical Assembly of HORMA Domain Proteins.” *Developmental Cell* 31 (4): 487–502. <https://doi.org/10.1016/j.devcel.2014.09.013>.
- Kleckner, Nancy. 1996. “Meiosis: How Could It Work?” *Proceedings of the National Academy of Sciences of the United States of America*. Proc Natl Acad Sci U S A. <https://doi.org/10.1073/pnas.93.16.8167>.
- Kneitz, Burkhard, Paula E. Cohen, Elena Avdievich, Liyin Zhu, Michael F. Kane, Harry Hou, Richard D. Kolodner, Raju Kucherlapati, Jeffrey W. Pollard, and Winfried Edelmann. 2000. “MutS Homolog 4 Localization to Meiotic Chromosomes Is Required for Chromosome Pairing during Meiosis in Male and Female Mice.” *Genes and Development* 14 (9): 1085–97. <https://doi.org/10.1101/gad.14.9.1085>.
- Kogo, Hiroshi, Makiko Tsutsumi, Hidehito Inagaki, Tamae Ohye, Hiroshi Kiyonari, and Hiroki Kurahashi. 2012. “HORMAD2 Is Essential for Synapsis Surveillance during Meiotic Prophase via the Recruitment of ATR Activity.” *Genes to Cells* 17 (11): 897–912. <https://doi.org/10.1111/gtc.12005>.
- Kogo, Hiroshi, Makiko Tsutsumi, Tamae Ohye, Hidehito Inagaki, Takaya Abe, and Hiroki Kurahashi. 2012. “HORMAD1-Dependent Checkpoint/Surveillance Mechanism Eliminates Asynaptic Oocytes.” *Genes to Cells* 17 (6): 439–54. <https://doi.org/10.1111/j.1365-2443.2012.01600.x>.
- Kojima, Mina L., Dirk G. De Rooij, and David C. Page. 2019. “Amplification of a Broad Transcriptional Program by a Common Factor Triggers the Meiotic Cell Cycle in Mice.” *ELife* 8 (February). <https://doi.org/10.7554/eLife.43738>.
- Kolas, N. K., and P. E. Cohen. 2004. “Novel and Diverse Functions of the DNA Mismatch Repair Family

- in Mammalian Meiosis and Recombination." *Cytogenetic and Genome Research*. Cytogenet Genome Res. <https://doi.org/10.1159/000080600>.
- Korutla, L., P. J. Wang, and S. A. Mackler. 2005. "The POZ/BTB Protein NAC1 Interacts with Two Different Histone Deacetylases in Neuronal-like Cultures." *Journal of Neurochemistry* 94 (3): 786–93. <https://doi.org/10.1111/j.1471-4159.2005.03206.x>.
- Korutla, Laxminarayana, Ryan Degnan, Peijie Wang, and Scott A. Mackler. 2007. "NAC1, a Cocaine-Regulated POZ/BTB Protein Interacts with CoREST." *Journal of Neurochemistry* 101 (3): 611–18. <https://doi.org/10.1111/J.1471-4159.2006.04387.X>.
- Koubova, Jana, Yueh-Chiang Hu, Tanmoy Bhattacharyya, Y. Q. Shirleen Soh, Mark E. Gill, Mary L. Goodheart, Cathryn A. Hogarth, Michael D. Griswold, and David C. Page. 2014a. "Retinoic Acid Activates Two Pathways Required for Meiosis in Mice." *PLoS Genetics* 10 (8): e1004541. <https://doi.org/10.1371/journal.pgen.1004541>.
- Koubova, Jana, Yueh Chiang Hu, Tanmoy Bhattacharyya, Y. Q. Shirleen Soh, Mark E. Gill, Mary L. Goodheart, Cathryn A. Hogarth, Michael D. Griswold, and David C. Page. 2014b. "Retinoic Acid Activates Two Pathways Required for Meiosis in Mice." *PLoS Genetics* 10 (8): e1001062. <https://doi.org/10.1371/journal.pgen.1004541>.
- Koubova, Jana, Douglas B. Menke, Qing Zhou, Blanche Cape, Michael D. Griswold, and David C. Page. 2006a. "Retinoic Acid Regulates Sex-Specific Timing of Meiotic Initiation in Mice." *Proceedings of the National Academy of Sciences of the United States of America* 103 (8): 2474–79. <https://doi.org/10.1073/pnas.0510813103>.
- . 2006b. "Retinoic Acid Regulates Sex-Specific Timing of Meiotic Initiation in Mice." *Proceedings of the National Academy of Sciences of the United States of America* 103 (8): 2474–79. <https://doi.org/10.1073/pnas.0510813103>.
- Kouznetsova, Anna, Hong Wang, Marina Bellani, R. Daniel Camerini-Otero, Rolf Jessberger, and Christer Höög. 2009. "BRCA1-Mediated Chromatin Silencing Is Limited to Oocytes with a Small Number of Asynapsed Chromosomes." *Journal of Cell Science* 122 (14): 2446–52. <https://doi.org/10.1242/jcs.049353>.
- Krausz, C., L. Hoefsloot, M. Simoni, and F. Tüttelmann. 2014. "EAA/EMQN Best Practice Guidelines for Molecular Diagnosis of Y-Chromosomal Microdeletions: State-of-the-Art 2013." *Andrology*. *Andrology*. <https://doi.org/10.1111/j.2047-2927.2013.00173.x>.
- Krausz, Csilla, and Antoni Riera-Escamilla. 2018. "Genetics of Male Infertility." *Nature Reviews Urology* 15 (6): 369–84. <https://doi.org/10.1038/s41585-018-0003-3>.
- Kretser, D M De, K L Loveland, A Meinhardt, D Simorangkir, and N Wreford. 1998. "Spermatogenesis." *Human Reproduction & Embryology* 13.
- Kudo, Nobuaki R., Martin Anger, Antoine H.F.M. Peters, Olaf Stemmann, Hans Christian Theussl, Wolfgang Helmhart, Hiromi Kudo, Christa Heyting, and Kim Nasmyth. 2009. "Role of Cleavage by Separase of the Rec8 Kleisin Subunit of Cohesin during Mammalian Meiosis I." *Journal of Cell Science* 122 (15): 2686–98. <https://doi.org/10.1242/jcs.035287>.
- Kueng, Stephanie, Björn Hegemann, Beate H. Peters, Jesse J. Lipp, Alexander Schleiffer, Karl Mechtler, and Jan Michael Peters. 2006. "Wapl Controls the Dynamic Association of Cohesin with Chromatin." *Cell* 127 (5): 955–67. <https://doi.org/10.1016/J.CELL.2006.09.040/ATTACHMENT/8DA5CD14-3CC1-4E70-A3D7-C9C3DDC10132/MMC1.PDF>.
- Kumar, Rajeev, Henri Marc Bourbon, and Bernard De Massy. 2010. "Functional Conservation of Mei4

- for Meiotic DNA Double-Strand Break Formation from Yeasts to Mice.” *Genes and Development* 24 (12): 1266–80. <https://doi.org/10.1101/gad.571710>.
- Kumar, Rajeev, Norbert Ghyselinck, Kei ichiro Ishiguro, Yoshinori Watanabe, Anna Kouznetsova, Christer Höög, Edward Strong, et al. 2015. “MEI4 - a Central Player in the Regulation of Meiotic DNA Double-Strand Break Formation in the Mouse.” *Journal of Cell Science* 128 (9): 1800–1811. <https://doi.org/10.1242/jcs.165464>.
- Kumar, Rajeev, Cecilia Oliver, Christine Brun, Ariadna B. Juarez-Martinez, Yara Tarabay, Jan Kadlec, and Bernard De Massy. 2018. “Mouse REC114 Is Essential for Meiotic DNA Double-Strand Break Formation and Forms a Complex with MEI4.” *Life Science Alliance* 1 (6). <https://doi.org/10.26508/lsa.201800259>.
- Kurzbauer, Marie Therese, Clemens Uanschou, Doris Chen, and Peter Schlögelhofer. 2012. “The Recombinases DMC1 and RAD51 Are Functionally and Spatially Separated during Meiosis in Arabidopsis.” *Plant Cell* 24 (5): 2058–70. <https://doi.org/10.1105/tpc.112.098459>.
- Lam, Isabel, and Scott Keeney. 2015. “Mechanism and Regulation of Meiotic Recombination Initiation.” *Cold Spring Harbor Perspectives in Biology* 7 (1): a016634. <https://doi.org/10.1101/cshperspect.a016634>.
- Lammers, J H, H H Offenberg, M van Aalderen, A C Vink, A J Dietrich, and C Heyting. 1994. “The Gene Encoding a Major Component of the Lateral Elements of Synaptonemal Complexes of the Rat Is Related to X-Linked Lymphocyte-Regulated Genes.” *Molecular and Cellular Biology* 14 (2): 1137–46. <https://doi.org/10.1128/mcb.14.2.1137>.
- Lan, Xianjiang, Boyko S. Atanassov, Wenqian Li, Ying Zhang, Laurence Florens, Ryan D. Mohan, Paul J. Galardy, Michael P. Washburn, Jerry L. Workman, and Sharon Y.R. Dent. 2016. “USP44 Is an Integral Component of N-CoR That Contributes to Gene Repression by Deubiquitinating Histone H2B.” *Cell Reports* 17 (9): 2382–93. <https://doi.org/10.1016/J.CELREP.2016.10.076>.
- Lange, Julian, Jing Pan, Francesca Cole, Michael P. Thelen, Maria Jasin, and Scott Keeney. 2011. “ATM Controls Meiotic Double-Strand-Break Formation.” *Nature* 479 (7372): 237–40. <https://doi.org/10.1038/nature10508>.
- Lao, Jessica P., Steve D. Oh, Miki Shinohara, Akira Shinohara, and Neil Hunter. 2008. “Rad52 Promotes Postinvasion Steps of Meiotic Double-Strand-Break Repair.” *Molecular Cell* 29 (4): 517–24. <https://doi.org/10.1016/j.molcel.2007.12.014>.
- Larose, Hailey, Adrienne Niederriter Shami, Haley Abbott, Gabriel Manske, Lei Lei, and Saher Sue Hammoud. 2019. “Gametogenesis: A Journey from Inception to Conception.” In *Current Topics in Developmental Biology*, 132:257–310. NIH Public Access. <https://doi.org/10.1016/bs.ctdb.2018.12.006>.
- Lee, Chih Ying, Henning F. Horn, Colin L. Stewart, Brian Burke, Ewelina Bolcun-Filas, John C. Schimenti, Michael E. Dresser, and Roberto J. Pezza. 2015. “Mechanism and Regulation of Rapid Telomere Prophase Movements in Mouse Meiotic Chromosomes.” *Cell Reports* 11 (4): 551. <https://doi.org/10.1016/J.CELREP.2015.03.045>.
- Lee, Jibak, and Tatsuya Hirano. 2011. “RAD21L, a Novel Cohesin Subunit Implicated in Linking Homologous Chromosomes in Mammalian Meiosis.” *Journal of Cell Biology* 192 (2): 263–76. <https://doi.org/10.1083/jcb.201008005>.
- Lee, Jibak, Toshiharu Iwai, Takehiro Yokota, and Masakane Yamashita. 2003. “Temporally and Spatially Selective Loss of Rec8 Protein from Meiotic Chromosomes during Mammalian Meiosis.” *Journal of Cell Science* 116 (13): 2781–90. <https://doi.org/10.1242/jcs.00495>.

- Lehti, M. S., and A. Sironen. 2016. "Formation and Function of the Manchette and Flagellum during Spermatogenesis." *Reproduction* 151 (4): R43–54. <https://doi.org/10.1530/REP-15-0310>.
- Lei, Lei, and Allan C. Spradling. 2016. "Mouse Oocytes Differentiate through Organelle Enrichment from Sister Cyst Germ Cells." *Science* 352 (6281): 95–99. <https://doi.org/10.1126/science.aad2156>.
- Lesch, Bluma J, and David C Page. 2012. "Genetics of Germ Cell Development." *Nature Reviews Genetics*. Nature Publishing Group. <https://doi.org/10.1038/nrg3294>.
- Leung, Wing-Kit, Neil Humphryes, Negar Afshar, Bilge Argunhan, Yaroslav Terentyev, Tomomi Tsubouchi, and Hideo Tsubouchi. 2015. "The Synaptonemal Complex Is Assembled by a PolySUMOylation-Driven Feedback Mechanism in Yeast." *Journal of Cell Biology* 211 (4): 785–93. <https://doi.org/10.1083/JCB.201506103>.
- Li, Rong, and David F. Albertini. 2013. "The Road to Maturation: Somatic Cell Interaction and Self-Organization of the Mammalian Oocyte." *Nature Reviews Molecular Cell Biology*. Nature Publishing Group. <https://doi.org/10.1038/nrm3531>.
- Li, Xin, and John C. Schimenti. 2007. "Mouse Pachytene Checkpoint 2 (Trip13) Is Required for Completing Meiotic Recombination but Not Synapsis." *PLoS Genetics* 3 (8): 1365–76. <https://doi.org/10.1371/journal.pgen.0030130>.
- Liebe, Bodo, Manfred Alsheimer, Christer Höög, Ricardo Benavente, and Harry Scherthan. 2004. "Telomere Attachment, Meiotic Chromosome Condensation, Pairing, and Bouquet Stage Duration Are Modified in Spermatocytes Lacking Axial Elements." *Molecular Biology of the Cell* 15 (2): 827–37. <https://doi.org/10.1091/mbc.E03-07-0524>.
- Lin, Yanfeng, Mark E. Gill, Jana Koubova, and David C. Page. 2008. "Germ Cell-Intrinsic and -Extrinsic Factors Govern Meiotic Initiation in Mouse Embryos." *Science* 322 (5908): 1685–87. <https://doi.org/10.1126/science.1166340>.
- Lin, Yi-Tzu, and Blanche Capel. 2015. "Cell Fate Commitment during Mammalian Sex Determination." *Current Opinion in Genetics & Development* 32 (June): 144–52. <https://doi.org/10.1016/j.gde.2015.03.003>.
- Lintern-Moore, S, and G P Moore. 1979. "The Initiation of Follicle and Oocyte Growth in the Mouse Ovary." *Biology of Reproduction* 20 (4): 773–78. <https://doi.org/10.1095/biolreprod20.4.773>.
- Lipkin, Steven M., Peter B. Moens, Victoria Wang, Michelle Lenzi, Dakshine Shanmugarajah, Abigail Gilgeous, James Thomas, et al. 2002. "Meiotic Arrest and Aneuploidy in MLH3-Deficient Mice." *Nature Genetics* 31 (4): 385–90. <https://doi.org/10.1038/ng931>.
- Liu, Jian Guo, Li Yuan, Eva Brundell, Birgitta Björkroth, Bertil Daneholt, and Christer Höög. 1996. "Localization of the N-Terminus of SCP1 to the Central Element of the Synaptonemal Complex and Evidence for Direct Interactions between the N-Termini of SCP1 Molecules Organized Head-to-Head." *Experimental Cell Research* 226 (1): 11–19. <https://doi.org/10.1006/excr.1996.0197>.
- Liu, Jianhua, Tzu Chen Wu, and Michael Lichten. 1995. "The Location and Structure of Double-Strand DNA Breaks Induced during Yeast Meiosis: Evidence for a Covalently Linked DNA-Protein Intermediate." *EMBO Journal* 14 (18): 4599–4608. <https://doi.org/10.1002/j.1460-2075.1995.tb00139.x>.
- Liu, Tiejun, Baocun Sun, Xiulan Zhao, Yanlei Li, Xueming Zhao, Ying Liu, Zhi Yao, et al. 2015. "USP44+ Cancer Stem Cell Subclones Contribute to Breast Cancer Aggressiveness by Promoting Vasculogenic Mimicry." *Molecular Cancer Therapeutics* 14 (9): 2121–31.

- <https://doi.org/10.1158/1535-7163.MCT-15-0114-T>.
- Liu, Xueqing, Veronica Castle, and Teruko Taketo. 2019. "Interplay between Caspase 9 and X-Linked Inhibitor of Apoptosis Protein (XIAP) in the Oocyte Elimination during Fetal Mouse Development." *Cell Death & Disease* 10 (11). <https://doi.org/10.1038/S41419-019-2019-X>.
- Lu, Jing, Yanling Gu, Jianrong Feng, Weihong Zhou, Xue Yang, and Yuequan Shen. 2014. "Structural Insight into the Central Element Assembly of the Synaptonemal Complex." *Scientific Reports* 4 (1): 1–6. <https://doi.org/10.1038/srep07059>.
- Lu, Wan Jin, Joseph Chapo, Ignasi Roig, and John M. Abrams. 2010. "Meiotic Recombination Provokes Functional Activation of the P53 Regulatory Network." *Science* 328 (5983): 1278–81. <https://doi.org/10.1126/science.1185640>.
- Luo, Mengcheng, Fang Yang, N. Adrian Leu, Jessica Landaiche, Mary Ann Handel, Ricardo Benavente, Sophie La Salle, and P. Jeremy Wang. 2013. "MEIOB Exhibits Single-Stranded DNA-Binding and Exonuclease Activities and Is Essential for Meiotic Recombination." *Nature Communications* 4 (1): 1–12. <https://doi.org/10.1038/ncomms3788>.
- Luo, Mengcheng, Jian Zhou, N. Adrian Leu, Carla M. Abreu, Jianle Wang, Montserrat C. Anguera, Dirk G. de Rooij, Maria Jasin, and P. Jeremy Wang. 2015. "Polycomb Protein SCML2 Associates with USP7 and Counteracts Histone H2A Ubiquitination in the XY Chromatin during Male Meiosis." *PLOS Genetics* 11 (1): e1004954. <https://doi.org/10.1371/JOURNAL.PGEN.1004954>.
- MacQueen, Amy J., and Andreas Hochwagen. 2011. "Checkpoint Mechanisms: The Puppet Masters of Meiotic Prophase." *Trends in Cell Biology* 21 (7): 393–400. <https://doi.org/10.1016/j.tcb.2011.03.004>.
- Mahadevaiah, Shantha K., Déborah Bourc'his, Dirk G. De Rooij, Timothy H. Bestor, James M.A. Turner, and Paul S. Burgoyne. 2008. "Extensive Meiotic Asynapsis in Mice Antagonises Meiotic Silencing of Unsynapsed Chromatin and Consequently Disrupts Meiotic Sex Chromosome Inactivation." *Journal of Cell Biology* 182 (2): 263–76. <https://doi.org/10.1083/jcb.200710195>.
- Malki, Safia, Godfried W. vanderHeijden, Kathryn A. O'Donnell, Sandra L. Martin, and Alex Bortvin. 2014. "A Role for Retrotransposon LINE-1 in Fetal Oocyte Attrition in Mice." *Developmental Cell* 29 (5): 521–33. <https://doi.org/10.1016/j.devcel.2014.04.027>.
- Mallepaly, Rathika, Peter R. Butler, Amin S. Herati, and Dolores J. Lamb. 2017. "Genetic Basis of Male and Female Infertility." *Monographs in Human Genetics* 21: 1–16. <https://doi.org/10.1159/000477275>.
- Manfrini, Nicola, Ilaria Guerini, Andrea Citterio, Giovanna Lucchini, and Maria Pia Longhese. 2010. "Processing of Meiotic DNA Double Strand Breaks Requires Cyclin-Dependent Kinase and Multiple Nucleases." *The Journal of Biological Chemistry* 285 (15): 11628. <https://doi.org/10.1074/JBC.M110.104083>.
- Manheim, Elizabeth A., and Kim S. McKim. 2003. "The Synaptonemal Complex Component C(2)M Regulates Meiotic Crossing over in *Drosophila*." *Current Biology* 13 (4): 276–85. [https://doi.org/10.1016/S0960-9822\(03\)00050-2](https://doi.org/10.1016/S0960-9822(03)00050-2).
- Marcet-Ortega, Marina, Sarai Pacheco, Ana Martínez-Marchal, Helena Castillo, Elsa Flores, Maria Jasin, Scott Keeney, and Ignasi Roig. 2017. "P53 and TAp63 Participate in the Recombination-Dependent Pachytene Arrest in Mouse Spermatocytes." *PLoS Genetics* 13 (6): 1–24. <https://doi.org/10.1371/journal.pgen.1006845>.
- Mark, Manuel, Hugues Jacobs, Mustapha Oulad-Abdelghani, Christine Dennefeld, Betty Féret, Nadège Vernet, Carmen Alina Codreanu, Pierre Chambon, and Norbert B. Ghyselinck. 2008.

- “STRA8-Deficient Spermatocytes Initiate, but Fail to Complete, Meiosis and Undergo Premature Chromosome Condensation.” *Journal of Cell Science* 121 (19): 3233–42.
<https://doi.org/10.1242/jcs.035071>.
- Marsolier-Kergoat, Marie Claude, Md Muntaz Khan, Jonathan Schott, Xuan Zhu, and Bertrand Llorente. 2018. “Mechanistic View and Genetic Control of DNA Recombination during Meiosis.” *Molecular Cell* 70 (1): 9–20.e6. <https://doi.org/10.1016/j.molcel.2018.02.032>.
- Martínez-Marchal, Ana, Yan Huang, Maria Teresa Guillot-Ferriols, Mònica Ferrer-Roda, Anna Guixé, Montserrat Garcia-Caldés, and Ignasi Roig. 2020. “The DNA Damage Response Is Required for Oocyte Cyst Breakdown and Follicle Formation in Mice.” *PLOS Genetics* 16 (11): e1009067.
<https://doi.org/10.1371/journal.pgen.1009067>.
- Martini, Emmanuelle, Robert L. Diaz, Neil Hunter, and Scott Keeney. 2006. “Crossover Homeostasis in Yeast Meiosis.” *Cell* 126 (2): 285–95. <https://doi.org/10.1016/j.cell.2006.05.044>.
- Mascarenhas, Maya N, Seth R Flaxman, Ties Boerma, Sheryl Vanderpoel, and Gretchen A Stevens. 2012. “National, Regional, and Global Trends in Infertility Prevalence since 1990: A Systematic Analysis of 277 Health Surveys.” *PLoS Medicine* 9 (12): e1001356.
<https://doi.org/10.1371/journal.pmed.1001356>.
- Matson, Clinton K., Mark W. Murphy, Michael D. Griswold, Shosei Yoshida, Vivian J. Bardwell, and David Zarkower. 2010. “The Mammalian Doublesex Homolog DMRT1 Is a Transcriptional Gatekeeper That Controls the Mitosis versus Meiosis Decision in Male Germ Cells.” *Developmental Cell* 19 (4): 612–24. <https://doi.org/10.1016/j.devcel.2010.09.010>.
- Matsuoka, Shuhei, Mingxia Huang, and Stephen J. Elledge. 1998. “Linkage of ATM to Cell Cycle Regulation by the Chk2 Protein Kinase.” *Science* 282 (5395): 1893–97.
<https://doi.org/10.1126/science.282.5395.1893>.
- Mazina, Olga M., Alexander V. Mazin, Takuro Nakagawa, Richard D. Kolodner, and Stephen C. Kowalczykowski. 2004. “Saccharomyces Cerevisiae Mer3 Helicase Stimulates 3’-5’ Heteroduplex Extension by Rad51: Implications for Crossover Control in Meiotic Recombination.” *Cell* 117 (1): 47–56. [https://doi.org/10.1016/S0092-8674\(04\)00294-6](https://doi.org/10.1016/S0092-8674(04)00294-6).
- McLaren, A., and M. Monk. 1981. “X-Chromosome Activity in the Germ Cells of Sex-Reversed Mouse Embryos.” *Journal of Reproduction and Fertility* 63 (2): 533–37.
<https://doi.org/10.1530/jrf.0.0630533>.
- McLaren, A. 1984. “Meiosis and Differentiation of Mouse Germ Cells.” *Symposia of the Society for Experimental Biology* 38: 7–23.
- McLean, Derek J, Patrick J Friel, Daniel S Johnston, and Michael D Griswold. 2003. “Characterization of Spermatogonial Stem Cell Maturation and Differentiation in Neonatal Mice.” *Biology of Reproduction* 69 (6): 2085–91. <https://doi.org/10.1095/biolreprod.103.017020>.
- Menke, Douglas B., Jana Koubova, and David C. Page. 2003. “Sexual Differentiation of Germ Cells in XX Mouse Gonads Occurs in an Anterior-to-Posterior Wave.” *Developmental Biology* 262 (2): 303–12. [https://doi.org/10.1016/S0012-1606\(03\)00391-9](https://doi.org/10.1016/S0012-1606(03)00391-9).
- Meuwissen, R. L.J., H. H. Offenbergh, A. J.J. Dietrich, A. Riesewijk, M. Van Iersel, and C. Heyting. 1992. “A Coiled-Coil Related Protein Specific for Synapsed Regions of Meiotic Prophase Chromosomes.” *EMBO Journal* 11 (13): 5091–5100. <https://doi.org/10.1002/j.1460-2075.1992.tb05616.x>.
- Mimitou, Eleni P., Shintaro Yamada, and Scott Keeney. 2017. “A Global View of Meiotic Double-Strand Break End Resection.” *Science* 355 (6320): 40–45.

- <https://doi.org/10.1126/science.aak9704>.
- Mitchell, Pamela J., and Robert Tjian. 1989. "Transcriptional Regulation in Mammalian Cells by Sequence-Specific DNA Binding Proteins." *Science* 245 (4916): 371–78. <https://doi.org/10.1126/science.2667136>.
- Miyamoto, Toshinobu, Shiga Hasuike, Leah Yogev, Maria R Maduro, Mutsuo Ishikawa, Heiner Westphal, and Dolores J Lamb. 2003. "Azoospermia in Patients Heterozygous for a Mutation in SYCP3." *Lancet (London, England)* 362 (9397): 1714–19. [https://doi.org/10.1016/S0140-6736\(03\)14845-3](https://doi.org/10.1016/S0140-6736(03)14845-3).
- Miyauchi, Hidetaka, Hiroshi Ohta, So Nagaoka, Fumio Nakaki, Kotaro Sasaki, Katsuhiko Hayashi, Yukihiro Yabuta, Tomonori Nakamura, Takuya Yamamoto, and Mitinori Saitou. 2017. "Bone Morphogenetic Protein and Retinoic Acid Synergistically Specify Female Germ-cell Fate in Mice." *The EMBO Journal* 36 (21): 3100–3119. <https://doi.org/10.15252/embj.201796875>.
- Moens, Peter B., Nadine K. Kolas, Madalena Tarsounas, Edyta Marcon, Paula E. Cohen, and Barbara Spyropoulos. 2002. "The Time Course and Chromosomal Localization of Recombination-Related Proteins at Meiosis in the Mouse Are Compatible with Models That Can Resolve the Early DNA-DNA Interactions without Reciprocal Recombination." *Journal of Cell Science* 115 (8): 1611–22. <https://doi.org/10.1242/JCS.115.8.1611>.
- Molyneaux, K A, J Stallock, K Schaible, and C Wylie. 2001. "Time-Lapse Analysis of Living Mouse Germ Cell Migration." *Developmental Biology* 240 (2): 488–98. <https://doi.org/10.1006/dbio.2001.0436>.
- Morelli, Meisha A., and Paula E. Cohen. 2005. "Not All Germ Cells Are Created Equal: Aspects of Sexual Dimorphism in Mammalian Meiosis." *Reproduction*. *Reproduction*. <https://doi.org/10.1530/rep.1.00865>.
- Morimoto, Akihiro, Hiroki Shibuya, Xiaoqiang Zhu, Jihye Kim, Kei Ichiro Ishiguro, Min Han, and Yoshinori Watanabe. 2012. "A Conserved KASH Domain Protein Associates with Telomeres, SUN1, and Dynactin during Mammalian Meiosis." *Journal of Cell Biology* 198 (2): 165–72. <https://doi.org/10.1083/jcb.201204085>.
- Mosbech, Anna, Claudia Lukas, Simon Bekker-Jensen, and Niels Mailand. 2013. "The Deubiquitylating Enzyme USP44 Counteracts the DNA Double-Strand Break Response Mediated by the RNF8 and RNF168 Ubiquitin Ligases." *Journal of Biological Chemistry* 288 (23): 16579–87. <https://doi.org/10.1074/jbc.M113.459917>.
- Moses, M J. 1969. "Structure and Function of the Synaptonemal Complex." *Genetics* 61 (1): Suppl:41-51.
- Mou, Lisha, Yadong Wang, Honggang Li, Yi Huang, Tao Jiang, Weiren Huang, Zesong Li, et al. 2013. "A Dominant-Negative Mutation of HSF2 Associated with Idiopathic Azoospermia." *Human Genetics* 132 (2): 159–65. <https://doi.org/10.1007/s00439-012-1234-7>.
- Muyt, Arnaud De, Lea Jessop, Elizabeth Kolar, Anuradha Sourirajan, Jianhong Chen, Yaron Dayani, and Michael Lichten. 2012. "BLM Helicase Ortholog Sgs1 Is a Central Regulator of Meiotic Recombination Intermediate Metabolism." *Molecular Cell* 46 (1): 43–53. <https://doi.org/10.1016/j.molcel.2012.02.020>.
- Muyt, Arnaud De, Alexandra Pyatnitskaya, Jessica Andréani, Lepakshi Ranjha, Claire Ramus, Raphaëlle Laureau, Ambra Fernandez-Vega, et al. 2018. "A Meiotic XPF–ERCC1-like Complex Recognizes Joint Molecule Recombination Intermediates to Promote Crossover Formation." *Genes and Development* 32 (3–4): 283–96. <https://doi.org/10.1101/gad.308510.117>.

- Muyt, Arnaud De, Liangran Zhang, Tristan Piolot, Nancy Kleckner, Eric Espagne, and Denise Zickler. 2014. "E3 Ligase Hei10: A Multifaceted Structure-Based Signaling Molecule with Roles within and beyond Meiosis." *Genes and Development* 28 (10): 1111–23. <https://doi.org/10.1101/gad.240408.114>.
- Nagaoka, So I., Yukihiko Yabuta, Fumio Nakaki, Hidetaka Miyauchi, Yoshiaki Nosaka, Hiroshi Ohta, Takuya Yamamoto, Kazuki Kurimoto, Katsuhiko Hayashi, Tomonori Nakamura, and Mitinori Saitou. 2020. "ZGLP1 Is a Determinant for the Oogenic Fate in Mice." *Science* 4115 (February): 1–15. <https://doi.org/10.1126/science.aaw4115.1>.
- Nakada, Shinichiro. 2016. "Opposing Roles of RNF8/RNF168 and Deubiquitinating Enzymes in Ubiquitination-Dependent DNA Double-Strand Break Response Signaling and DNA-Repair Pathway Choice." *Journal of Radiation Research* 57 (S1): i33–40. <https://doi.org/10.1093/JRR/RRW027>.
- Nakagawa, Takuro, and Richard D. Kolodner. 2002. "The MER3 DNA Helicase Catalyzes the Unwinding of Holliday Junctions." *Journal of Biological Chemistry* 277 (31): 28019–24. <https://doi.org/10.1074/jbc.M204165200>.
- Nambiar, Mridula, and Gerald R. Smith. 2018. "Pericentromere-Specific Cohesin Complex Prevents Meiotic Pericentric DNA Double-Strand Breaks and Lethal Crossovers." *Molecular Cell* 71 (4): 540–553.e4. <https://doi.org/10.1016/j.molcel.2018.06.035>.
- Namwanje, Maria, and Chester W Brown. 2016. "Activins and Inhibins: Roles in Development, Physiology, and Disease." *Cold Spring Harbor Perspectives in Biology* 8 (7). <https://doi.org/10.1101/cshperspect.a021881>.
- Nasmyth, Kim, and Christian H. Haering. 2009. "Cohesin: Its Roles and Mechanisms." *Annual Review of Genetics* 43 (1): 525–58. <https://doi.org/10.1146/annurev-genet-102108-134233>.
- National Institute for Health and Care Excellence [NICE]. 2013. "National Institute for Health and Care Excellence." *Fertility: Assessment and Treatment for People with Fertility Problems*, [NICE Guideline CG156]. <https://www.nice.org.uk/guidance/cg156>.
- Neale, Matthew J., Jing Pan, and Scott Keeney. 2005. "Endonucleolytic Processing of Covalent Protein-Linked DNA Double-Strand Breaks." *Nature* 436 (7053): 1053–57. <https://doi.org/10.1038/nature03872>.
- Nègre, Nicolas, Christopher D. Brown, Parantu K. Shah, Pouya Kheradpour, Carolyn A. Morrison, Jorja G. Henikoff, Xin Feng, et al. 2010. "A Comprehensive Map of Insulator Elements for the *Drosophila* Genome." *PLOS Genetics* 6 (1): e1000814. <https://doi.org/10.1371/JOURNAL.PGEN.1000814>.
- Newman, John R.S., Ethan Wolf, and Peter S. Kim. 2000. "A Computationally Directed Screen Identifying Interacting Coiled Coils from *Saccharomyces Cerevisiae*." *Proceedings of the National Academy of Sciences of the United States of America* 97 (24): 13203–8. <https://doi.org/10.1073/pnas.97.24.13203>.
- Nilsson, E, J A Parrott, and M K Skinner. 2001. "Basic Fibroblast Growth Factor Induces Primordial Follicle Development and Initiates Folliculogenesis." *Molecular and Cellular Endocrinology* 175 (1–2): 123–30. [https://doi.org/10.1016/s0303-7207\(01\)00391-4](https://doi.org/10.1016/s0303-7207(01)00391-4).
- Niu, Hengyao, Xue Li, Emily Job, Caroline Park, Danesh Moazed, Steven P. Gygi, and Nancy M. Hollingsworth. 2007. "Mek1 Kinase Is Regulated To Suppress Double-Strand Break Repair between Sister Chromatids during Budding Yeast Meiosis." *Molecular and Cellular Biology* 27 (15): 5456–67. <https://doi.org/10.1128/mcb.00416-07>.

- Niu, Hengyao, Lihong Wan, Bridget Baumgartner, Dana Schaefer, Josef Loidl, and Nancy M. Hollingsworth. 2005. "Partner Choice during Meiosis Is Regulated by Hop1-Promoted Dimerization of Mek1." *Molecular Biology of the Cell* 16 (12): 5804–18. <https://doi.org/10.1091/mbc.E05-05-0465>.
- Niu, Hengyao, Lihong Wan, Valeria Busygina, Young Ho Kwon, Jasmina A. Allen, Xue Li, Ryan C. Kunz, et al. 2009. "Regulation of Meiotic Recombination via Mek1-Mediated Rad54 Phosphorylation." *Molecular Cell* 36 (3): 393–404. <https://doi.org/10.1016/j.molcel.2009.09.029>.
- Novak, Ivana, Hong Wang, Ekaterina Revenkova, Rolf Jessberger, Harry Scherthan, and Christer Höög. 2008. "Cohesin Smc1 β Determines Meiotic Chromatin Axis Loop Organization." *Journal of Cell Biology* 180 (1): 83–90. <https://doi.org/10.1083/jcb.200706136>.
- O'Donnell, Liza, Peter Stanton, and David M de Kretser. 2000. *Endocrinology of the Male Reproductive System and Spermatogenesis. Endotext*. <http://www.ncbi.nlm.nih.gov/pubmed/25905260>.
- O'Flynn O'Brien, Katherine L., Alex C. Varghese, and Ashok Agarwal. 2010. "The Genetic Causes of Male Factor Infertility: A Review." *Fertility and Sterility* 93 (1): 1–12. <https://doi.org/10.1016/j.fertnstert.2009.10.045>.
- Oatley, Jon M., and Michael D. Griswold. 2020. "MEIOSIN: A New Watchman of Meiotic Initiation in Mammalian Germ Cells." *Developmental Cell* 52 (4): 397–98. <https://doi.org/10.1016/j.devcel.2020.02.002>.
- Oatley, Jon M, and Ralph L Brinster. 2008. "Regulation of Spermatogonial Stem Cell Self-Renewal in Mammals." *Annual Review of Cell and Developmental Biology* 24: 263–86. <https://doi.org/10.1146/annurev.cellbio.24.110707.175355>.
- . 2012. "The Germline Stem Cell Niche Unit in Mammalian Testes." *Physiological Reviews*. <https://doi.org/10.1152/physrev.00025.2011>.
- Obeso, David, Roberto J. Pezza, and Dean Dawson. 2014. "Couples, Pairs, and Clusters: Mechanisms and Implications of Centromere Associations in Meiosis." *Chromosoma*. Chromosoma. <https://doi.org/10.1007/s00412-013-0439-4>.
- Offenberg, Hildo H, Johanna A C Schalk, Ralph L J Meuwissen, Mirjam Van Aalderen, Henri A Kester, Axel J J Dietrich, and Christa Heyting. 1998. "SCP2: A Major Protein Component of the Axial Elements of Synaptonemal Complexes of the Rat." *Nucleic Acids Research*. Vol. 26.
- Oh, Steve D., Jessica P. Lao, Patty Yi Hwa Hwang, Andrew F. Taylor, Gerald R. Smith, and Neil Hunter. 2007. "BLM Ortholog, Sgs1, Prevents Aberrant Crossing-over by Suppressing Formation of Multichromatid Joint Molecules." *Cell* 130 (2): 259–72. <https://doi.org/10.1016/j.cell.2007.05.035>.
- Öllinger, Rupert, Manfred Alsheimer, and Ricardo Benavente. 2005. "Mammalian Protein SCP1 Forms Synaptonemal Complex-like Structures in the Absence of Meiotic Chromosomes." *Molecular Biology of the Cell* 16 (1): 212–17. <https://doi.org/10.1091/mbc.E04-09-0771>.
- Oulad-Abdelghani, Mustapha, Philippe Bouillet, Didier Décimo, Anne Gansmuller, Sophie Heyberger, Pascal Dollé, Sylviane Bronner, Yves Lutz, and Pierre Chambon. 1996. "Characterization of a Premeiotic Germ Cell-Specific Cytoplasmic Protein Encoded by Stra8, a Novel Retinoic Acid-Responsive Gene." *Journal of Cell Biology* 135 (2): 469–77. <https://doi.org/10.1083/jcb.135.2.469>.
- Pacheco, Sarai, Andros Maldonado-Linares, Montserrat Garcia-Caldés, and Ignasi Roig. 2019. "ATR Function Is Indispensable to Allow Proper Mammalian Follicle Development." *Chromosoma* 128

- (3): 489–500. <https://doi.org/10.1007/s00412-019-00723-7>.
- Pacheco, Sarai, Andros Maldonado-Linares, Marina Marcet-Ortega, Cristina Rojas, Ana Martínez-Marchal, Judit Fuentes-Lazaro, Julian Lange, et al. 2018. “ATR Is Required to Complete Meiotic Recombination in Mice.” *Nature Communications* 9 (1). <https://doi.org/10.1038/s41467-018-04851-z>.
- Pacheco, Sarai, Marina Marcet-Ortega, Julian Lange, Maria Jasin, Scott Keeney, and Ignasi Roig. 2015. “The ATM Signaling Cascade Promotes Recombination-Dependent Pachytene Arrest in Mouse Spermatocytes.” *PLoS Genetics* 11 (3): 1–27. <https://doi.org/10.1371/journal.pgen.1005017>.
- Page, Jesus, José A. Suja, Juan L. Santos, and Julio S. Rufas. 1998. “Squash Procedure for Protein Immunolocalization in Meiotic Cells.” *Chromosome Research* 6 (8): 639–42. <https://doi.org/10.1023/A:1009209628300>.
- Paigen, Kenneth, and Petko M. Petkov. 2018a. “PRDM9 and Its Role in Genetic Recombination.” *Trends in Genetics*. Nature Publishing Group. <https://doi.org/10.1016/j.tig.2017.12.017>.
- . 2018b. “PRDM9 and Its Role in Genetic Recombination.” *Trends in Genetics*. Elsevier Ltd. <https://doi.org/10.1016/j.tig.2017.12.017>.
- Pangas, Stephanie A, Youngsok Choi, Daniel J Ballow, Yangu Zhao, Heiner Westphal, Martin M Matzuk, and Aleksandar Rajkovic. 2006. “Oogenesis Requires Germ Cell-Specific Transcriptional Regulators *Sohlh1* and *Lhx8*.” *Proceedings of the National Academy of Sciences of the United States of America* 103 (21): 8090–95. <https://doi.org/10.1073/pnas.0601083103>.
- Papanikos, Frantzeskos, Julie A.J. Clément, Erika Testa, Ramya Ravindranathan, Corinne Grey, Ihsan Dereli, Anastasiia Bondarieva, et al. 2019. “Mouse ANKRD31 Regulates Spatiotemporal Patterning of Meiotic Recombination Initiation and Ensures Recombination between X and Y Sex Chromosomes.” *Molecular Cell* 74 (5): 1069–1085.e11. <https://doi.org/10.1016/j.molcel.2019.03.022>.
- Park, Jae Min, Jae Eun Lee, Chan Mi Park, and Jung Hwa Kim. 2019. “USP44 Promotes the Tumorigenesis of Prostate Cancer Cells through EZH2 Protein Stabilization” 41 (September 2018): 1–11.
- Parra, María Teresa, Alberto Viera, Rocío Gómez, Jesús Page, Ricardo Benavente, Juan Luis Santos, Julio S. Rufas, and José A. Suja. 2004. “Involvement of the Cohesin Rad21 and SCP3 in Monopolar Attachment of Sister Kinetochores during Mouse Meiosis I.” *Journal of Cell Science* 117 (7): 1221–34. <https://doi.org/10.1242/JCS.00947>.
- Parra, María Teresa, Alberto Viera, Rocío Gómez, Jesús Page, Mar Carmena, William C. Earnshaw, Julio S. Rufas, and José A. Suja. 2003. “Dynamic Relocalization of the Chromosomal Passenger Complex Proteins Inner Centromere Protein (INCENP) and Aurora-B Kinase during Male Mouse Meiosis.” *Journal of Cell Science*. *J Cell Sci*. <https://doi.org/10.1242/jcs.00330>.
- Parvanov, Emil D., Hui Tian, Timothy Billings, Ruth L. Saxl, Catrina Spruce, Rakesh Aithal, Lumir Krejci, Kenneth Paigen, Petko M. Petkov, and Yukiko Yamashita. 2017. “PRDM9 Interactions with Other Proteins Provide a Link between Recombination Hotspots and the Chromosomal Axis in Meiosis.” *Molecular Biology of the Cell* 28 (3): 488–99. <https://doi.org/10.1091/mbc.E16-09-0686>.
- Pattabiraman, Divya, Baptiste Roelens, Alexander Woglar, and Anne M. Villeneuve. 2017. “Meiotic Recombination Modulates the Structure and Dynamics of the Synaptonemal Complex during *C. Elegans* Meiosis.” *PLoS Genetics* 13 (3): e1006670.

- <https://doi.org/10.1371/journal.pgen.1006670>.
- Pelttari, Jeanette, Mary-Rose Hoja, Li Yuan, Jian-Guo Liu, Eva Brundell, Peter Moens, Sabine Santucci-Darmanin, et al. 2001. "A Meiotic Chromosomal Core Consisting of Cohesin Complex Proteins Recruits DNA Recombination Proteins and Promotes Synapsis in the Absence of an Axial Element in Mammalian Meiotic Cells." *Molecular and Cellular Biology* 21 (16): 5667–77. <https://doi.org/10.1128/mcb.21.16.5667-5677.2001>.
- Pepling, M E, and A C Spradling. 1998. "Female Mouse Germ Cells Form Synchronously Dividing Cysts." *Development (Cambridge, England)* 125 (17): 3323–28.
- Pepling, Melissa E. 2012. "Follicular Assembly: Mechanisms of Action." *Reproduction*. BioScientifica. <https://doi.org/10.1530/REP-11-0299>.
- Pepling, Melissa E., and Allan C. Spradling. 2001. "Mouse Ovarian Germ Cell Cysts Undergo Programmed Breakdown to Form Primordial Follicles." *Developmental Biology* 234 (2): 339–51. <https://doi.org/10.1006/dbio.2001.0269>.
- Perera, David, Livia Perez-Hidalgo, Peter B. Moens, Kaarina Reini, Nicholas Lakin, Juhani E. Syväoja, Pedro A. San-Segundo, and Raimundo Freire. 2004. "TopBP1 and ATR Colocalization at Meiotic Chromosomes: Role of TopBP1/Cut5 in the Meiotic Recombination Checkpoint." *Molecular Biology of the Cell* 15 (4): 1568–79. <https://doi.org/10.1091/mbc.E03-06-0444>.
- Peternel, Špela, Simona Jevševar, Marjan Bele, Vladka Gaberc-Porekar, and Viktor Menart. 2008. "New Properties of Inclusion Bodies with Implications for Biotechnology." *Biotechnology and Applied Biochemistry* 49 (4): 239. <https://doi.org/10.1042/ba20070140>.
- Petukhova, Galina V., Roberto J. Pezza, Filip Vanevski, Mickael Ploquin, Jean Yves Masson, and R. Daniel Camerini-Otero. 2005. "The Hop2 and Mnd1 Proteins Act in Concert with Rad51 and Dmc1 in Meiotic Recombination." *Nature Structural and Molecular Biology* 12 (5): 449–53. <https://doi.org/10.1038/nsmb923>.
- Petukhova, Galina V., Peter J. Romanienko, and R. Daniel Camerini-Otero. 2003. "The Hop2 Protein Has a Direct Role in Promoting Interhomolog Interactions during Mouse Meiosis." *Developmental Cell* 5 (6): 927–36. [https://doi.org/10.1016/S1534-5807\(03\)00369-1](https://doi.org/10.1016/S1534-5807(03)00369-1).
- Pezza, Roberto J., Oleg N. Voloshin, Filip Vanevski, and R. Daniel Camerini-Otero. 2007. "Hop2/Mnd1 Acts on Two Critical Steps in Dmc1-Promoted Homologous Pairing." *Genes and Development* 21 (14): 1758–66. <https://doi.org/10.1101/gad.1562907>.
- Pezza, Roberto J., Oleg N. Voloshin, Alexander A. Volodin, Kingsley A. Boateng, Marina A. Bellani, Alexander V. Mazin, and R. Daniel Camerini-Otero. 2014. "The Dual Role of HOP2 in Mammalian Meiotic Homologous Recombination." *Nucleic Acids Research* 42 (4): 2346–57. <https://doi.org/10.1093/nar/gkt1234>.
- Pinto, Fernando Lopes, and Peter Lindblad. 2010. "A Guide for In-House Design of Template-Switch-Based 5' Rapid Amplification of cDNA Ends Systems." *Analytical Biochemistry* 397 (2): 227–32. <https://doi.org/10.1016/j.ab.2009.10.022>.
- Pittman, Douglas L., John Cobb, Kerry J. Schimenti, Lawriston A. Wilson, Deborah M. Cooper, Ember Brignull, Mary Ann Handel, and John C. Schimenti. 1998. "Meiotic Prophase Arrest with Failure of Chromosome Synapsis in Mice Deficient for Dmc1, a Germline-Specific RecA Homolog." *Molecular Cell* 1 (5): 697–705. [https://doi.org/10.1016/S1097-2765\(00\)80069-6](https://doi.org/10.1016/S1097-2765(00)80069-6).
- Pochart, Pascale, Dana Woltering, and Nancy M. Hollingsworth. 1997. "Conserved Properties between Functionally Distinct MutS Homologs in Yeast." *Journal of Biological Chemistry* 272 (48): 30345–49. <https://doi.org/10.1074/jbc.272.48.30345>.

- Prasada Rao, H. B.D., Huanyu Qiao, Shubhang K. Bhatt, Logan R.J. Bailey, Hung D. Tran, Sarah L. Bourne, Wendy Qiu, et al. 2017. "A SUMO-Ubiquitin Relay Recruits Proteasomes to Chromosome Axes to Regulate Meiotic Recombination." *Science* 355 (6323): 403–7. <https://doi.org/10.1126/science.aaf6407>.
- Prieto, Ignacio, José A. Suja, Nieves Pezzi, Leonor Kremer, Carlos Martínez-A., Julio S. Rufas, and José L. Barbero. 2001. "Mammalian STAG3 Is a Cohesin Specific to Sister Chromatid Arms in Meiosis I." *Nature Cell Biology* 3 (8): 761–66. <https://doi.org/10.1038/35087082>.
- Qiao, Huanyu, Jefferson K. Chen, April Reynolds, Christer Höög, Michael Paddy, and Neil Hunter. 2012. "Interplay between Synaptonemal Complex, Homologous Recombination, and Centromeres during Mammalian Meiosis." *PLoS Genetics* 8 (6): e1002790. <https://doi.org/10.1371/journal.pgen.1002790>.
- Qiao, Huanyu, H. B.D. Prasada Rao, Ye Yang, Jared H. Fong, Jeffrey M. Cloutier, Dekker C. Deacon, Kathryn E. Nagel, et al. 2014. "Antagonistic Roles of Ubiquitin Ligase HEI10 and SUMO Ligase RNF212 Regulate Meiotic Recombination." *Nature Genetics* 46 (2): 194–99. <https://doi.org/10.1038/ng.2858>.
- Rampalli, Shravanti, L. Pavithra, Altaf Bhatt, Tapas K. Kundu, and Samit Chattopadhyay. 2005. "Tumor Suppressor SMAR1 Mediates Cyclin D1 Repression by Recruitment of the SIN3/Histone Deacetylase 1 Complex." *Molecular and Cellular Biology* 25 (19): 8415–29. <https://doi.org/10.1128/mcb.25.19.8415-8429.2005>.
- Ranjha, Lepakshi, Sean M. Howard, and Petr Cejka. 2018. "Main Steps in DNA Double-Strand Break Repair: An Introduction to Homologous Recombination and Related Processes." *Chromosoma*. Springer Science and Business Media Deutschland GmbH. <https://doi.org/10.1007/s00412-017-0658-1>.
- Rato, Luis, Marco G Alves, Silvia Socorro, Ana I Duarte, Jose E Cavaco, and Pedro F Oliveira. 2012. "Metabolic Regulation Is Important for Spermatogenesis." *Nature Reviews. Urology* 9 (6): 330–38. <https://doi.org/10.1038/nrurol.2012.77>.
- Raverdeau, Mathilde, Aurore Gely-Pernot, Betty Féret, Christine Dennefeld, Gérard Benoit, Irwin Davidson, Pierre Chambon, Manuel Marka, and Norbert B. Ghyselinck. 2012. "Retinoic Acid Induces Sertoli Cell Paracrine Signals for Spermatogonia Differentiation but Cell Autonomously Drives Spermatocyte Meiosis." *Proceedings of the National Academy of Sciences of the United States of America* 109 (41): 16582–87. <https://doi.org/10.1073/pnas.1214936109>.
- Raynard, Steven, Weixing Zhao, Wendy Bussen, Lucy Lu, Yang Yang Ding, Valeria Busygina, Amom Ruhikanta Meetei, and Patrick Sung. 2008. "Functional Role of BLAP75 in BLM-Topoisomerase III α -Dependent Holliday Junction Processing." *Journal of Biological Chemistry* 283 (23): 15701–8. <https://doi.org/10.1074/jbc.M802127200>.
- Reddy, Pradeep, Lian Liu, Deepak Adhikari, Krishna Jagarlamudi, Singareddy Rajareddy, Yan Shen, Chun Du, et al. 2008. "Oocyte-Specific Deletion of Pten Causes Premature Activation of the Primordial Follicle Pool." *Science (New York, N.Y.)* 319 (5863): 611–13. <https://doi.org/10.1126/science.1152257>.
- Refolio, Esther, Santiago Cavero, Edyta Marcon, Raimundo Freire, and Pedro A. San-Segundo. 2011. "The Ddc2/ATRIP Checkpoint Protein Monitors Meiotic Recombination Intermediates." *Journal of Cell Science* 124 (14): 2488–2500. <https://doi.org/10.1242/jcs.081711>.
- Reinholdt, Laura G., and John C. Schimenti. 2005. "Mei1 Is Epistatic to Dmc1 during Mouse Meiosis." *Chromosoma* 114 (2): 127–34. <https://doi.org/10.1007/s00412-005-0346-4>.

- Revenkova, E., M. Eijpe, C. Heyting, B. Gross, and R. Jessberger. 2001. "Novel Meiosis-Specific Isoform of Mammalian SMC1." *Molecular and Cellular Biology* 21 (20): 6984–98. <https://doi.org/10.1128/MCB.21.20.6984-6998.2001>.
- Revenkova, Ekaterina, Maureen Eijpe, Christa Heyting, Craig A. Hodges, Patricia A. Hunt, Bodo Liebe, Harry Scherthan, and Rolf Jessberger. 2004. "Cohesin SMC1 β Is Required for Meiotic Chromosome Dynamics, Sister Chromatid Cohesion and DNA Recombination." *Nature Cell Biology* 6 (6): 555–62. <https://doi.org/10.1038/ncb1135>.
- Reyes-Turcu, Francisca E., Karen H. Ventii, and Keith D. Wilkinson. 2009. "Regulation and Cellular Roles of Ubiquitin-Specific Deubiquitinating Enzymes." *Annual Review of Biochemistry*. NIH Public Access. <https://doi.org/10.1146/annurev.biochem.78.082307.091526>.
- Reynolds, April, Huanyu Qiao, Ye Yang, Jefferson K. Chen, Neil Jackson, Kajal Biswas, J. Kim Holloway, et al. 2013. "RNF212 Is a Dosage-Sensitive Regulator of Crossing-over during Mammalian Meiosis." *Nature Genetics* 45 (3): 269–78. <https://doi.org/10.1038/ng.2541>.
- Rinaldi, Vera D., Jordana C. Bloom, and John C. Schimenti. 2020. "Oocyte Elimination through DNA Damage Signaling from CHK1/CHK2 to P53 and P63." *Genetics* 215 (2): 373–78. <https://doi.org/10.1534/genetics.120.303182>.
- Rinaldi, Vera D., Ewelina Bolcun-Filas, Hiroshi Kogo, Hiroki Kurahashi, and John C. Schimenti. 2017. "The DNA Damage Checkpoint Eliminates Mouse Oocytes with Chromosome Synapsis Failure." *Molecular Cell* 67 (6): 1026-1036.e2. <https://doi.org/10.1016/j.molcel.2017.07.027>.
- Robert, T., A. Nore, C. Brun, C. Maffre, B. Crimi, H. M. Bourbon, and B. De Massy. 2016. "The Topo VIB-Like Protein Family Is Required for Meiotic DNA Double-Strand Break Formation." *Science* 351 (6276): 943–49. <https://doi.org/10.1126/science.aad5309>.
- Robert, Thomas, Nathalie Vrielynck, Christine Mézard, Bernard de Massy, and Mathilde Grelon. 2016. "A New Light on the Meiotic DSB Catalytic Complex." *Seminars in Cell and Developmental Biology* 54: 165–76. <https://doi.org/10.1016/j.semcdb.2016.02.025>.
- Roeder, G. 2000. "The Pachytene Checkpoint." *Trends in Genetics* 16 (9): 395–403. [https://doi.org/10.1016/S0168-9525\(00\)02080-1](https://doi.org/10.1016/S0168-9525(00)02080-1).
- Roig, I., B. Liebe, J. Egozcue, I. Cabero, Montserrat Garcia, and H. Scherthan. 2004. "Female-Specific Features of Recombinational Double-Stranded DNA Repair in Relation to Synapsis and Telomere Dynamics in Human Oocytes." *Chromosoma* 113 (1): 22–33. <https://doi.org/10.1007/s00412-004-0290-8>.
- Romanienko, Peter J., and R. Daniel Camerini-Otero. 2000. "The Mouse Spo11 Gene Is Required for Meiotic Chromosome Synapsis." *Molecular Cell* 6 (5): 975–87. [https://doi.org/10.1016/S1097-2765\(00\)00097-6](https://doi.org/10.1016/S1097-2765(00)00097-6).
- Rooij, D G de, and L D Russell. 2000. "All You Wanted to Know about Spermatogonia but Were Afraid to Ask." *Journal of Andrology* 21 (6): 776–98.
- Rosenberg, Scott C., and Kevin D. Corbett. 2015. "The Multifaceted Roles of the HOR MA Domain in Cellular Signaling." *Journal of Cell Biology*. Rockefeller University Press. <https://doi.org/10.1083/jcb.201509076>.
- Rossetti, R., I. Ferrari, M. Bonomi, and L. Persani. 2017. "Genetics of Primary Ovarian Insufficiency." *Clinical Genetics*. John Wiley & Sons, Ltd. <https://doi.org/10.1111/cge.12921>.
- Rosu, Simona, Diana E. Libuda, and Anne M. Villeneuve. 2011. "Robust Crossover Assurance and Regulated Interhomolog Access Maintain Meiotic Crossover Number." *Science* 334 (6060):

- 1286–89. <https://doi.org/10.1126/science.1212424>.
- Royo, H el ene, Haydn Prosser, Yaroslava Ruzankina, Shantha K. Mahadevaiah, Jeffrey M. Cloutier, Marek Baumann, Tomoyuki Fukuda, et al. 2013. “ATR Acts Stage Specifically to Regulate Multiple Aspects of Mammalian Meiotic Silencing.” *Genes and Development* 27 (13): 1484–94. <https://doi.org/10.1101/gad.219477.113>.
- Royo, H el ne, Grzegorz Polikiewicz, Shantha K. Mahadevaiah, Haydn Prosser, Mike Mitchell, Allan Bradley, Dirk G. De Rooij, Paul S. Burgoyne, and James M.A. Turner. 2010. “Evidence That Meiotic Sex Chromosome Inactivation Is Essential for Male Fertility.” *Current Biology* 20 (23): 2117–23. <https://doi.org/10.1016/j.cub.2010.11.010>.
- Russell, Lonnie D, Robert A Ettl, Amiya P Sinha Hikim, and Eric D Clegg. 1993. “Histological and Histopathological Evaluation of the Testis.” *International Journal of Andrology* 16 (1): 83. <https://doi.org/doi:10.1111/j.1365-2605.1993.tb01156.x>.
- Ruth, Katherine S., Felix R. Day, Jazib Hussain, Ana Mart inez-Marchal, Catherine E. Aiken, Ajuna Azad, Deborah J. Thompson, et al. 2021. “Genetic Insights into Biological Mechanisms Governing Human Ovarian Ageing.” *Nature* 2021 596:7872 596 (7872): 393–97. <https://doi.org/10.1038/s41586-021-03779-7>.
- Sakuno, Takeshi, and Yoshinori Watanabe. 2009. “Studies of Meiosis Disclose Distinct Roles of Cohesion in the Core Centromere and Pericentromeric Regions.” *Chromosome Research*. Chromosome Res. <https://doi.org/10.1007/s10577-008-9013-y>.
- Salle, Sophie La, Kristina Palmer, Marilyn O’Brien, John C. Schimenti, John Eppig, and Mary Ann Handel. 2012. “Spata22, a Novel Vertebrate-Specific Gene, Is Required for Meiotic Progress in Mouse: Germ Cells.” *Biology of Reproduction* 86 (2). <https://doi.org/10.1095/biolreprod.111.095752>.
- Salle, Sophie La, and Jacquetta M. Trasler. 2006. “Dynamic Expression of DNMT3a and DNMT3b Isoforms during Male Germ Cell Development in the Mouse.” *Developmental Biology* 296 (1): 71–82. <https://doi.org/10.1016/J.YDBIO.2006.04.436>.
- San Filippo, Joseph, Patrick Sung, and Hannah Klein. 2008. “Mechanism of Eukaryotic Homologous Recombination.” *Annual Review of Biochemistry* 77 (1): 229–57. <https://doi.org/10.1146/annurev.biochem.77.061306.125255>.
- Santucci-Darmanin, Sabine, Sophie Neyton, Fran oise Lespinasse, Anne Sauni eres, Patrick Gaudray, and V eronique Paquis-Flucklinger. 2002. “The DNA Mismatch-Repair MLH3 Protein Interacts with MSH4 in Meiotic Cells, Supporting a Role for This MutL Homolog in Mammalian Meiotic Recombination.” *Human Molecular Genetics* 11 (15): 1697–1706. <https://doi.org/10.1093/hmg/11.15.1697>.
- Sathyan, Kizhakke M., Zhen Shen, Vidisha Tripathi, Kannanganattu V. Prasanth, and Supriya G. Prasanth. 2011. “A BEN-Domain-Containing Protein Associates with Heterochromatin and Represses Transcription.” *Journal of Cell Science* 124 (18): 3149–63. <https://doi.org/10.1242/jcs.086603>.
- Scarpa, Aldo, David K. Chang, Katia Nones, Vincenzo Corbo, Ann Marie Patch, Peter Bailey, Rita T. Lawlor, et al. 2017. “Whole-Genome Landscape of Pancreatic Neuroendocrine Tumours.” *Nature* 543 (7643): 65–71. <https://doi.org/10.1038/nature21063>.
- Scherthan, Harry. 2001. “A Bouquet Makes Ends Meet.” *Nature Reviews Molecular Cell Biology*. Nature Publishing Group. <https://doi.org/10.1038/35085086>.
- Schmidt, Dirk, Catherine E. Ovitt, Katrin Anlag, Sandra Fehsenfeld, Lars Gredsted, Anna Corina Treier,

- and Mathias Treier. 2004. "The Murine Winged-Helix Transcription Factor Foxl2 Is Required for Granulosa Cell Differentiation and Ovary Maintenance." *Development (Cambridge, England)* 131 (4): 933–42. <https://doi.org/10.1242/DEV.00969>.
- Schramm, Sabine, Johanna Fraune, Ronald Naumann, Abraham Hernandez-Hernandez, Christer Höög, Howard J. Cooke, Manfred Alsheimer, and Ricardo Benavente. 2011. "A Novel Mouse Synaptonemal Complex Protein Is Essential for Loading of Central Element Proteins, Recombination, and Fertility." *PLoS Genetics* 7 (5): e1002088. <https://doi.org/10.1371/journal.pgen.1002088>.
- Schücker, Katharina, Thorge Holm, Christian Franke, Markus Sauer, and Ricardo Benavente. 2015. "Elucidation of Synaptonemal Complex Organization by Super-Resolution Imaging with Isotropic Resolution." *Proceedings of the National Academy of Sciences of the United States of America* 112 (7): 2029–33. <https://doi.org/10.1073/pnas.1414814112>.
- Schücker, Katharina, Markus Sauer, and Ricardo Benavente. 2018. "Superresolution Imaging of the Synaptonemal Complex." In *Methods in Cell Biology*, 145:335–46. <https://doi.org/10.1016/bs.mcb.2018.03.033>.
- Serrentino, Maria Elisabetta, and Valérie Borde. 2012. "The Spatial Regulation of Meiotic Recombination Hotspots: Are All DSB Hotspots Crossover Hotspots?" *Experimental Cell Research*. Academic Press Inc. <https://doi.org/10.1016/j.yexcr.2012.03.025>.
- Sharan, Shyam K., April Pyle, Vincenzo Coppola, Janice Babus, Srividya Swaminathan, Jamie Benedict, Deborah Swing, et al. 2004. "BRCA2 Deficiency in Mice Leads to Meiotic Impairment and Infertility." *Development*. The Company of Biologists Ltd. <https://doi.org/10.1242/dev.00888>.
- Shibuya, Hiroki, Akihiro Morimoto, and Yoshinori Watanabe. 2014. "The Dissection of Meiotic Chromosome Movement in Mice Using an In Vivo Electroporation Technique." *PLoS Genetics* 10 (12): e1004821. <https://doi.org/10.1371/journal.pgen.1004821>.
- Shin, Yong Hyun, Youngsok Choi, Serpil Uckac Erdin, Svetlana A. Yatsenko, Malgorzata Kloc, Fang Yang, P. Jeremy Wang, Marvin L. Meistrich, and Aleksandar Rajkovic. 2010. "Hormad1 Mutation Disrupts Synaptonemal Complex Formation, Recombination, and Chromosome Segregation in Mammalian Meiosis." *PLoS Genetics* 6 (11): e1001190. <https://doi.org/10.1371/journal.pgen.1001190>.
- Shinohara, T, K E Orwig, M R Avarbock, and R L Brinster. 2001. "Remodeling of the Postnatal Mouse Testis Is Accompanied by Dramatic Changes in Stem Cell Number and Niche Accessibility." *Proceedings of the National Academy of Sciences of the United States of America* 98 (11): 6186–91. <https://doi.org/10.1073/pnas.111158198>.
- Shoji, Masanobu, Shinichiro Chuma, Kayo Yoshida, Takashi Morita, and Norio Nakatsuji. 2005. "RNA Interference during Spermatogenesis in Mice." *Developmental Biology* 282 (2): 524–34. <https://doi.org/10.1016/J.YDBIO.2005.03.030>.
- Siebert, Paul D., Alex Chenchik, David E. Kellogg, Konstantin A. Lukyanov, and Sergey A. Lukyanov. 1995. "An Improved PCR Method for Walking in Uncloned Genomic DNA." *Nucleic Acids Research* 23 (6): 1087–88. <https://doi.org/10.1093/nar/23.6.1087>.
- Smith, Gerald R., and Mridula Nambiar. 2020. "New Solutions to Old Problems: Molecular Mechanisms of Meiotic Crossover Control." *Trends in Genetics*. Elsevier Ltd. <https://doi.org/10.1016/j.tig.2020.02.002>.
- Smith, Samuel, Samantha M Pfeifer, and John A Collins. 2003. "Diagnosis and Management of Female Infertility." *JAMA* 290 (13): 1767–70. <https://doi.org/10.1001/jama.290.13.1767>.

- Snowden, Timothy, Samir Acharya, Charles Butz, Mark Berardini, and Richard Fishel. 2004. "HMSH4-HMSH5 Recognizes Holliday Junctions and Forms a Meiosis-Specific Sliding Clamp That Embraces Homologous Chromosomes." *Molecular Cell* 15 (3): 437–51. <https://doi.org/10.1016/j.molcel.2004.06.040>.
- Soh, Y. Q. Shirleen, Jan Philipp Junker, Mark E. Gill, Jacob L. Mueller, Alexander van Oudenaarden, and David C. Page. 2015. "A Gene Regulatory Program for Meiotic Prophase in the Fetal Ovary." *PLoS Genetics* 11 (9): e1005531. <https://doi.org/10.1371/journal.pgen.1005531>.
- Soh, Y. Q. Shirleen, Maria M. Mikedis, Mina Kojima, Alexander K. Godfrey, Dirk G. de Rooij, and David C. Page. 2017. "Meioc Maintains an Extended Meiotic Prophase I in Mice." *PLoS Genetics* 13 (4). <https://doi.org/10.1371/journal.pgen.1006704>.
- Soper, Sarah F.C., Godfried W. van der Heijden, Tara C. Hardiman, Mary Goodheart, Sandra L. Martin, Peter de Boer, and Alex Bortvin. 2008. "Mouse Maelstrom, a Component of Nuage, Is Essential for Spermatogenesis and Transposon Repression in Meiosis." *Developmental Cell* 15 (2): 285. <https://doi.org/10.1016/J.DEVCEL.2008.05.015>.
- Souquet, Benoit, Emilie Abby, Roxane Hervé, Friederike Finsterbusch, Sophie Tourpin, Ronan Le Bouffant, Clotilde Duquenne, et al. 2013. "MEIOB Targets Single-Strand DNA and Is Necessary for Meiotic Recombination." *PLoS Genetics* 9 (9): e1003784. <https://doi.org/10.1371/journal.pgen.1003784>.
- Sowa, Mathew E., Eric J. Bennett, Steven P. Gygi, and J. Wade Harper. 2009. "Defining the Human Deubiquitinating Enzyme Interaction Landscape." *Cell* 138 (2): 389. <https://doi.org/10.1016/J.CELL.2009.04.042>.
- Stanzione, Marcello, Marek Baumann, Frantzeskos Papanikos, Ihsan Dereli, Julian Lange, Angelique Ramlal, Daniel Tränkner, et al. 2016. "Meiotic DNA Break Formation Requires the Unsynapsed Chromosome Axis-Binding Protein IHO1 (CCDC36) in Mice." *Nature Cell Biology* 18 (11): 1208–20. <https://doi.org/10.1038/ncb3417>.
- Stegmeier, Frank, Michael Rape, Viji M. Draviam, Grzegorz Nalepa, Mathew E. Sowa, Xiaolu L. Ang, E. Robert McDonald, et al. 2007. "Anaphase Initiation Is Regulated by Antagonistic Ubiquitination and Deubiquitination Activities." *Nature* 446 (7138): 876–81. <https://doi.org/10.1038/nature05694>.
- Stracker, Travis H., and John H.J. Petrini. 2011. "The MRE11 Complex: Starting from the Ends." *Nature Reviews Molecular Cell Biology*. Nature Publishing Group. <https://doi.org/10.1038/nrm3047>.
- Sturm, Dominik, Brent A. Orr, Umut H. Toprak, Volker Hovestadt, David T.W. Jones, David Capper, Martin Sill, et al. 2016. "New Brain Tumor Entities Emerge from Molecular Classification of CNS-PNETs." *Cell* 164 (5): 1060–72. <https://doi.org/10.1016/J.CELL.2016.01.015>.
- Su, Xiaohua, Deepavali Chakravarti, and Elsa R. Flores. 2013. "P63 Steps into the Limelight: Crucial Roles in the Suppression of Tumorigenesis and Metastasis." *Nature Reviews Cancer*. Nat Rev Cancer. <https://doi.org/10.1038/nrc3446>.
- Subramanian, Vijayalakshmi V., and Andreas Hochwagen. 2014. "The Meiotic Checkpoint Network: Step-by-Step through Meiotic Prophase." *Cold Spring Harbor Perspectives in Biology* 6 (10). <https://doi.org/10.1101/cshperspect.a016675>.
- Sun, Fei, Paul Turek, Calvin Greene, Evelyn Ko, Alfred Rademaker, and Renée H Martin. 2007. "Abnormal Progression through Meiosis in Men with Nonobstructive Azoospermia." *Fertility and Sterility* 87 (3): 565–71. <https://doi.org/10.1016/j.fertnstert.2006.07.1531>.

- Suresh, Bharathi, Junwon Lee, Seok Ho Hong, Kye Seong Kim, and Suresh Ramakrishna. 2015. "The Role of Deubiquitinating Enzymes in Spermatogenesis." *Cellular and Molecular Life Sciences* 72 (24): 4711–20. <https://doi.org/10.1007/s00018-015-2030-z>.
- Suzuki, Ayumu, Masataka Hirasaki, Tomoaki Hishida, Jun Wu, Daiji Okamura, Atsushi Ueda, Masazumi Nishimoto, et al. 2016. "Loss of MAX Results in Meiotic Entry in Mouse Embryonic and Germline Stem Cells." *Nature Communications* 7 (1): 1–15. <https://doi.org/10.1038/ncomms11056>.
- Székvölgyi, Lóránt, Kunihiro Ohta, and Alain Nicolas. 2015. "Initiation of Meiotic Homologous Recombination: Flexibility, Impact of Histone Modifications, and Chromatin Remodeling." *Cold Spring Harbor Perspectives in Biology* 7 (5): 1–18. <https://doi.org/10.1101/cshperspect.a016527>.
- Takemoto, Kazumasa, Naoki Tani, Yuki Takada-Horisawa, Sayoko Fujimura, Nobuhiro Tanno, Mariko Yamane, Kaho Okamura, Michihiko Sugimoto, Kimi Araki, and Kei ichiro Ishiguro. 2020. "Meiosis-Specific C19orf57/4930432K21Rik/BRME1 Modulates Localization of RAD51 and DMC1 to DSBs in Mouse Meiotic Recombination." *Cell Reports* 31 (8): 107686. <https://doi.org/10.1016/j.celrep.2020.107686>.
- Tam, P P, and M H Snow. 1981. "Proliferation and Migration of Primordial Germ Cells during Compensatory Growth in Mouse Embryos." *Journal of Embryology and Experimental Morphology* 64 (August): 133–47.
- Tharp, Marla E., Safia Malki, and Alex Bortvin. 2020. "Maximizing the Ovarian Reserve in Mice by Evading LINE-1 Genotoxicity." *Nature Communications* 2020 11:1 11 (1): 1–13. <https://doi.org/10.1038/s41467-019-14055-8>.
- Touati, Sandra A., and Katja Wassmann. 2016. "How Oocytes Try to Get It Right: Spindle Checkpoint Control in Meiosis." *Chromosoma*. Springer Science and Business Media Deutschland GmbH. <https://doi.org/10.1007/s00412-015-0536-7>.
- Tournaye, Herman, Csilla Krausz, and Robert D Oates. 2017. "Novel Concepts in the Aetiology of Male Reproductive Impairment." *The Lancet. Diabetes & Endocrinology* 5 (7): 544–53. [https://doi.org/10.1016/S2213-8587\(16\)30040-7](https://doi.org/10.1016/S2213-8587(16)30040-7).
- Traven, Ana, and Jörg Heierhorst. 2005. "SQ/TQ Cluster Domains: Concentrated ATM/ATR Kinase Phosphorylation Site Regions in DNA-Damage-Response Proteins." *BioEssays* 27 (4): 397–407. <https://doi.org/10.1002/bies.20204>.
- Tropel, Philippe, Cécile André, Stéphane Viville, Adeline Ndandougou, and Laura Jung. 2017. "CpG Island Methylation Correlates with the Use of Alternative Promoters for USP44 Gene Expression in Human Pluripotent Stem Cells and Testes ." *Stem Cells and Development* 26 (15): 1100–1110. <https://doi.org/10.1089/scd.2017.0057>.
- Turner, James M.A. 2015. "Meiotic Silencing in Mammals." *Annual Review of Genetics* 49 (1): 395–412. <https://doi.org/10.1146/annurev-genet-112414-055145>.
- Turner, James M.A., Olga Aprelikova, Xiaoling Xu, Ruihong Wang, Sangsoo Kim, Gadisetti V.R. Chandramouli, J. Carl Barrett, Paul S. Burgoyne, and Chu Xia Deng. 2004. "BRCA1, Histone H2AX Phosphorylation, and Male Meiotic Sex Chromosome Inactivation." *Current Biology* 14 (23): 2135–42. <https://doi.org/10.1016/j.cub.2004.11.032>.
- Turner, James M.A., Shantha K. Mahadevaiah, Peter J.I. Ellis, Michael J. Mitchell, and Paul S. Burgoyne. 2006. "Pachytene Asynapsis Drives Meiotic Sex Chromosome Inactivation and Leads to Substantial Postmeiotic Repression in Spermatids." *Developmental Cell* 10 (4): 521–29.

- <https://doi.org/10.1016/j.devcel.2006.02.009>.
- Tüttelmann, Frank, Christian Ruckert, and Albrecht Röpke. 2018. "Disorders of Spermatogenesis. Perspectives for Novel Genetic Diagnostics after 20 Years of Unchanged Routine." *Medizinische Genetik* 30 (1): 12–20. <https://doi.org/10.1007/s11825-018-0181-7>.
- Uhlén, Mathias, Linn Fagerberg, Bjö M. Hallström, Cecilia Lindskog, Per Oksvold, Adil Mardinoglu, Åsa Sivertsson, et al. 2015. "Tissue-Based Map of the Human Proteome." *Science* 347 (6220). https://doi.org/10.1126/SCIENCE.1260419/SUPPL_FILE/1260419_UHLEN.SM.PDF.
- Urrutia, Raul. 2003. "KRAB-Containing Zinc-Finger Repressor Proteins." *Genome Biology* 4 (10): 231. <https://doi.org/10.1186/GB-2003-4-10-231>.
- Vara, Covadonga, Andreu Paytuví-Gallart, Yasmina Cuartero, François Le Dily, Francisca Garcia, J. Salvà-Castro, L. Gómez-H, et al. 2019. "Three-Dimensional Genomic Structure and Cohesin Occupancy Correlate with Transcriptional Activity during Spermatogenesis." *Cell Reports* 28 (2): 352–367.e9. <https://doi.org/10.1016/j.celrep.2019.06.037>.
- Vasmatzis, George, Farhad Kosari, Jeffrey L. Salisbury, Ying Zhang, Paul J. Galdary, Jan van Deursen, Dennis A. Wigle, and Oded Foreman. 2012. "USP44 Regulates Centrosome Positioning to Prevent Aneuploidy and Suppress Tumorigenesis." *Journal of Clinical Investigation* 122 (12): 4362–74. <https://doi.org/10.1172/jci63084>.
- Visconti, Roberta, Luca Palazzo, Rosa Della Monica, and Domenico Grieco. 2012. "Fcp1-Dependent Dephosphorylation Is Required for M-Phase-Promoting Factor Inactivation at Mitosis Exit." *Nature Communications* 3 (May): 810–94. <https://doi.org/10.1038/ncomms1886>.
- Vitt, U A, E A McGee, M Hayashi, and A J Hsueh. 2000. "In Vivo Treatment with GDF-9 Stimulates Primordial and Primary Follicle Progression and Theca Cell Marker CYP17 in Ovaries of Immature Rats." *Endocrinology* 141 (10): 3814–20. <https://doi.org/10.1210/endo.141.10.7732>.
- Voelkel-Meiman, Karen, Cassandra Johnston, Yashna Thappeta, Vijayalakshmi V. Subramanian, Andreas Hochwagen, and Amy J. MacQueen. 2015. "Separable Crossover-Promoting and Crossover-Constraining Aspects of Zip1 Activity during Budding Yeast Meiosis." *PLoS Genetics* 11 (6): e1005335. <https://doi.org/10.1371/journal.pgen.1005335>.
- Voelkel-Meiman, Karen, Sarah S. Moustafa, Philippe Lefrançois, Anne M. Villeneuve, and Amy J. MacQueen. 2012. "Full-Length Synaptonemal Complex Grows Continuously during Meiotic Prophase in Budding Yeast." *PLOS Genetics* 8 (10): e1002993. <https://doi.org/10.1371/JOURNAL.PGEN.1002993>.
- Vrielynck, Nathalie, Aurélie Chambon, Daniel Vezon, Lucie Pereira, Liudmila Chelysheva, Arnaud De Muyt, Christine Mézard, Claudine Mayer, and Mathilde Grelon. 2016. "A DNA Topoisomerase VI-like Complex Initiates Meiotic Recombination." *Science* 351 (6276): 939–43. <https://doi.org/10.1126/science.aad5196>.
- Vries, Femke A.T. De, Esther De Boer, Mike Van Den Bosch, Willy M. Baarends, Marja Ooms, Li Yuan, Jian Guo Liu, Albert A. Van Zeeland, Christa Heyting, and Albert Pastink. 2005. "Mouse Sycp1 Functions in Synaptonemal Complex Assembly, Meiotic Recombination, and XY Body Formation." *Genes and Development* 19 (11): 1376–89. <https://doi.org/10.1101/gad.329705>.
- Vries, Sandra S. De, Esther B. Baart, Marleen Dekker, Ariaan Siezen, Dirk G. De Rooij, Peter De Boer, and Hein Te Riele. 1999. "Mouse MutS-like Protein Msh5 Is Required for Proper Chromosome Synapsis in Male and Female Meiosis." *Genes and Development* 13 (5): 523–31. <https://doi.org/10.1101/gad.13.5.523>.
- Wang, Jia-hao, Yan Li, Shou-long Deng, Yi-xun Liu, and Zheng-xing Lian. 2019. "Recent Research

- Advances in Mitosis During." *Cells* 567 (8): 1–15.
- Wang, Jian, Wenxiang Zhang, Hong Jiang, and Bai-Lin Wu. 2014. "Mutations in HFM1 in Recessive Primary Ovarian Insufficiency." *New England Journal of Medicine* 370 (10): 972–74. <https://doi.org/10.1056/nejmc1310150>.
- Wear, Hannah M., Matthew J. McPike, and Karen H. Watanabe. 2016. "From Primordial Germ Cells to Primordial Follicles: A Review and Visual Representation of Early Ovarian Development in Mice." *Journal of Ovarian Research* 9 (1): 1–11. <https://doi.org/10.1186/s13048-016-0246-7>.
- Wei, Kaichun, Alan B. Clark, Edmund Wong, Michael F. Kane, Dan J. Mazur, Tchaiko Parris, Nadine K. Kolas, et al. 2003. "Inactivation of Exonuclease I in Mice Results in DNA Mismatch Repair Defects, Increased Cancer Susceptibility, and Male and Female Sterility." *Genes and Development* 17 (5): 603–14. <https://doi.org/10.1101/gad.1060603>.
- Wendt, Kerstin S., Keisuke Yoshida, Takehiko Itoh, Masashige Bando, Birgit Koch, Erika Schirghuber, Shuichi Tsutsumi, et al. 2008. "Cohesin Mediates Transcriptional Insulation by CCCTC-Binding Factor." *Nature* 2008 451:7180 451 (7180): 796–801. <https://doi.org/10.1038/nature06634>.
- West, Alan M.V., Scott C. Rosenberg, Sarah N. Ur, Madison K. Lehmer, Qiaozhen Ye, Götz Hagemann, Iracema Caballero, et al. 2019. "A Conserved Filamentous Assembly Underlies the Structure of the Meiotic Chromosome Axis." *ELife* 8: e40372. <https://doi.org/10.7554/eLife.40372>.
- Western, Patrick. 2009. "Foetal Germ Cells: Striking the Balance between Pluripotency and Differentiation." *The International Journal of Developmental Biology* 53 (2–3): 393–409. <https://doi.org/10.1387/ijdb.082671pw>.
- Widger, Alexander, Shantha K Mahadevaiah, Julian Lange, Elias Elinati, Jasmin Zohren, Takayuki Hirota, Sarai Pacheco, et al. 2018. "ATR Is a Multifunctional Regulator of Male Mouse Meiosis." *Nature Communications* 9 (1). <https://doi.org/10.1038/s41467-018-04850-0>.
- Williams, Carmen J, and Gregory F Erickson. 2000. "Morphology and Physiology of the Ovary." In . South Dartmouth (MA).
- Williamson, Laura M., Michael Steel, Jasleen K. Grewal, My Lihn Thibodeau, Eric Y. Zhao, Jonathan M. Loree, Kevin C. Yang, et al. 2019. "Tumor BEN FUSTION Genomic Characterization of a Welldifferentiated Grade 3 Pancreatic Neuroendocrine Tumor." *Cold Spring Harbor Molecular Case Studies* 5 (3): 1–14. <https://doi.org/10.1101/mcs.a003814>.
- Winkel, Karoline, Manfred Alsheimer, Rupert Öllinger, and Ricardo Benavente. 2009. "Protein SYCP2 Provides a Link between Transverse Filaments and Lateral Elements of Mammalian Synaptonemal Complexes." *Chromosoma* 118 (2): 259–67. <https://doi.org/10.1007/s00412-008-0194-0>.
- Wojtasz, Lukasz, Jeffrey M. Cloutier, Marek Baumann, Katrin Daniel, János Varga, Jun Fu, Konstantinos Anastasiadis, et al. 2012. "Meiotic DNA Double-Strand Breaks and Chromosome Asynapsis in Mice Are Monitored by Distinct HORMAD2-Independent and -Dependent Mechanisms." *Genes & Development* 26 (9): 958–73. <https://doi.org/10.1101/gad.187559.112>.
- Wojtasz, Lukasz, Katrin Daniel, Ignasi Roig, Ewelina Bolcun-Filas, Huiling Xu, Verawan Boonsanay, Christian R. Eckmann, et al. 2009. "Mouse HORMAD1 and HORMAD2, Two Conserved Meiotic Chromosomal Proteins, Are Depleted from Synapsed Chromosome Axes with the Help of TRIP13 AAA-ATPase." *PLoS Genetics* 5 (10). <https://doi.org/10.1371/journal.pgen.1000702>.
- Wu, Hsin Yen, Hsuan Chung Ho, and Sean M. Burgess. 2010. "Mek1 Kinase Governs Outcomes of Meiotic Recombination and the Checkpoint Response." *Current Biology* 20 (19): 1707–16. <https://doi.org/10.1016/j.cub.2010.09.016>.

- Wu, Leonard, Csanad Z. Bachrati, Jiongwen Ou, Chang Xu, Jinhu Yin, Michael Chang, Weidong Wang, Lei Li, Grant W. Brown, and Ian D. Hickson. 2006. "BLAP75/RMI1 Promotes the BLM-Dependent Dissolution of Homologous Recombination Intermediates." *Proceedings of the National Academy of Sciences of the United States of America* 103 (11): 4068–73. <https://doi.org/10.1073/pnas.0508295103>.
- Xiao, Yuxuan, Daniel Pollack, Miriam Andrusier, Avi Levy, Myrasol Callaway, Edward Nieves, Prabhakara Reddi, and Margarita Vigodner. 2016. "Identification of Cell-Specific Targets of Sumoylation during Mouse Spermatogenesis." *Reproduction* 151 (2): 149–66. <https://doi.org/10.1530/REP-15-0239>.
- Xu, Huizhong, Zhisong Tong, Qing Ye, Tengqian Sun, Zhenmin Hong, Lunfeng Zhang, Alexandra Bortnick, et al. 2019. "Molecular Organization of Mammalian Meiotic Chromosome Axis Revealed by Expansion STORM Microscopy." *Proceedings of the National Academy of Sciences of the United States of America* 116 (37): 18423–28. <https://doi.org/10.1073/pnas.1902440116>.
- Xuan, C., Q. Wang, X. Han, Y. Duan, L. Li, L. Shi, Y. Wang, L. Shan, Z. Yao, and Y. Shang. 2012. "RBB, a Novel Transcription Repressor, Represses the Transcription of HDM2 Oncogene." *Oncogene* 2013 32:32 32 (32): 3711–21. <https://doi.org/10.1038/onc.2012.386>.
- Yamaguchi, Shinpei, Kwonho Hong, Rui Liu, Li Shen, Azusa Inoue, Dinh Diep, Kun Zhang, and Yi Zhang. 2012. "Tet1 Controls Meiosis by Regulating Meiotic Gene Expression." *Nature* 492 (7429): 443–47. <https://doi.org/10.1038/nature11709>.
- Yan, C, P Wang, J DeMayo, F J DeMayo, J A Elvin, C Carino, S V Prasad, et al. 2001. "Synergistic Roles of Bone Morphogenetic Protein 15 and Growth Differentiation Factor 9 in Ovarian Function." *Molecular Endocrinology (Baltimore, Md.)* 15 (6): 854–66. <https://doi.org/10.1210/mend.15.6.0662>.
- Yan, Wei, Lang Ma, Kathleen H Burns, and Martin M Matzuk. 2004. "Haploinsufficiency of Kelch-like Protein Homolog 10 Causes Infertility in Male Mice." *Proceedings of the National Academy of Sciences of the United States of America* 101 (20): 7793–98. <https://doi.org/10.1073/pnas.0308025101>.
- Yang, Fang, Rabindranath De La Fuente, N. Adrian Leu, Claudia Baumann, K. John McLaughlin, and P. Jeremy Wang. 2006. "Mouse SYCP2 Is Required for Synaptonemal Complex Assembly and Chromosomal Synapsis during Male Meiosis." *Journal of Cell Biology* 173 (4): 497–507. <https://doi.org/10.1083/jcb.200603063>.
- Yang, Fang, Sherman Silber, N Adrian Leu, Robert D Oates, Janet D Marszalek, Helen Skaletsky, Laura G Brown, Steve Rozen, David C Page, and P Jeremy Wang. 2015. "TEX11 Is Mutated in Infertile Men with Azoospermia and Regulates Genome-Wide Recombination Rates in Mouse." *EMBO Molecular Medicine* 7 (9): 1198–1210. <https://doi.org/10.15252/emmm.201404967>.
- Yatsenko, Alexander N, Andrew P Georgiadis, Albrecht Röpke, Andrea J Berman, Thomas Jaffe, Marta Olszewska, Birgit Westernströer, et al. 2015. "X-Linked TEX11 Mutations, Meiotic Arrest, and Azoospermia in Infertile Men." *The New England Journal of Medicine* 372 (22): 2097–2107. <https://doi.org/10.1056/NEJMoa1406192>.
- Yatsenko, Svetlana A., and Aleksandar Rajkovic. 2019. "Genetics of Human Female Infertility." *Biology of Reproduction* 101 (3): 549–66. <https://doi.org/10.1093/biolre/iox084>.
- Ye, Qiaozhen, Dong Hyun Kim, Ihsan Dereli, Scott C Rosenberg, Goetz Hagemann, Franz Herzog, Attila Tóth, Don W Cleveland, and Kevin D Corbett. 2017. "The AAA + ATP Ase TRIP 13 Remodels HORMA Domains through N-terminal Engagement and Unfolding." *The EMBO*

- Journal* 36 (16): 2419–34. <https://doi.org/10.15252/emj.201797291>.
- Yokobayashi, Shihori, Ching Yeu Liang, Hubertus Kohler, Peter Nestorov, Zichuan Liu, Miguel Vidal, Maarten Van Lohuizen, Tim C. Roloff, and Antoine H.F.M. Peters. 2013. “PRC1 Coordinates Timing of Sexual Differentiation of Female Primordial Germ Cells.” *Nature* 495 (7440): 236–40. <https://doi.org/10.1038/nature11918>.
- Yokoo, Rayka, Karl A. Zawadzki, Kentaro Nabeshima, Melanie Drake, Swathi Arur, and Anne M. Villeneuve. 2012. “COSA-1 Reveals Robust Homeostasis and Separable Licensing and Reinforcement Steps Governing Meiotic Crossovers.” *Cell* 149 (1): 75–87. <https://doi.org/10.1016/j.cell.2012.01.052>.
- Yoshida, Kayo, Gen Kondoh, Yoichi Matsuda, Toshiyuki Habu, Yoshitake Nishimune, and Takashi Morita. 1998. “The Mouse RecA-like Gene Dmc1 Is Required for Homologous Chromosome Synapsis during Meiosis.” *Molecular Cell* 1 (5): 707–18. [https://doi.org/10.1016/S1097-2765\(00\)80070-2](https://doi.org/10.1016/S1097-2765(00)80070-2).
- Yoshida, Shosei, Mamiko Sukeno, Toshinori Nakagawa, Kazuyuki Ohbo, Go Nagamatsu, Toshio Suda, and Yo-ichi Nabeshima. 2006. “The First Round of Mouse Spermatogenesis Is a Distinctive Program That Lacks the Self-Renewing Spermatogonia Stage” 1505: 1495–1505. <https://doi.org/10.1242/dev.02316>.
- Yuan, Li, Jian Guo Liu, Jian Zhao, Eva Brundell, Bertil Daneholt, and Christer Höög. 2000. “The Murine SCP3 Gene Is Required for Synaptonemal Complex Assembly, Chromosome Synapsis, and Male Fertility.” *Molecular Cell* 5 (1): 73–83. [https://doi.org/10.1016/S1097-2765\(00\)80404-9](https://doi.org/10.1016/S1097-2765(00)80404-9).
- Yuan, Li, Jeanette Pelttari, Eva Brundell, Birgitta Björkroth, Jian Zhao, Jian Guo Liu, Hjalmar Brismar, Bertil Daneholt, and Christer Höög. 1998. “The Synaptonemal Complex Protein SCP3 Can Form Multistranded, Cross-Striated Fibers in Vivo.” *Journal of Cell Biology* 142 (2): 331–39. <https://doi.org/10.1083/jcb.142.2.331>.
- Zakharyevich, Kseniya, Yunmei Ma, Shangming Tang, Patty Yi Hwa Hwang, Serge Boiteux, and Neil Hunter. 2010. “Temporally and Biochemically Distinct Activities of Exo1 during Meiosis: Double-Strand Break Resection and Resolution of Double Holliday Junctions.” *Molecular Cell* 40 (6): 1001–15. <https://doi.org/10.1016/j.molcel.2010.11.032>.
- Zakharyevich, Kseniya, Shangming Tang, Yunmei Ma, and Neil Hunter. 2012. “Delineation of Joint Molecule Resolution Pathways in Meiosis Identifies a Crossover-Specific Resolvase.” *Cell* 149 (2): 334–47. <https://doi.org/10.1016/j.cell.2012.03.023>.
- Zelensky, Alex, Roland Kanaar, and Claire Wyman. 2014. “Mediators of Homologous DNA Pairing.” *Cold Spring Harbor Perspectives in Biology* 6 (12). <https://doi.org/10.1101/cshperspect.a016451>.
- Zeleznik, Anthony J. 2004. “The Physiology of Follicle Selection.” *Reproductive Biology and Endocrinology*. BioMed Central. <https://doi.org/10.1186/1477-7827-2-31>.
- Zhang, Bin, Zhenghui Tang, Lejun Li, and Lin Yu Lu. 2020. “NBS1 Is Required for SPO11-Linked DNA Double-Strand Break Repair in Male Meiosis.” *Cell Death and Differentiation* 27 (7): 2176–90. <https://doi.org/10.1038/s41418-020-0493-4>.
- Zhang, Hong Yan, Bo Wei Liao, Zhi Sheng Xu, Yong Ran, Dong Peng Wang, Yan Yang, Wei Wei Luo, and Yan Yi Wang. 2020. “USP44 Positively Regulates Innate Immune Response to DNA Viruses through Deubiquitinating MITA.” *PLoS Pathogens* 16 (1): e1008178. <https://doi.org/10.1371/journal.ppat.1008178>.
- Zhang, Jingjing, Yasuhiro Fujiwara, Shohei Yamamoto, and Hiroki Shibuya. 2019. “A Meiosis-Specific

- BRCA2 Binding Protein Recruits Recombinases to DNA Double-Strand Breaks to Ensure Homologous Recombination." *Nature Communications* 2019 10:1 10 (1): 1–14. <https://doi.org/10.1038/s41467-019-08676-2>.
- Zhang, Jingjing, Manickam Gurusaran, Yasuhiro Fujiwara, Kexin Zhang, Meriem Echbarthi, Egor Vorontsov, Rui Guo, et al. 2020. "The BRCA2-MEILB2-BRME1 Complex Governs Meiotic Recombination and Impairs the Mitotic BRCA2-RAD51 Function in Cancer Cells." *Nature Communications* 2020 11:1 11 (1): 1–18. <https://doi.org/10.1038/s41467-020-15954-x>.
- Zhang, Liangran, Nancy E. Kleckner, Aurora Storlazzi, and Keun P. Kim. 2011. "Meiotic Double-Strand Breaks Occur Once per Pair of (Sister) Chromatids and, via Mec1/ATR and Tel1/ATM, Once per Quartet of Chromatids." *Proceedings of the National Academy of Sciences of the United States of America* 108 (50): 20036–41. <https://doi.org/10.1073/pnas.1117937108>.
- Zhang, Liangran, Zhangyi Liang, John Hutchinson, and Nancy Kleckner. 2014. "Crossover Patterning by the Beam-Film Model: Analysis and Implications." *PLoS Genetics* 10 (1): e1004042. <https://doi.org/10.1371/journal.pgen.1004042>.
- Zhang, Liangran, Shunxin Wang, Shen Yin, Soogil Hong, Keun P. Kim, and Nancy Kleckner. 2014. "Topoisomerase II Mediates Meiotic Crossover Interference." *Nature* 511 (7511): 551–56. <https://doi.org/10.1038/nature13442>.
- Zhang, Qianting, Shu Yan Ji, Kiran Busayavalasa, and Chao Yu. 2019. "SPO16 Binds SHOC1 to Promote Homologous Recombination and Crossing-over in Meiotic Prophase I." *Science Advances* 5 (1): eaau9780. <https://doi.org/10.1126/sciadv.aau9780>.
- Zhang, Wenxiang, Xiaomin Song, Feng Ni, Jinbao Cheng, Bai Lin Wu, and Hong Jiang. 2017. "Association Analysis between HFM1 Variations and Idiopathic Azoospermia or Severe Oligozoospermia in Chinese Men." *Science China Life Sciences*. Science in China Press. <https://doi.org/10.1007/s11427-016-0274-9>.
- Zhang, Ying, Jan van Deursen, and Paul J. Galaray. 2011. "Overexpression of Ubiquitin Specific Protease 44 (USP44) Induces Chromosomal Instability and Is Frequently Observed in Human T-Cell Leukemia." *PLoS ONE* 6 (8). <https://doi.org/10.1371/journal.pone.0023389>.
- Zhao, Weixing, Sivaraja Vaithiyalingam, Joseph San Filippo, David G. Maranon, Judit Jimenez-Sainz, Gerald V. Fontenay, Youngho Kwon, et al. 2015. "Promotion of BRCA2-Dependent Homologous Recombination by DSS1 via RPA Targeting and DNA Mimicry." *Molecular Cell* 59 (2): 176–87. <https://doi.org/10.1016/J.MOLCEL.2015.05.032>.
- Zickler, D, and N Kleckner. 1999. "Meiotic Chromosomes: Integrating Structure and Function." *Annual Review of Genetics*. <https://doi.org/10.1146/annurev.genet.33.1.603>.
- Zickler, Denise. 2006. "From Early Homologue Recognition to Synaptonemal Complex Formation." *Chromosoma* 115 (3): 158–74. <https://doi.org/10.1007/s00412-006-0048-6>.
- Zickler, Denise, and Nancy Kleckner. 2015. "Recombination, Pairing, and Synapsis of Homologs during Meiosis." *Cold Spring Harbor Laboratory Press*, 1,2. <https://doi.org/10.1101/cshperspect.a016626>.
- Zorrilla, Michelle, and Alexander N. Yatsenko. 2013. "The Genetics of Infertility: Current Status of the Field." *Current Genetic Medicine Reports* 1 (4): 247–60. <https://doi.org/10.1007/s40142-013-0027-1>.

Supplementary Tables

Supplementary Table 1 Information of candidate genes. List of all the putative novel genes derived from 14 dpp mouse testis, displaying the code, number of exons, length in base pairs, location, homology, similarity to other proteins, and GO terms associated with the similar protein.

Name	#Exons	Length (bp)	Location	Homology	Similarity	GO TERMS
002P1	3	9682	17:22772621-22782303	All animals (low coverage)	Zinc finger protein 271	
010P1	7	34877	17:22285251-22320128	All animals (low coverage)	Zinc finger protein 761; Zinc finger protein 845	
010P2	7	34877	17:22285251-22320128	All animals (low coverage)	Zinc finger protein 761; Zinc finger protein 845	DNA binding, transcription, DNA-templated, regulation of transcription, DNA-templated, nucleus, metal ion binding
012P1	1	329	17:33146800-33147129	Mostly Mammals	Zinc finger protein 709	
014P1	4	35535	17:17005247-17040782	All animals (low coverage)	Zinc finger protein 709	vesicle organization, proteasome-mediated ubiquitin-dependent protein catabolic process, nucleolus, cytoplasm, plasma membrane, cytosol, protein binding, endocytic vesicle, negative regulation of transforming growth factor beta 1 production, cell migration, filamentous actin, ruffle, regulation of actin cytoskeleton reorganization, cell-cell junction, cell cortex, perinuclear region of cytoplasm, positive regulation of protein localization to nucleus, regulation of receptor-mediated endocytosis, cell-cell adhesion, mitotic cell cycle
017P1	1	2825	17:3311406-3314231	All animals (low coverage)	CD2-associated protein	DNA binding, transcription, DNA-templated, regulation of transcription, DNA-templated, nucleus, metal ion binding
018P1	1	302	17:33148024-33148326	Rodents	Zinc finger protein 124	regulation of bone mineralization, ATP binding, nucleus, regulation of catalytic activity, protein kinase activity, regulation of protein stability, membrane, positive regulation of phosphatidylinositol 3-kinase activity, regulation of protein kinase activity, positive regulation of pseudopodium assembly, filopodium, regulation of protein catabolic process, cardiac conduction system development, plasma membrane, cytosol, microtubule organizing center, protein binding, GTP binding, midbody, establishment of cell polarity, secretory granule, regulation of exocytosis, keratinocyte development, neuron projection, hair follicle morphogenesis, neuronal cell body, establishment of Golgi localization, positive regulation of neuron apoptotic process, regulation of protein heterodimerization activity, positive regulation of intracellular protein transport, actin filament branching, epithelial cell-cell adhesion, regulation of filopodium assembly, mitogen-activated protein kinase kinase binding, keratinization, negative regulation of protein-containing complex assembly, multicellular organism growth, spindle midzone, Golgi membrane, sprouting angiogenesis, actin filament bundle assembly, organelle transport along microtubule, canonical Wnt signaling pathway, epithelial-mesenchymal cell signaling, apical part of cell, positive regulation of peptide-serine phosphorylation, hair follicle placode formation, establishment or maintenance of apical/basal cell polarity, heart contraction, obsolete GTP catabolic process, positive regulation of DNA replication, mitotic spindle, submandibular salivary gland formation, GTPase activity, positive regulation of hair follicle cell proliferation, neuron fate determination, positive regulation of substrate adhesion-dependent cell spreading, adherens junction organization, positive regulation of JNK cascade, positive regulation of synapse
020P1	1	1738	16:24379363-24381101	All animals (low coverage)	BMP-2-inducible protein kinase	
022P1	1	589	7:11845107-11845696	All animals	Cell division control protein 42 homolog	

						structural plasticity, regulation of attachment of spindle microtubules to kinetochore, response to glucose, actin filament organization, cellular protein localization, Golgi organization, nuclear migration, regulation of mitotic nuclear division, negative regulation of gene expression, positive regulation of gene expression, positive regulation of cytokinesis, small GTPase mediated signal transduction, filopodium assembly, positive regulation of catalytic activity
025P1	4	6731	7:43257525-43264256	All animals (low coverage)	Zinc finger protein 431	core promoter sequence-specific DNA binding, chromatin binding, transcription, DNA-templated, cell differentiation, histone deacetylase binding, nucleus, negative regulation of osteoblast differentiation
029P1	1	1997	7:7100330-7102327	Mostly Mammals	Zinc finger protein 37	DNA binding, transcription, DNA-templated, regulation of transcription, DNA-templated, nucleus, zinc ion binding, multicellular organism development, germ cell development, spermatogenesis
033P1	1	428	7:4909038-4909466	Mostly Mammals	D-3-phosphoglycerate dehydrogenase	neural tube development, L-serine metabolic process, L-serine biosynthetic process, theonine metabolic process, glutamine metabolic process, glycine metabolic process, phosphoglycerate dehydrogenase activity, G1 to G0 transition, spinal cord development, glial cell development, neuron projection development, neurogenesis, gamma-aminobutyric acid metabolic process, regulation of gene expression, taurine metabolic process
036P1	4	9376	7:11979393-11988769	Mostly Mammals	Zinc finger and SCAN domain containing protein 4C	chromosome, telomeric region, DNA binding, negative regulation of mitotic recombination, transcription, DNA-templated, regulation of transcription by RNA polymerase II, cytoplasm, nucleus, DNA-binding transcription factor activity, stem cell differentiation, telomere maintenance via telomere lengthening, metal ion binding
046P1	5	15820	7:6976337-6992157	Mus musculus	Zinc finger protein 264	DNA binding, transcription, DNA-templated, regulation of transcription, DNA-templated, nucleus, metal ion binding
060P1	6	7361	7:24687897-24695258	Mus musculus	CD177 antigen	
060P2	6	7361	7:24687897-24695258	Rattus norvegicus	CD177 antigen	anchored component of membrane, plasma membrane, leukocyte migration, blood coagulation
060P3	6	7361	7:24687897-24695258	Mus musculus	CD177 antigen	
062P1	5	7611	7:102119400-102127011	Mostly Mammals	Nuclear pore complex protein Nup98-Nup96	DNA replication, nucleus, nucleoplasm, structural constituent of nuclear pore, peptide binding, nuclear inclusion body, obsolete protein import into nucleus, docking, nuclear membrane, nuclear pore complex assembly, mRNA transport, nuclear periphery, kinetochore, nuclear pore nuclear basket
062P2	5	7611	7:102119400-102127011	Mostly Mammals	Nuclear pore complex protein Nup98-Nup96	
064P1	5	12361	7:6343668-6356029	All animals (low coverage)	Zinc finger protein 582	DNA binding, transcription, DNA-templated, regulation of transcription, DNA-templated, nucleus, metal ion binding
064P2	5	12361	7:6343668-6356029	All animals (low coverage)	Zinc finger protein 582	
066P1	1	2082	7:128040805-128042887	Mostly Mammals	Armadillo repeat-containing X-linked protein 3	positive regulation of transcription by RNA polymerase II, integral component of mitochondrial outer membrane, protein binding, cellular protein localization
067P1	1	467	7:43264906-43265373	Mostly Mammals	Zinc finger protein 120	DNA binding, transcription, DNA-templated, regulation of transcription, DNA-templated, nucleus, metal ion binding
068P1	1	8236	7:27880839-27889075	All animals	Protein kinase C zeta type	neuron projection extension, activation of phospholipase D activity, axon hillock, cell leading edge, cytoplasm, endosome, plasma membrane, cytosol, microtubule organizing center, protein binding, ATP binding, nuclear envelope, nucleus, establishment of cell polarity, protein kinase C signaling, peptidyl-serine phosphorylation, positive regulation of interleukin-4 production, positive regulation of T-helper 2 cell differentiation, negative regulation of apoptotic process, actin cytoskeleton reorganization, cell migration, inflammatory response, apical plasma membrane, nuclear matrix, positive regulation of NF-kappaB transcription factor activity, protein

					phosphorylation, negative regulation of protein-containing complex assembly, negative regulation of peptidyl-tyrosine phosphorylation, positive regulation of ERK1 and ERK2 cascade, membrane raft, zinc ion binding, insulin receptor signaling pathway, positive regulation of cell population proliferation, negative regulation of hydrolase activity, protein heterooligomerization, protein kinase activity, protein serine/threonine kinase activity, protein kinase C activity, positive regulation of cell-matrix adhesion, vesicle transport along microtubule, apical cortex, myelin sheath abaxonal region, positive regulation of excitatory postsynaptic potential, membrane hyperpolarization, long-term synaptic potentiation, protein localization to plasma membrane, cell-cell junction, bicellular tight junction, cell cortex, potassium channel regulator activity, positive regulation of T-helper 2 cell cytokine production, perinuclear region of cytoplasm, positive regulation of glucose import, microtubule cytoskeleton organization, positive regulation of insulin receptor signaling pathway, negative regulation of insulin receptor signaling pathway, activation of protein kinase B activity, long-term memory, protein-containing complex, positive regulation of interleukin-5 production, positive regulation of interleukin-13 production, positive regulation of interleukin-10 production	
070P1	11	4792	14:546927729-54697521	Mostly Mammals	Leishmanolysin-like peptidase	membrane, cytoplasm, lipid droplet, metalloendopeptidase activity, focal adhesion, cell adhesion, metal ion binding, mitotic cell cycle
071P1	1	2782	14:61557070-61559852	All animals	Proteasome subunit alpha type-2	proteasome core complex, nucleus, proteasome core complex, alpha-subunit complex, ubiquitin-dependent protein catabolic process, threonine-type endopeptidase activity, P-body, response to virus
072P1	1	329	8:129284441-129284770	Mostly Mammals	Zinc finger protein 120	DNA binding, transcription, DNA-templated, regulation of transcription, DNA-templated, nucleus, metal ion binding
073P1	1	551	8:83477471-83478022	All animals (low coverage)	Pescadillo homolog	peribosome, large subunit precursor, rRNA processing, nucleolus, protein binding, nucleus, nucleoplasm, PeBoW complex, ribosome biogenesis, ribonucleoprotein complex binding, regulation of cell cycle, protein localization to organelle, cell population proliferation, maturation of LSU-rRNA from tritestic RNA transcript (SSU-rRNA, 5.8S rRNA, LSU-rRNA), maturation of 5.8S rRNA from tritestic rRNA transcript (SSU-rRNA, 5.8S rRNA, LSU-rRNA), condensed chromosome, nucleolus organization
079P1	1	812	8:129283469-129284281	All animals (low coverage)	Zinc finger protein 431	core promoter sequence-specific DNA binding, chromatin binding, transcription, DNA-templated, cell differentiation, histone deacetylase binding, nucleus, negative regulation of osteoblast differentiation, negative regulation of DNA-binding transcription factor activity, negative regulation of transcription by RNA polymerase II, metal ion binding
080P1	4	19720	8:129263722-129283442	All animals (low coverage)	Zinc finger protein 431	
083P1	3	6181	8:111748507-111754688	Mus musculus	Zinc finger protein 431	
086P1	4	24827	8:69560509-69585336	Mammals & birds, fishes	Cadherin-11	integral component of membrane, corticospinal tract morphogenesis, cytoplasm, plasma membrane, calcium ion binding, homophilic cell adhesion via plasma membrane adhesion molecules
089P1	1	876	19:37784217-37785093	Mammals & birds, fishes	26S protease regulatory subunit 4	protein catabolic process, cytoplasm, ATP binding, nucleus, ATP hydrolysis activity, obsolete ATP catabolic process, proteasome accessory complex, TBP-class protein binding
091P1	1	1765	19:12905227-12906992	Mammals & birds	Regulatory for meiotic nuclear division protein 1 homolog	mitochondrion, translation
094P1	13	41692	19:40748788-40790480	Mostly Mammals	Uncharacterized protein C10orf131 homolog	
094P2	13	41692	19:40748788-40790480	Mostly Mammals	Uncharacterized protein C10orf131 homolog	

096P1	3	7548	19:40821650-40829198	Mostly Mammals	Coiled-coil and C2 domain-containing protein 2A	cilium assembly, cytoplasm, cytoskeleton, protein binding, MKS complex, ciliary transition zone, smoothened signaling pathway
096P2	3	7548	19:40821650-40829198	Mostly Mammals	Coiled-coil and C2 domain-containing protein 2A	
105P1	3	3527	160P2	Mus musculus	Coiled-coil and C2 domain-containing protein 2A	
105P2	3	3527	160P2	Mus musculus	Coiled-coil and C2 domain-containing protein 2A	
109P1	1	590	1:191939937-191940527	Mus musculus	Glycoprotein 55	Integral component of membrane, structural molecule activity, virion membrane, viral envelope, host cell plasma membrane, viral capsid, virion attachment to host cell, fusion of virus membrane with host plasma membrane, host cell endoplasmic reticulum membrane
119P4	25	67109	1:181576524-181643633	Mostly Mammals	Dynein heavy chain 14, axonemal	cytoplasm, microtubule, ATP binding, dynein complex, cilium, microtubule motor activity, microtubule-based movement
134P1	4	21478	11:121903898-121925376	All animals (low coverage)	Zinc finger protein 431	core promoter sequence-specific DNA binding, chromatin binding, transcription, DNA-templated, cell differentiation, histone deacetylase binding, nucleus, negative regulation of osteoblast differentiation, negative regulation of DNA-binding transcription factor activity, negative regulation of transcription by RNA polymerase II, metal ion binding
134P2	4	21478	11:121903898-121925376	All animals (low coverage)	Zinc finger protein 431	
136P1	11	23340	11:105034974-105058314	Mus musculus	Zinc finger protein 431	
142P1	2	16607	11:121940152-121956759	All animals (low coverage)	Zinc finger protein 431; Zinc finger protein 658	core promoter sequence-specific DNA binding, chromatin binding, DNA binding, transcription, DNA-templated, regulation of transcription, DNA-templated, cell differentiation, histone deacetylase binding, nucleus, negative regulation of osteoblast differentiation, negative regulation of DNA-binding transcription factor activity, negative regulation of transcription by RNA polymerase II, DNA-binding transcription factor activity, metal ion binding
142P3	2	16607	11:121940152-121956759	All animals (low coverage)	Zinc finger protein 431; Zinc finger protein 658	
151P1	1	455	17:33147379-33147834	Mostly Mammals	Zinc finger protein 844	DNA binding, transcription, DNA-templated, regulation of transcription, DNA-templated, nucleus, metal ion binding
154P1	4	22658	16:98059784-98082442	All animals (low coverage)	Zinc finger protein 431	core promoter sequence-specific DNA binding, chromatin binding, transcription, DNA-templated, cell differentiation, histone deacetylase binding, nucleus, negative regulation of osteoblast differentiation, negative regulation of DNA-binding transcription factor activity, negative regulation of transcription by RNA polymerase II, metal ion binding
154P2	4	22658	16:98059784-98082442	Mostly Mammals	Zinc finger protein 431	
160P1	4	16453	18:90579618-90596071	All animals (low coverage)	Zinc finger protein 431	cytoplasm, microtubule, ATP binding, dynein complex, cilium, microtubule motor activity, microtubule-based movement
160P2	4	16453	18:90579618-90596071	All animals (low coverage)	Zinc finger protein 431	
160P2	25	67109	1:181576524-181643633	Mostly Mammals	Dynein heavy chain 14, axonemal	
161P1	2	7861	18:38359214-38367075	All animals	Glutamine synthetase	perikaryon, cytoplasm, mitochondrion, rough endoplasmic reticulum, protein binding, ATP binding, manganese ion binding, glutamate binding, glutamine biosynthetic process, glutamate metabolic process, glutamate decarboxylase activity, glutamate-ammonia ligase activity, axon terminus, protein homooligomerization, cell

					population proliferation, positive regulation of epithelial cell proliferation, glial cell projection, cellular response to starvation, magnesium ion binding, positive regulation of synaptic transmission, glutamatergic, response to glucose, positive regulation of insulin secretion, cell body, protein-containing complex
162P1	7	27228	18:84792800-84820028	Mostly Mammals	Uncharacterized protein C18orf63
165P1	1	413	12:18648570-18648983	Mostly Mammals	Zinc finger protein 120
169P1	1	1439	12:22584104-22585543	All animals (low coverage)	core promoter sequence-specific DNA binding, chromatin binding, transcription, DNA-templated, cell differentiation, histone deacetylase binding, nucleus, negative regulation of osteoblast differentiation, negative regulation of DNA-binding transcription factor activity, negative regulation of transcription by RNA polymerase II, metal ion binding
170P1	1	1523	12:22867994-22869517	All animals (low coverage)	Zinc finger protein 709
171P1	1	2252	12:21878703-21880955	All animals (low coverage)	Zinc finger protein 120
172P1	1	2506	12:20457757-20460263	Mostly Mammals	Hippocalcin-like protein 1 calcium ion binding
174P1	1	314	12:19975735-19976049	All animals (low coverage)	Zinc finger protein 431 core promoter sequence-specific DNA binding, chromatin binding, transcription, DNA-templated, cell differentiation, histone deacetylase binding, nucleus, negative regulation of osteoblast differentiation, negative regulation of DNA-binding transcription factor activity, negative regulation of transcription by RNA polymerase II, metal ion binding
175P1	1	413	12:22869607-22870020	All animals (low coverage)	Zinc finger protein 700 DNA binding, transcription, DNA-templated, regulation of transcription, DNA-templated, nucleus, metal ion binding
176P1	1	4031	12:19406041-19410072	All animals (low coverage)	Zinc finger protein 658 DNA binding, transcription, DNA-templated, regulation of transcription, DNA-templated, nucleus, DNA-binding transcription factor activity, metal ion binding
177P1	1	329	12:23782047-23782376	All animals (low coverage)	Zinc finger protein 120 DNA binding, transcription, DNA-templated, regulation of transcription, DNA-templated, nucleus, metal ion binding
178P1	1	1607	12:24213899-24215506	All animals (low coverage)	Zinc finger protein 160 DNA binding, transcription, DNA-templated, regulation of transcription, DNA-templated, nucleus, hemopoiesis, metal ion binding
180P1	1	2231	12:10156001-10158232	All animals	Acetyl-CoA carboxylase 1 fatty acid biosynthetic process, lipid metabolic process, biotin carboxylase activity, mitochondrion, cytosol, protein binding, ATP binding, acetyl-CoA metabolic process, lipid homeostasis, protein homotetramerization, tissue homeostasis, acetyl-CoA carboxylase activity, malonyl-CoA biosynthetic process, metal ion binding, protein metabolic process
181P1	1	1019	12:18648990-18650009	All animals (low coverage)	Zinc finger protein 431 core promoter sequence-specific DNA binding, chromatin binding, transcription, DNA-templated, cell differentiation, histone deacetylase binding, nucleus, negative regulation of osteoblast differentiation, negative regulation of DNA-binding transcription factor activity, negative regulation of transcription by RNA polymerase II, metal ion binding
185P1	1	1253	12:22724964-22726217	All animals (low coverage)	Zinc finger protein 431 DNA binding, transcription, DNA-templated, regulation of transcription, DNA-templated, nucleus, metal ion binding
186P1	1	413	12:24215513-24215926	All animals (low coverage)	Zinc finger protein 700
188P1	3	62611	12:77129105-77191716	Mus musculus	Zinc finger protein 700
188P2	3	62611	12:77129105-77191716	Mus musculus	Zinc finger protein 700

190P1	1	1076	12:10154850-10155926	All animals	Acetyl-CoA carboxylase 1	fatty acid biosynthetic process, lipid metabolic process, biotin carboxylase activity, mitochondrion, cytosol, protein binding, ATP binding, acetyl-CoA metabolic process, lipid homeostasis, protein homotetramerization, tissue homeostasis, acetyl-CoA carboxylase activity, malonyl-CoA biosynthetic process, metal ion binding, protein metabolic process
191P1	1	1537	12:21992931-21994468	Mostly Mammals	Zinc finger protein 700	DNA binding, transcription, DNA-templated, regulation of transcription, DNA-templated, nucleus, metal ion binding
193P1	1	4255	12:18871742-18875997	All animals (low coverage)	Zinc finger protein 658	DNA binding, transcription, DNA-templated, regulation of transcription, DNA-templated, nucleus, DNA-binding transcription factor activity, metal ion binding
194P1	1	767	12:20322022-20322789	All animals (low coverage)	Zinc finger protein 120	DNA binding, transcription, DNA-templated, regulation of transcription, DNA-templated, nucleus, metal ion binding
195P1	1	6682	12:19861064-19867746	All animals (low coverage)	Zinc finger protein 431	core promoter sequence-specific DNA binding, chromatin binding, transcription, DNA-templated, cell differentiation, histone deacetylase binding, nucleus, negative regulation of osteoblast differentiation, negative regulation of DNA-binding transcription factor activity, negative regulation of transcription by RNA polymerase II, metal ion binding
196P1	1	329	12:22585550-22585879	All animals (low coverage)	Zinc finger protein 120	DNA binding, transcription, DNA-templated, regulation of transcription, DNA-templated, nucleus, metal ion binding
197P1	1	299	12:20321368-20321667	Mostly Mammals	Zinc finger protein 120	DNA binding, transcription, DNA-templated, regulation of transcription, DNA-templated, nucleus, metal ion binding
198P1	1	1439	12:23780601-23782040	Mostly Mammals	Zinc finger protein 709	
199P1	1	1814	12:24337167-24338981	All animals (low coverage)	Zinc finger protein 431	core promoter sequence-specific DNA binding, chromatin binding, transcription, DNA-templated, cell differentiation, histone deacetylase binding, nucleus, negative regulation of osteoblast differentiation, negative regulation of DNA-binding transcription factor activity, negative regulation of transcription by RNA polymerase II, metal ion binding
200P1	1	4810	12:23143970-23148780	Mostly Mammals	Zinc finger protein 431	
201P1	1	1271	12:19976053-19977324	All animals (low coverage)	Zinc finger protein 431	DNA binding, transcription, DNA-templated, regulation of transcription, DNA-templated, nucleus, metal ion binding
202P1	1	299	12:22726338-22726637	Mostly Mammals	Zinc finger protein 700	
204P1	1	6835	12:19301346-19308181	Mostly Mammals	Zinc finger protein 431	core promoter sequence-specific DNA binding, chromatin binding, transcription, DNA-templated, cell differentiation, histone deacetylase binding, nucleus, negative regulation of osteoblast differentiation, negative regulation of DNA-binding transcription factor activity, negative regulation of transcription by RNA polymerase II, metal ion binding
206P1	1	329	12:23929820-23930149	All animals (low coverage)	Zinc finger protein 120	DNA binding, transcription, DNA-templated, regulation of transcription, DNA-templated, nucleus, metal ion binding
207P1	1	826	12:21671882-21672708	Mostly Mammals	Zinc finger protein 120	
208P1	1	299	12:19975399-19975698	Mostly Mammals	Zinc finger protein 120	
209P1	1	1439	12:23928374-23929813	All animals (low coverage)	Zinc finger protein 431	core promoter sequence-specific DNA binding, chromatin binding, transcription, DNA-templated, cell differentiation, histone deacetylase binding, nucleus, negative regulation of osteoblast differentiation, negative regulation of DNA-binding transcription factor activity, negative regulation of transcription by RNA polymerase II, metal ion binding
210P1	1	2703	15:3217049-3219752	Mammals & alligator	RNA-binding protein EWS	RNA binding, transcription, DNA-templated, regulation of transcription, DNA-templated, cytoplasm, plasma membrane, identical protein binding, protein binding, nucleus, nucleotide binding, zinc ion binding

212P1	3	9490	15:19207680-19217170	Mus musculus	RNA-binding protein EWS	
216P2	2	73971	X:140361491-140435462	All animals (low coverage)	FERM and PDZ domain-containing protein 3	cytoskeleton
219P1	1	5982	X:22243205-22249187	Mus musculus	Testis-expressed sequence 13A protein	zinc ion binding
222P1	5	16146	X:56277090-56293236	Rattus norvegicus +1	Zinc finger protein 449	
222P2	5	16146	X:56277090-56293236	Rattus norvegicus +1	Zinc finger protein 449	DNA binding, transcription, DNA-templated, nucleus, DNA-binding transcription factor activity, metal ion binding
251P1	7	10437	X:101695773-101706210	Rattus norvegicus	Circumsporozite protein	
251P10	7	10437	X:101695773-101706210	Rattus norvegicus	Circumsporozite protein	
251P11	7	10437	X:101695773-101706210	Rattus norvegicus	Circumsporozite protein	
251P12	7	10437	X:101695773-101706210	Rattus norvegicus	Circumsporozite protein	
251P13	7	10437	X:101695773-101706210	Rattus norvegicus	Circumsporozite protein	
251P14	7	10437	X:101695773-101706210	Rattus norvegicus	Circumsporozite protein	
251P15	7	10437	X:101695773-101706210	Rattus norvegicus	Circumsporozite protein	
251P16	7	10437	X:101695773-101706210	Rattus norvegicus	Circumsporozite protein	cell surface
251P17	7	10437	X:101695773-101706210	Rattus norvegicus	Circumsporozite protein	
251P18	7	10437	X:101695773-101706210	Rattus norvegicus	Circumsporozite protein	
251P19	7	10437	X:101695773-101706210	Rattus norvegicus	Circumsporozite protein	
251P2	7	10437	X:101695773-101706210	Rattus norvegicus	Circumsporozite protein	
251P20	7	10437	X:101695773-101706210	Rattus norvegicus	Circumsporozite protein	
251P21	7	10437	X:101695773-101706210	Rattus norvegicus	Circumsporozite protein	
251P22	7	10437	X:101695773-101706210	Rattus norvegicus	Circumsporozite protein	

251P23	7	10437	X:101695773-101706210	Rattus norvegicus	Circumsporozoite protein	
251P24	7	10437	X:101695773-101706210	Rattus norvegicus	Circumsporozoite protein	
251P25	7	10437	X:101695773-101706210	Rattus norvegicus	Circumsporozoite protein	
251P26	7	10437	X:101695773-101706210	Rattus norvegicus	Circumsporozoite protein	
251P3	7	10437	X:101695773-101706210	Rattus norvegicus	Circumsporozoite protein	
251P4	7	10437	X:101695773-101706210	Rattus norvegicus	Circumsporozoite protein	
251P5	7	10437	X:101695773-101706210	Rattus norvegicus	Circumsporozoite protein	
251P6	7	10437	X:101695773-101706210	Rattus norvegicus	Circumsporozoite protein	
251P7	7	10437	X:101695773-101706210	Rattus norvegicus	Circumsporozoite protein	
251P8	7	10437	X:101695773-101706210	Rattus norvegicus	Circumsporozoite protein	
251P9	7	10437	X:101695773-101706210	Rattus norvegicus	Circumsporozoite protein	
255P1	8	34017	X:1613332234-161366251	Rattus norvegicus +1 sp	BEN domain-containing protein 2	
260P1	1	1687	4:129928611-129930298	Rattus norvegicus +1 sp	SPOC domain-containing protein 1	transcription, DNA-templated, negative regulation of phosphatase activity
273P1	6	17150	2:68561621-68578771	Rodents	POTE ankyrin domain family member A	
273P2	6	17150	2:68561621-68578771	Rodents	POTE ankyrin domain family member A	
303P1	11	18213	9:75468476-75486689	All animals (low coverage)	RNA polymerase-associated protein LEO1	Wnt signaling pathway, positive regulation of transcription by RNA polymerase II, mRNA polyadenylation, transcription, DNA-templated, nucleolus, protein binding, nucleus, stem cell population maintenance, histone H2B ubiquitination, spinal cord oligodendrocyte cell differentiation, melanocyte differentiation, negative regulation of myeloid cell differentiation, positive regulation of transcription elongation from RNA polymerase II promoter, Cdc73/Paf1 complex, positive regulation of mRNA 3'-end processing, endodermal cell fate commitment, neural crest cell development, xanthophore differentiation, glial cell development, histone monoubiquitination, embryonic cranial skeleton morphogenesis, heart development
303P10	11	18213	9:75468476-75486689	Mammals	RNA polymerase-associated protein LEO1	
303P11	11	18213	9:75468476-75486689	All animals (low coverage)	RNA polymerase-associated protein LEO1	
303P2	11	18213	9:75468476-75486689	Mammals	RNA polymerase-associated protein LEO1	

303P3	11	18213	9:-75468476-75486689	All animals (low coverage)	RNA polymerase-associated protein LEO1	integral component of membrane, cytoplasm, microtubule organizing center, protein binding, protein ubiquitination, ligase activity, zinc ion binding	
303P4	11	18213	9:-75468476-75486689	Mammals	RNA polymerase-associated protein LEO1		
303P5	11	18213	9:-75468476-75486689	Mammals	RNA polymerase-associated protein LEO1		
303P6	11	18213	9:-75468476-75486689	Mammals	RNA polymerase-associated protein LEO1		
303P7	11	18213	9:-75468476-75486689	Mammals	RNA polymerase-associated protein LEO1		
303P8	11	18213	9:-75468476-75486689	All animals (low coverage)	RNA polymerase-associated protein LEO1		
303P9	11	18213	9:-75468476-75486689	Mammals	RNA polymerase-associated protein LEO1		
305P1	1	3510	9:56027491-56031001	All animals	E3 ubiquitin-protein ligase RNF19A		
310P1	1	11097	9:122903236-122914333	All animals (low coverage)	Zinc finger protein 660		DNA binding, transcription, DNA-templated, regulation of transcription, DNA-templated, nucleus, metal ion binding
319P1	1	365	13:65249837-65250202	Mostly Mammals	Zinc finger protein 20		
321P1	3	16581	13:74505897-74522478	All animals (low coverage)	Zinc finger protein 431	core promoter sequence-specific DNA binding, chromatin binding, transcription, DNA-templated, cell differentiation, histone deacetylase binding, nucleus, negative regulation of osteoblast differentiation, negative regulation of DNA-binding transcription factor activity, negative regulation of transcription by RNA polymerase II, metal ion binding	
321P2	3	16581	13:74505897-74522478	All animals (low coverage)	Zinc finger protein 431		
323P1	5	13479	13:74550898-74564377	All animals (low coverage)	Zinc finger protein 431		
324P1	1	305	13:65337385-65337690	Mostly Mammals	Zinc finger protein 431		
325P1	4	13777	13:81826068-81839845	Mus musculus	Zinc finger protein 431		
327P1	4	19570	13:62665774-62685344	All animals (low coverage)	Zinc finger protein 431	core promoter sequence-specific DNA binding, chromatin binding, transcription, DNA-templated, cell differentiation, histone deacetylase binding, nucleus, negative regulation of osteoblast differentiation, negative regulation of DNA-binding transcription factor activity, negative regulation of transcription by RNA polymerase II, metal ion binding	
327P2	4	19570	13:62665774-62685344	All animals (low coverage)	Zinc finger protein 431		
333P1	5	15210	13:74603075-74618285	All animals (low coverage)	Zinc finger protein 431		

33P2	5	15210	13:74603075-74618285	All animals (low coverage)	Zinc finger protein 431	
341P1	3	6462	13:49762460-49768922	Mostly Mammals	Sperm motility kinase X	ATP binding, protein serine/threonine kinase activity
345P1	1	761	13:65249008-65249769	All animals (low coverage)	Zinc finger protein 120	DNA binding, transcription, DNA-templated, regulation of transcription, DNA-templated, nucleus, metal ion binding
346P1	3	8287	13:49820663-49828950	Rodents	Sperm motility kinase X	ATP binding, protein serine/threonine kinase activity
347P1	1	3061	10:130573979-130577040	All animals (low coverage)	Zinc finger protein 431	core promoter sequence-specific DNA binding, chromatin binding, transcription, DNA-templated, cell differentiation, histone deacetylase binding, nucleus, negative regulation of osteoblast differentiation, negative regulation of DNA-binding transcription factor activity, negative regulation of transcription by RNA polymerase II, metal ion binding
355P1	4	8108	10:93850061-93858169	All animals	Ubiquitin carboxyl-terminal hydrolase 44 (Usp44)	proteasome-mediated ubiquitin-dependent protein catabolic process, nucleus, regulation of mitotic cell cycle spindle assembly checkpoint, cysteine-type peptidase activity, zinc ion binding, mitotic cell cycle
356P1	1	674	5:109478138-109478812	All animals (low coverage)	Zinc finger protein 120	DNA binding, transcription, DNA-templated, regulation of transcription, DNA-templated, nucleus, metal ion binding
361P1	4	18312	5:110076130-110094442	All animals (low coverage)	Zinc finger protein 431	core promoter sequence-specific DNA binding, chromatin binding, transcription, DNA-templated, cell differentiation, histone deacetylase binding, nucleus, negative regulation of osteoblast differentiation, negative regulation of DNA-binding transcription factor activity, negative regulation of transcription by RNA polymerase II, metal ion binding
361P2	4	18312	5:110076130-110094442	All animals (low coverage)	Zinc finger protein 431	DNA binding, transcription, DNA-templated, regulation of transcription, DNA-templated, nucleus, metal ion binding
362P1	1	311	5:109479106-109479417		Zinc finger protein 497	
364P1	4	92821	5:49787426-49880247	Mus musculus	Zinc finger protein 497	
368P1	5	19178	5:109866698-109885876	All animals (low coverage)	Zinc finger protein 431	core promoter sequence-specific DNA binding, chromatin binding, transcription, DNA-templated, cell differentiation, histone deacetylase binding, nucleus, negative regulation of osteoblast differentiation, negative regulation of DNA-binding transcription factor activity, negative regulation of transcription by RNA polymerase II, metal ion binding
368P2	5	19178	5:109866698-109885876	All animals (low coverage)	Zinc finger protein 431	
369P1	1	374	5:136205011-136205385	Mus musculus	IgE-binding protein	DNA integration, nucleic acid binding, viral process

